PHARMACOLOGICAL CHARACTERISATION OF SELECTED PYRROLOBENZODIAZEPINES AS ANTI-CANCER AGENTS

Pharmacokinetic and pharmacodynamic characterisation of the pyrrolobenzodiazepine dimer SJG-136 and the monomers D709119, MMY-SJG and SJG-303

Gary Paul WILKINSON

Submitted for the degree of Doctor of Philosophy

Tom Connors Cancer Research Centre

University of Bradford

2004

Gary Paul Wilkinson

Pharmacological Characterisation Of Selected Pyrrolobenzodiazepines As Anti-Cancer Agents

Abstract

This study aimed to investigate the pharmacology of selected pyrrolobenzodiazepine (PBD) compounds shown to have cytotoxic activity with predicted DNA sequence selectivity. Research focused upon the PBD dimer, SJG-136, selected for clinical trials, and the novel PBD monomer compounds D709119, MMY-SJG and SJG-303.

SJG-136, a novel sequence-selective DNA minor groove cross-linking agent, was shown to have potent tumour cell type selective cytotoxicity in *in vitro* assays. Pharmacokinetic studies in mice via both the i.p. and i.v. route (dosed at the maximum tolerated dose (MTD)) showed that SJG-136 reaches concentrations in plasma well in excess of the *in vitro* IC_{50} values for 1 h exposure, and was detected in tumour and brain samples also above the *in vitro* IC_{50} values. Furthermore, SJG-136 showed linear pharmacokinetics over a 3-fold drug dose range. Metabolism studies showed SJG-136 is readily metabolised *in vitro* by hepatic microsomes, predominantly to a monodemethylated metabolite; this metabolite could be detected *in vivo*. Analytical method development work was also conducted for the imminent Phase I clinical trial of SJG-136 resulting in a sensitive and selective bio-analytical detection protocol. Comet analysis showed that SJG-136 dosed at the MTD and ⅓MTD causes significant interstrand DNA cross-linking in lymphocytes *in vivo*. *In vitro* studies demonstrated that SJG-136 localises within the cell nucleus, and acts to disrupt cell division via a G_2/M block in the cell cycle at realistic concentrations and exposure times that are achievable *in vivo*.

In vivo pharmacokinetic studies of D709119 showed the compound is easily detectable in mouse plasma following i.p. dosing at the MTD, but could not be detected in either tumour or brain samples. *In vitro* cytotoxicity studies revealed D709119 to have potent activity across a selection of tumour cell lines.

SJG-136, D709119, MMY-SJG, SJG-303 and DC-81 demonstrated a non-enzyme-catalysed reactivity with the biologically relevant thiol, reduced glutathione (GSH). Studies demonstrated that reactivity of the PBD compounds toward GSH was dependent on GSH concentrations. At levels of GSH found in plasma, the PBD compounds showed considerably lower reactivity with GSH than at intracellular GSH levels.

SJG-136 and D709119 also showed favourable pharmacokinetic profiles in mice, and warrant further study for anti-tumour activity *in vivo* and progression to use in patients.

Keywords: Pyrrolobenzodiazepine (PBD), anti-cancer, SJG-136, D709119, DNA-interactive agent, pharmacokinetics, pharmacodynamics, HPLC, glutathione, pre-clinical

Table of Contents

For my parents, Patricia and Michael Wilkinson
and my fiancée Jen

Acknowledgements

I would like to thank Dr Paul Loadman and Professor Terry Jenkins for their invaluable help, guidance and support throughout the project.

Many thanks to everyone at the Tom Connors Cancer Research Unit for their help, especially James (Jim-Bob) Taylor, Dave Swaine, Steve Shnyder and Patricia Cooper for their expert assistance, without whom life would have been much more difficult. I would also like to thank Professor David Thurston and Dr Philip Howard for assistance and providing the compounds to work on. Thanks to Dr Victoria Spanswick and Professor John Hartley for teaching me the Comet assay (and for putting up with me in their labs). For much "spiritual" guidance and coffee break conversation, thanks go to Tracey Norris.

Thanks go to my Mum and Dad for their continued support.

Finally, thanks to my fiancée Jen for her unshakable belief that I'd get this far (and for several proof reads).

Table of Figures

Table of Tables

Table of Equations

Abbreviations

$[M + X]^{\bullet+}$	Denotes ion detected by mass spectrometer. M = mass of analysed compound; X denotes additional elements or compounds increasing the detected mass to charge ratio of the resulting ion.
Ang-1	Angioprotein 1.
AP	Apurinic / apyrimidinic.
AUC	Area underneath the concentration vs. time curve.
BER	Base excision repair.
BSO	D,L-buthionine-*S,R*-sulfoxamine.
$C(0)$	Estimation of plasma concentration at time $t = 0$ h.
CL	Clearance.
C_{max}	Maximum plasma concentration.
COMPARE	NCI 60-cell line screen pattern recognition algorithm.
CV	Coefficient of variation.
DMA	*N,N*-dimethylacetamide.
DMSO	Dimethyl sulfoxide.
DNA	Deoxyribonucleic acid.
dNTP	Any or all of the four deoxyribonucleoside phosphates required for DNA synthesis.
DSB	DNA double-strand break.
EDTA	Ethylenediaminetetraacetic acid.
Em	Emission.
ERK	Extracellular-signal-regulated kinase.
Ex	Excitation.
FACS	Fluorescence-activated cell sorting.
FTase	Ras farnesyltransferase.
GI50	Growth inhibition of 50%. The drug concentration resulting in a 50% reduction in the net protein increase (as measured by SRB staining) in control cells during the drug incubation.
GSH	Reduced glutathione.
HBSS	Hank's balanced salt solution.
HhH	Helix-hairpin-helix.
HPLC	High performance liquid chromatography.

HR	Homologous recombination.
hTERT	The human telomerase reverse transcriptase catalytic subunit.
hTR	The human RNA component of telomerase.
i.p.	Intra-peritoneal.
i.v.	Intravenous.
IC_{50}	Inhibitory concentration at which 50% growth inhibition is observed versus untreated controls.
ICL	DNA interstrand crosslink.
k_{el}	Elimination rate constant.
LC50	Concentration of drug resulting in 50% decrease in net protein compared to $t = 0$ measurement.
LD_{50}	Median lethal dose.
LOQ	Limit of quantification; the lowest concentration of analyte determined with acceptable accuracy and precision.
m/z	Mass to charge ratio.
MAPK	Mitogen-activated protein kinase.
MeCN	Acetonitrile.
MeOH	Methanol.
MMP	Matrix metalloproteinases.
MRM	Multiple reaction monitoring (used to monitor the transition between quadrupoles in MS/MS analysis).
MS	Mass spectrometer (single quadrupole).
MS/MS	Mass spectrometer (twin quadrupole).
MTD	Maximum tolerated dose.
MTT	3,[4,5-Dimethylthiazol-2-yl]-2,5-diphenyltetrazolium bromide.
MUG	Mismatch-specific DNA glycosylase.
MW	Molecular weight.
n / a	Not applicable.
n / d	Not detected.
NADH	Reduced nicotinamide adenine dinucleotide.
NADPH	Reduced nicotinamide adenine dinucleotide phosphate.
NAT2	*N*-acetyltransferase 2.
NCI	National Cancer Institutes of the USA.

NER	Nucleotide excision repair.
NHEJ	Non-homologous end-joining.
NMR	Nuclear magnetic resonance.
p53	Product of tumour suppressor gene *p53*.
PBD	Pyrrolobenzodiazepine; specifically pyrrolo[2,1-*c*][1,4]benzodiazepine.
PBS	Phosphate-buffered saline.
PD	Pharmacodynamic.
P-gp	P-glycoprotein.
PK	Pharmacokinetic.
Pu	Purine base.
Py	Pyrimidine base.
QIVT	Quantitative *in vitro* transcription.
r^2	Coefficient of determination.
RNA	Ribonucleic acid.
RSD	Relative standard deviation.
s.c.	Subcutaneous.
S9 fraction	Subcellular fraction used for *in vitro* metabolism studies, prepared by 9000*g* centrifugation of liver homogenate to remove nucleii and mitochondria. Contains microsomal and cytosolic enzymes.
SAR	Structure-activity relationship.
SD	Standard deviation.
SIR	Single ion recording.
SPE	Solid phase extraction.
SRB	Sulforhodamine B.
$t_{½}$	Half life.
TGI50	Drug concentration resulting in total growth inhibition. Where there is no net protein increase (as measured by SRB staining).
TIC	Total ion current.
TMci	Tail moment of untreated irradiated control.
TMcu	Tail moment of untreated irradiated control.
TMdi	Tail moment of drug treated irradiated sample.
TNM	Tumour, Node, Metastasis system of tumour classification.

UDG	Uracil-DNA glycosylase.
UK	United Kingdom
USA	United States of America
UV	Ultraviolet.
VEGF	Vascular endothelial growth factor.
V_{ss}	Volume of distribution at steady state.
V_z	Volume of distribution of terminal elimination phase.

1 What is Cancer?

1.1 The history of cancer

Cancer has become an increasingly prominent disease and is one of the leading causes of death in the western world, although the disease itself has ancient roots.

The Greek physician Hippocrates is thought to have originated the word "cancer" used today, due to his usage of the terms "carcinos" and "carcinoma", to describe non-ulcer forming and ulcer-forming tumours. These words refer to a crab in Greek, and were used to describe the finger-like projections formed by the tumour. Hippocrates believed the body contained four humours or body fluids, blood, phlegm, yellow bile, and black bile. Good health was thought to depend upon a balance of these fluids, and imbalance was considered to cause illness and disease. Cancer was thought to arise from an excess of black bile. This theory was widely accepted and held sway for over 1300 years, perhaps a result of religious prohibitions preventing the study of the body and thereby disallowing practices such as autopsy (Diamandopoulos, 1996).

One of the theories that replaced the humoral theory proposed by Hippocrates suggested the formation of cancer from another body fluid, lymph. At this point in time (18th century), life was thought to consist of the continuous movement of fluids through solids; blood and lymph were thought to be the most important of these fluids. Proposed by Stahl and Hofman, it was believed that cancer was composed of fermenting and degenerating lymph, varying in density, acidity and alkalinity (Diamandopoulos, 1996).

An investigation by Sir Percival Pott in 1775 provided one of the first scientific studies into the cause of cancer (Shindell & Goldberg, 1981). This linked the high incidence of death from cancer of the scrotum in males in their twenties to earlier occupation as chimneysweeps, and suggested that the causative agent responsible was soot. This study identified both a suspected carcinogen, and further characterised cancer as a disease with a notable latent period.

Johannes Muller, a German pathologist, demonstrated in 1838 that cancer is composed of cells, not lymph. However, he believed that cancer cells did not originate from normal cells, but from budding elements (blastema) between normal tissue. It was his student, Rudolf Virchow, who determined that all cells (including cancer cells) are derived from other cells (Diamandopoulos, 1996).

The recognition of cancer as a condition arising from the uncontrolled proliferation of cells was not possible until the advent of the microscope. Examination by the eminent 19th century pathologist Rudolf Virchow, prompted the declaration that “every cell is born from another cell”. Consequently cancer became established as a cellular disease, and the science of oncology was born. This enhanced the ability and usefulness of surgery for cancer treatment, as body tissues removed by the surgeon could now be microscopically examined and a precise diagnosis could be made (Ackerknecht, 1953). Virchow proposed that cancer is caused by chronic irritation. He also believed that cancers could spread “like a liquid”. It was shown later by a German surgeon, Karl Thiersch, that cancers metastasise through the spread of malignant cells in the bloodstream.

A theory that was entertained for much of the 17th and 18th centuries was that cancer may be contagious. This manifested itself predominantly in France; the first cancer hospital there was forced to move out of Paris in 1779 as a result of fears that cancer may spread through the city. In a similar vein, a Nobel Prize was mistakenly awarded in 1926 for work which indicated that cancer could be caused by a parasitic worm (e-Museum, 1926). The parasite theory was not confirmed, and rapidly fell out of favour.

1.2 Cancer – the problem

Despite numerous medical advances in the treatment of cancer, it remains a significant health problem. During 2001, in the UK alone malignant neoplasm (excluding benign, in situ, other and unspecified neoplasms) was responsible for 154,460 deaths. This places cancer as the cause of a quarter (26%) of all deaths in the UK (Cancer Research UK, 2003). Additionally, more than 262,000 new cases of cancer were diagnosed in the UK in 1998 (Cancer Research UK, 2002). Excluding non-melanoma skin cancers, the three most common cancers are responsible for the largest number of deaths; 22% of deaths are attributed to lung cancer, cancers of the large bowel (colon and rectum) are responsible for 10%, and breast cancer (despite a very low incidence in men) is responsible for 8% of all cancer deaths (Cancer Research UK, 2002; 2003). While there are over 200 different types of cancer only a few occur frequently, and of these lung, breast, large bowel (colorectal) and prostate account for over half of new cases (Cancer Research UK, 2002).

1.3 The biology of cancer

1.3.1 What is cancer?

Cancer is a broad umbrella term used to describe any of over a hundred different diseases characterised by uncontrolled cell proliferation. It is important to be aware of the distinction between different types of cancer, as the clinical implication and outcome for a patient can be vastly different depending on the type and location of cancer manifested. This is further complicated as cancers arising from the same cell-type can behave differently.

There are somewhere in the region of 5×10^{13} cells which make up the component parts of the human body, and each of these cells is carefully controlled and regulated in order to meet the needs of the body as a whole. Bearing in mind that the entire body originates from the formation of one cell from the fusion of two gametes, there are a vast number of cell divisions occurring to form the final organism. This system is subjected to tight and rigorous control to ensure that the rate at which cells are formed matches that at which cells are removed (Ruddon, 1995).

Cancer results from a defect in the regulation of cell growth and proliferation. A single cancerous cell can divide to form two cells; the two cancerous cells can further split to form four, and the rate of growth can continue onwards exponentially. Thus a tumour can be formed from the malfunction of a single cell. If this cancerous growth goes unchecked, it can progress to invade surrounding tissue, enter the circulation and spread, and interfere with the normal functions of the body ultimately leading to the death of the individual (Ruddon, 1995).

1.3.2 Types of cancer / cancer classification

There is a major distinction between types of neoplasm: benign (non-cancerous) or malignant (cancerous). The primary characteristic of a benign neoplasm is the confinement of the growth to its original location. It is generally enclosed in a fibrous capsule, and does not invade surrounding tissue or metastasise to other parts of the body. The common skin wart is an example of a benign growth and, as it is localised, it is almost invariably treatable by surgery resulting in the total removal of neoplastic cells. The complete removal of the neoplastic tissue and lack of invasive characteristics mean that this type of tumour is generally not life-threatening unless it occurs in an inoperable location. Benign growths tend to grow relatively slowly, and more closely resemble their tissue of origin than their malignant counterparts (Ruddon, 1995).

Alternatively the growth may be malignant; this can both invade adjacent tissue, and can spread to become established in other parts of the body via metastasis. Malignant neoplasms are growths generally considered to be cancers. It is the ability of these tumours to invade normal non-neoplastic tissue, and to spread to other parts of the body (metastasise) that makes this growth highly dangerous and difficult to treat. Once metastases (secondary growths that have travelled to other parts of the body) have become established in other areas of the body the option to completely remove the cancer by localised surgery is no longer possible, and alternative modes of treatment become necessary (Ruddon, 1995).

1.3.3 Cancer classification

Neoplasms are classified according to the type of cell and tissue from which they originate. There is a subdivision into three types of malignant tumour: the carcinomas, sarcomas, lymphomas and leukaemias. Approximately 90% of human cancers fall into the carcinoma classification, and are a result of malignancies formed from epithelial cells. Sarcomas are formed from connective tissues such as muscle and bone, and are rare in humans. Lymphomas and leukaemias constitute about 8% of human cancers, and are cancers derived from cells of the lymphatic and blood systems, respectively (Franks & Teich, 1997).

The diversity of cancers and the complexity of classification has resulted in the development of clinical staging systems in order to describe the extent of tumour progression. One of the most common techniques for classifying cancers is known as the TNM (Tumour, Node, Metastasis) system. This system can be used to describe the size of a primary tumour, whether the cancer has spread to the lymph nodes, and whether the cancer has metastasised to other parts of the body. An example of this staging system can be seen in Table 1.1.

Classification	Description
Primary Tumour	
Tis	Means 'in situ' – cancerous cells have been found but they have not yet begun to move into surrounding tissues in the testicle.
T1	Means the tumour is contained within the testicle and epididymis.
T2	Means there are signs that the tumour has grown into blood or lymphatic vessels.
T3	Means the tumour has grown as far as the spermatic cord (and there are may also be blood or lymphatic vessel involvement).
T4	Means the tumour has grown into the scrotum.
Regional Lymph Nodes	
N0	There are no lymph nodes containing cancer cells.
N1	The lymph nodes are all smaller than 2 cm across.
N2	At least one of the lymph nodes is bigger than 2 cm, but smaller than 5 cm across.
N3	At least one of the lymph nodes is bigger than 5 cm across.
Distant Metastases	
M0	Means there are no signs of spread to other body organs.
M1a	Means there is cancer spread to the lungs OR there are lymph nodes a long way from the testicles, for example near the collar bone.
M1b	Means there is spread to other body organs such as the liver or brain.

Table 1.1 The TNM system of tumour classification for testicular cancer (adapted from the Cancer Research UK website, www.cancerhelp.co.uk).

1.4 Causes of cancer

1.4.1 What leads to tumour formation?

In normal continually renewing tissue there are two types of cell: (i) the stem cell, which has a high capacity for proliferation (although normally the rate of division is slow), and (ii) the differentiated cell, which arises from a stem cell but has progressed through a process of maturation and differentiation to become a particular type of cell. A stem cell normally divides asymmetrically producing two daughter cells, one of which retains its growth potential and remains a stem cell (a copy of the mother cell), whereas the other becomes a differentiated cell. In most cases tumours arise from a single transformed stem cell, rather than from a differentiated cell.

There is an extensive amount of evidence that genetic mutation can cause cancer. This can include changes within the genome such as insertions, deletions, point mutations, translocations or amplifications. It was observed by Ames (Ames, 1983) that the majority of carcinogens are also mutagens. There are findings that show that genetically determined traits associated with a deficiency in DNA repair enzymes can be linked with incidence of cancer. This led to the general acceptance of a genetic component to cancer formation, and therefore the link that damage to genetic material could lead to tumour formation.

Initiation of tumour formation can occur in several ways. The mechanisms by which this may transpire are:

- **Activation of oncogenes.** Often this involves the conversion of a proto-oncogene into an activated oncogene. Oncogenes can be activated by mutations, viral oncogenesis (insertion of an oncogene by a viral vector), gene amplification, or by chromosomal abnormalities. Viral oncogenesis is relatively rare and results from either the incorporation of viral sequences (normally modified versions of proto-oncogenes) into the host genome, from insertional mutagenesis (viral integration into host DNA causing the disruption of a host growth control factor), or by transactivation of an unrelated growth regulatory protein by a virally encoded protein (Hodgson & Maher, 1999).
- **Inactivation of tumour suppressor genes.** Tumour suppressor genes act in a recessive manner as the *loss* of a tumour suppressor gene may lead to tumour formation. An example of this is the tumour suppressor gene, p53. p53 has been shown to initiate apoptosis in cells that have been subjected to DNA-damaging agents, such as ionising γ radiation and various chemotherapy agents (Canman & Kastan, 1995). Hence loss of the p53 gene can result in the survival of cells with DNA damage, and the potential for the accumulation of mutations may result in the activation of oncogenic factors. The mechanisms by which p53 elicits its effects are still not fully understood, although it is widely agreed that p53 plays an important role in the cellular response to DNA damage.
- **Heritable cancer.** This type of cancer is usually caused by inheritance of a defective DNA repair mechanism, a metabolism that is overly efficient at metabolising chemicals into carcinogens, or an inappropriate immune response. A defect in DNA repair mechanisms can lead to conditions such as retinoblastoma (a tumour of the eye) and familial adenomatous polyposis (a predisposition to

colorectal cancer), both of which are dominantly inherited (Hodgson & Maher, 1999).

1.4.2 Environmental aspects of cancer

A high proportion of cancer is attributed to environmental factors, with categories ranging from the use of substances such as tobacco and alcohol, to the more general categories of diet and exposure to solar radiation. In the USA, there is evidence that over 70% of cancers are linked to environmental factors, and therefore are potentially avoidable (Doll & Peto, 1981).

2 Treatment of Cancer

2.1 Surgery

Surgery is the primary and most preferred method of treating cancer. Correctly used, surgery can often eradicate primary or localised disease. Even in a situation where a cancer is not confined to one region of the body the removal of a large focal tumour mass may help by lowering the overall tumour burden. For the removal of easily operable neoplasms, such as the basal cell carcinoma (the commonest form of skin cancer), surgical procedures such as curettage and cautery, surgical excision or cryotherapy, are commonly used procedures that result in a high cure rate. In more complicated situations, where the tumour has begun to invade surrounding tissue, it is common for surgical excision of the growth to be combined with either radiotherapy or chemotherapy to increase the likelihood of removing all of the cancerous cells.

2.2 Radiotherapy

Radiotherapy is similar to surgery as it is primarily useful in the treatment of localised cancers, but has the advantage that it can be used to treat cancers that have grown out of reach of the surgeons' knife, and have become inoperable. As radiotherapy is less invasive some localised tumours are treated solely with radiation. Other tumours are treated with a combination of surgery and radiation in order to remove the bulk of the tumour surgically and eliminate any cancerous cells that may have invaded the surrounding tissue with radiotherapy. As some types of tumour are particularly sensitive to radiation, this can be a highly effective tool.

Damage by radiation is a noted cause of cancer due to the genetic damage that can occur as a result of exposure to non-lethal doses, resulting in random mutations to the host DNA. Used in high doses radiation can result in cell death; this is the main principle of radiotherapy. This method of treatment is similar to surgery, as it is not specific for cancerous cells and will also kill normal cells. This limits the usefulness of radiation therapy, as it can pose a highly toxic threat to the patient. Lack of specificity is one of the main problems with current treatments for cancer.

There are several types of radiation in use for the treatment of cancer: X-rays or γ radiation are used to excite electrons within the biological matter and cause the further ionisation of other atoms, and electrons (produced by a particle accelerator) are used to directly interact with the atoms of molecules present in the target cells, are two examples. Generally, radiotherapy uses an external radiation source and beams of radiation are directed at the tumour in order to destroy the cancerous cells.

In order to control tumour growth by the use of radiotherapy, it is important to consider the concept that tumours contain a fraction of cells that have unlimited proliferative capacity. Therefore, in order to control tumour growth all of the tumour stem cells need to be killed. Thus the dose of radiation required to control a tumour depends on both the sensitivity of the cells to radiation and the number of cells present. Many different factors can influence the effectiveness of radiotherapy. This includes the type of radiation used, factors that can influence the effectiveness of the radiotherapy such as the presence or absence of oxygen (which can alter the dose of low-LET (linear energy transfer – X or γ rays) radiation needed by up to 3 times) (Chapman *et al.*, 1974;

Cheong *et al.*, 1993; Bristow & Hill, 1998). Types of radiation used include UV radiation, X-rays, β-rays, or γ-rays.

2.3 Chemotherapy

Chemotherapy is the concept of treating cancer with drugs. Treatment of cancer in this way is thought to be at least 500 years old, when preparations of zinc, mercury and silver were used, although the first documented treatment was in 1865 when potassium arsenite was used to treat a patient with leukaemia where a positive effect was noted (Lissauer, 1865). However, it was not until some 80 years later that the first successful systemic cancer treatment emerged as a spin-off from the development of nitrogen mustard for warfare use. Nitrogen mustard was used in a clinical trial for the treatment of lymphosarcoma in 1942, and a review of its effectiveness in the treatment of cancer was published in 1946 when it became more widely known. This publication is regarded as marking the beginning of modern cancer chemotherapy (Gilman & Philips, 1946). Mechlorethamine, one of the first nitrogen mustards to be shown to be clinically effective, is still used today in the treatment of cancer.

2.3.1 Principles and practice

Currently, chemotherapy is used in clinical practice in one of three roles:

- As the major curative agent for a few selected malignancies, e.g. Hodgkins disease (and other lymphomas), acute leukaemia in children, and testicular cancer in males.
- As a palliative treatment for many types of advanced cancers.
- As an adjuvant treatment before, during, or after localised treatments (such as surgery or radiotherapy) to enhance cell kill and eliminate possible metastases.

In addition to the desired antitumour effects, all current anticancer drugs are toxic to normal tissue, so there is a limited dose that may be given to a patient before the benefit of tumour cytotoxicity develops into the detrimental effects of systemic toxicity. This places a constraint on the clinical efficacy of the drugs. The overall goal in the development and design of antitumour drugs is to widen the therapeutic window and allow large doses of drug to be given, without causing major toxicity to normal tissue. This has led to many different strategies for enhancing toxicity to tumour cells while reducing toxicity to normal tissues, including strategies such as using pro-drugs, chemotherapeutic drugs which are not activated until they reach the tumour site, as well as the currently used drug therapies.

Chemotherapeutic agents are divided into separate classes based upon their mechanism of action or the cellular target upon which they act:

- Antimetabolites. Interfere with production of nucleic acids. There are several distinct subclasses:
    - Folate antagonists. Competitive inhibitors of dihydrofolate reductase prevent regeneration of reduced folate and lead to diminished DNA synthesis due to lack of purines and thymidine monophosphate (Pratt *et al.*, 1994).
    - Pyrimidine antagonists. Inhibitors of thymidylate synthase decrease thymidine production resulting in decreased DNA synthesis (Ivanetich & Santi, 1988).

  - Purine antagonists. Inhibit nucleotide production (at PRPP amidotransferase and IMP dehydrogenase) and act as pseudonucleotides (Pratt *et al.*, 1994; Moore & Erlichman, 1998).
  - Ribonucleoside reductase inhibitors. Hydroxyurea destabilises the haem centre of ribonucleoside reductase disrupting deoxyribonucleoside synthesis (Pratt *et al.*, 1994).
- Alkylating agents. Transfer an alkyl group to an intracellular molecule (typically an amine, phosphate, sulfhydryl or hydroxyl moiety), forming a covalent bond. Monofunctional (one reactive alkyl group) or bifunctional (two reactive alkyl groups and capacity for crosslink formation). Effects believed to be elicited from interaction with DNA bases, causing strand-breakage (Kohn, 1979; Garcia *et al.*, 1988). There are several classes:
  - Nitrogen mustards. N-7 position on guanine is most susceptible position for alkylation; form covalent cross-links. Several in current clinical use.
  - Nitrosoureas. Bifunctional alkylating agents. Single clinically useful agent (streptozotocin). Able to cross blood-brain barrier (Moertel *et al.*, 1992).
  - Alkanesulfonates. Bifunctional alkylating agents that react with N-7 position of guanine. Shown to form interstrand DNA crosslinks (Tong & Ludlum, 1980; Bedford & Fox, 1983; Farmer, 1987).
  - Aziridines. Bifunctional alkylating agents. Can form DNA crosslinks.
- Platinum compounds. Similar mechanism of action to alkylating agents. Preferred binding sites at N-7 of guanine and adenine (Roberts *et al.*, 1988). Can form interstrand crosslinks and adducts (DNA-DNA binding and DNA-protein binding) (Fichtinger-Schepman *et al.*, 1987).

- DNA-intercalating drugs:
    - Anthracyclines. Act by intercalating non-covalently and disrupting DNA structure and synthesis. Induce protein-linked double-strand breaks in DNA (Glisson *et al.*, 1986; Myers *et al.*, 1988).
    - Mitoxantrone. Interferes with topoisomerase II function preventing reannealing of DNA strands and causing double-strand protein-linked breaks (Harker *et al.*, 1989).

3 Anticancer drug development

3.1 A brief history of anticancer drug development

There have been many different approaches to the development and testing of anticancer drugs over the years. The majority of historic and current drug development systems revolve around the use of *in vivo* screens. These screens have the advantage that the effects of a potential agent can be observed in a whole-body environment, taking into account distribution of the drug, metabolic processes and rate of excretion of the drug as well as the effect of the drug on the tumour.

The idea of a primary *in vivo* screen was initially formalised in 1934 at the National Cancer Institutes of the USA (NCI) (Zubrod, 1979). This screen used randomly bred mice and the implantation of sarcoma-37. From the 1940s onwards many other tumours of various rodents came into use across the international scientific community, although again this used randomly bred animals, and thus rendered the systems highly immunogenic. In 1955, with the establishment of the Cancer Chemotherapy National Service Centre, the L1210 leukaemia became the primary screen, which was later superseded by the P388 leukaemia. Approximately 700,000 compounds were put through this screen (Frei, 1982). This practice of *in vivo* primary screening fell out of favour in 1985 with the initiation of the NCI human tumour cell line screen, and increasing pressure from ethical issues on the use of animals for a screen showing such a low hit-rate for new compounds (less than 0.1% at that time), coupled with the significantly lower amount of novel compound needed for evaluation in the *in vitro* system.

The advent of modern chemotherapy in the 1940s gave way to the serious usage of *in vitro* chemosensitivity assays for use in the prediction of *in vivo* cytotoxicity. Human tumour explants were used to assess the cytotoxicity of compounds. However, many factors were uncontrolled in these experiments as chemically defined cell culture medium was not available, and purely qualitative measurement was used, factors which made assessment of the data difficult. Improvements to cell culture techniques occurred during subsequent years helping to make this type of assay easier and more viable as a screening test. However, it was not until the implementation of the NCI human tumour cell line screen that this type of technique was elevated from a pre-screen to a primary screen.

While the progression of drugs from synthesis to clinical trials is still evolving, the actual clinical phase of drug development has remained relatively consistent. Phase I trials define basic parameters such as maximum tolerated dose (MTD) in a patient (to estimate an efficacious dose for use in phase II trials), toxicity of the compound, and study the clinical pharmacology of the drug. Phase II trials are designed to investigate therapeutic value of the compound, using information determined in phase I. Phase III trials are used to compare the new therapy to an existing standard to assess whether the new therapy has a significant advantage over current treatments.

3.2 The process of drug development

Much of current anticancer drug development preclinical work revolves around the practices put in place by the NCI. The NCI has a comprehensive human tumour cell line screening procedure in place, to which organisations have open access, and subsequent *in vivo* studies (such as hollow fibre and tumour xenograft) as used by the

NCI also tend to be used across the board. Thus, current preclinical work tends to follow the pattern described in Figure 3.1, with phase II and III trials following on. The usage of a panel of tumour cells has resulted in a shift of drug discovery from the previous "compound-oriented" approach to a "disease-oriented" approach, as compounds are now tested from the outset with the aim of finding out which tumour cell line the compound will be most effective against.

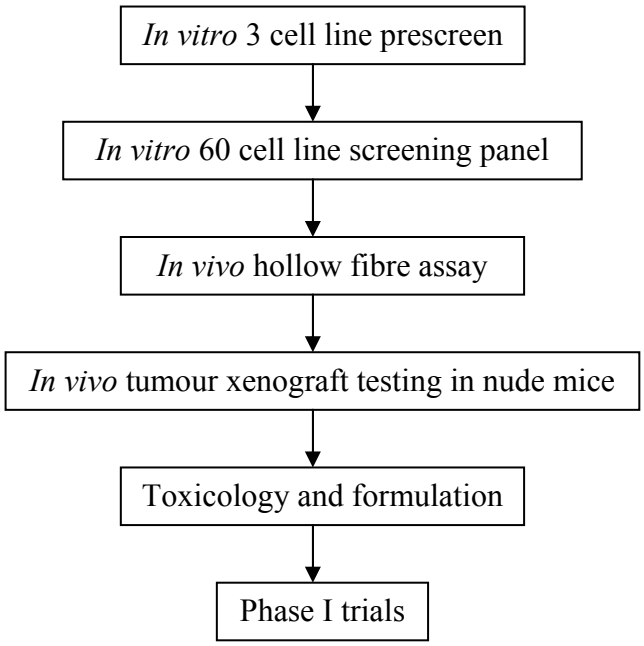

Figure 3.1 The preclinical drug development process.

3.2.1 Human tumour cell screening

Measurement of cytotoxicity in human tumour cell lines as an indicator of anticancer agent efficacy has become a fairly common practice over recent years. One of the most valuable resources for the testing of new chemical entities is the 60-cell-line based *In Vitro* Cell Line Screening Project (IVCLSP) run by the NCI. Fully operational as a primary screen in 1990 after five years of development, this project was set up with the intention of screening up to 20,000 compounds a year through a panel of 60 human

tumour cells lines representing different tumour types (leukaemia, melanoma, cancers of the lung, colon, brain, ovary, breast, prostate and kidney), and generating dose-response curves for the compound in each cell line. The aim of this type of screen is to enable a ranking of compounds as to which is most likely to possess biological activity, and thus prioritise which compounds should progress to further stages in development for evaluation in more complex tumour models. Due to the nature of the screen and the broad spectrum of cancer cells involved in the screen, it is also thought that this would enable an indication as to which type of cancer the potential drug may be useful in treating, as bias in the cell type killed may point to tumour selectivity (NCI, 2001).

In 1995, the NCI cell screening process was further streamlined, due to a large number of inactive compounds finding their way into the system. This resulted in the development of a 3-cell line pre-screen (MCF-7, NCI-H460, and SF-268 cell lines), which is significantly less labour intensive and costly than the 60 cell-line screen. This was designed to filter out as many of the inactive compounds as possible, without missing any of the active compounds, and involved a relatively high concentration (10^{-4} M), single-dose regimen to detect any cytotoxicity elicited by the test drugs. It is estimated that up to 50% of compounds can be eliminated from the full screen using this process (NCI, 2001).

The actual screen itself generates a 5 point dose-response curve for each compound in each cell line, using sulforhodamine B (SRB) protein binding stain to assess growth and viability after incubation with the test drug over a 48 h period (Skehan *et al.*, 1990). Results obtained from this assay are used to generate a "fingerprint" or mean-graph display, and their profile can then be compared by use of the COMPARE pattern-

recognition algorithm to relate the novel compound to other compounds in the NCI database. It has been stated that the profiles for drugs acting by similar mechanisms of action have been shown to correlate using the COMPARE function. Therefore, it is considered that use of the algorithm to look for compounds that show profiles that do not correlate well to other drugs in the database, and yet still show cytotoxicity in some cell lines, may result in the discovery of compounds acting by novel pathways (Boyd, 1997).

This first-line level of cell-based screening of compounds tends to now constitute what would be considered the "discovery" level of the drug research process. Complemented by rational drug design processes and *in silico* modelling of compounds, this should allow a significant streamlining of compounds that progress to the more resource-intensive levels of research involving whole animal models.

3.2.2 *In vivo* secondary screens

The time and expense involved in the *in vivo* screening of potential anticancer agents, has split the process of *in vivo* screening into two parts. The current NCI drug development programme uses a "hollow fibre assay" as the initial *in vivo* exposure stage of a drug, as it allows a quantitative assessment of drug efficacy, while using a minimal level of resources, and compounds proving to be of continued interest are then investigated in a tumour xenograft model.

3.2.2.1 The hollow fibre assay

The hollow fibre assay involves the culturing of cells within a polyvinylidene fluoride membrane hollow fibre, and subsequent implantation *in vivo*. The fibres used have a

molecular weight cut-off of 500 kDa, which allows the interaction of host and tumour cell soluble factors (including proteins) across the membrane, without allowing the tumour cells to leave the fibre, or host cells to penetrate. The fibres are implanted both i.p. (intraperitoneal) and s.c. (subcutaneous), and the animals are exposed to the drug continuously for 4 days. After the final dosing, the fibres are collected from the animal and the cells removed from the fibres and subjected to the MTT assay to determine viability, and hence efficacy of the compound (Hollingshead *et al.*, 1995). The main advantage of this technique is that several fibres can be implanted per animal, allowing assessment of the activity of the compound on many more tumour cell lines in a much shorter time period than a xenograft study would (see section 3.2.2.2). Used in conjunction with the cell-line screen, this further facilitates the decision as to what tumours the compound should be aimed at in later stages of development.

3.2.2.2 Tumour xenograft studies

Human tumour xenografts are used in order to better assess the tumour-specific cytotoxic effects of a potential anticancer agent. This involves the implantation of a human-derived tumour (derived from a human tumour cell line) onto, most commonly, the congenitally athymic nude mouse (immunocompromised, and thus less likely to react to the implanted foreign material). The xenograft has advantages over the assays used earlier in the drug discovery process in that it provides an intact tumour model, which means that it is closer to how the tumour would appear in humans and may express similar levels of enzyme activity or detoxifying molecules as would be observed *in situ*. However, this technique is very time-consuming compared to the methods described earlier, as it may take up to 8 weeks in total to perform the experiment for slower-growing tumours and is expensive in numbers of mice, as often

50-100% more than the required number of mice must be used in order to compensate for mice in which the tumours do not take (Plowman *et al.*, 1997). Hence the wisdom in using the faster and cheaper methods mentioned earlier to both screen out inactive compounds and to select for which tumour type the potential drug should be tested in when at the xenograft stage, should increase the chances of finding a positive response and possible tumour selectivity in a shorter time.

3.2.3 Preclinical toxicology

Having reached this point, there is sufficient confidence in the drug for it to be considered for use in man; therefore, appropriate toxicology studies must be carried out in animals to determine a safe starting dose before the drug can progress to the clinic. It has been established that preclinical studies in rodent species, specifically the mouse, are sufficient for prediction of toxicity in humans, a conclusion based on extensive data comparing toxicity in animals to that in humans (Newell *et al.*, 1999). Thus toxicity studies are performed in the mouse to establish a safe starting dose, typically defined as one tenth of the mouse MTD, and this is confirmed by testing in a second species, often rat or dog before the drug advances to phase I clinical trials (Toppmeyer, 1997).

3.3 Clinical evaluation

3.3.1 Phase I trials

Once a candidate compound has shown favourable characteristics in non-human models, and appropriate parameters for the drug have been established, such as the tumour type for which the drug is to be indicated and safe starting dose, the drug can progress to phase I trials.

Due to the nature of anticancer drugs, their inherent toxicity, narrow therapeutic window and often non-linear pharmacokinetics, it is considered unethical for an anticancer compound to be tested in a normal healthy volunteer, as therapy could prove life-threatening or harmful at efficacious doses. Thus, the first line of testing of anticancer drugs is generally in cancer patients for whom all other therapeutic options have been exhausted. However, recent trends moving away from conventional cytotoxic agents to biological agents that manipulate the host response or perturb cell signalling mechanisms is altering this approach.

The principle aim of phase I trials is to establish the maximum tolerated dose (MTD), which is defined as the highest dose that can be safely administered to a patient. With conventional cytotoxic agents, this is typically achieved by beginning dosing at one-tenth of the murine equivalent LD_{10}, and incrementing dose levels using a modified Fibonacci dose escalation scheme (dose levels incremented as sequential 67%, 50%, 40%, and 33% increases) until an MTD is seen (Collins *et al.*, 1986). Usually 2-3 patients are used per dose escalation (Simon *et al.*, 1997). If none of the patients experiences dose limiting toxicity (DLT), dose is escalated to the next level. If one of the three patients experiences a DLT, three additional patients are treated at the same dose. If two or more out of the total of six patients this dose level experience DLTs, then the MTD is considered to have been exceeded and additional patients are treated at the previous dose level to confirm the safety of that dose for future studies.

With newer biological agents the compound is not designed as a cytotoxic agent and often does not need to be dosed at the MTD to achieve optimum efficacy; therefore

conventional trial design is inappropriate. These trials have evolved to identify an optimum biological dose (or pharmacodynamic endpoint), to combine maximum efficacy with minimum adverse effects (Blackledge & Averbuch, 2004).

Phase I studies enable the setting of a safe dose level for further studies in phase II. Other purposes of the phase I trial are to characterise the toxicity profile of the drug (expected and unexpected toxicities), and to examine the clinical pharmacology of the compound. While phase I trials are not designed to characterise the efficacy of compounds, any antitumour effect will be noted. The sample size for this phase of investigation is often small, and several sources quote differing sample sizes, however a range of 15 -60 patients depending on compound and study design appears typical (Lewis & Weiner, 2002; Voorhees *et al.*, 2003; Blackledge & Averbuch, 2004; Harris, 2004).

3.3.2 Phase II trials

The purpose of a phase II trial is to determine if a compound is having a therapeutic effect against a tumour or cancer to a degree that is worthy of further study. This type of study usually includes patients that have been selected based upon the type of cancer they are suffering, so that it is matched to the cancer that the drug is considered to be efficacious against, and rely on tumour response to the therapy as the primary measure of effectiveness. This trial is generally conducted on a larger scale than phase I trials, and the number of patients needed in the trial is calculated beforehand and decided upon the basis necessary to achieve statistical significance (Teicher, 1997; Lewis & Weiner, 2002).

3.3.3 Phase III trials

Phase III trials are aimed at proving the value of a novel drug over an existing therapy. At this stage the activity of the drug has been proven, but for the drug to become routinely used in the clinic there is a requirement for evidence of an advantage of the novel therapy, due to either a reduced side-effect profile or an increase in potency against a tumour (Teicher, 1997; Lewis & Weiner, 2002).

4 New targets in cancer research

Current chemotherapeutic approaches to cancer are nowhere near ideal, as treatment often results in an incomplete cure, and toxicity of anticancer drugs is an accepted norm. Chemotherapy has improved dramatically since its inception, with improvements in survival being the most notable landmark by which to judge this advance (McVie, 1999). The difficulty in finding an effective treatment arises mainly from the incredibly difficult task of designing or finding a treatment that is able to distinguish normal cells from cancerous cells. Therefore, there is still tremendous scope for development of cancer therapies to enable the selective elimination of cancerous cells, with minimal or no tissue toxicity.

Strategies for the development of new therapies have involved the synthesis of analogues in the hope of finding a better drug based on the efficacy of an existing lead compound or agent, i.e. improving the cytotoxicity or maintaining the same levels of cytotoxicity and reducing toxicity. However, this "handle turning" technique has not been particularly successful, producing only a relative few useful agents (Verweij & de Jonge, 2000).

In an attempt to produce drugs more intelligently, research has evolved to look at the processes involved in cellular division and differentiation to see what makes a cancer cell different from a normal cell. Efforts are underway to characterise these differences and to exploit these anomalies in order to use the machinery of cancer against itself.

4.1 p53

p53 is a tumour suppressor gene found to be mutated in over 50% of human cancers, and as such is one of the genes most commonly altered in tumours (Hollstein *et al.*, 1999; Soussi *et al.*, 2000). The central role of p53, the product of which is a nuclear transcription factor, is to act in response to DNA damage and to induce cell cycle arrest or apoptosis. This helps to ensure the integrity of the genome in that if a cell is able to repair its DNA, it can do so before undergoing division; if not, it is eliminated. The role of p53 is thus to act to prevent the division of cells with an altered genome. Cells with damaged or mutated forms of p53 do not have this mechanism; this can result in increased genetic instability and increased chance of damaged cells progressing to a cancerous state. Furthermore, mutated p53 is associated with increased resistance to chemotherapy believed to arise from interference in the normal apoptotic pathway by mutated p53. Such mutants are thought to confer "gain of function" characteristics upon tumour cells, bestowing additional properties upon the cell over and above simply the loss of wild-type p53 function and potentially affecting the sensitivity of the cell to anticancer agents (Wattel *et al.*, 1994; Rusch *et al.*, 1995; Gasco & Crook, 2003; Soussi, 2003).

The major cellular role of p53 and its involvement in the occurrence of such a large number of cancers [estimated to be involved in over 35% of world-wide new cancer cases (Harris, 1996)] have presented it as an attractive target for the design of new therapies to specifically target p53-mutated/deficient tumours.

One of the strategies used to attempt to target tumours lacking p53 is to replace the damaged copy of the p53 gene with a working copy, through the use of gene therapy.

Gene therapy as a technique itself poses significant problems, as currently there is no regular use of gene therapy due to a combination of ethical and practical problems. However, several attempts have been made using both viral and non-viral means of delivery to insert working copies of p53 into tumour cells.

Phase I clinical trials have indicated that the use of a viral vector for the p53 gene has potential for success. Both retroviral and adenoviral methods have been shown to work, although adenoviral vectors are preferred, as this confers only a transient expression of the transfected p53 gene as the viral DNA is not integrated into the host genome (Roth *et al.*, 1996; Clayman *et al.*, 1999). Transient expression should be all that is necessary, as damaged cells should undergo apoptosis almost immediately upon the expression of p53, and this avoids ethical issues arising such as the germline transmission of transfected DNA. It has also been observed that this affords a higher level of efficiency of transfection and resultant higher levels of expression over retroviral vectors. However, it has become apparent from these experiments that transfection with p53 is not enough to completely abolish an established tumour. Transfection with p53 appears to sensitise cells to other anticancer agents, such as ionising radiation and chemotherapeutic agents. However, transfection of p53 via a viral vector has drawbacks, as immunological complications arise and there is a lack of specificity for tumour cells.

Non-viral transfer of an undamaged copy of the p53 gene has also been considered, and presents fewer problems than a viral delivery system. Cationic liposomes have been used to this end (Chene, 2001). The cationic lipids bind to the anionic DNA, and can then be injected. However, this method is currently relatively inefficient as interactions

with plasma constituents and the immune system can have a drastic effect on the amount of DNA delivered to the tumour site. This is coupled with a lack of tumour specificity, and as a transfection technique cationic liposomes produce poor transfection efficiencies.

Other techniques are also being developed in pursuit of p53 as an antitumour target. There is interest in using p53 deficiency as a target at which to aim adenoviruses; in this case, p53 acts by binding to a section of the adenovirus and to cause its inactivation. Thus cells are protected from the cellularly lethal effects of the virus by p53, but cells possessing either no p53 or a mutated form are not (Heise *et al.*, 1997). There is also interest in the fixing or reactivation of aberrant p53. It is thought that it may be possible in some cases to alter the mutated p53, shifting it into an active or more stable form, thus allowing stimulation of apoptosis in tumour cells (Chene, 2001).

4.2 Angiogenesis

It is well established that the formation of new blood vessels is critical for tumour progression and metastasis. Therefore, inhibition of this blood vessel formation (angiogenesis) as a method of disrupting tumour growth presents an attractive target. There have been many targets identified to this end. Among these are the growth factors (foremost of these is VEGF or vascular endothelial growth factor), the MMPs (matrix metalloproteinases), and the integrins.

VEGF is instrumental in the induction of angiogenesis. It is currently understood that the process of angiogenesis in tumours is primarily mediated by VEGF, driving endothelial cell proliferation, migration and tubule formation. In association with

VEGF, Ang-1 (angioprotein-1) causes vessel maturation and stabilisation *in vivo*, although this can be destabilised by Ang-2 and another cycle of angiogenesis can proceed if VEGF is present. In the absence of VEGF, the vessels will degenerate (Matter, 2001). In addition to this, although separate from the regulatory systems involved in controlling VEGF levels, the matrix metalloproteinases (MMPs) have been shown to exert considerable influence over angiogenesis. MMPs are involved in the tissue remodelling that occurs during angiogenesis, and are therefore also implicated in modulating tumour invasiveness and metastatic potential of tumours, as tissue remodelling is vital for vessel formation and tumour spread.

There are surface receptors implicated in the processes of angiogenesis, as well as metastatic progression: these are the integrins. This association arises from the observation of an anti-angiogenic effect of αv-integrin antagonists. Further observations of factors interacting with integrins and resulting in anti-angiogenic effects, have supported their role in angiogenesis (e.g. endostatin, tumstatin and thrombospondin) (Eliceiri & Cheresh, 2001).

These numerous targets have led to a wealth of research into agents to exploit angiogenesis as an anticancer key. VEGF tyrosine kinase receptor inhibitors have proved popular, as the target has been validated by use of anti-VEGF antibodies (Kim *et al.*, 1993). This area has now resulted in drugs in clinical trials: SU5416 (semaxanib), a VEGF-R2 inhibitor, reached phase III trials but has recently been found ineffective in colorectal cancer (Peapack, 2004), and PTK787/ZK222584, a general VEGF receptor kinase inhibitor, is in phase I trials.

MMPs are a large family of zinc-binding proteins, of which there are several subtypes (MMPs 1, 2, 3, 7, 8, 9, 11, 12 & 13) expressing differing substrate specificities. MMPs come into the classifications of collegenases, stromelysins, elastases and membrane type MMPs (Buolamwini, 1999). MMP inhibitors targeted at these enzymes have been reasonably successful as a therapeutic target, resulting in several potential drugs. One such drug is marimastat, a broad-spectrum MMP inhibitor with activity against many of the major enzymatic subtypes. A competitive, reversible substrate inhibitor, marimastat has reached phase III clinical trials as a cytostatic agent. There are several other compounds in various stages of development for inhibition of MMPs.

The integrins are transmembrane proteins that function as receptors for matrix proteins such as fibronectin, collagen, laminin and vitronectin. This has led to attempts to exploit this role in angiogenesis for cancer chemotherapy, and has prompted the use of synthetic peptides to antagonise integrin interactions, providing a degree of success (El-Hariry & Pignatelli, 1997). It is thought that this area has special value in the prevention of metastatic disease, although present knowledge of the interactions and functions of the cell adhesion molecules is not sufficient to allow a rational approach to therapy design.

The epidermal growth factor receptor (EGFR) and its downstream signalling pathway has become the target of much interest over recent years (Woodburn, 1999). EGFR mediated signalling has been linked to the production of increased amounts of angiogenic factors such as VEGF. Several novel strategies have been attempted to modulate this pathway. Small molecule inhibitors have been developed for the inhibition of EGFR tyrosine kinase. Gefitinib has recently received approval for

clinical use, and is the first EGFR directed agent to achieve this status; erlotinib is following closely behind and is in follow-up stage of phase III trials (Blackledge & Averbuch, 2004). Monoclonal antibodies have also become successful and reached the clinic as anticancer therapies. The chimeric monoclonal antibody Cetuximab, is directed against EGFR and has been approved for use against metastatic colorectal cancer (Harris, 2004). Similarly, Trastuzumab is a monoclonal antibody directed against another member of the ErbB family, Her2/neu, and has shown positive clinical benefit in breast cancer and is approved for use in the clinic (Harris, 2004).

4.3 Ras farnesyltransferase

There has been much effort into the development of *Ras*-targeted drugs for anticancer therapy, stimulated by the fact that *Ras* mutations occur in up to 30% of human cancers. Oncogenic mutation of the *Ras* gene, can lead to constitutive activation of the protein, resulting in continuous activation of its downstream effectors irrespective of growth signals, and mitotic activity where none is required. Activated *Ras* triggers the mitogen-activated protein kinase (MAPK) cascade, ultimately resulting in the activation of extracellular-signal-regulated kinase (ERK), which enters the nucleus and stimulates mitosis by phosphorylating and activating appropriate transcription factors. Ras farnesyltransferase (FTase), is instrumental in the transfer of a farnesyl moiety to the newly transcribed Ras protein (Buolamwini, 1999). The farnesyl group is needed to anchor Ras to the cell membrane and allow it to perform its signalling function. Thus, the inhibition of FTase would potentially provide a target that may have anticancer properties via inactivation (or lack of activation) of *Ras*. Thus far, FTase inhibitors have proven effective in animal models, and have progressed to clinical trials (Lobell & Kohl, 1998).

4.4 Telomerase

At the end of chromosomes are caps of repeating DNA base sequences called telomeres. In humans, this repeating sequence is a 6 base-pair (bp) sequence 5'-(TTAGGG), typically 5-15 kb pairs long. Telomeres are often referred to as a mitotic clock, as with each cell division the length of the telomeres are shortened by some 50-200 bp as a result of a mitotic DNA synthesis aberration, termed the 'end replication problem', and when telomeres reach a critical length the cell undergoes growth arrest (cellular senescence). This confers a limited number of replications on any given cell. When a cell reaches senescence, it has effectively entered a stable state where further cell division does not occur; however, senescence does not result in cell death. Should a cell continue to divide beyond senescence, the telomere will reach a critical length and undergo crisis, a condition in which the telomeres are so short that end-to-end fusion and chromosome breakage and fusion can occur, leading to chromosomal abnormalities and apoptosis (White *et al.*, 2001). In occasional cases, the cell can escape senescence or crisis (and therefore death), by regenerating its telomere, and this phenomenon has been associated with the enzyme telomerase (Wright & Shay, 1992; Kim *et al.*, 1994).

Telomerase is a ribonucleoprotein consisting of two main components, hTR (the human RNA component, the template for the 6 base pair repeat) and the hTERT (the human telomerase reverse transcriptase) catalytic subunit. The limiting factor for telomerase activity in normal cells is the expression of hTERT, as hTR is constitutively expressed in all human somatic cells, whereas hTERT is not expressed in normal somatic tissues (Feng *et al.*, 1995). Telomerase has been found to be expressed in around 85% of human tumours, and thus it is believed that for a cancerous cell to continue proliferating

beyond its normal life span, telomerase must be reactivated to maintain the telomere and prevent senescence or crisis occurring (White *et al.*, 2001). Hence inhibition of telomerase presents an attractive target for potential anticancer therapy as a mechanism of removing the immortality of the cancerous cells, thus allowing them to divide and senesce or apoptose. Telomerase inhibitors have shown remarkable activity in preclinical tests, but have yet to progress to clinical trial.

4.5 Proteasome

The proteasome is a proteinase complex crucial to cell cycle regulation and apoptosis and is responsible for the degradation of most intracellular proteins. It was discovered that the caspases, part of the protease family, are involved in the apoptotic pathway and garnered interest in the potential role of the proteasome in this process. Inhibition of the proteasome has been shown to induce apoptosis of cancer cells and have *in vivo* efficacy against tumours (Fujita *et al.*, 1996; Orlowski *et al.*, 1998). Bortezomib, a proteasome inhibitor, has demonstrated a broad spectrum of antitumour activity in the NCI tumour cell line screen and antitumour activity in several murine tumour xenograft models. It is thought that proteasome inhibitors act in a synergistic manner with DNA damaging agents by preventing transcription of genes involved in DNA repair by inhibiting translocation of nuclear factor κB, and also by interfering with P-glycoprotein maturation thus inhibiting one of the best characterised mechanisms of chemotherapy resistance (Loo & Clarke, 1999; Orlowski & Baldwin, 2002; Mitsiades *et al.*, 2003). Bortezomib has been approved for use in the clinic as part of combination therapy, and is the only such proteasome inhibitor thus far to have entered clinical trials.

4.6 BCR-ABL

BCR-ABL is a tyrosine kinase implicated in chronic myeloid leukaemia (CML). In CML, there is a genetic abnormality caused by reciprocal translocation of chromosomes 9 and 22, and this results in the expression of the constitutively active tyrosine kinase, BCR-ABL. It has been shown that expression of this kinase alone is sufficient to cause CML, and as such it presents an attractive and selective target for anticancer agents(Druker *et al.*, 2001). The BCR-ABL inhibitor, Imatinib (STI571), acts by competitive inhibition of the ATP-binding site of BCR-ABL, resulting in inhibition of the tyrosine phosphorylation of proteins involved in the BCR-ABL mediated signal transduction pathway. Imatinib is approved for use in the clinic, and is the first of the molecular targeting drugs to directly act on a protein known to be implicated carcinogenesis.

5 DNA repair mechanisms and cancer

Many of the successful chemotherapeutic agents, such as the nitrogen mustards and platinum-containing compounds, target DNA in order to produce cytotoxic effects. This often results in the alkylation of DNA and may subsequently produce strand breaks and possibly inter-strand cross-links. Damage to DNA by these agents is seldom limited to cancerous cells, and the often seen side-effects of chemotherapy arise as a direct result of damage to normal cells (Ferber, 1999). As early as the 1960's, reports appeared examining the effects of chemotherapeutic agents on bone marrow and peripheral blood cells, touting the gross chromosomal damage inflicted on these normal cells by therapeutic doses of chemotherapeutic agents (Bell *et al.*, 1966; Whang-Peng *et al.*, 1969). From a current perspective, it seems obvious that this damage arose from the inability of cellular DNA repair mechanisms to cope with the damage inflicted by the chemotherapy used. Knowledge of the apoptotic events that occur in a normal cell when DNA becomes damaged beyond repair allows explanation of why the induced chromosomal damage did not itself result in secondary tumours.

Nuclear DNA is constantly under attack from environmental stresses, and DNA repair mechanisms have evolved to combat these cellular insults. These mechanisms consist of base-excision repair, nucleotide-excision repair, recombinational repair and mismatch repair. Repair mechanisms most important in relation to chemotherapy are excision repair and recombinational repair, as these processes are responsible for repair of single strand breaks and alkylation events, and double-strand breaks and inter-strand cross-links, respectively. These types of damage are often induced by chemotherapeutic agents. Among other mechanisms resistance to chemotherapy has been linked with an increase in the activity of cellular DNA repair mechanisms possibly acting to prevent

sufficient damage to cause cell death (Masuda *et al.*, 1988; Wang *et al.*, 2001). It is suggested that certain pyrrolobenzodiazepine (PBD) compounds may bind to DNA in a manner that allows circumvention of the DNA repair pathways that act to provide resistance to conventional anticancer drugs.

5.1 Base excision repair

The base excision repair (BER) pathway is a critical repair mechanism for dealing with single-strand breaks, and is involved in the removal of chemically altered bases. The repair pathway consists of four key stages at which individual enzymes performs tasks imperative to the complete pathway (Figure 5.1).

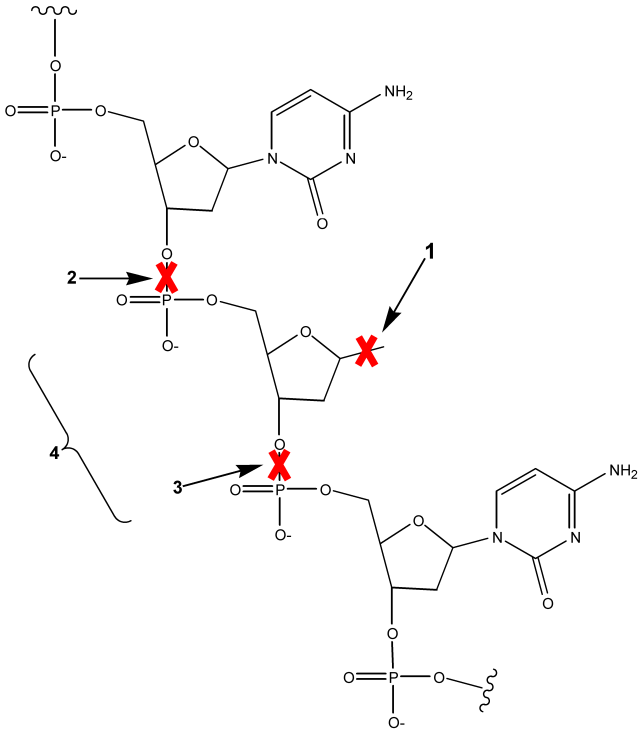

Figure 5.1 DNA base excision repair pathway. 1) Glycosylase enzyme removes damaged base, 2) endonuclease cleaves sugar phosphate backbone 5' to the AP site, 3) DNA polymerase removes sugar phosphate and fills resulting gap, 4) DNA ligase seals remaining nick and repair is complete. Red X markers denote bonds broken in the processes. Adapted from (Parikh *et al.*, 1997).

5.1.1 DNA glycosylases and damage detection

The DNA glycosylases are key enzymes involved in the detection and instigation of BER. These enzymes are responsible for recognising distinct forms of DNA damage, and removing the damaged and/or inappropriate bases by hydrolysis of the glycosyl bond (Krokan *et al.*, 1997). This results in the generation of a non-coding apurinic/apyrimidinic (AP) sites. There are a number of different DNA glycosylases, each thought to be responsible for the recognition of different types of DNA damage (Mol *et al.*, 1999). DNA glycosylases fall into two categories: the pure glycosylases and the AP lyase/glycosylases. The pure glycosylases leave an abasic site in the DNA strand whereas the AP lyase/glycosylases leave an AP site with a 3' nick.

It is currently believed that there are distinct enzymes involved in the recognition of lesions that are repaired via the BER pathway. A brief description follows for the enzymes thought to be involved in repair of these lesions and their proposed mechanism of action:

- Deamination:
    - Uracil-DNA glycosylase (UDG). Cleaves the N-C1' glycosyl bond between a target uracil and the deoxyribose sugar. Acts to remove uracil from single-stranded DNA and from U-G or U-A pairings in double-stranded DNA, but will not act on RNA (Slupphaug *et al.*, 1995). Thought to act by flipping out target base from DNA base stack.
    - G-T/U mismatch-specific DNA glycosylase (MUG). Cellular cytosine is often methylated at its 5' position, and this can result in deamination to form 5-methyluracil or thymine and result in G-T mismatches in DNA. MUG cleaves thymine or uracil mismatches with G, C and T, but will not act on A-

T/U pairs or single strand DNA (Neddermann & Jiricny, 1993). This enzyme is also thought to act by flipping out the target base.

- Oxidation:
    - MutY mismatched-adenine glycosylase. MutY specifically acts to remove adenine mispaired with 8-oxoguanine, guanine or cytosine (Gogos *et al.*, 1996; Manuel *et al.*, 1996). It is 1000-fold more active towards an 8-oxoguanine mismatch than for A-C mispairs (Bulychev *et al.*, 1996). This enzyme belongs to the Helix-hairpin-Helix (HhH) superfamily of DNA repair enzymes. This enzyme is also thought to act by flipping out the target base.
    - Endonuclease III oxidised-pyrimidine glycosylase/lyase. Endo III has broad specificity, and acts to cleave oxidised pyrimidine bases. It also acts as an AP lyase to nick DNA at abasic sites (Katcher & Wallace, 1983; Doetsch & Cunningham, 1990). This enzyme also belongs to the HhH superfamily and is believed to act by flipping the damaged base out of the DNA base stack.
- Alkylation:
    - AlkA 3-methyladenine DNA glycosylase. AlkA has broad range of substrate activity, recognising and excising not only 3-methyladenine, but also alkylated purines and pyrimidines, oxidative lesions, and even undamaged normal bases (Berdal *et al.*, 1998). This enzyme also belongs to the HhH superfamily and is believed to act by flipping the damaged base out of the DNA base stack.

5.1.2 AP endonucleases and AP site recognition

The second stage of the BER cascade involves AP endonuclease enzymes. This enzyme is responsible for recognition of AP sites. After generation of an AP site by the glycosylase enzyme, AP endonuclease recognises the non-coding site and cleaves the phosphodiester backbone of DNA 5' to the AP site. This acts to prime the section of DNA for repair by leaving a 3'-hydroxyl group (Parikh *et al.*, 1997; Wilson & Barsky, 2001). The predominant AP endonuclease present in mammalian cells is human AP endonuclease (HAP1, also called APE1 or APEX), and is thought to comprise ~95% of total cellular AP site-cleaving activity (Chen *et al.*, 1991).

5.1.3 DNA polymerase and damage repair

The DNA polymerase enzyme, DNA polymerase β, acts in BER to bind to the nicked DNA produced by endonuclease activity and cleaves out the abasic site (Matsumoto & Kim, 1995). The enzyme then proceeds to bind dNTP, move the dNTP into the gap site and subsequently catalyse nucleotidyl transfer (Parikh *et al.*, 1997).

5.1.4 DNA ligase finish

DNA ligase joins up the remaining nick left after the activity of DNA polymerase β, completing the repair. This is done by the catalysed annealing of the 5' phosphate-terminated donor strand to the 3' hydroxyl terminated acceptor. DNA ligases I and III have been implicated in mammalian BER (Parikh *et al.*, 1997).

5.2 Nucleotide excision repair

Nucleotide excision repair (NER) is principally responsible for the repair of DNA adducts that result in large, helix-distorting lesions. Dipyrimidine lesions such as those

resulting from exposure to UV light are an example of this type of damage (Friedberg *et al.*, 1995; Batty & Wood, 2000).

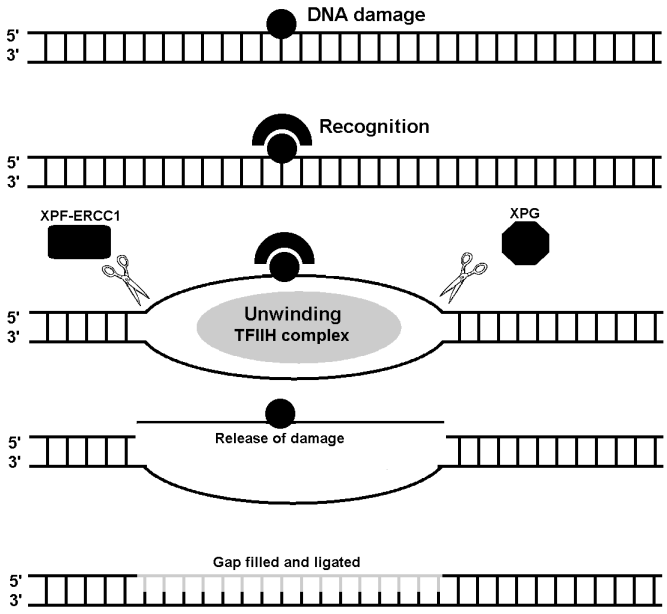

Figure 5.2 Nucleotide excision repair. Damage is recognised by XPC-hHR23B and/or XPA-RPA. DNA is unwound by the TFIIH complex using helicases XPB and XPD; the structure created is a target for the endonucelases XPG and XPF-ERCC1 which cleave DNA and release the damaged section of DNA. The gap remaining is subsequently filled and ligated.

NER is a multi-step process (Figure 5.1) thought to involve in the region of 20 proteins in the repair pathway (Wood, 1997). The initial step is the recognition of DNA damage. This is currently believed to involve the XPC-hHR23B and XPA-RPA proteins, although the order in which the proteins bind is unclear (Batty & Wood, 2000). The TFIIH transcription factor is then enrolled, which contains the helicases XPB and XPD which are vital in the unwinding of DNA in the region of the lesion (Evans *et al.*, 1997). The protein complex clustered around the lesion then provides a landmark for the nucleolytic incisions of XPG (3' of the lesion) and XPF-ERCC1 (5' of the lesion), which

leads to the release of a nucleotide containing the lesion, of approximately 30 nucleotides in length (Huang *et al.*, 1992). This is followed by DNA synthesis across the gap left by oligonucleotide excision, thought to be by DNA polymerase δ / ε (Wood, 1997). The double helix is finally restored by ligation, thought to be performed by DNA ligase I (Barnes *et al.*, 1992).

5.3 Double-strand break repair

Events that cause double-strand breaks (DSB) in DNA are especially cytotoxic. DSBs if left unrepaired are generally lethal to cells, and if repaired erroneously can result in chromosomal abnormalities such as translocation and subsequent alterations in gene function. Cells have evolved two key mechanisms for the repair of DSBs: homologous recombination (HR) and non-homologous end-joining (NHEJ).

HR repairs DNA using an undamaged sister chromatid as a repair template, this removes damage in an error free process. The Rad52 epistasis group of proteins are implicated in the HR-mediated repair of DSBs, although it is unclear in the literature as to which enzyme mediates each part of the reparation process. HR proceeds (Kanaar *et al.*, 1998; Braithwaite *et al.*, 1999; Fojo, 2001; Martin, 2001; McHugh *et al.*, 2001; Pierce *et al.*, 2001) by:

1. Recognition of the damaged DNA ends.
2. Nucleolytic processing of the DNA ends to give a single-stranded 3' overhang at each broken end.
3. Searching for the homologous template on the sister chromatid.
4. Formation of a complex between the 3' end on the broken DNA and the complementary sequence on the homologous strand.

5. Extension of the 3' ends by synthesis of DNA complementary to the template.
6. Dissociation of the recombination complex and ligation of repaired DNA.

NHEJ is a more error-prone mechanism of DSB repair as it relies on pasting the broken ends of DNA together, and there is no homologous template required to ensure sequence fidelity. This somewhat simplifies the process of DSB repair as there are less proteins involved. The human Ku (derived from the first two letters of the family name of a Japanese patient in which it was recognised) protein is a heterodimeric complex composed of two protein subunits Ku70 and Ku80 (also termed Ku86). The binding of Ku to the broken ends of DSBs is believed to initiate the process of NHEJ. Ku is thought to stabilise the ends of DNA in order to allow rejoining by DNA ligase IV in association with XRCC4. NHEJ appears to be the main form of DSB repair in mammalian cells (Kanaar *et al.*, 1998; Braithwaite *et al.*, 1999; Fojo, 2001; Martin, 2001; McHugh *et al.*, 2001; Pierce *et al.*, 2001).

5.4 Repair of interstrand crosslinks

Current understanding of the mammalian mechanisms of DNA interstrand crosslink (ICL) repair is poorly understood. Repair of ICLs have been characterised in bacterial cells in more detail and suggest that there is interplay between NER and HR. This model suggests an initial incision either side of the lesion on one strand of the DNA duplex releasing an oligonucleotide (still linked via the crosslink to the complimentary strand) as with NER, considered an ‘unhooking’ of the crosslink. This is followed by an HR event, replacing the missing oligonucleotide and repairing that strand of the DNA duplex. To complete the repair, a second NER process takes place to excise the remaining lesion and is followed by completion of the NER process to fill in the

remaining gap. It was found that although there was potential for 'unhooking' of both strands simultaneously, and subsequent DSB formation, this was not observed to occur.

Studies in yeast showed a different story for eukaryotic cells: DSBs were seen to form in yeast cells treated with DNA crosslinking agents. However, the proposed double-NER reaction was not found to account for all DSBs formed. It was observed that there was a high proportion of DSBs formed in rapidly-dividing cells, whereas virtually no DSB formation was seen in non-dividing cells (McHugh *et al.*, 2000). This led to the proposal that the formation of DSBs was as a result of DNA replication forks running into an ICL, which is likely an impassable block. The following collapse of the replication fork is believed to result in the formation of a DSB.

In mammals, the mechanisms by which ICLs are repaired are somewhat less well understood. It has been shown that a combined NER + HR mechanism, as proposed for bacteria (Cole, 1973), is not likely to be a major contributor to repair of ICLs, as mutation studies aimed to remove key proteins involved in the NER process did not cause the increase in sensitivity to crosslinking agents that would be expected if this was the main mechanism of repair. It has been shown however, that mutation of XPF (also ERCC-4) or ERCC-1 (both required for nicking DNA 5' of the lesion) results in extreme sensitivity to crosslinking agents versus other proteins in the NER pathway (Damia *et al.*, 1996; De Silva *et al.*, 2000). Further studies have shown a role for Xrcc3, a protein linked to the HR repair pathway, in the repair of ICLs via its apparent influence on Rad51 foci formation (Wang *et al.*, 2001).

Therefore current understanding of ICL repair in mammals and humans appears to indicate a role for ERCC1, XPF and Xrcc3 and Rad51 foci in the repair pathway. The current diversity of opinion would perhaps also indicate the possibility of several differing repair mechanisms, as differing reports indicate implication of HR, NER and NHEJ in ICL repair, and indeed several reports appear to implicate a combination of individual elements of each repair pathway.

5.5 DNA repair mechanisms and cancer chemotherapy

Many of the more effective chemotherapeutic treatments for cancers centre on actions on DNA, directly or indirectly. These include the alkylating or platinating agents (nitrogen mustards, cisplatin, carboplatin), inhibitors of DNA topsimerases I (topotecan, camptothecin) and II (mitoxantrone) and antimetabolites (methotrexate, capecitabine, fluorouracil, mercaptopurine). Despite the proven efficacy of these DNA active drugs, DNA as a target has in many circles now lost favour, largely as a result of the perceived lack of specificity afforded by this mechanism of cytotoxicity. Furthermore cancers can often become resistant to these DNA-directed therapies. Obvious culprits for the noted resistance to DNA directed drugs are DNA-damage repair mechanisms. It has been noted in several tumour lines that resistance to drugs acting on DNA is associated with the upregulation or overexpression of proteins linked to DNA repair. This has led to the development of therapies designed to circumvent these repair mechanisms such as drug-based inactivation of aspects of DNA repair mechanisms (Middleton & Margison, 2003), and it has been suggested that modulation of DNA repair proteins may be achieved using gene therapy strategies (Wang *et al.*, 2001). Other approaches have centred on attempting to increase the cytotoxicity and therefore yield of ICLs induced by drugs in order to overwhelm DNA repair pathways. However, it is likely that this

increased cytotoxicity to tumour cells would have implications on side-effects, and thus prodrug approaches have also become popular in attempting to deliver enhanced cytotoxicity compounds to the tumour. Another approach is to design drugs that have minimal effect on the structure of DNA and thus evade the repair mechanisms employed by the cell. The pyrrolobenzodiazepine class of agents has been engineered to behave in this fashion through DNA minor groove-mediated events.

6 The pyrrolobenzodiazepines

6.1 Background to the compound family

The PBDs or pyrrolobenzodiazepines (also termed pyrrolo[2,1-*c*][1,4]benzodiazepines) are a group of antitumour antibiotics first discovered in 1963. Prior to their discovery, many [1,4]benzodiazepines had been developed as potential antianxiety drugs, but it had not been thought that fusion of a pyrrole ring to this system would evoke antitumour activity. There has been a high level of interest in the biological activity of this group of compounds, but as yet there have been no PBDs accepted as therapeutic agents, despite compounds progressing to clinical trials, although some anticancer activity for this class of compound has been documented.

The first of the PBD compounds to be studied was anthramycin. It was discovered in 1963 that the addition of ammonium sulfate to a fermentation broth derived from *Streptomyces refuineus* resulted in a precipitate that showed activity against a spectrum of Gram-positive bacteria. It was also shown to be active against sarcoma 180 in mice and carcinoma 755 in rats. This active precipitate was denoted refuin, and was assumed at that point to be a protein. Further work resulted in the development of an extraction and purification method to isolate the active molecules in this broth. It was discovered that the active element was not a protein, but the heterocyclic compound anthramycin, so named due to the presence of anthranilic acid as part of its structure. Comparisons between refuin and anthramycin indicated that refuin contained only 0.5% anthramycin. Pure anthramycin is highly active against Gram-positive bacteria and active to a lesser extent against Gram-negative bacteria and fungi.

Further PBDs were discovered over later years with the advent of sibiromycin (derived from extracts from *Streptosporangium sibiricum* in 1969), tomaymycin (derived from *Streptomyces achromogenes* in 1972), and neothramycin (derived from *Streptomyces* No. MC916-C4 in 1976). All were shown to have activity against bacteria, and some degree of antitumour activity. There are now 12 known naturally occurring PBDs, in addition to numerous synthetic analogues (Thurston, 1999).

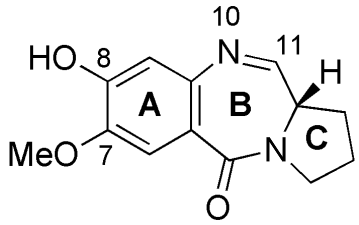

Figure 6.1 The PBD monomer DC-81 showing the numbering system and ring lettering of the PBD nucleus.

The PBD molecule consists of a fused tricyclic system (see structure 2 in Figure 6.1), namely an aromatic A-ring, a pyrrolidine C-ring, and a 1,4-diazepin-5-one B-ring bearing a N10-C11 imine carbinolamine moiety (Baraldi *et al.*, 1999). All naturally-occurring forms of this compound possess the (*S*) configuration at C11a, which provides the molecules with a right-handed twist when viewed from the C-ring towards the A-ring. This provides the isohelicity with the DNA minor groove needed for an effective interaction with the nucleic acid, and hence biological efficacy.

6.2 Mechanism of action

Pyrrolobenzodiazepines elicit their antitumour effects through strong covalent binding with DNA, the result of this being interference with DNA and RNA synthesis. This

interference is a function of their ability to form adducts in the minor groove of B-form DNA. The mechanism involved in the binding of a PBD molecule to DNA is believed to be a two-stage process with the initial interaction being non-covalent. The shape of the drug molecule allows a snug fit into the minor groove, followed by the formation of a covalent bond with the C11 of the drug and the exocyclic 2-amino group of a guanine residue (Remers, 1988; Thurston, 1993).

Anthramycin, the first discovered PBD, has had its mode of DNA interaction well studied. Shown to bind to DNA, and to result in the formation of a strongly bound drug-DNA complex (Kohn *et al.*, 1974), anthramycin displays a marked preference for double-stranded DNA over single-strand DNA, but shows no reactivity with RNA (Kohn & Spears, 1970). Interestingly, the time taken to reach saturation binding of DNA with anthramycin has been shown to be significantly longer than that of typical intercalating drugs such as actinomycin, taking minutes to hours rather than the milliseconds to seconds of the intercalating drugs (Konishi *et al.*, 1984). Initially the anthramycin-DNA adduct was shown to be covalent in nature by the use of UV spectroscopy, thermal denaturation, dialysis, gel filtration and alcohol precipitation techniques (Kohn & Spears, 1970; Kohn *et al.*, 1974; Kohn, 1975). Further investigation using enzymatic (S1-nuclease) and chemical (BND-cellulose chromatography) probes indicated that the bonding of the drug causes little or no distortion of local DNA structure (Petrusek *et al.*, 1981). However, these studies were not able to identify the finer details of the binding, such as the orientation in the minor groove, or the configuration at the C11 position. Further work was able to identify the C11 position of the PBD as the point of adduct formation, in support of earlier suggestions that this was the point of bond formation (Kohn & Spears, 1970). Other

possible sites for alkylation were identified as C6, C7, C8, and N3 and were subsequently eliminated (Petrusek *et al.*, 1981). Direct evidence for the involvement of C11 was provided by the use of NMR comparing the ^{13}C spectra of [11-^{13}C]-anthramycin methyl ether and the [11-^{13}C]-anthramycin adduct formed with calf thymus DNA (Graves *et al.*, 1984).

The interaction of PBD compounds with DNA is proposed to be in a relatively sequence-selective manner, with a preference being shown for binding to a guanine base flanked on either side by a purine base revealed by footprinting-type studies (Hertzberg *et al.*, 1986; Hurley *et al.*, 1988; Thurston, 1993). It has been shown that PBD compounds form covalent adducts with the exocyclic N2 of guanine, in the minor groove of DNA (Remers, 1988; Thurston, 1993). The site within the PBD molecule that is involved in binding to DNA (the N10-C11 region), can exist in three different forms, all possessing the ability to alkylate N2-guanine residues: a) imine (Figure 6.2, **2**), b) carbinolamine (Figure 6.2, **3**), and c) carbinolamine methyl ether (Figure 6.2, **4**,).

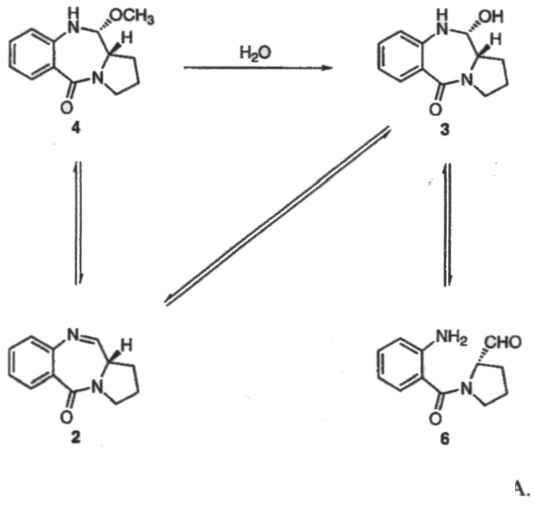

Figure 6.2 Possible forms of PBDs that can interact with duplex DNA (from (Baraldi *et al.*, 1999)).

There are three potential mechanisms by which this bond may form (Figure 6.3):

1. There may be a direct SN2Ca-type attack of the protonated carbinolamine (Figure 6.3, **6**) or its 11-methyl ether (**7**), by the guanine, resulting in the adduct (**9**) (Hurley, 1977).
2. The mechanism may involve Schiffs base formation between N2-guanine functionality and the acyclic amino aldehyde of the DNA-drug adduct (Figure 6.3, **8**) (Ostrander *et al.*, 1981), followed by intramolecular cyclisation via attack of the aromatic amino acid function.
3. Or there could be a direct attack of the biological nucleophile on the imine function (Figure 6.3, **2**) (Kopka *et al.*, 1994).

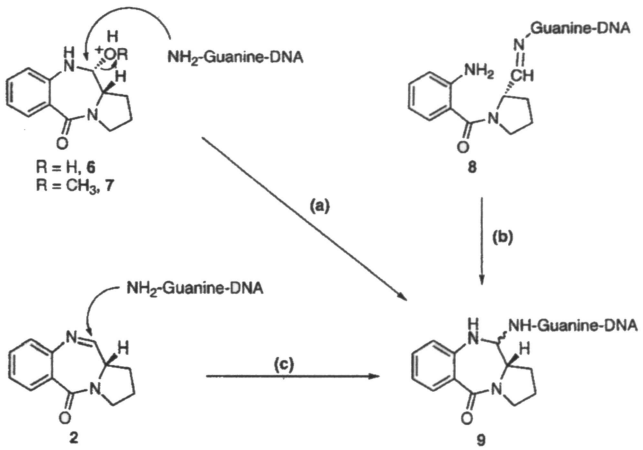

Figure 6.3 Possible mechanism of DNA alkylation by PBDs (from (Baraldi *et al.*, 1999)).

There has been some interest in separately studying the non-covalent and covalent components involved in the binding of a PBD molecule to DNA. To investigate the non-covalent portion of the reaction, a series of compounds was studied that lacks the

N10-C11 function by which the covalent bond is formed. Molecules studied in this experiment were shown to retain the ability to form non-covalent bonds, provided hydroxyl or acetoxy groups were maintained at the C2 and C8 positions, and a further requirement of an (*R*)-configuration at C2 was met (Jones *et al.*, 1990).

Covalent bond formation was studied using a model nucleophile (thiophenol), in order to deduce the reactive species of PBD molecule involved, and attempt to measure the rate of reaction (Morris *et al.*, 1990).

The sequence selectivity of the PBDs could be partly due to the ability of the PBD molecule to bind to DNA, and then migrate to another site where it binds more strongly, prompting the suggestion that the compound could bind to DNA and then "creep" along the minor groove to a more favourable site without actually dissociating from the DNA (Hertzberg *et al.*, 1986; Remers, 1988).

It has been shown, by use of thermal denaturation, ethidium bromide displacement, and endonuclease digestion studies, that there is a distinct order of DNA reactivity of the naturally-occurring PBDs (sibiromycin > anthramycin > tomaymycin > DC-81 > neothramycin) (Puvvada *et al.*, 1993). However, there has been less success in elucidating a link between DNA-binding affinity, sequence selectivity, *in vitro* cytotoxicity or *in vivo* antitumour activity.

6.3 Biological activity of PBD compounds

Biological assessment of the PBD series of compounds has mostly centred around the naturally-occurring PBDs, anthramycin, tomaymycin, sibiromycin, neothramycin and

DC-81. Furthermore, not all PBDs have been tested in all systems, so direct comparison required to identify a structure-activity relationship is not particularly easy. This has been further hampered by the limited number of available compounds, and the difficulty in synthesising further analogues.

Work in the late 1970's has indicated the cytotoxic effects of the naturally-occurring PBDs covers a wide range of biological systems, ranging from the inactivation of viruses and bacteriophages to their antibacterial and antitumour effects.

Anthramycin has been shown to inhibit a broad spectrum of bacteria and fungi in culture. However this has not been noted to translate into a useful *in vivo* property, as no activity in animals has been observed other than some effects on parasites such as *Trichomas vaginalis*, *Entamoeba histolitica* and *Syphcia obvelata* (Horwitz, 1975). Some derivatives of anthramycin have shown activity in one or more biological systems, although a substantial deviation from the original PBD structure tends to result in a loss of activity (Hurley, 1977). Antibacterial activity was also observed with tomaymycin and derivatives (Arima *et al.*, 1972; Shimizu *et al.*, 1982; Tozuka *et al.*, 1983). The most active of the naturally-occurring PBDs is sibiromycin. This has been found to be active against many bacteria, as well as showing activity against a number of tumours (Gauze *et al.*, 1969; Dudnik *et al.*, 1971). Neothramycins show weak antibacterial activity, but have good antitumour potency (Takeuchi *et al.*, 1976). The simple PBD molecule, DC-81, has also proved to be less cytotoxic than tomaymycin in selected cell lines (Bose *et al.*, 1992c).

Current research into the use of PBDs as antitumour agents has resulted in two distinct classes of agent. There is interest in both using original PBD-style compound analogues, referred to as monomers, and in exploring the creation of PBD dimers where two PBD sub-unit molecules are linked.

6.4 PBD monomers

This class of PBD originates from the original series of naturally-occurring compounds, such as anthramycin, tomaymycin, sibiromycin, neothramycin and DC-81. The original work on the pyrrolobenzodiazepine group of compounds was able to identify the primary mechanism of action of PBDs as a function of DNA binding. This produces a consequential inhibition of DNA/RNA synthesis, resulting in toxicity as a product of the inhibition of vital cellular processes, although direct evidence for this as the only cause of toxicity has not yet been forthcoming. Thus far, sibiromycin has remained the favourite PBD monomer in terms of ability to bind DNA as measured by thermal denaturation studies, ethidium bromide displacement, and restriction endonuclease digestion studies (Puvvada *et al.*, 1993). It has been suggested that there is a structure-activity relationship (SAR) between strong DNA binding, as indicated in these experiments, and cytotoxicity when translated into a biological system (Thurston, 1993; Thurston *et al.*, 1999). However, this is difficult to observe, as there is a limited number of studies that have been performed that allow comparison of these characteristics. Sibiromycin especially, has been neglected as far as biological characterisation is concerned, having only had a rough characterisation of efficacy against a tumour model. While the results obtained against the tumour model with sibiromycin were impressive (lyo-1 > 90% tumour inhibition, OG-5 = 100% tumour inhibition), the actual dosage was recorded only as “maximum tolerated” (Brazhnikova *et al.*, 1972), and therefore

could not be compared with other results. Sibiromycin has been examined in preliminary clinical trials, and effectiveness against squamous cell carcinoma was suggested (Gauze *et al.*, 1972). However, this does not appear to have been pursued, probably as a result of earlier research that indicated cardiotoxicity of sibiromycin in dogs (Bazhanov & Shepelevtseva, 1974). A similar fate appears to have befallen anthramycin and neothramycin, the other two naturally-occurring PBD monomers to have reached clinical trials. Almost half the number of terminal patients responded to crude anthramycin; however, a quarter of those given pure anthramycin went into irreversible shock, and some showed abnormal electrocardiograms (Korman & Tendler, 1965). Neothramycin indicated responses to some types of cancer, without the cardiotoxic aspect, but this PBD agent has not progressed further (Hisamatsu *et al.*, 1980; Fujita *et al.*, 1982; Tsugaya *et al.*, 1986).

The monomers anthramycin, neothramycin, tomaymycin, sibiromycin, and DC-81 have all been shown to inhibit transcription *in vitro* in a bacteriophage T7 RNA polymerase model. A quantitative *in vitro* transcription (QIVT) assay was used to assess the level of inhibition of the compounds to ascertain whether the binding of PBD monomer to DNA was able to inhibit transcription. This allowed quantitation of the level of transcription inhibition by each compound, and resulted in an experimental rank order of inhibiting ability as: sibiromycin > tomaymycin > anthramycin > DC-81 > neothramycin. This was accompanied by *in vitro* transcription footprinting assay, which led to the conclusion that agents involved primarily favoured binding to a 5'-AGA sequence, although binding was influenced by bases flanking this sequence (Puvvada *et al.*, 1997).

Other work has attempted to assess the influence of the A ring of the PBD nucleus, by synthesising a range of compounds with different modifications to the A-ring. However, it was found that no changes to the A-ring conformation resulted in either an increase in *in vitro* cytotoxicity or DNA-binding ability of the compounds (Thurston *et al.*, 1999).

An alternative strategy to increasing the cytotoxicity of PBD-based compounds has been to examine C2-exo-unsaturated PBDs. A selection of these compounds was synthesised and assessed in a selection of ovarian carcinoma cell lines. Of the new compounds, two managed to produce a higher denaturation temperature for double-stranded DNA, indicating stronger DNA binding. These agents also effected an increase in cytotoxicity in two of the cell lines used, relative to DC-81. However, this is not necessarily useful, as tomaymycin itself is noted to have over 270-fold higher toxicity in the CH1 cell line, although it assists in the elucidation of a SAR as the only difference involves one hydroxyl group (Gregson *et al.*, 2000). However, sibiromycin, previously noted to be most strongly bound to DNA of the naturally-occurring PBDs (Puvvada *et al.*, 1993), was not considered in this study.

6.5 PBD dimers

Interest in the PBD series has diversified over recent years, with the linking of two PBD-based molecules together to form a dimer. This was initially started with the synthesis of a dimer of DC-81 (Figure 6.4), termed DSB-120 (Figure 6.5) (Bose *et al.*, 1992a). It was reported that this molecule allows recognition of an increased number of bases, and binds with an increased affinity compared to the PBD monomer DC-81, resulting in an increased level of *in vitro* cytotoxicity (measured as decreased IC_{50}) in

the cell lines used (Bose *et al.*, 1992b). The effect of the length of the linker used between PBD units was studied, and the conclusion drawn from the data found that an odd number of linker units gave the best cytotoxic activity (Bose *et al.*, 1992b). DSB-120 was found to be the most cytotoxic of the compounds examined.

This led to further work to study the cellular pharmacology of a series of C8-linked PBD dimers, with varying linker length. Results showed DSB-120 to be the most potent in terms of cytotoxicity, with an odd number of linker units resulting in better activity than that observed for an even number of linker units (Smellie *et al.*, 1994). It was further noted that the agents used produced a cell-cycle block in the G2/M phase of the cell cycle, noted to be a characteristic of agents that interfere with DNA (Konopa, 1988), more specifically a characteristic of cross-linking drugs such as mephalan and cisplatin (Brox *et al.*, 1980; Sorenson & Eastman, 1988). It was noted that in the A2780cisR cell line (cisplatin-resistant), a similar pattern of resistance to DSB-120 was observed as that shown with cisplatin. It was noted that GSH levels in this cell line are elevated compared to other cell lines, and hence it was suggested that GSH may responsible for inactivation of the drug. This was tested by depleting cellular GSH using BSO (D,L-buthionine-*S,R*-sulfoximine), and partial reversal of resistance was observed (Smellie *et al.*, 1994). Evidence that the A2780cisR cell line shows increased expression of ECRCC-1 mRNA (the translated protein being involved in NER) suggests that DSB-120 induced DNA interaction may be modulated via the NER pathway as well (Li *et al.*, 1998; Aquilina *et al.*, 2000; Massey *et al.*, 2003). Other evidence has shown an increased IC_{50} for cell line HX62 compared to 41M, which may be attributable to HX62 having up to 4-fold higher GSH levels than 41M (Mistry *et al.*, 1991; Smellie *et al.*, 1994), and thus suggests GSH binding may be a metabolic route for this compound.

Interestingly, a cell line with acquired doxorubicin resistance (41MdoxR), showed a resistance to DSB-120. This appears to be correlated with the high level of resistance to other compounds noted in this cell line (vinblastine, taxol, colchicine) conferred by elevated levels of P-glycoprotein (P-gp), the multidrug resistance protein responsible for efflux of several therapeutic compounds (Smellie *et al.*, 1994). P-gp was blocked by use of verapamil (Smellie *et al.*, 1994), a well-known inhibitor of P-gp function (Wils *et al.*, 1994; Wilkinson, 2000), and partial reversal of resistance was observed. This indicated that DSB-120 may be a substrate for this efflux mechanism, a potential pharmacokinetic problem, as P-gp has been observed to be implicated in several cancers and the resulting occurrence of multidrug resistance.

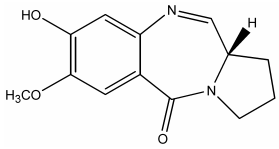

Figure 6.4 Structure of DC-81.

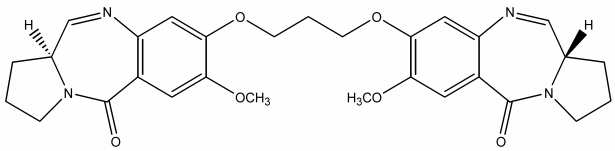

Figure 6.5 Structure of DSB-120.

Work by Walton and colleagues (Walton *et al.*, 1996) has produced some of the only pharmacokinetic data currently available in the literature on the behaviour of a PBD molecule *in vivo*. The PBD dimer, DSB-120, was studied both *in vitro* for cytotoxicity in cultured cell lines, and stability in blood and plasma, and were investigated *in vivo*

for clearance and tumour distribution data. The cell panel cytotoxicity data was consistent with earlier data from other studies, in that DSB-120 showed marked cytotoxicity in all cell lines. Furthermore, DSB-120 appeared to be stable in plasma, although a rapid degradation in whole blood was observed. In contrast to the *in vitro* data, DSB-120 showed very poor activity *in vivo*, with a significantly lower therapeutic index compared to other DNA-crosslinking drugs used in the study (cisplatin, carboplatin), and thus a markedly higher toxicity to the mice used in the experiment. Plasma pharmacokinetics showed biexponetial characteristics, with an initial short distribution phase ($t_{½}$ = 4 min), and a longer elimination phase ($t_{½}$ = 38 min). However, the steady-state tumour/plasma ratio was about 5%, and thus the drug showed poor specificity for the tumour relative to normal tissue. LD50 data also showed DSB-120 to be much more toxic than either cisplatin or carboplatin. Hence, despite strong DNA binding and good *in vitro* data, DSB -120 looks to be of no use as an *in vivo* compound.

Refinement work to improve the DNA binding of PBD dimers has resulted in the synthesis of SJG-136 (Gregson *et al.*, 1999; Gregson *et al.*, 2001). This analogue of DSB-120 has been reported to have an increased ability to thermally stabilise double-stranded calf thymus DNA significantly more than any previously studied compound, indicating a much higher affinity for DNA than previous agents. SJG-136 has been shown to have increased toxicity (pM rather than μM) compared to DSB-120 and cisplatin in an A2780cisR cell line, and does not appear to suffer from the proposed reactivity with glutathione as reported previously (Smellie *et al.*, 1994). In fact a 320-fold increase in cytotoxicity to the cell line was reported compared to DSB-120. However, as yet no *in vivo* data has been reported, therefore it is unknown as to whether this increase in toxicity of SJG-136 will translate in a similar manner to that of DSB-

120, and result in unfavourable pharmacokinetics and inauspicious toxicity, as observed with this other dimer (Walton *et al.*, 1996).

6.6 Sequence selectivity of the PBDs

The antitumour activity of many of the early PBDs was thought to be attributed to the ability of the compounds to covalently bind to the N2 of guanine in double-stranded or duplex DNA (Hurley & Petrusek, 1979; Graves *et al.*, 1984). The adducts formed by this binding were observed to neatly fit into the minor groove of the double helix, with the right-handed twist of the PBD molecule following the curve of the DNA (Petrusek *et al.*, 1981; Hertzberg *et al.*, 1986; Hurley *et al.*, 1988; Thurston, 1993). This observation that the twist of the drug and the twist of the DNA were closely matched led to interest as to whether the drug-DNA interaction may be sequence-dependent, and therefore if alteration in the 3-dimensional structure of the drug would influence its DNA binding selectivity (Hertzberg *et al.*, 1986).

Early evidence to indicate a level of sequence selectivity of the PBD compounds was found. Competitive binding experiments showed incomplete competition for binding sites between anthramycin and tomaymycin (Hurley, 1977) and between anthramycin and CC-1065 (Swenson *et al.*, 1982), suggesting that different PBD molecules have a preference for binding to different areas within DNA. Work by Petrusek and co-workers (Petrusek *et al.*, 1981), indicated that anthramycin expressed a preference for binding to G (guanine) when flanked by G, rather than C (cytosine). This was further confirmed by other studies that showed that anthramycin produces greater inhibition of the action of restriction enzymes whose recognition sequences include a 5'-GG over those including a 5'-GC (Sumner & Bennett, 1981; Kaplan, 1982).

A more direct method of establishing a degree of PBD sequence selectivity was shown by the use of methidiumpropyl-EDTA-iron(II) footprinting (Hertzberg *et al.*, 1986). This study showed that anthramycin, tomaymycin and sibiromycin exhibited 2 - 3 base pair sequence selectivity, centred around the covalently-bound G residue. It was shown that a 5'-PuGPu sequence was the most preferred sequence, while 5'-PyGPy was the least preferred. However, it is important to be aware that while there is a degree of selectivity, binding was still observed to the less preferred sequences. Other work has confirmed this 5'-PuGPu selectivity, and has further allowed a rank order of preference of these sequences to be established, this being 5'-PuGPu > 5'-PuGPy ~ 5'-PyGPu >5'-PyGPy (Hurley *et al.*, 1988; Thurston, 1993).

Further work using IVTF (*in vitro* transcription footprinting) techniques has allowed the characterisation of sequences to which PBD compounds bind preferentially, by looking at the sequences which result in a blockage of transcription by bacteriophage T7 RNA polymerase *in vitro*. Anthramycin and sibiromycin showed an exclusive preference for 5'-AGA sequences. Tomaymycin and neothramycin showed a similar affinity for 5'-AGA (i.e. blocked transcription at the same sites), but in addition blockages of transcription were observed at sites corresponding to 5'-AGG, 5'-GGA, and 5'-TGA (Puvvada *et al.*, 1997). It was also proposed that the base sequences flanking the 5'-AGA sequence, preferred by anthramycin and sibiromycin, influence the degree of transcription block observed, with 7 bases purportedly involved in this selectivity (Puvvada *et al.*, 1997).

The use of PBD dimers is currently thought to be a route by which the number of base pairs recognised by the molecule can be expanded. The use of dimers has led to an increase in cytotoxicity of the PBD compound; however, thus far there is no practical demonstration of the increased sequence selectivity and recognition of a larger number of base pairs. Molecular modelling (Jenkins *et al.*, 1994) and NMR (Mountzouris *et al.*, 1994) studies have indicated that a larger 6 base pair sequence may be recognised, with the DSB-120 molecule actively recognising a 5'-Pu-GATC-Py or 5'-Py-GATC-Pu sequences, although this has yet to be demonstrated in an *in vitro* situation. Similar molecular modelling studies have indicated a similar increased number of base pair recognition by the SJG-136 dimer (Gregson *et al.*, 2001).

7 Aims of the research

The pyrrolobenzodiazepine (PBD) class of DNA-interactive compounds has been demonstrated to show a sequence-selective binding affinity for DNA, and as such are of particular interest as DNA-interactive agents with a selective mechanism of action.

This study aims to investigate the pharmacological characteristics of the novel PBD dimer SJG-136, and the PBD monomers, D709119, SJG-303 and MMY-SJG. To this end, analytical methods will be developed to allow extraction and analysis of the compounds in biological fluids and tissues. Furthermore, *in vitro* systems will be used to characterise the pharmacodynamic and pharmacokinetic behaviours of these agents. Where possible, *in vivo* models will be used to investigate the pharmacokinetics of these agents and assess pharmacodynamic endpoints. The proposed reactivity of PBD agents with reduced glutathione (GSH) will also be investigated.

This main focus of these studies will centre on the PBD dimer, SJG-136, as this agent is of particular interest due to selection for progression into man in forthcoming phase I clinical trials. This selection was the result of demonstrably potent *in vivo* antitumour activity and a novel pattern of action as assessed by the NCI COMPARE analysis algorithm (personal communication, Prof. D. E. Thurston).

8 Materials and methods

8.1 Test compounds

SJG-136, D709119, MMY-SJG, SJG-303 and DC-81 were supplied as pale yellow powders and were obtained from Professor D. E. Thurston (University of London, UK). Purity and identity data was unavailable, however molecular weights were confirmed using mass spectrometry.

SJG-136 (Figure 8.1) is a novel PBD dimer shown to bind to DNA with high affinity, and is believed to bind to DNA in a sequence-selective manner (Gregson *et al.*, 1999; Gregson *et al.*, 2001). SJG-136 has previously been shown to have potent cytotoxicity in *in vitro* tumour cell line models, and has shown a novel pattern of action in the NCI 60-cell-line screen COMPARE analysis.

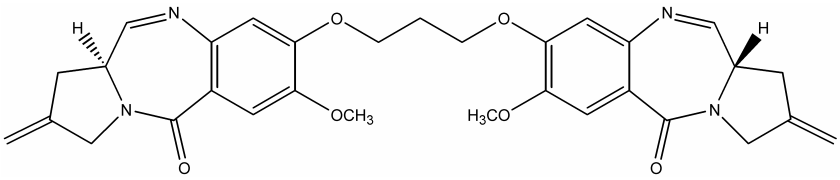

Figure 8.1 Structure of SJG-136. Molecular weight 556.61 (monoisotopic MW 556.23).

D709119 (Figure 8.2) is a PBD monomer that has shown a novel mechanism of action in the NCI 60-cell-line COMPARE analysis (unpublished data).

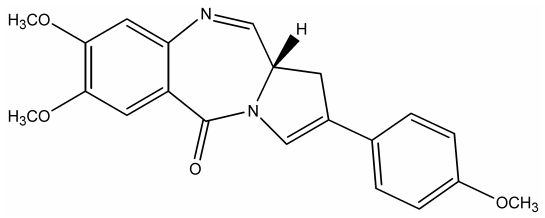

Figure 8.2 Structure of D709119. Molecular weight 364.39 (monoisotopic MW 364.14).

MMY-SJG (Figure 8.3) is the monomeric form of SJG-136. MMY-SJG has been shown to have potent cytotoxic activity in the NCI 60-cell-line screen (unpublished data).

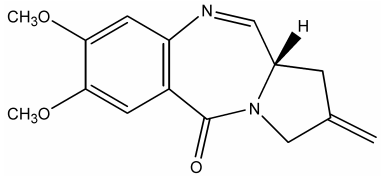

Figure 8.3 Structure of MMY-SJG. Molecular weight 272.30 (monoisotopic MW 272.12).

SJG-303 (Figure 8.4) is a PBD monomer shown to have potent cytotoxicity in the NCI 60-cell-line screen (unpublished data).

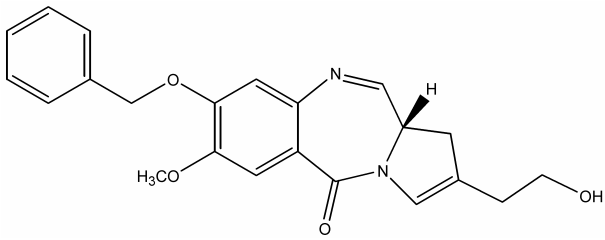

Figure 8.4 Structure of SJG-303. Molecular weight 378.42 (monoisotopic MW 378.16).

DC-81 (Figure 8.5) is a PBD monomer used for preparation of the first synthesised PBD dimer, DSB-120 (Jenkins *et al.*, 1994; Mountzouris *et al.*, 1994) and has been shown to bind to DNA and have potent cytotoxicity (Bose *et al.*, 1992c; Puvvada *et al.*, 1993).

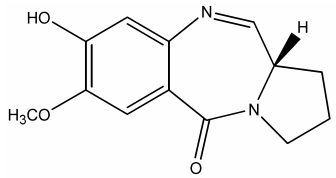

Figure 8.5 Structure of DC-81. Molecular weight 246.26 (monoisotopic MW 246.10).

8.2 *In vivo* studies

8.2.1 Animals

Female NMRI (B and K Universal, Hull, UK) and NCR-Nu (NCI, USA) mice aged 6-8 weeks were used in *in vivo* studies. Mice were housed in an air-conditioned room with regular 12 h cycles of light and dark, and received CRM diet (SDS, Witham, UK) and water ad libitum. All animal procedures were carried out under a project licence issued by the UK Home Office, and UKCCCR guidelines (UKCCCR, 1997) were followed throughout.

8.2.2 Compound formulation

D709119 was dissolved in DMSO and then diluted to the required concentration in 10% DMSO / arachis oil. D709119 was administered via the intra-peritoneal (i.p.) route as a single bolus injection at the maximum tolerated dose (MTD) of 0.5 mg kg^{-1}.

SJG-136 was dissolved in DMSO (for i.p. studies) or DMA (for intravenous studies) and then diluted in physiological saline to a final solution containing < 1% DMSO. SJG-136 was administered via the i.p. route at the MTD of 0.2 mg kg^{-1}. SJG-136 was administered via the intravenous (i.v.) route at the MTD of 0.3 mg kg^{-1}.

8.2.3 Determination of MTD

Test compound in solvent was administered to 2 mice once daily and mice were weighed daily and assessed for signs of toxicity. Toxicity is defined as weight loss of greater than 15% of the initial body weight. Dose was incremented daily until toxicity was observed. A solvent control group (administered dose vehicle only) was set up and observed in parallel. MTD was defined as the maximum dose at which test compound could be administered without evidence of toxicity.

8.2.4 Tumour models

Tumour pieces were removed form storage in liquid nitrogen, defrosted and implanted subcutaneously into the flanks of 2 mice under aseptic conditions. Once grown, tumours were removed, placed in sterile saline containing antibiotics and cut into approximately 1 – 2 mm fragments. Fragments were implanted subcutaneously into the flanks of experimental animals. Animals were used when tumours had grown to approximately 8 – 12 mm in diameter.

8.3 Analytical method development

8.3.1 Chemicals and reagents

All chemicals and reagents were of analytical grade and were obtained from Sigma (Poole, UK). Al solvents were of analytical grade and were obtained from Fisher (Loughborough, UK). All PBD compounds were obtained from Professor D. E. Thurston (University of London, UK).

8.3.2 Characterisation of fluorescence of compounds

Test compound was diluted in methanol or acetonitrile to a final concentration of 1 mM. The compound solution was manually infused into the flow cell of a Waters 454 scanning fluorescence detector (Waters, Hertsford, UK) using a syringe, and was allowed to remain in the flow cell for determination of fluorescent parameters. The scan function of the detector was used to obtain excitation and emission spectra of the compound over a wavelength range of 200 to 900 nm. Wavelengths derived from initial scans were used to fine tune parameters for each compound. Detailed instructions on the operation of excitation and emission scans are published in the operator's manual for the scanning fluorescence detector.

8.3.3 Characterisation of UV absorbance of compounds

UV absorbance characterisation was determined following development of initial HPLC separation of compound. Compound was injected onto the HPLC system at a concentration of 1 mM. A Waters 996 photodiode array detector (Waters, Hertsford, UK) was set to record wavelengths from 210 to 700 nm during sample acquisition. Waters Millennium software (Waters, Hertsford, UK) was used to obtain the UV

absorbance spectrum as determined by the photodiode array detector at the time of compound elution.

8.3.4 Mass spectral characterisation of compounds

Mass spectrometry was performed unless otherwise stated using a Micromass ZMD single quadrupole mass spectrometer (Manchester, UK). A Micromass Quattro Ultima tandem mass spectrometer was used where stated. An electrospray ionisation probe was used in positive mode throughout all mass spectrometry work. Mass spectral compounds were characterised by infusion into the mass spectrometer (MS) at a flow rate of 100 µl min^{-1} and concentration of 100 µM in selected solvent. Gas flows, voltages and MS conditions were adjusted until optimal detection of the compound parent ion could be seen ($[M + H]^{\bullet+}$).

8.3.5 HPLC method development

Method development for the PBD compounds investigated in this study centred initially around the compound MMY-SJG due to lack of availability of the other PBD compounds. Upon receipt of further PBD monomer compounds DC-81, SJG-303 and D709119, method development on these new compounds progressed rapidly as initial method development was found to be largely transferable, likely to be a result of structural similarities. The compound SJG-136, a dimer of MMY-SJG, was found to be compatible with the methods developed for the monomers with minor alterations.

Method development for the test compounds aimed to create a MS-compatible method to allow transference to an MS-based platform as required.

8.3.5.1 Chromatographic system

The HPLC system consisted of a Waters 2690 separations module (Waters, Hertsford, UK) for solvent delivery and autosampling. Detection was performed using a Merck L-7480 fluorescence detector (Merck KGaA, Darmstadt Germany), a Waters 996 photodiode array detector (Waters), a Micromass ZMD MS or a Micromass Quattro Ultima MS/MS (Micromass). The detectors were used alone where appropriate, or connected in series to investigate several parameters per run. When flow was directed into a mass spectrometer, a flow splitter was employed to ensure flow into the MS was within instrument specifications (<200 µl min^{-1}). A 0.5 µm pre-column filter (HiChrom, Theale, UK) was used to protect the HPLC column from any residual particulate matter in samples, and was found to affect chromatography less than a pre-column cartridge.

8.3.5.2 MMY-SJG, SJG-303 and DC-81

During the course of method development, several combinations of conditions were tested to obtain optimal chromatography.

8.3.5.2.1 Methanol-based method

Initial method development was performed with the compound MMY-SJG. Conditions used were methanol (MeOH) and water running isocratically in a 35:65% ratio, with a flow rate of 1 ml min^{-1}, using a reverse-phase LiChrosorb RP8 C8 endcapped (5 µm x 250 mm x 4 mm) column, and detection using a Waters 996 Photodiode Array detector (set to perform a full-scan 200 to 700 nm) and a Waters 474 fluorescence detector (excitation at 260 nm and emission at 420 nm, as determined from fluorescence

characterisation of MMY-SJG). 30 µl of a 0.1 µg ml^{-1} solution of MMY-SJG in MeOH was injected onto the column to assess chromatography.

To improve peak shape, column selection was changed to a reverse-phase HiRPB C18 endcapped (5 µm x 150 mm x 4.6 mm) column. Buffering capacity was introduced into the mobile phase to enhance peak reproducibility. Loss of peak was observed when using a 0.1 M phosphate buffer at pH 7. Choice of buffer was altered to 0.01 M ammonium formate, adjusted to pH 4.0 using formic acid. This replaced the previous aqueous component of the mobile phase. A flow rate of 1 ml min^{-1} and a mobile phase composition of 47.5% MeOH and 52.5% 0.01 M ammonium formate (pH 4.0) running isocratically was used.

Both SJG-303 and DC-81 were found to produce satisfactory peak shapes and reproducible retention times on this system, although mobile phase composition of aqueous and organic solvents was altered. DC-81 was analysed using a flow rate of 1 ml min^{-1} with mobile phase composition of 35% MeOH with 65% 0.01 M (pH 4.0) ammonium formate. SJG-303 was analysed using a flow rate of 1 ml min^{-1} and mobile phase composition 55% MeOH with 45% 0.01 M (pH 4.0) ammonium formate.

8.3.5.2.2 Acetonitrile-based method

In order to inhibit the formation of the carbinolamine methyl ether form of the PBD imine compounds (as was observed by MS with MeOH in the analytical solution; see results sections 9.1.4, 10.1.3 and 11.3), it became apparent that it would be advantageous to develop a non-MeOH HPLC method. This was achieved by substituting acetonitrile (MeCN) for the MeOH in the existing method. This altered the

retention times and peak shapes of the compounds such that it became necessary to alter the choice of HPLC column to a reverse-phase Hypersil phenyl (5 µm x 150 mm x 4.6 mm) endcapped column. Reproducible peak shapes and retention times were achieved with this column/mobile phase combination with the conditions described in Table 8.1 and a flow rate of 1 ml min^{-1}.

Compound	% MeCN	% 0.01M (pH 4.0) ammonium formate
MMY-SJG	14	86
DC-81	9.5	90.5
SJG-303	20.75	79.25

Table 8.1 HPLC mobile phase conditions for selected PBD monomer compounds.

8.3.5.2.3 Mass spectrometry

Both methods described above were assessed for use with MS detection. The mobile phase conditions, flow rate, and column described above were used to analyse samples using a Micromass ZMD mass spectrometer (Micromass). Flow into the mass spectrometer was reduced to 100 µl min^{-1} by use of a flow splitter. Mass spectrometer conditions were optimised to:

- Desolvation gas, 340 l h^{-1}.
- Cone gas, 160 l h^{-1}.
- Capillary, 3.13 kV.
- Sample cone, 34 V.
- Extraction cone, 9 V.
- Rf lens, 0.1 V.
- Source block temperature, 100 ºC.
- Desolvation temperature, 150 ºC.

8.3.5.3 D709119

Chromatographic separation of D709119 used a reverse-phase Hypersil phenyl (5 μm x 150 mm x 4.6 mm) endcapped column (Sigma). Initial chromatographic conditions used a methanol (MeOH)/ammonium formate based method, however it was found that D709119 could exist as an alternate form with methanol present so choice of organic solvent was switched to acetonitrile. Isocratic conditions were developed for elution of D709119 using 30% MeCN and 70% 0.01 M ammonium formate (pH 4.0). Flow rate was 1.8 ml min^{-1}.

Detection of D709119 was via use of a Micromass ZMD single quadrupole mass spectrometer detecting the parent ion ($[M + H]^{\bullet+}$) at a mass to charge ratio (*m/z*) of 365.2. High concentrations of D709119 were detectable using a Waters 996 photodiode array detector with optimal detection at λ 260 nm. D709119 was not detectible by fluorescence detection. MS conditions were optimised to:

- Desolvation gas, 340 l h^{-1}.
- Cone gas, 160 l h^{-1}.
- Capillary, 3.00 kV.
- Sample cone, 35 V.
- Extraction cone, 17 V.
- Rf lens, 0.5 V.
- Source block temperature, 125 ºC.
- Desolvation temperature, 350 ºC.

8.3.5.4 SJG-136

Chromatographic separation of SJG-136 was achieved using a reverse-phase Hypersil phenyl (5 μm x 150 mm x 4.6 mm) endcapped column (Sigma).

Isocratic conditions were developed for elution of SJG-136 using 20% MeCN and 80% 0.01 M ammonium formate (pH 4.0). Flow rate was 1.8 ml min^{-1}. It was observed that retention time and peak shape degraded with time using the isocratic method, therefore a gradient method was developed to attempt to address this problem. Gradient separation gave better performance in terms of peak separation and resolution.

Gradient elution of SJG-136 was performed using MeCN and 0.01 M ammonium formate (pH 4.0). Changes in gradient conditions over time were linear. Gradient conditions were as follows; MeCN 14% at time 0 increased to 19% over 5 min, then further increased to 26% between 5 and 26 minutes, increased from 26% to 48% MeCN between 26 and 30 min and held at 48% MeCN for 15 min and finally allowed to re-equilibrate at 14% MeCN for 15 min. Flow rate was 1.8 ml min^{-1}.

Detection of SJG-136 was primarily by use of a Merck 4780 fluorescence detector [excitation λ 260 nm and emission λ 420 nm]. SJG-136 could be detected at high concentrations using a Waters 996 photodiode array detector, with optimal detection at λ 260 nm. SJG-136 could be detected using a Micromass ZMD single quadrupole mass spectrometer, with the parent ion appearing at a *m/z* of 557.4 ($[M + H]^+$) using single-ion recording mode.

8.3.6 Calibration and limit of detection

Calibration curves were performed by spiking test compound into 100 µl of drug-free mouse plasma to achieve set final concentrations in plasma. Samples were then extracted as described (section 8.3.8) and checked for linear response over the range examined. Replicate samples at a midpoint along the calibration curve were examined to ensure reproducibility. The limit of detection was considered to be the lowest concentration that could be reliably detected following a 70 µl injection onto the HPLC system. These data were used to obtain the relationship between peak area and amount of drug in the spiked mouse plasma.

8.3.7 Stability in biological fluids

Blood or plasma was placed on ice and spiked with test compound to desired concentration. At time $t = 0$, a 100 µl aliquot was removed and extracted as described (section 8.3.8). Spiked blood or plasma was then incubated at 37 °C with 100 µl aliquots removed for extraction at required time points. The half-life for the test compound in plasma or blood was calculated by log-linear regression.

8.3.8 Extraction from biological samples

It was necessary to develop methods of extraction of analyte from pre-clinical samples for all compounds and a separate method for extraction from clinical samples for SJG-136 due to its imminent progression towards clinical trials.

8.3.8.1 Pre-clinical samples

Extraction methodology for pre-clinical samples was designed to extract test compound from murine samples for use in *in vivo* pharmacokinetic studies as well as to be used for extraction from *in vitro* samples studying drug characteristics.

8.3.8.1.1 Plasma; MeCN protein precipitation

To 100 µl mouse plasma in a 1.5 ml microcentrifuge tube, 200 µl MeCN was added and the sample was vortex mixed. Sample was centrifuged at room temperature for 20 min at 20,000 *g*. Supernatant was removed to a fresh 1.5 ml microcentrifuge tube and spun in a Jouan RC 10.10 centrifugal evaporator (Jouan Ltd, Ilkeston, UK) under vacuum at room temperature until dry. Sample was reconstituted in 100 µl of mobile phase, and centrifuged for 20 min at 20,000 *g* to remove any residual particulate matter. 70 µl of supernatant was injected onto the HPLC system for analysis.

Extraction efficiencies were calculated by spiking 10 µl of test compound diluted in PBS to a total 100 µl of mouse plasma to give a set concentration, and extracting using the MeCN protein precipitation protocol. Standards were prepared by spiking the same solution of test compound into 90 µl of water to give and total volume of 100 µl and thus identical amount of drug in plasma and standard. Extraction efficiency was considered to be the percentage of drug recovered from plasma versus drug seen in the standard. Controls used consisted of plasma spiked with 10 µl of PBS containing no test compound.

8.3.8.1.2 Tissue; MeCN protein precipitation

Tissue was weighed, and 3 volumes per unit weight of PBS were added to the tumour in a universal tube. Tissue was homogenised using an Ultra Turrax homogeniser (IKA Labortechnik, Staufen, Germany) until homogenous.

200µl of tissue homogenate was aliquoted into a 1.5 ml microcentrifuge tube, and 400 µl of MeCN was added and the sample was vortex mixed. Sample was centrifuged at room temperature for 20 min at 20,000 *g*. Supernatant was removed to a fresh 1.5 ml microcentrifuge tube and spun in a Jouan RC 10.10 centrifugal evaporator (Jouan Ltd, Ilkeston, UK) under vacuum at room temperature until dry. Sample was reconstituted in 100 µl of mobile phase, and centrifuged for 20 min at 20,000 *g* to remove any residual particulate matter. 70 µl of supernatant was injected onto the HPLC system for analysis.

Efficiency of extraction from tissue was calculated by spiking tissue homogenate with 10 µl of test compound solution diluted in PBS to desired final concentration in 200 µl homogenate and extracting. An identical 10 µl of test compound solution was pipetted into 90 µl of water as a standard. To 200 µl of homogenate 10 µl of PBS was added as control, and was extracted. Extraction efficiency was considered the percentage of drug recovered from homogenate versus the standard.

8.3.8.2 SJG-136 phase I clinical trial

The PBD dimer SJG-136 is expected to go into clinical trials in the near future, therefore an extraction method was developed here to enable extraction of SJG-136 from clinical samples. The criteria desired for a clinical extraction method differ as

sample volume will be much higher (1 – 2 ml plasma / sera from human samples versus 100 – 200 µl from mice) and starting dose will be much lower than that used in pre-clinical *in vivo* studies. This necessitates a more sensitive method and the use of concentrating steps.

8.3.8.2.1 MeCN Protein precipitation

The method described in section 8.8.1.1 was used. There was also development of an augmented method in which 0.5 ml of human sera was extracted by addition of 1 ml MeCN. All other steps were identical to section 8.8.1.1.

8.3.8.2.2 Solid phase extraction

In all instances 100 mg, 1 ml solid phase extraction (SPE) cartridges were used. CN-endcapped Bond Elut (Varian) SPE cartridges were routinely used after method development which additionally investigated C18-endcapped, C8-endcapped, C2-endcapped and phenyl-endcapped (Varian) cartridges.

Liquid was pulled through the SPE cartridge by use of a SPS24 vacuum manifold (Varian). SPE cartridges were primed with 2 ml of MeCN, conditioned with 2 ml of water, sample was loaded onto the cartridge, and cartridge was washed with 2 ml of water. Cartridge was air dried by passing 10 ml of air through the cartridge. Analyte was eluted in 500 µl of MeCN, and evaporated to dryness using a centrifugal evaporator (Jouan). Sample was reconstituted in mobile phase (14% MeCN) and injected onto the HPLC system for analysis.

8.3.8.2.3 Ethyl acetate

To 200 µl of plasma sample 1 ml of ethyl acetate was added, and the sample was vortex mixed. The sample was then centrifuged at 10,000 *g* for 5 min. Supernatant was removed to a fresh tube and transferred to a centrifugal evaporator and evaporated to dryness. Sample was reconstituted in 100 µl mobile phase.

Extraction efficiency was calculated by spiking plasma with 20 µl SJG-136 at 1 µM in PBS to give a final concentration of 0.1 µM and extracting. 20 µl SJG-136 at 1 µM in PBS was spiked into 80 µl of PBS as a standard, and extraction efficiency considered the percentage of SJG-136 recovered from plasma versus the standard. PBS and sera were extracted as blanks.

8.3.8.2.4 Influence of temperature

1 ml MeCN was spiked with SJG-136 to a final concentration of 0.1 µM. Samples were placed in a centrifugal evaporator and evaporated under vacuum at either at room temperature or 35 °C until dry. Samples were reconstituted in 100 µl of mobile phase (14% MeCN) and injected onto the HPLC system. Recovery of SJG-136 after evaporation was compared to unevaporated standards.

8.3.8.2.5 Influence of pH

SJG-136 was spiked into human sera to a final concentration of 0.1 µM. Samples were then extracted by solid phase extraction as described, with a modification (section 8.8.2.2). After elution from the SPE cartridge, 10 µl of concentrated ammonia solution (Sigma) was added to the eluant to increase the alkalinity of the sample. Sample was then evaporated to dryness using a centrifugal evaporator (Jouan) and reconstituted in

100 µl mobile phase (14% MeCN). Samples alkalinised with ammonia were compared to samples extracted without the added ammonia, and both were compared to SJG-136 standards to assess extraction efficiency.

8.3.8.2.6 Influence of silicon coating and tube material

Polypropylene and glass sample tubes, both uncoated and silicon coated were used, as well as uncoated polystyrene tubes (Sigma). MeCN was spiked with SJG-136 to a final concentration of 0.1 µM, and 1 ml aliquots were distributed into each type of tube, placed in a centrifugal evaporator (Jouan) and evaporated until dry. Samples were reconstituted in 1 ml of mobile phase (14% MeCN) and injected onto the HPLC system. Samples were compared to each other and to SJG-136 standards to determine effect of material on SJG-136 recovery.

8.3.8.2.7 Zinc sulphate protein precipitation

Sample processing to be conducted at room temperature. To 1000 µl of sample add 100 µl of 1 M $ZnSO_4$ in a 1.5 ml microcentrifuge tube. Vortex mix briefly and centrifuge at 20,000*g* for 20 min. Remove supernatant and dispose of. Reconstitute pellet in 500 µl MeOH. Mix thoroughly and centrifuge at 20,000*g* for 20 min. Transfer supernatant to fresh 1.5 ml microcentrifuge tube. Add 50 µl ammonia solution (30% w/w), vortex mix briefly and evaporate to dryness in at room temperature in Jouan RC 10.10 centrifugal evaporator (Jouan Ltd, Ilkeston, UK).

Reconstitute sample in 100 µl mobile phase. Centrifuge at 20,000*g* for 20 min to remove any residual particulate matter and inject 70 µl of supernatant onto HPLC system for analysis.

8.4 Glutathione reactivity studies

Reactivity of the compounds with reduced glutathione (GSH) was assessed.

8.4.1 Reaction with GSH versus time

The reactivity of test compound with GSH over time was investigated as a function of disappearance of compound (as determined by HPLC) over time.

Test compound was spiked into phosphate buffer (19.7% KH_2PO_4 0.2 M : 80.3% Na_2HPO_4 0.2 M ; pH 7.4) containing GSH at concentrations of 50 mM, 5 mM, 500 µM or 50 µM on ice, to a final concentration of 50 µM. Samples were briefly vortex mixed and 100 µl immediately transferred to the HPLC autosampler at room temperature, whereon 10 µl of sample was injected onto the HPLC system for analysis. A repeat injection from the same sample vial was injected every 4 h up to 24 h. Controls assayed on the HPLC system were: GSH without test compound, buffer solution with test compound at 50 µM, and buffer solution containing neither GSH or test compound. Samples were compared to the control 50 µM test compound in buffer (no GSH) to determine relative loss of compound.

8.4.2 Reaction with increasing concentrations of GSH

The reactivity of test compound with increasing concentrations of GSH was investigated as a function of disappearance of compound with altered GSH concentration as determined by HPLC.

Solutions of GSH were made up in phosphate buffer (19.7% KH_2PO_4 0.2 M : 80.3% Na_2HPO_4 0.2 M ; pH 7.4) at concentrations of 50, 30, 16, 8, 4, 2 and 1 mM, and 500

and 50 µM. Test compound was spiked into 100 µl of each of the GSH solutions to a final concentration of 50 µM. Samples were vortex mixed briefly, and 30 µl was injected onto the HPLC system. Controls assayed on the HPLC system were: GSH without test compound, buffer solution with test compound at 50 µM, and buffer solution containing neither GSH or test compound. Samples were compared to the control 50 µM test compound in buffer (no GSH) to determine the relative loss of compound.

8.4.3 Effect of GSH on pH

The effect of GSH on the pH of buffered solutions was investigated, as mimicking of biological pH was considered highly important.

GSH was made up fresh in PBS at concentrations of 50 mM, 5 mM, 500 µM and 50 µM by addition of GSH as a powder and vortex mixing until GSH dissolved. pH was measured in the resulting solutions using Hanna 209 pH meter (Hanna Instruments Ltd, Beds., UK).

GSH was also made up fresh (as above) in 0.067 M phosphate buffer (19.7% KH_2PO_4 0.067 M: 80.3% Na_2HPO_4 0.067 M; pH 7.4) and in 0.2 M phosphate buffer (19.7% KH_2PO_4 0.2 M: 80.3% Na_2HPO_4 0.2 M; pH 7.4). pH was measured in the resulting solutions using an Hanna 209 pH meter (Hanna Instruments Ltd, Beds., UK).

8.5 Protein binding

Assessment of binding of test compound to human sera proteins was performed in order to predict potential effects this may have on pharmacokinetics and tissue distribution of the compounds.

8.5.1 Ultrafiltration

100 µl of human sera (Sigma) or PBS was spiked with test compound to a final concentration of 500 nM. Samples were vortex mixed briefly, and then placed in low binding regenerated cellulose Ultrafree-MC centrifugal filter units (Millipore, Watford, UK) with a molecular weight cut-off of 30,000. Samples were centrifuged for 40 min at 12,000 *g*. Filtrate was collected and assayed by HPLC, and percentage of binding to protein or non-specific binding to the filter membrane was calculated by comparing filtered serum to filtered PBS controls and unfiltered PBS controls.

8.5.2 Ultracentrifugation

500 µl of human sera (Sigma) or PBS was spiked with test compound to a final concentration of 10, 100 or 1000 nM. Samples were vortex mixed briefly, and transferred into polycarbonate thick-walled ultracentrifuge tubes. Samples were then centrifuged at 250,000 *g* for 16 h at 4 °C. Supernatants were collected and analysed on the HPLC system. Both sera and PBS samples were compared to PBS samples that had not been centrifuged, and percentage of compound protein bound was calculated compound recovered from sera samples versus compound recovered from PBS samples.

8.6 Metabolism studies

In order to attempt to predict the formation of metabolites *in vivo*, the formation of metabolites of SJG-136 *in vitro* in metabolically intact systems was investigated. This is especially relevant to SJG-136 as extensive metabolism can complicate pharmacological characteristics of a compound and the progression of this agent into clinical trials, making this an especially important issue.

8.6.1 S9 fraction incubations

NMRI mice were sacrificed by cervical dislocation and liver was removed and placed immediately on ice. Liver was weighed, placed in a conical based centrifuge tube and 3 volumes per unit weight of PBS were added. Liver was homogenised, and homogenate was centrifuged at 9000 *g* for 20 min. The S9 fraction (supernatant) was removed to a fresh tube and placed on ice.

Test compound was spiked into 700 µl of S9 fraction to a final concentration of 1 µM. Co-factors NADPH and NADH were added to the S9 fraction to a final concentration of 1 mM, vortex mixed briefly and S9/compound/co-factor solution was incubated at 37 °C. 100 µl samples were removed at times 0, 0.5, 1, 1.5 and 2 h, were extracted as described in section 8.8.1 and injected onto the HPLC system.

8.6.2 Microsomal incubations

NMRI mice were sacrificed by cervical dislocation and liver was removed and placed immediately on ice. Liver was weighed, placed in a conical based centrifuge tube and 3 volumes per unit weight of PBS were added. Liver was homogenised and homogenate was centrifuged 12,000 *g* for 20 min. Supernatant was removed to a fresh tube and

centrifuged at 100,000 *g* for 60 min at 4 °C. Supernatant was removed and pellet was resuspended in PBS (1 ml per 1 g of liver) to produce a suspension of microsomes.

Test compound was spiked into 1 ml of microsome suspension containing co-factors NADPH at 1 mM and $MgCl_2$ at 2.5 mM to a final concentration of 1 µM, and incubated at 37 °C. 100 µl samples were taken at time 0, 5, 15, 30, 45, 60 and 90 min. Samples were extracted as described in section 8.8.1, and injected onto the HPLC system for analysis.

8.7 Pharmacokinetic studies

The pharmacokinetic profile of SJG-136 was assessed in NCR-Nu mice. Plasma profile was assessed after dosing via the i.p. and i.v. route at the appropriate MTDs (0.2 mg kg^{-1} i.p.; 0.3 mg kg^{-1} i.v.) and also at ⅓ MTD via the i.v. route. The i.p. study investigated the plasma concentration profile only in non-tumour-bearing mice. The i.v. studies used HL-60 tumour-bearing mice and investigated plasma, tumour and brain levels of test compound. Plasma, tumour and brain levels of test compound were investigated in the i.v. studies. Mice were treated (n = 3 per time point) and samples were collected up to 24 h post dose.

The pharmacokinetic profile of D709119 was assessed in MAC15A or MAC29 tumour bearing NMRI mice. Mice were dosed via the i.p. route at the MTD (0.5 mg kg^{-1}). The study investigated the plasma time course in the MAC15A tumour-bearing mice, and tumour levels of test compound in both MAC15A and MAC29 tumour-bearing mice. Mice were treated (n = 3 per time point) and samples were collected up to 24 h post dose.

8.7.1 Sample treatment

Blood samples were obtained using cardiac puncture under terminal anaesthesia. Samples were immediately transferred onto ice for transportation and centrifuged at 7000 *g* to separate plasma within 10 min of sampling. Samples were stored at -20 °C prior to extraction and analysis. Brains and tumours were removed, snap frozen in liquid nitrogen and stored at -80 °C prior to extraction and analysis. Extraction procedures are described in detail elsewhere (see section 8.3.8).

8.7.2 Pharmacokinetic parameters

Pharmacokinetic parameters were calculated using previously described methods (Gibaldi, 1984; Rowland & Tozer, 1989). Sigmaplot (SPSS, Surrey, UK) was used to perform curve fitting according to the equations described below, with $1/y^2$ weighting applied to data points.

The area under the plasma/tissue concentration time curve (AUC) was calculated using the trapezoidal rule. AUC is defined as the sum of all trapezoids (to last time point at which concentration is determined; Equation 1) plus the extrapolated area to infinity (Equation 2).

$$\text{Area of trapezoid} = (C_1 + C_2)/2 \times (t_2 - t_1)$$

Equation 1 Formula to calculate area of trapezoid where C_1 is concentration at t_1 and C_2 is concentration at t_2.

$$\text{Extrapolated area to infinity} = C_{last} / k_{el}$$

Equation 2 Formula to extrapolate area to infinity where C_{last} is concentration at last determined time point and k_{el} is the elimination rate constant.

The elimination rate constant, k_{el}, was calculated by non-linear regression of the concentration time curve using Equation 3 to account for the distribution and elimination phases of drug disposition. Equation 4 was used to account for an absorption component to enable curve fitting to i.p. derived data.

$$C(t) = C_1 e^{-k\mathrm{el}1t} + C_2 e^{-k\mathrm{el}2t}$$

Equation 3 Equation to describe bi-exponential kinetics of compound elimination. C denotes concentration, $k_{\mathrm{el}n}$ denotes the elimination rate constant and t denotes time.

$$C(t) = C_1 e^{-k\mathrm{el}1t} + C_2 e^{-k\mathrm{el}2t} - (C_1 + C_2) e^{kat}$$

Equation 4 Equation to describe bi-exponential kinetics of compound elimination and absorption. C denotes concentration, $k_{\mathrm{el}n}$ denotes the elimination rate constant k_{a} denotes absorption rate constant and t denotes time.

C_{max} was determined from observations of the plasma concentration time data as the maximum observed concentration of drug in plasma.

Half life ($t_{½}$) was calculated using Equation 5.

$$t_{½} = ln2 / k_{\mathrm{el}}$$

Equation 5 Equation to calculate half life ($t_{½}$).

Initial volume of distribution (V_{i}) was calculated using Equation 6.

$$V_{\mathrm{i}} = \mathrm{Dose} / C_0$$

Equation 6 Equation to calculate initial volume of distribution (V_{i}). Where dose is the amount of compound administered and C_0 is concentration at time $t = 0$.

Volume of distribution at steady state (V_{ss}) was calculated using Equation 7.

$$V_{ss} = (AUMC / AUC) \times (Dose / AUC)$$

Equation 7 Equation to calculate volume of distribution at steady state (V_{ss}). Where dose is the amount of compound administered and AUMC is the area under the first moment curve and AUC is the area under the curve.

Clearance (CL) was calculated using Equation 8.

$$CL = Dose / AUC$$

Equation 8 Equation to calculate clearance (CL). Dose is the amount of compound administered and AUC is the area under the concentration vs. time curve.

8.8 *In vitro* studies

8.8.1 Cell culture

Selected cell lines were cultured in RPMI-1640 medium containing 10% foetal bovine serum and 2 mM L-glutamine. Cells were cultured in either 25 cm^2 or 75 cm^2 bottomed tissue culture treated non-vented flasks (depending upon numbers of cells required) in a 5% CO_2 atmosphere at 37 °C.

All cell lines used were adherent. Cells were subcultured by removing all medium, washing cells with 5 ml of Hanks Balanced Salt Solution (HBSS), and addition of 1 ml (25 cm^2 flasks) or 2 ml (75 cm^2 flasks) of trypsin/EDTA and incubation at 37 °C until cells became detached. Cells were vigorously drawn up into and expelled from a 10 ml pipette to break up cell clumps. Cells were split 1 flask into 3 flasks for further growth. Subculturing was performed when cells were approximately 80% confluent.

8.8.2 Cytotoxicity studies

Cytotoxicity of test compounds was assessed using the MTT assay, in which the tetrazolium salt, 3-[4,5-dimethylthiazol-2-yl]-2,5-diphenyltetrazolium bromide (MTT), is reduced to insoluble formazan crystals by metabolically active cells. In this manner the MTT assay was used as a measure of cell viability, as described originally by Mosmann and co-workers (Mosmann, 1983).

Cells were passaged as described (section 2.1) and the number of cells per unit volume was determined using a haemocytometer. Cells were diluted if necessary to a final concentration of 10,000 cells per ml in culture medium. 200 µl of cell suspension was

aliquoted into wells on a 96-well microtitre plate, so as to give 2000 cells per well, excepting in columns 1 and 12 of the plates, in which culture medium only was dispensed. Cells were allowed to attach overnight. Test compound was diluted out in cell culture media to final concentrations in 10-fold dilution steps of 1 mM to 10 pM. Medium was removed from the microtitre plate wells and was replaced with culture medium in 8 replicates (1 column of the plate) of either test compound containing medium at each concentration, or of culture medium alone (1 column). Plates were incubated at 37 °C in a 5% CO_2 atmosphere for 96 h.

MTT was dissolved in PBS at a final concentration of 5 mg ml^{-1} and filtered by passing the solution through a 0.2 μm syringe filter (Corning, Schiphol-Rijk, The Netherlands). Media was removed from wells and replaced with 180 μl of fresh culture medium to which 10 μl of MTT solution was added. The plates were incubated for 4 h at 37 °C. 200 μl of MTT/media solution was removed from wells taking care not to disturb formed formazan crystals. 150 μl of DMSO was dispensed into each well and gently pipetted up and down to dissolve formazan crystals. Plates were then read using a Labsystems Multiskan PLUS plate reader (Vantaa, Finland) at an absorbance wavelength of 550 nm.

8.8.3 Cellular localisation studies

The favourable fluorescent characteristics of SJG-136 implied possibilities of using fluorescence microscopy or ultraviolet confocal microscopy to locate SJG-136 within the cell. As there is a distinct proposed site of action of the PBD compounds in their activity within the nucleus of the cell the possibility of localisation of SJG-136 within the nucleus would support delivery of the compound to its target site.

Glass coverslips (BDH, Poole, UK) were disinfected by immersion in 70% ethanol: 30% distilled water. Cells were passaged as described (section 8.8.1), counted using a haemocytometer and diluted if necessary in culture medium to a final concentration of 10^5 cells per ml. Coverslips were placed in 6-well plates and 2 ml of cell suspension was pipetted into each well. Cells were allowed to attach to the coverslips and grow until approximately 50% confluent.

SJG-136 was spiked into the culture medium to a final concentration of either 100 nM or 1 μM. Cells were incubated with or without compound present for 1, 6 or 18 h. Coverslips with attached cells (live) were mounted by inverting and placing on a microscope slide. Slides were viewed immediately by fluorescence microscopy using a Leica DMRB fluorescence (Leica, Milton Keynes, UK) microscope with UV illumination and a filter allowing excitation wavelengths of 340–380 nm.

8.8.4 Chromosomal staining

8.8.4.1 Preparation of chromosomal DNA

Cells were prepared so that chromosomal DNA could be observed. Cells were grown in a 75 cm^2 tissue culture flask, and were used when 80% confluent. To the culture medium, demecolcine solution (10 μg ml^{-1}, Sigma) was added to give a final concentration of 0.04 μg ml^{-1}, and cells were incubated for 4 h. Medium was removed and cells were harvested as described (section 8.8.1). The cell suspension was transferred to a conical-based centrifuge tube and centrifuged at 1000 *g* for 10 min. Supernatant was discarded and cells were resuspended in 10 ml of 0.075 M KCl and

allowed to sit for 15 min. Cells were centrifuged at 1000 *g* for 10 min and all supernatant, other than 0.5 ml, was removed and 10 ml of ice-cold fixative (Methanol:Glacial acetic acid, 3:1 ratio) was added and mixed well. This step was repeated.

Cell suspension was centrifuged at 1000 *g* for 10 min, and supernatant was removed. Cells were gently resuspended in 1 ml of ice-cold fixative. Slides were cleaned to remove traces of grease and placed on a flat surface. 3 drops of cell suspension were dropped from a height of approximately 15 cm onto the centre of a slide, allowed to dry, and then a further 3 drops were dropped onto slide. This was repeated until 9 drops had been dropped onto the slide, the slide was then allowed to dry completely. Slides were examined using phase contrast microscopy to view chromosomal DNA.

8.8.4.2 Staining of DNA

Slides were incubated with 100 nM SJG-136 for 18 h at 4 °C. Slides were viewed either using a Leica DMRB fluorescence microscope (Leica, Milton Keynes, UK) with UV illumination and filters set to excite the slide at 340 – 380 nm, or a Leica TCS-SP confocal microscope (Leica, Milton Keynes, UK) with pseudo-UV illumination (wavelength = 360 nm).

8.9 Flow cytometry

Effects of the PBD dimer SJG-136 on the cell cycle were assessed using flow cytometry.

8.9.1 Treatment of cells

Cells were seeded into 75 cm^2 tissue culture treated flasks (as described in section 8.8.1), and allowed to grow until approximately 80% confluent. Cells were then exposed to SJG-136 at 10 nM in cell culture medium, a concentration close to the 1 h IC_{50} for each cell line (as determined in section 8.8.2). Exposure was either for 1 h, after which cells were washed in culture media and allowed to recover, or continuous exposure over the entire time. Cells were exposed continuously or allowed to recover for 24, 48 or 72 h, alongside untreated controls. At the end of treatment/recovery period, cells were harvested as described earlier (section 8.8.1) and additional pipetting was used to ensure a single cell suspension.

8.9.2 DNA measurement using ethanol fixation

Measurement of DNA content of cells was performed as previously described (Ormerod, 2000). The prepared single cell suspension was centrifuged at 1000 *g* for 5 min, the supernatant was discarded, and cells were resuspended in 200 µl PBS. 2 ml of ice-cold ethanol:distilled water (70:30 v/v ratio) was added, the suspension was briefly vortex mixed and the left of ice for 30 min. Cells were harvested by centrifugation at 300 *g* for 5 min, supernatant was discarded, and cells were resuspended in 400 µl PBS. Cells were checked microscopically to ensure minimal clumping. 50 µl of RNase solution (1 mg ml^{-1} in PBS) and 50 µl propidium iodide solution (400 µg ml^{-1} in water) were added, and the suspension was incubated at 37 °C for 30 min. Cells were vortex

mixed briefly and passed through a 50 μm syringe filter (Corning, Schiphol-Rijk, The Netherlands) immediately before injection onto the FACS (fluorescence activated cell sorter) to prevent potential cell clumps.

Cells were analysed using a FACSCalibur flow cytometer (BD Biosciences, Oxford, UK), with an argon ion laser tuned to 488 nm, and measuring forward and orthagonal light scatter and red fluorescence (measuring area and width).

Cell counts were plotted as width versus area using Cellquest software (BD Biosciences, Oxford, UK), and were gated to ensure inclusion only of single cells. Histograms produced were processed using WinMDI (Joe Trotter, Scripps Institute, La Jolla, CA) software and analysed using Cylchred software (Terry Hoy, Cardiff, UK) to determine the proportion of cells in each of the G_1, S and G_2/M phases.

8.10 Pharmacodynamic studies

The single-cell gel electrophoresis (Comet) assay was used to assess interstrand crosslinking as a pharmacodynamic endpoint *in vivo* in the lymphocytes and tumour cells of mice exposed to the PBD dimer SJG-136. All chemicals and reagents were obtained from Sigma unless otherwise indicated.

8.10.1 Sample preparation

8.10.1.1 Isolation of lymphocytes

Whole blood was obtained from mice under terminal anaesthesia by cardiac puncture following drug administration, and transferred directly to a heparinised tube on ice. Blood (up to 0.5 ml) was layered onto 0.75 ml Ficoll-Paque (Pharmacia Biotech, St. Albans, UK) in a 1.5 ml polypropylene microcentrifuge tube. Sample was centrifuged at room temperature for 20 min at 450 *g*. The fluffy mononuclear layer at the interface of the Ficoll-Paque and plasma water was removed to a fresh tube, resuspended in cold RPMI 1640 (Sigma) and centrifuged at 4 °C for 5 min at 200 *g*. Supernatant was discarded, and the pellet was resuspended in 1 ml of ice cold freezing mixture (70% RPMI 1640, 20% foetal calf serum and 10% DMSO) and transferred to cryovials. Samples were immidiately placed in a -80 °C freezer for storage until analysis.

8.10.1.2 Preparation of tumours

Tumour was removed from killed mice as quickly as possible and placed in cold RMPI 1640 medium on ice. Tumour was placed in a petri dish in a small volume of RPMI 1640 and chopped finely to form a cell suspension. Cell suspension was transferred to a fresh universal tube and cold medium was added to a total volume of 5 ml. The

suspension was centrifuged at 200 *g* for 5 min at 4 °C. Supernatant was discarded and cells were resuspended in 1 ml of freezing mixture (70% RPMI 1640, 20% Foetal calf serum and 10% DMSO) and transferred into cryovials. The suspension was immediately transferred to a -80 °C freezer for storage until analysis.

8.10.2 Comet assay for detection of interstrand crosslinks

The procedure for the use of the Comet assay to measure ICLs has been described in detail previously (Spanswick *et al.*, 1999). All procedures were carried out on ice and in subdued lighting. Cells were irradiated with 10 Gy of X-ray radiation immediately prior to analysis to deliver a fixed number of random DNA strand breaks. Cells were embedded in 1% agarose on a precoated microscope slide and lysed for 1 h in lysis buffer (100 mM disodium EDTA, 2.5 M NaCl, 10 mM Tris-HCl, pH 10.5; to which 1% Triton X-100 was added immediately prior to analysis), after which the slides were washed with distilled water every 15 min for 1 h. Slides were incubated in alkali buffer (50 mM NaOH, 1 mM disodium EDTA, pH 12.5) for 45 min, and the electrophoresed in the same buffer for 25 min at 18 V (0.6 V cm^{-1}), 250 mM. The slides were then rinsed with neutralising buffer (0.5 M Tris-HCl, pH 7.5) and then with saline.

Slides were allowed to dry, and were then stained with propidium iodide (2.5 μg ml^{-1}) for 30 min, after which they were rinsed with distilled water. Slides were examined using a NIKON inverted microscope using a high pressure mercury light source (NIKON UK Ltd, Kingston Upon Thames, UK) with a 510 – 560 nm filter and a 590 barrier filter at x20 magnification. Pictures were captured using a charge-coupled device (CCD) camera and analysed by use of Komet Analysis software (Kinetic Imaging, Liverpool, UK). 25 cells were analysed for each duplicate slide. Tail moment

was calculated using Komet Analysis software, based on the definition of Olive and co-workers (Olive *et al.*, 1990). Crosslinking was expressed as: percentage of decrease in tail moment = [1 – (*TMdi* –*TMcu*/*TMci* – *TMcu*)] x 100. *TMdi* is tail moment of drug treated irradiated sample, *TMcu* is tail moment of untreated irradiated control, and *TMci* is tail moment of untreated irradiated control.

9 The PBD dimer, SJG-136

SJG-136 (NSC D694501; Figure 9.1) is s PBD dimer compound investigated in this study as a result of evidence of potent cytotoxicity (and novel mechanism of action as indicated by NCI COMPARE analysis), proposed sequence-selective DNA binding and current progress towards phase I clinical trials. As such there is much interest in this compound. Further understanding of the pharmacology of SJG-136 is vital in predicting and understanding the properties of the agent as it progresses towards use in man.

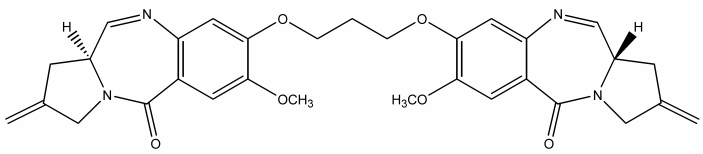

Figure 9.1 Structure of the PBD dimer, SJG-136.

The study is the first to characterise SJG-136 for analytical detection and the pharmacological description for behaviour of the compound in *in vivo* and *in vitro* models.

9.1 Compound characterisation

To facilitate analysis of SJG-136, the compound was assessed for detection using several available methods. This allowed selection of optimal detection parameters for analytical method development.

9.1.1 UV absorbance spectra

UV spectral characteristics of SJG-136 were identified using photodiode array detection. This allowed a UV absorbance spectrum to be generated and optimal wavelengths for detection to be determined from these data (Figure 9.2). UV

absorbance spectra were determined by development of a basic MeCN/water HPLC method, injection of the compound onto the system using this method (at 1 mM), and subsequent analysis of the spectral properties of the eluted peak (as described in section 8.3.3).

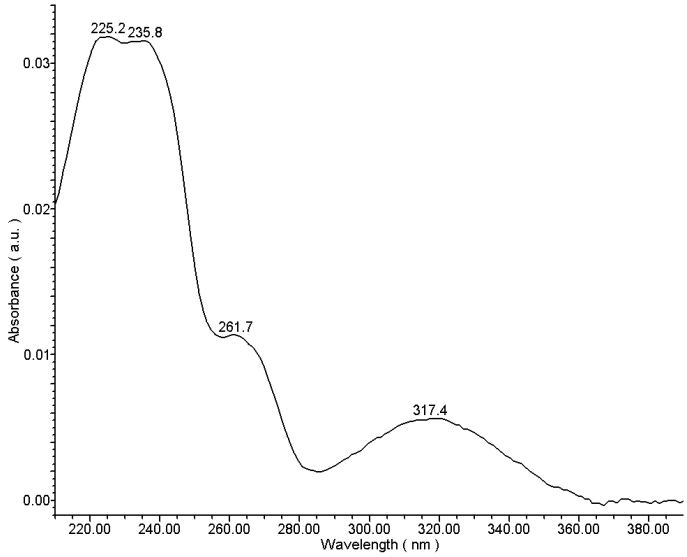

Figure 9.2 UV absorbance spectrum of SJG-136. Useful maxima for optical detection are seen at 225, 236, 262 and 317 nm.

The spectrum demonstrated peaks for detection at 225, 236, 262 and 317 nm, although spectral peaks were observed to be broad.

9.1.2 Fluorescence characterisation

The fluorescent spectral characteristics of SJG-136 were investigated over the wavelength range 210 – 900 nm. SJG-136 was trapped in the flow cell of the scanning fluorescence detector as described (section 8.3.2) and the solution was scanned to obtain excitation and emission spectra. Excitation scans were performed by detecting emission at a wavelength of 400 nm (Figure 9.3); emission scans were performed by excitation at

a wavelength of 235 nm (Figure 9.4). These wavelengths were determined from preliminary work suggesting optimal excitation and emission at approximately these wavelengths in PBD compounds.

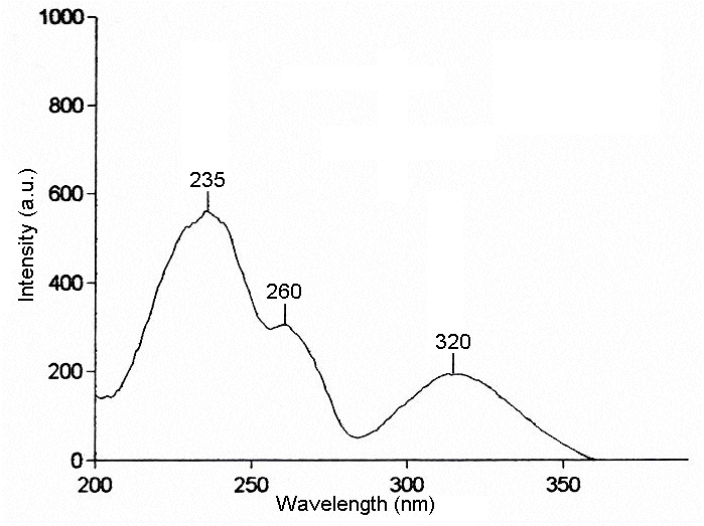

Figure 9.3 Excitation fluorescence spectrum of SJG-136 (using emission wavelength 400 nm). Optimal wavelength for detection seen at 235 nm; optimal selectivity at 260 nm due to reduction in background noise.

Results showed the optimal excitation wavelength for SJG-136 as 235 nm, although spectral peaks were observed to be broad with excitation peaks of lower fluorescence intensity at 260 and 320 nm. A wavelength of 260 nm was chosen for detection due to the decreased background noise and interference generally observed at this wavelength versus 235 nm. Optimal emission wavelength was seen at 420 nm.

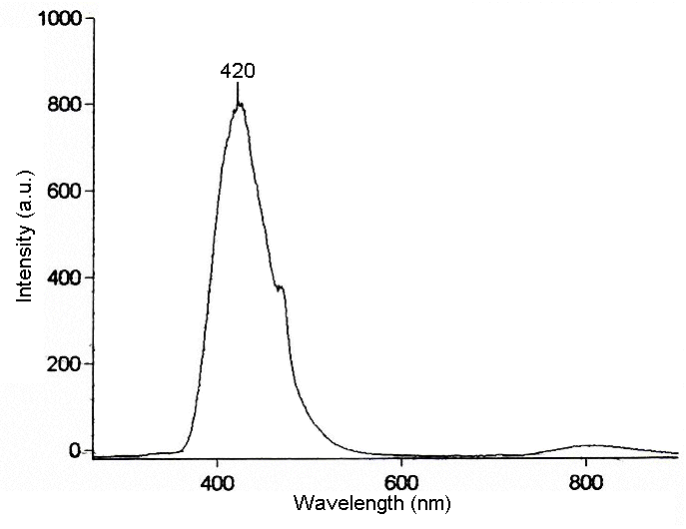

Figure 9.4 Emission fluorescence spectrum of SJG-136 (using excitation wavelength of 235 nm). Optimal wavelength for emission seen at 420 nm.

9.1.3 Effect of solvent on fluorescence intensity

The effect of solvent upon the intensity of fluorescence of SJG-136 was investigated in solvents typically involved in the detection or handling of the compound (Figure 9.5). It was found that SJG-136 fluoresced most intensely in MeOH or 50% MeCN:50% water (no significant difference between the two groups; $P > 0.05$, two tailed unpaired Students t-test). The intensity of fluorescence in either of these solvents was significantly higher than that in any of the other investigated solvents ($P < 0.005$, two tailed unpaired Students t-test).

Analytically, there are implications in the effect of solvent on the intensity of SJG-136 fluorescence, as the limit of detection may be affected by the choice of solvent. However, due to other unique properties for SJG-136, solvent choice for analysis of the agent was constrained and choice of MeOH was not viable (see section 9.1.4).

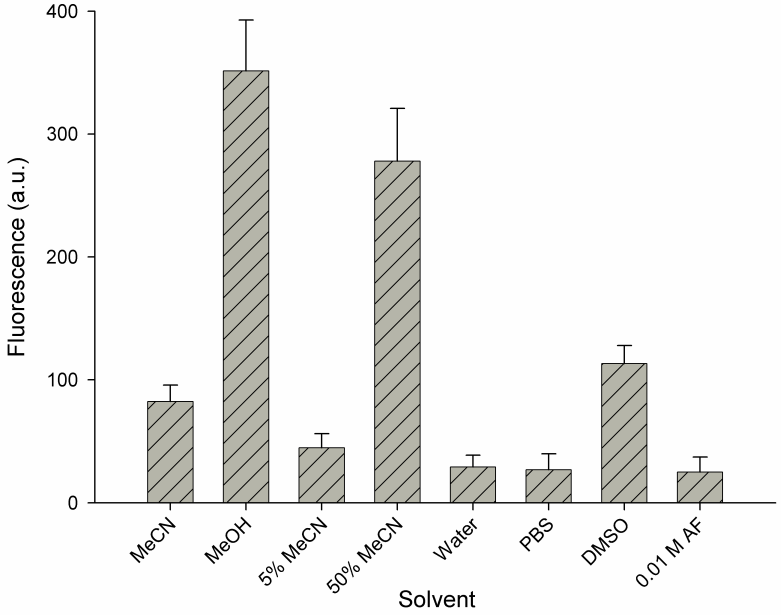

Figure 9.5 The effect of solvent on fluorescence intensity of SJG-136 (mean ± SD; n = 3). Note: 0.01 M AF = 0.01 M ammonium formate, pH 4.

9.1.4 Mass spectral characteristics

The mass spectral characteristics of SJG-136 were obtained by infusing SJG-136 directly into the mass spectrometer with no chromatography, and tuning of the mass spectrometer (MS) to maximise the intensity of the SJG-136 ion (see section 8.3.4).

9.1.4.1 Single quadrupole mass spectrometry

Single quadrupole mass spectrometry was used to identify the dominant ion for SJG-136 as it was envisioned that MS may be used for detection of compound and identification of metabolites. SJG-136 was infused directly into the MS, and tune page conditions were adjusted to give optimal detection of the ionised parent compound at mass + 1 ($[M + H]^{\bullet+}$); detected as a mass to charge (m/z) ratio of 557.1 (Figure 9.6a). The exact or monoisotopic molecular weight of SJG-136 is calculated as 556.2. It was proposed that the imine functional groups of SJG-136 possess the potential to react with

water and/or methanol to form carbinolamine or carbinolamine methyl ether versions of the compound respectively (illustrated in Figure 9.7); this was investigated to examine the impact on method development. This phenomenon has been speculated for many PBD compounds, but no successful attempts to prove the existence of these forms have been published to date.

In order to detect these additional forms of SJG-136, the compound was infused into the MS in either 100% MeCN, 50% water: 50% MeCN or 100% MeOH. The carbinolamine form of SJG-136 was detected at *m/z* 615.1 and 631.1, corresponding to an addition of a water molecule at both imine groups (+36) plus a sodium (+23; $[M + 2H_2O + Na]^{\bullet+}$) or potassium (+39; $[M + 2H_2O + K]^{\bullet+}$) adduct formed within the MS (Figure 9.6b). In this instance the most intense ion is still the parent compound ion at 557.1. The carbinolamine methyl ether form of the compound was detected at 589.4, 643.1 and 659.1, corresponding to the addition of one MeOH molecule (+32; $[M + MeOH]^{\bullet+}$) or two MeOH molecules (+64) plus either sodium (+23; $[M + 2MeOH + Na]^{\bullet+}$) or potassium (+39; $[M + 2MeOH + K]^{\bullet+}$) adducts (Figure 9.6c). These data demonstrate that SJG-136 in the presence of MeOH will react with MeOH to form the carbinolamine methyl ether. This formation produced a molecular ion of equivalent intensity to the SJG-136 imine form. As a consequence of this discovery, it was decided to avoid using MeOH in HPLC method development as detection using MS may show decreased sensitivity if the SJG-136 ion is present in two forms. The reactivity of SJG-136 with water appeared to be relatively insignificant, as SJG-136 parent ion remained the obviously most intense ion. This, coupled with the impracticality of removing water from the analytical systems and the impossibility of

removing water from biological systems, precluded removal of water from method development.

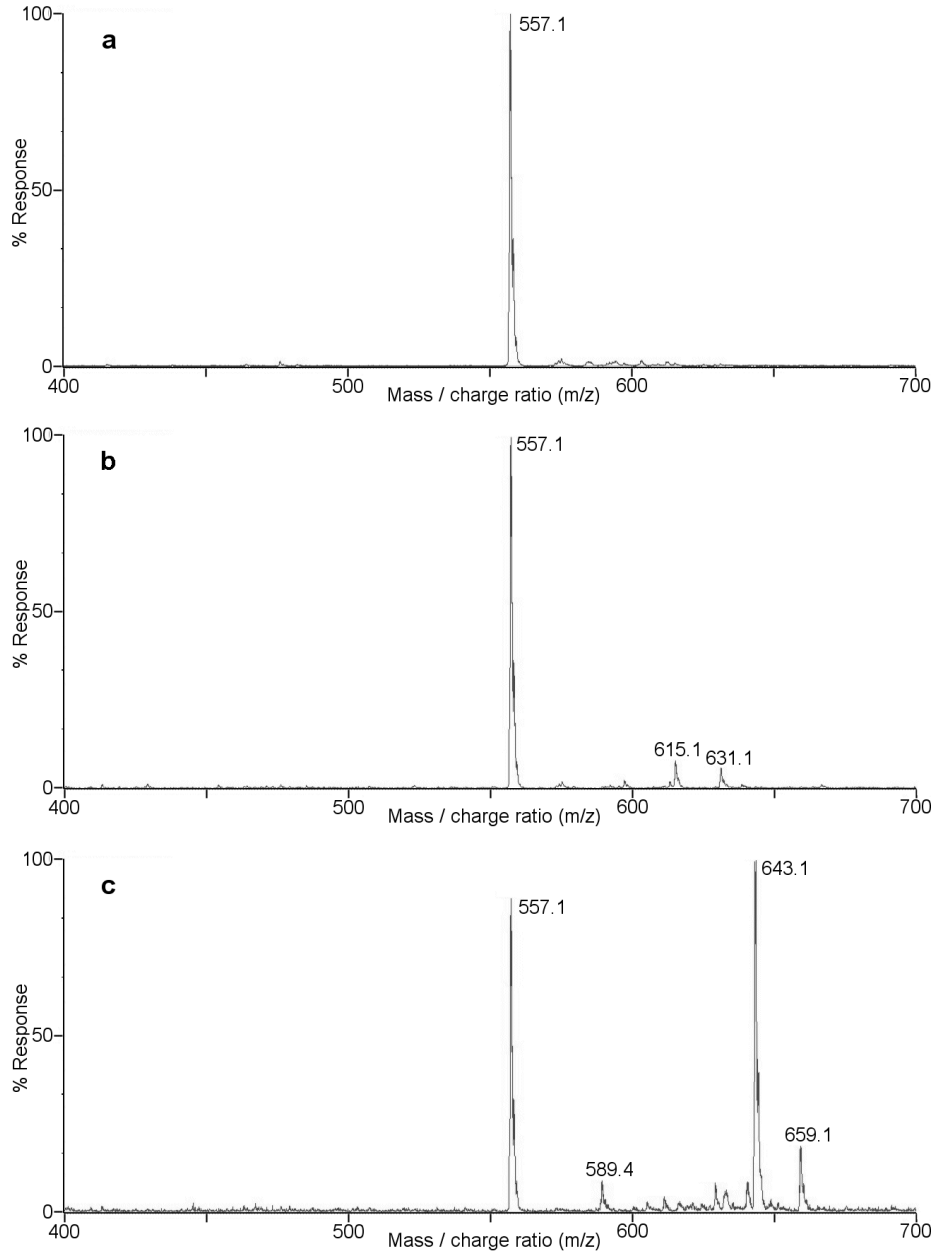

Figure 9.6 Mass spectra of SJG-136 showing potential of SJG-136 to react with water and methanol. SJG-136 with: a) MeCN showing SJG-136 in imine form at *m/z* 557.1; b) water present showing imine (557.1), and carbinolamine (+Na adduct at 615.1 or +K adduct at 631.1); c) MeOH present showing imine (557.1), mono-carbinolamine methyl ether (589.4) and bis-carbinolamine methyl ether (+Na adduct at 643.1 or +K adduct at 659.1).

These data indicate that SJG-136 can exist in 3 forms depending upon the solvent in which it is dissolved. The imine form (as illustrated in both Figure 9.1 and Figure 9.7-**1**), the bis-carbinolamine form (Figure 9.7-**2**) and the bis-carbinolamine methyl ether form (Figure 9.7-**3**). This behaviour was seen in all the PBD compounds investigated (see sections 10.1.3 and 11.3). However, due to the dimeric form of SJG-136, this is further complicated as it is possible that each arm of the dimer may be in a different form, for which there is evidence (Figure 9.6c indicates the formation of a mono-carbinolamine methyl ether form of SJG-136).

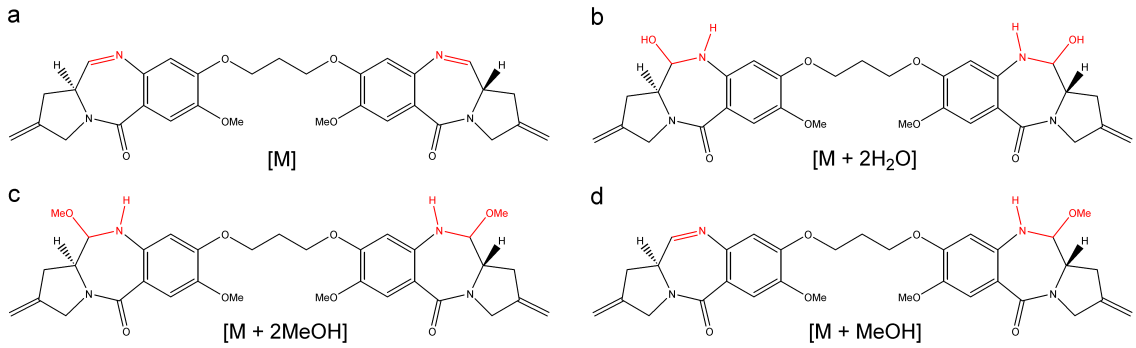

Figure 9.7 The three forms of PBD compounds illustrated by showing the reactive imine element of PBD compounds. a) The bis-imine form. b) The bis-carbinolamine form (resulting from the addition of water). c) The bis-carbinolamine methyl ether form (resulting from the addition of MeOH). d) The mono-carbinolamine methyl ether form. Red colouring denotes the reactive groups.

9.1.4.2 Tandem quadrupole mass spectrometry

SJG-136 was characterised using MS/MS to enable the use of this technique as a sensitive and selective form of detection. SJG-136 was infused into the mass spectrometer, and the tune conditions of the first quadrupole were optimised to give

maximal intensity of the SJG-136 parent ion. The second quadrupole was then used to perform a daughter ion scan, and collision cell conditions and gases were tuned to identify the most intense daughter ion for SJG-136 (Figure 9.8). Finally, these data were used to fine-tune a sensitive and selective MRM (multiple reaction monitoring) detection method which afforded approximately 10-fold lower limit of quantification versus single quadrupole detection.

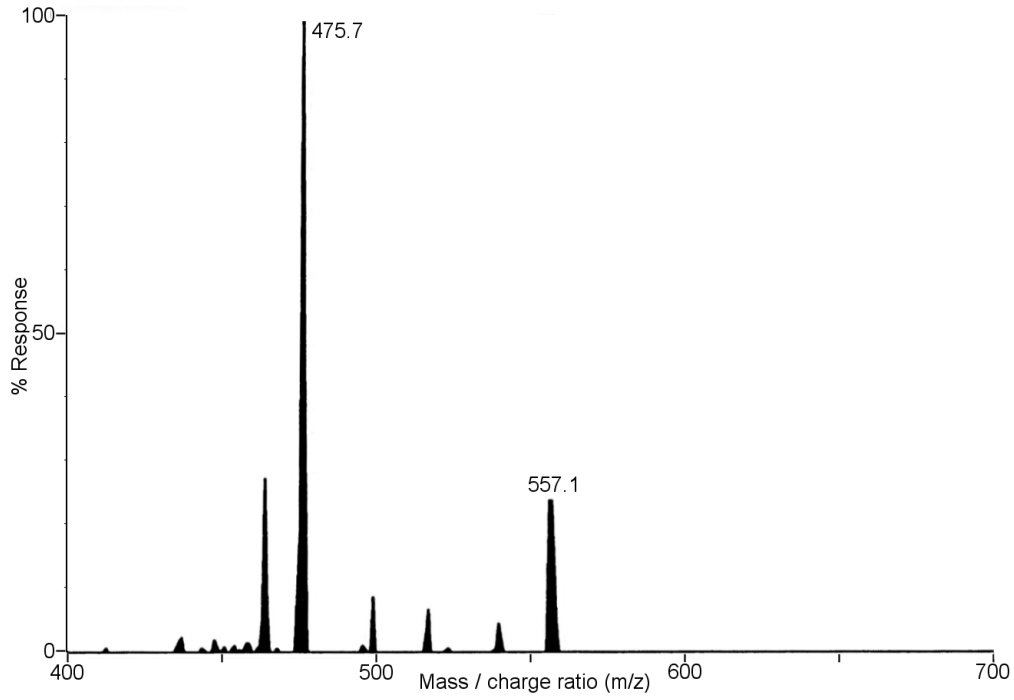

Figure 9.8 Daughter ion scan of SJG-136 showing major fragment at *m/z* 475.7. SJG-136 parent ion can be seen at *m/z* 557.1.

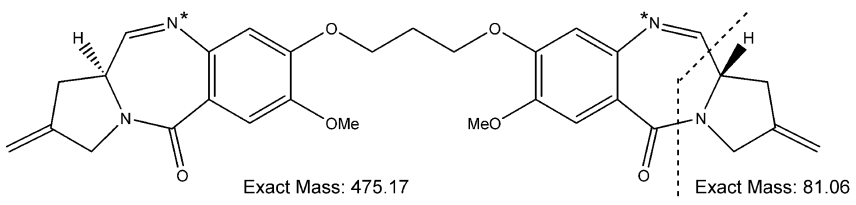

Figure 9.9 Diagram of SJG-136 showing probable fragmentation of the molecule for MS/MS analysis. * deontes possible site/s of protonation.

The major fragment of SJG-136 was determined to be at an *m/z* of 475.7, corresponding to the loss of one of the c-ring pyrrolidine structures from the molecule (Figure 9.9).

9.2 Analytical method development

It was evident that a highly sensitive method for detection of SJG-136 was needed due to the low MTD of SJG-136 (0.2 mg kg^{-1}). A MeCN-based mobile phase was chosen for method development of SJG-136 based on data indicating reactivity of the compound with MeOH (section 9.1.4.1). Fluorescence detection was chosen as the primary mode of detection, as it provided greater than 10-fold lower limit of quantification in early method development versus UV absorbance detection using a photodiode array detector (Figure 9.10).

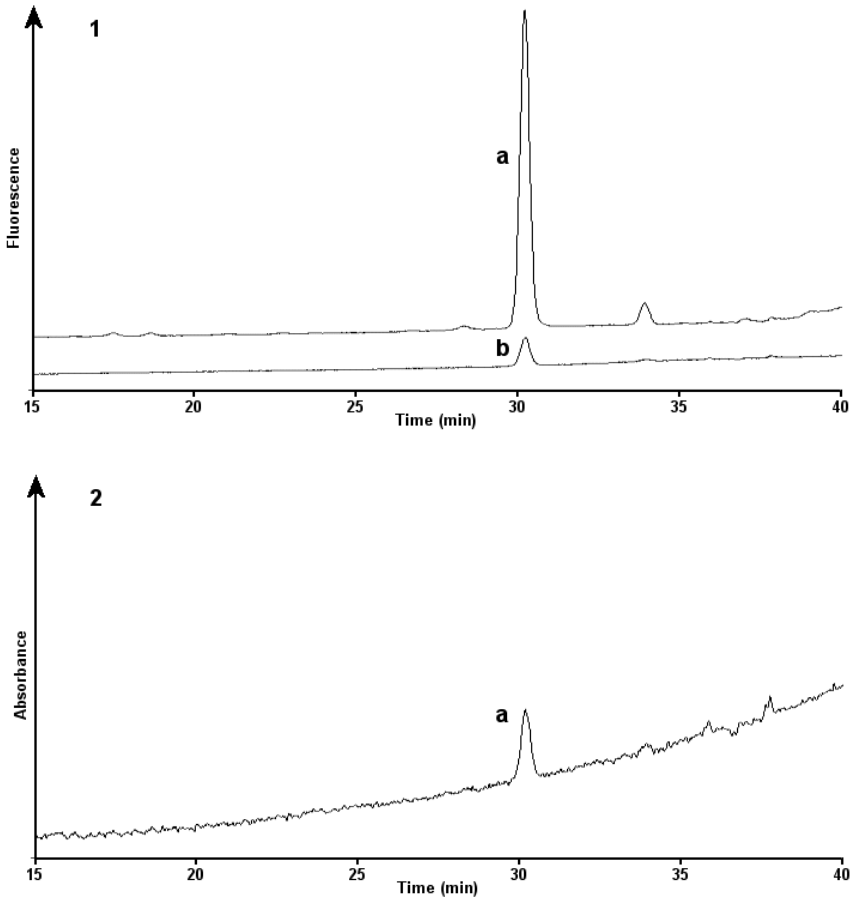

Figure 9.10 Early method development chromatograms illustrating relative sensitivity of detection for SJG-136 via (1) fluorescence detection (Ex λ 260 nm, Em λ 420 nm) or (2) UV absorbance detection with photodiode array detector (260 nm). Peaks labelled (a) show injection of SJG-136 at 1 μM (39 ng on column) on both (1) and (2); peak labelled (b) shows 0.1 μM (3.9 ng on column) injection (no peak found with UV absorbance detection).

Furthermore, fluorescence detection was found to be more sensitive than single quadrupole MS detection using the selected ion recording (SIR) function. Fluorescence resulted in a 10% better signal-to-noise ratio than MS detection, as calculated using MassLynx software.

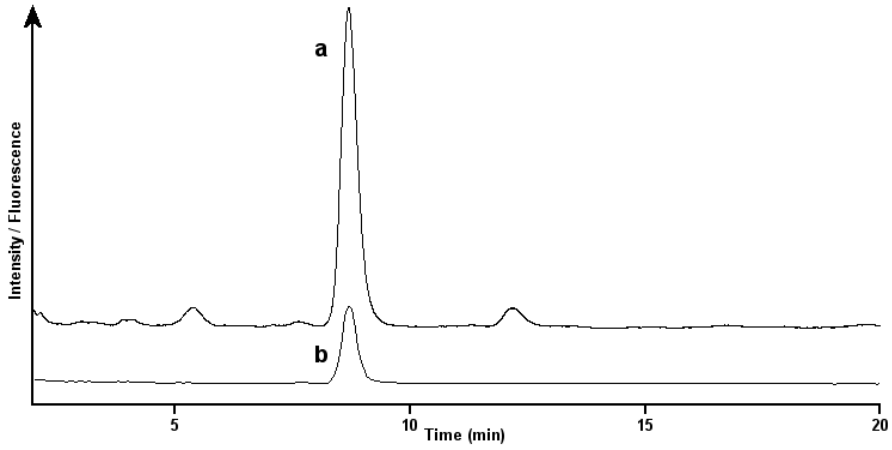

Figure 9.11 Comparison of SJG-136 detection with: (a) fluorescence detection (Ex λ 260 nm, Em λ 420 nm) or (b) mass spectrometer detection using the SIR function (39 ng SJG-136 injected on column). Intensity / fluorescence are not directly comparable; however fluorescence detection (a) shows a 10% better signal-to-noise ratio versus MS detection (b).

Though twin quadrupole (MS/MS) detection was found to be as sensitive as fluorescence detection, MS/MS detection was not available for routine analytical work and was therefore not considered for mainstream method development.

9.2.1 Isocratic separation

Initial development focused on developing an isocratic method with a short run time (< 20 min) to facilitate rapid sample processing. Method development for SJG-136 was based on earlier work in this study on PBD monomer compounds (section 11). The

structural similarity of SJG-136 to the PBD monomer compounds meant that it was probable that the analytical conditions would be largely transferable (in terms of mobile phase and column selection), although the organic/aqueous balance of solvents would likely need to be optimised. Fluorescence detection of SJG-136 was preferred, as this was found to be the most sensitive form of detection compared to UV absorbance and single quadrupole mass spectrometry. Excitation λ of SJG-136 was 260 nm and emission was 420 nm.

SJG-136 was injected onto the HPLC system as a 70 µl injection of a 100 nM SJG-136 solution. Mobile phase conditions were found to be optimal at 20% MeCN: 80% 0.01 M ammonium formate (pH 4.0), giving a symmetrical peak shape and highly reproducible retention time (standard deviation of 0.027 min during a sample run; *n* = 10) during individual sample runs (Figure 9.12).

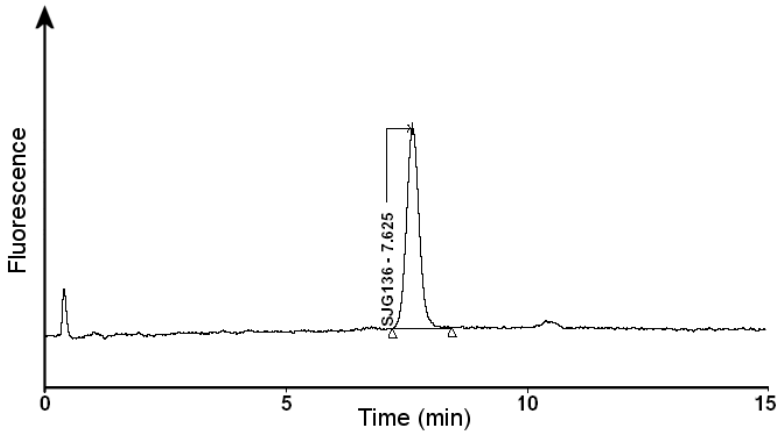

Figure 9.12 Example chromatographic trace for SJG-136, using the isocratic method. Trace shows a 70 µl injection of a 100 nM solution of SJG-136 (3.9 ng on column injection).

Following the development of an extraction method for SJG-136 from plasma (section 9.3.1) there was observation of a gradual build up of plasma interference on the column

(Figure 9.13), as well as intermittent interference close to the retention time of SJG-136 which became progressively worse following subsequent injections. As detection limits were intended to be in the low nM range, this problem was considered severe enough to switch to a gradient method of separation.

9.2.2 Gradient separation

The use of a gradient method for SJG-136 elution resulted in better peak separation from plasma interferences following extraction (Figure 9.14), while maintaining symmetrical peak shape (Figure 9.15). Including a strong organic component (50% MeCN) at the end of the gradient method resulted in the removal of build-up of material on the column. Retention times for SJG-136 with the gradient method were highly reproducible within sample sets (standard deviation of 0.032 min during a sample run; n = 20). The gradient method resulted in much improved separation, although the analytical run time was much increased. The improvement in peak separation was sufficient to warrant the extended run time, and thus the gradient method was used in further studies.

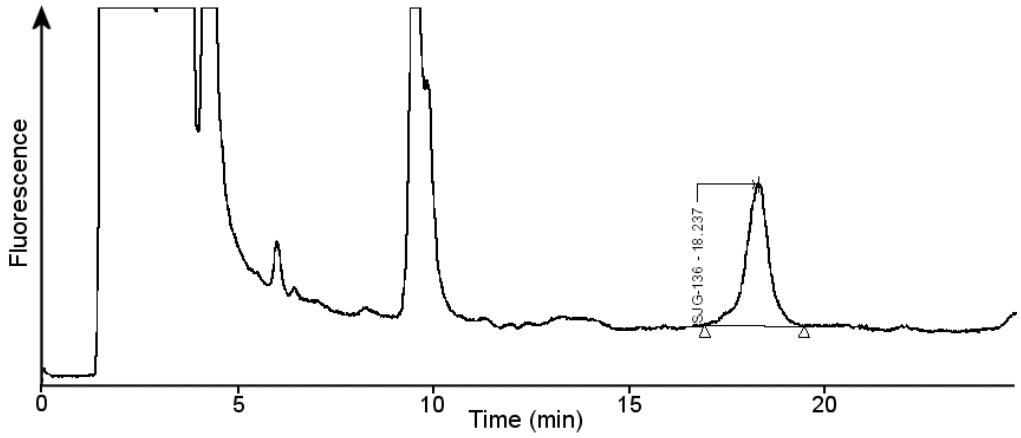

Figure 9.13 Example chromatogram showing a gradient separation of SJG-136 from plasma interference in murine plasma. Trace shows a 70 µl injection of an extraction from 100 nM SJG-136 in murine plasma (3.9 ng on column injection).

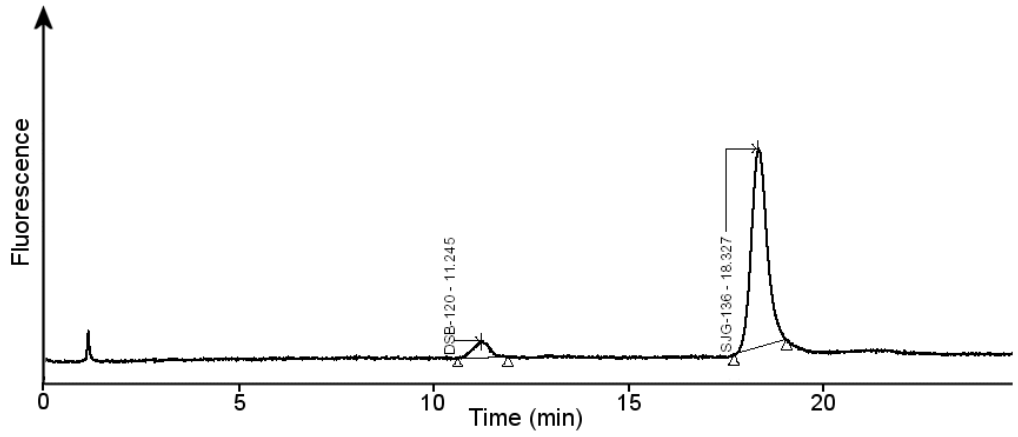

Figure 9.14 Example chromatographic trace for SJG-136, using the gradient method. Peaks shown are SJG-136 at 18.3 min (39 ng on column injection) and the PBD monomer DSB-120 at 11.3 min (3.9 ng on column injection).

9.3 Pre-clinical method development

9.3.1 Extraction from biological samples

Extraction efficiencies of SJG-136 from plasma and tissue homogenate were calculated by spiking SJG-136 into plasma or tissue homogenate to a final concentration of 100 nM (described in section 8.3.8), a concentration likely to be pharmacokinetically relevant (i.e. achievable *in vivo*). Extraction from preclinical murine plasma and tissue samples resulted in the extraction efficiencies detailed in Table 9.1. High recovery of SJG-136 from plasma and simplicity of the MeCN protein precipitation method made this technique the method of choice. The lower extraction efficiencies of SJG-136 from tissues, while not ideal were considered to be adequate. Investigations into the use of solid phase extraction for use with tissue homogenate proved impractical (the particulate nature of the homogenate caused blockage of the cartridges). It is important to consider these data alongside plasma protein binding data (section 9.5.1), as this indicates that the process of MeCN protein precipitation is liberating protein-bound drug during the extraction process. It would not be possible to achieve such high extraction efficiency if SJG-136 remained protein-bound, as approximately 80% of drug would remain in the protein pellet.

Biological sample	**Extraction efficiency (% ± 1 SD)**
Plasma	98.1 ± 0.07
Brain	53.6 ± 0.06
Tumour	52.6 ± 0.03

Table 9.1 Plasma and tissue extraction efficiencies of SJG-136 using MeCN protein precipitation (n = 3; mean ± SD).

9.3.2 Calibration

9.3.2.1 Calibration curve

Calibration curves for SJG-136 were produced in murine plasma and were found to be linear over the range 5 to 1000 nM, with low intra-day variation (coefficient of variation = 0.06) as tested by repeat injections at the midpoint of the calibration curve, 100 nM (Figure 9.15). Calibration curves were performed as recommended (Shah *et al.*, 1992) before analysis of any pharmacokinetic samples to ensure inter-day reliability of the assay.

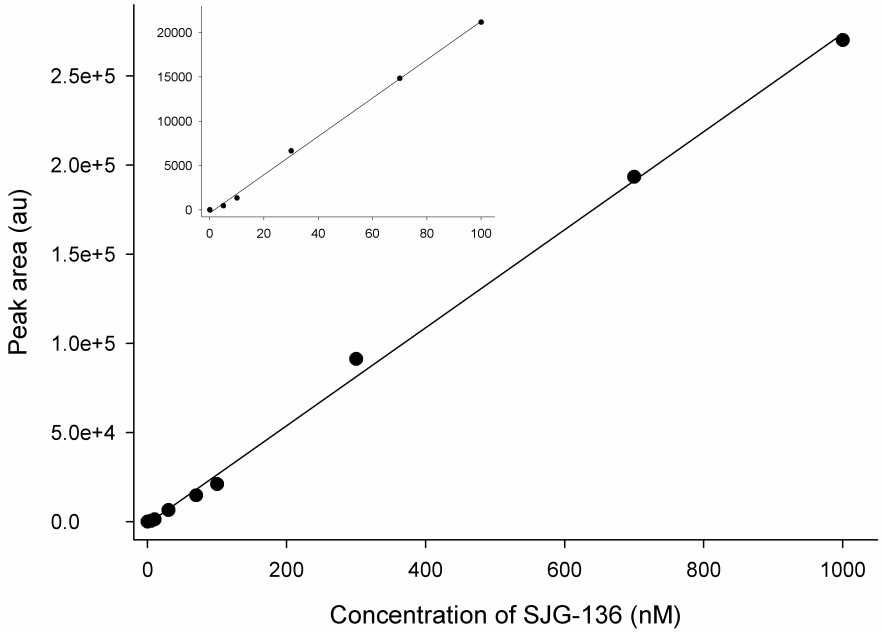

Figure 9.15 Calibration curve for SJG-136 in murine plasma (5 – 1000 nM; 2.8 – 556 ng ml^{-1}; n = 1); inset shows calibration curve over 5 – 100 nM (r^2 = 0.99; linear curve fit is defined as $y = 274.8x - 1053$ using $1/y^2$ weighting).

Calibration of SJG-136 showed a linear relationship between integrated peak area and concentration over the range studied (5 – 1000 nM), with good correlation as assessed by the coefficient of determination (r^2; calculated by the method of least-squares) and by back calculating values for points on the calibration curve from the fitted curve

(Table 9.2). The deviation from nominal values was found to be within acceptable parameters as previously defined (Shah *et al.*, 1992). The use of the structurally similar PBD dimer DSB-120 was investigated as an internal standard for the method, although due to the reactivity of the compound this increased the variation of the assay.

Standard Concentration (nM)	Calculated Concentration (nM)	% Dev
5	5.4	7.9
10	8.7	13.2
30	28.1	6.4
70	59.8	14.6
100	85.1	14.9
300	336.3	12.1
700	708.1	1.2
1000	987.2	1.3

Table 9.2 Back calculation of points on the calibration curve for SJG-136 in murine plasma (from Figure 9.15) showing back calculated concentrations and % deviation from the standard concentration.

9.3.2.2 Reproducibility of analysis

Day-to-day variation of calculated concentrations of SJG-136 were assessed by repeating calibration curves on different days. Inter-day variation was calculated as the coefficient of variation (Table 9.3). CV was found to be within acceptable limits (Shah *et al.*, 1992).

Intra-day variation was found to be low; repeated injections of SJG-136 at 100 nM during one day gave a coefficient of variation of 6% ($n = 6$).

Day	Calculated concentration (nM)		
	10	**100**	**1000**
1	8.6	89.6	985.1
2	8.7	80.8	986.6
3	12.8	87.5	1001.2
CV (%)	24.1	5.3	0.9

Table 9.3 Inter-day variation of calculated concentrations of SJG-136 extracted from mouse plasma samples; CV = coefficient of variation.

9.3.2.3 Limit of detection

Limit of quantification (LOQ) was found to be 5 nM in mouse plasma, with a signal to noise ratio of >5:1 (Figure 9.16) as calculated using MassLynx software. Figure 9.16 shows a 70 µl injection of extract at 5 nM (2.78 ng ml^{-1}), which equates to an injection of 0.2 ng onto the column.

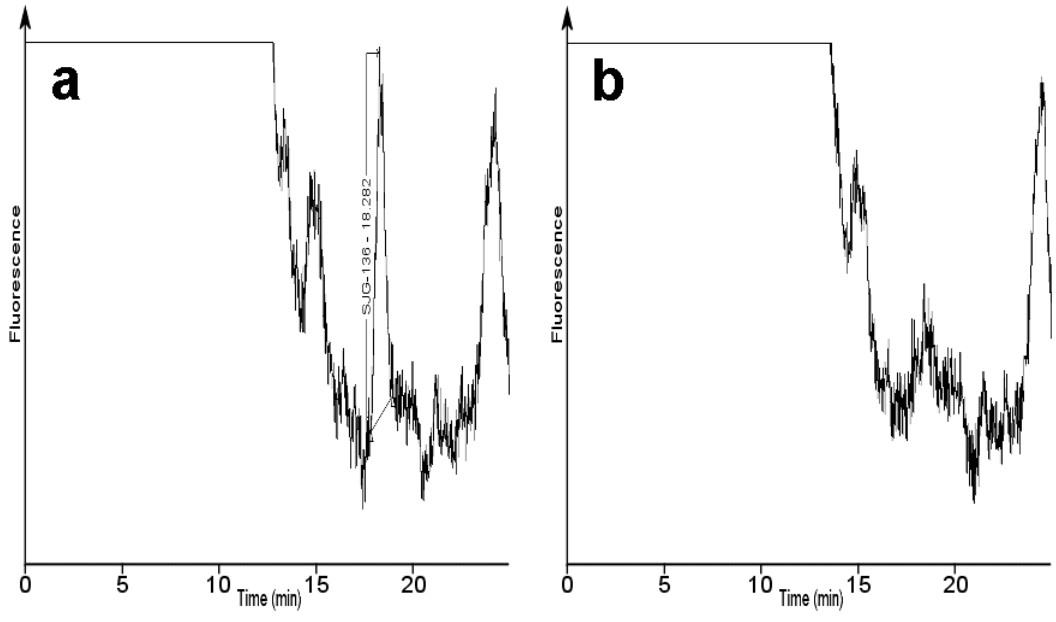

Figure 9.16 a) 5 nM SJG-136 extracted from mouse plasma. b) Blank extracted mouse plasma without added compound.

9.4 Clinical method development

The progression of SJG-136 to phase I clinical trials necessitated the development of an appropriate method for extraction of SJG-136 from human samples. All work was performed using pooled human sera (Sigma) due to ethical problems in obtaining fresh human blood and plasma. While there was no technical reason why the extraction method developed for murine samples could not be used for human samples, the starting dose for SJG-136 in man will be many times lower than the MTD in mice. This reduced starting dose will probably require a lower limit of detection, therefore a method that will make use of the increased sample volume obtained from patients (typically 1 ml or above) to extract drug and concentrate it to enable increased detection of drug was required. Extracting drug from 1 ml of sera and concentrating the sample into 100 µl to give a 10-fold increase in drug concentration (and thus a lower limit of detection) was desirable. To this end, alternative methods of extraction were investigated.

9.4.1 MeCN protein precipitation

Extraction of SJG-136 from 100 µl of sera using an identical method to that described (section 8.3.8.1) for extraction from murine samples, yielded an extraction efficiency of 60.9 ± 10% (mean ± %RSD). While this extraction efficiency was adequate, it did not include a concentration step and thus there is no increase in sensitivity of the assay overall. Using 100 µl rather than all of the available 1 ml ignores the possibility of increased limit of detection via use of a concentrating step.

Optimisation of this method in view of the evaporation issues discussed in section 9.4.3.2, and increasing the volume of sera extracted from 100 µl to 500 µl (to which 1

ml of MeCN was added for protein precipitation) indicated potential extraction efficiencies of approximately 95% while still including a concentration step. However, it was not possible to further investigate the reproducibility and validation of this method due to time constraints.

9.4.2 Ethyl acetate extraction

Ethyl acetate protein precipitation was investigated as a potential extraction procedure, however preliminary investigations indicated an unacceptably low extraction efficiency using this method (20%; $n = 2$). Consequentially this was not investigated further.

9.4.3 Solid phase extraction

Solid phase extraction (SPE) was investigated for extraction of SJG-136 from human sera. There were several steps in the development and optimisation of this method as it is a chromatography-based extraction method and as such requires selection of optimal SPE cartridge packing material (the solid phase), elution solvents and factors such as modulation of pH.

9.4.3.1 SPE cartridge selection

SJG-136 was extracted from 1 ml of human sera using a simple water/MeCN-based extraction method for selection of cartridge packing material. It was found that cyanopropyl endcapped (CN-E) cartridge packing material produced the highest extraction efficiency (Table 9.4). This extraction method development did not initially include a concentrating evaporation step, but was used purely to assess the efficiency of the cartridges investigated.

Extraction cartridge	Extraction efficiency ± CV
CN-E	82 ± 7.4%
C18-E	66.8 ± 3%
C8-E	68.6 ± 2.2%
C2-E	56.4 ± 29.8%
Phenyl	56.1 ± 26.8%

Table 9.4 Comparative extraction efficiencies for SJG-136 from human sera using a variety of available solid phase extraction cartridges (mean ± SD; $n = 3$).

Due to the selection of a phenyl column for HPLC analysis, it was expected that the phenyl SPE cartridge would give the highest extraction efficiency. However, the data showed that CN-E based cartridges offered an approximate 15% advantage over the next best cartridge. Consequently, CN-E cartridges were selected for further development of the SPE extraction method.

9.4.3.2 Effect of evaporation on extraction efficiency

In order to achieve a 10-fold increase in concentration of drug from a 1 ml sample as desired, it was necessary to include an evaporation step in the extraction process. The MeCN eluate from the SPE was evaporated to dryness and reconstituted to one tenth of the original volume in mobile phase and analysed. This was designed to produce a 10-fold increase in peak area relative to the un-evaporation concentrated eluate, and therefore a tenfold increase in the limit of detection. However it was found that the inclusion of an evaporation step into the extraction process resulted in a drastic drop in relative extraction efficiency from 82% when not evaporated to 30-45% when

concentrated by evaporation. Inter-day reproducibility of the extraction technique became highly variable alongside this development.

To isolate the step within the extraction process causing loss of compound, each step of the process was investigated. The evaporation step proved to be the cause, as it was observed that spiking drug into MeCN alone and evaporating to dryness did not result in 100% recovery of compound as expected. Factors investigated to identify the cause of this loss of compound during evaporation were microcentrifuge tube selection and temperature.

9.4.3.2.1 Tube selection

The possibility of sample tube material contributing to the loss of compound during the evaporation step was considered. Several different sample tube types were used; siliconized tubes were investigated as siliconization may alter binding of compound to sample tube surfaces. Several sample tube types were used, and the full extraction procedure was performed to assess impact of tube material.

It was observed that the polypropylene sample tubes previously used in method development resulted in the highest extraction efficiency (Figure 9.1). However, only a small difference in extraction efficiency was observed by changing sample tube material (difference between most inefficient and efficient tubes was observed to be 15%). Interestingly, siliconisation, which was used to reduce loss of compound by preventing binding to sample tube material, actually resulted in a lower recovery of compound.

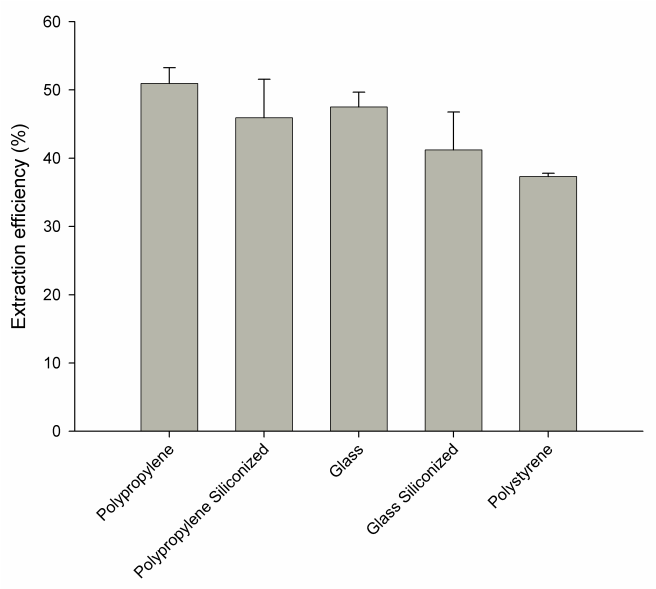

Figure 9.17 Effect of sample tube selection on extraction efficiency of SJG-136 using SPE method (mean ± SD; $n = 4$).

9.4.3.2.2 Temperature

To assess the effect of temperature on recovery from evaporation, MeCN spiked with SJG-136 was aliquoted into polypropylene sample tubes and samples were evaporated to dryness then reconstituted in mobile phase and analysed on the HPLC system. No extraction step was included. Samples were either evaporated at 37 °C or at room temperature.

Analysis showed that after evaporation at 37 °C only 41% of SJG-136 was recovered, whereas evaporation at room temperature resulted in recovery of 86% of compound. This indicated that temperature at which the evaporation step is performed (routinely 37 °C) leads to a loss of compound and a reduced extraction efficiency. This may be due to temperature-induced degeneration of compound, or could be a result of temperature-induced binding of SJG-136 to the sample tubes. Ideally, radiolabelling of the compound would allow the loss of compound to be traced, but this facility was

unavailable for the present study. As a result of these data, all further evaporation was carried out at room temperature to minimise loss of compound.

9.5 Pre-clinical pharmacokinetics

9.5.1 Protein binding

9.5.1.1 Ultrafiltration

Preliminary studies of protein binding of SJG-136 using ultrafiltration indicted that this method would be unsuitable for use with SJG-136. SJG-136 was observed to show a high level of binding to the filter membrane. This was assessed by comparing SJG-136 diluted in PBS passed through the filter to SJG-136 in PBS not passed through the filter membrane. While it may be possible to estimate protein binding by comparison of filtered SJG-136 in PBS to an unfiltered standard to calculate percentage of compound bound to the filter membrane, the binding of drug to filter would be liable to introduce a significant margin of error.

At an SJG-136 concentration of 500 nM, only 11.3 ± 2.2% (n = 3) of compound was recovered from a filtered standard (SJG-136 diluted in PBS), indicating extensive binding of SJG-136 to the filter membrane. From murine plasma, 4.8 ± 2% (n = 3) of SJG-136 was recovered by ultrafiltration. This method of assessment of protein binding indicates moderate binding of SJG-136 to plasma proteins (approximately 57% drug bound). However, due to the high degree of non-specific binding to the filter, alternate methods of assessing protein binding were investigated.

9.5.1.2 Ultracentrifugation

Using ultracentrifugation to precipitate sera proteins enabled circumvention of the filter membrane binding seen with ultrafiltration. Recovery from ultracentrifuged samples was checked by comparison of standards of SJG-136 in PBS after centrifugation with samples that had not been centrifuged, and was found to be 91.4 ± 10.8% (mean ± SD) in human sera. Human serum was used in these studies as ethical issues prevented the sacrifice of animals to obtain the increased volume of plasma needed for ultracentrifugation studies; human plasma was unavailable. However, the use of human biological fluids should give a more accurate prediction of pharmacokinetic parameters in man.

Protein binding was calculated by comparison of spiked SJG-136 samples with identical spiked PBS standards after ultracentrifugation. Protein binding was calculated to be 78.2% and 82.3% at 1000 nM and 100 nM respectively (Table 9.5), SJG-136 could not be detected in 10 nM samples due to chromatographic interference.

SJG-136 concentration (nM) in human sera	% protein bound (mean ± SD)
1000	78.2 ± 10.6%
100	82.3 ± 13.1%
10	n / d

Table 9.5 Assessment of % of SJG-136 bound to human sera protein using ultracentrifugation (n = 4).

The major difference between plasma and serum is the lack of fibrinogen and clotting factors in serum. Studies have suggested that in the majority of cases there is little drug

binding to fibrin, fibrinogen or other components of the blood clot, making use of plasma or serum essentially identical. The major pharmacokinetically important components such as albumin and α1-acid glycoprotein are present in both serum and plasma at equivalent levels (Lum & Gambino, 1974; Sadee *et al.*, 1980). Other sources suggest that use of serum is preferable to plasma as this avoids the possibility of interference with anticoagulants necessary to prevent clotting when using plasma (Kwon, 2001). These data indicate that SJG-136 shows a moderate level of protein binding, as it could be estimated that at any given time in systemic circulation approximately 20% of drug present will be unbound to plasma/serum proteins.

It is of note that total plasma protein in man is comparable to total plasma protein found in mouse (per unit weight). However, of the two major plasma proteins, albumin and α_1-acid-glycoprotein, albumin levels in man are similar to those found in the mouse whereas there is a 10-fold difference in the amount of α_1-acid-glycoprotein found (Davies & Morris, 1993). It may be of use to characterise the level of binding of SJG-136 to α_1-acid-glycoprotein in order to better predict pharmacokinetic differences that may be seen moving from mouse to man (i.e. more or less free drug in plasma); it would also be helpful to characterise the level of plasma or sera protein binding seen in the mouse for the same reason.

9.5.2 Stability in blood and plasma

Stability of SJG-136 in murine blood and plasma was assessed to determine the possibility of degradation of drug *ex vivo* during sample handling. Characterisation of SJG-136 stability was performed over a 6 h period, with SJG-136 spiked into blood and

plasma to a final concentration of 100 nM and incubated at 37 °C for the duration of the experiment.

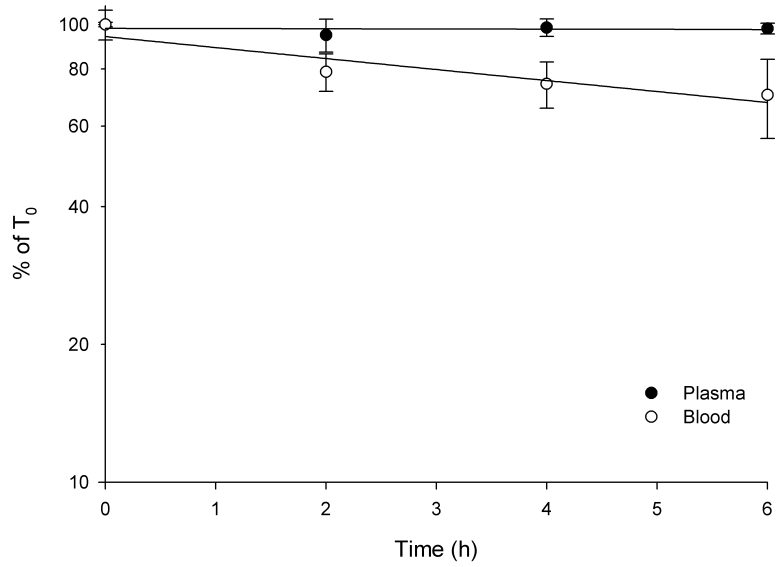

Figure 9.18 Stability of SJG-136 in murine plasma over time at 37 °C. Values are expressed as a % of drug recovered at t = 0 h (mean ± SD; *n* = 3).

SJG-136 was stable in plasma, with no appreciable loss of compound up to 6 h. In blood, SJG-136 showed a gradual loss of recovery of compound over the 6 h of the experiment. The half-life of SJG-136 in plasma and blood was calculated by fitting a log-linear curve to the plasma and blood data points, and extrapolating to 50% recovery. Due to the apparent lack of degradation of SJG-136 over the 6 h time period of the experiment, extrapolation of the curve indicated a half-life in plasma of SJG-136 in excess of 24 h. Half-life in blood was calculated as 11.5 h. These data imply that sample processing should be rapid in that plasma should be separated from blood as soon as possible *ex vivo*. As demonstrated, the plasma stability indicates that there is unlikely to be any significant loss of compound from plasma during sample handling.

9.5.3 *In vivo* intra-peritoneal pharmacokinetics

The pharmacokinetic plasma time-course of SJG-136 in the NCR-Nu mouse was evaluated following i.p. administration of SJG-136 at the i.p. MTD of 0.2 mg kg^{-1} (Figure 9.19).

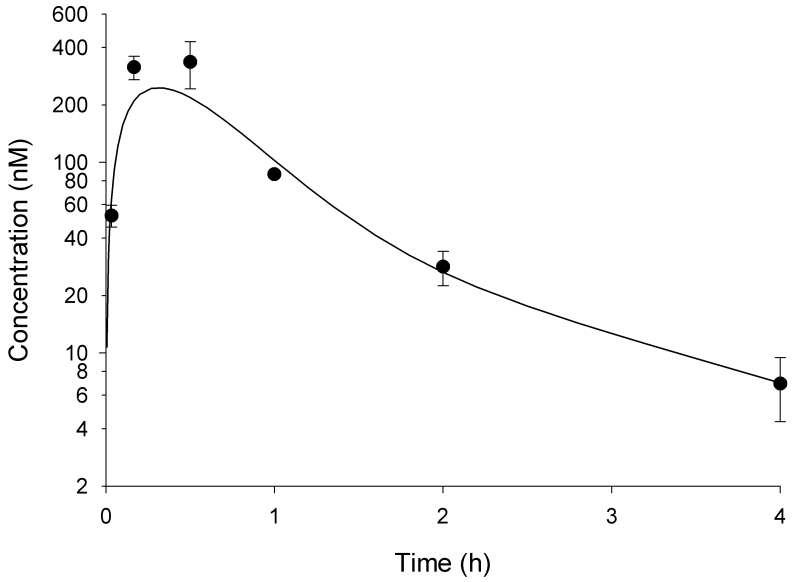

Figure 9.19 SJG-136 concentration (mean ± SD) versus time profile in NCR-Nu mouse plasma following i.p. administration at 0.2 mg kg^{-1} (n = 3, LOQ = 5 nM). Curve shows fit using 3 compartment model (Equation 4: C_1 = 2776, C_2 = 70, k_a = 3.8, k_{el1} = 3.1, k_{el2} = 0.6).

The area under the concentration time curve (AUC) was calculated to be 337.9 nM h (188.1 ng h ml^{-1}). Terminal elimination half life from plasma was moderate, with a calculated $t_{½}$ of 1.2 h (k_{el} calculated as 0.58 h^{-1} by curve fitting, $t_{½}$ calculated as $ln2$ / k_{el}). A moderate plasma clearance of 17.7 ml min^{-1} kg^{-1} (approximately 20% of murine hepatic blood flow; calculated assuming complete absorption from the peritoneal cavity) was calculated for SJG-136. SJG-136 was not detectable after 4 h post dose. C_{max} of SJG-136 was detected at 30 min post-dose as 315.7 nM (175.7 ng ml^{-1}).

9.5.4 *In vivo* intravenous pharmacokinetics

Further to the i.p.-dosed pharmacokinetic study, SJG-136 was administered i.v. at the MTD (0.3 mg kg^{-1} via the i.v. route) and ⅓MTD (0.1 mg kg^{-1}) to HL-60 (a human-derived promyelocytic leukaemia cell line) tumour-bearing NCR-Nu mice. Plasma, tumour and brain were analysed at each time point for concentration of SJG-136 in order to determine pharmacokinetic parameters. Tumour and brain were assessed in this case principally to establish whether SJG-136 reaches the tumour following i.v. dosing, and brain was analysed to determine SJG-136 penetration into the central nervous system.

9.5.4.1 Intravenous MTD pharmacokinetics

SJG-136 was easily detectable in plasma, tumour and brain following i.v. administration of drug at the MTD (Figure 9.20). SJG-136 appeared to have a low terminal elimination half-life in plasma of 0.66 h (k_{el} calculated as 1.05 h^{-1} using a two compartment model curve fit). A moderate plasma clearance of 11.8 ml min^{-1} kg^{-1} (approximately 14% of murine hepatic blood flow), similar to the value obtained for plasma clearance following i.p. dosing, was calculated. The AUC was shown to be 759.8 nM h (422.9 ng h ml^{-1}) with C_{max} of 4.8 μM (2.7 μg ml^{-1}) at 2 min post-dose. Volume of distribution was calculated as V_{ss} 239 ml kg^{-1} or V_z 743 ml kg^{-1}. The i.v. AUC data was used to calculate the bioavailability of SJG-136 via the i.p. route; SJG-136 was found to be 67% bioavailable via the i.p. route.

Levels of SJG-136 in the tumour reached an easily detectable C_{max} of 72.4 nM at 2 min, with an AUC of 22.2 nM h (12.4 ng h ml^{-1}). The elimination half life of SJG-136 from the tumour was 0.18 h (with an elimination rate constant of 3.6 h^{-1}). Levels of drug in the brain were found to reach a C_{max} of 30.2 nM at 2 min post-dose, with an AUC of 5.1 nM h (2.8 ng h ml^{-1}). The elimination rate constant was calculated to be 3.78 h^{-1}, resulting in an elimination half life of 0.18 h.

SJG-136 was below the limit of detection in plasma after 4 h post-dose, after either 30 min in tumour or 15 min in brain. Curve fits on all 3 concentration time profiles showed good correlation for data fitted using a 2 compartment pharmacokinetic model.

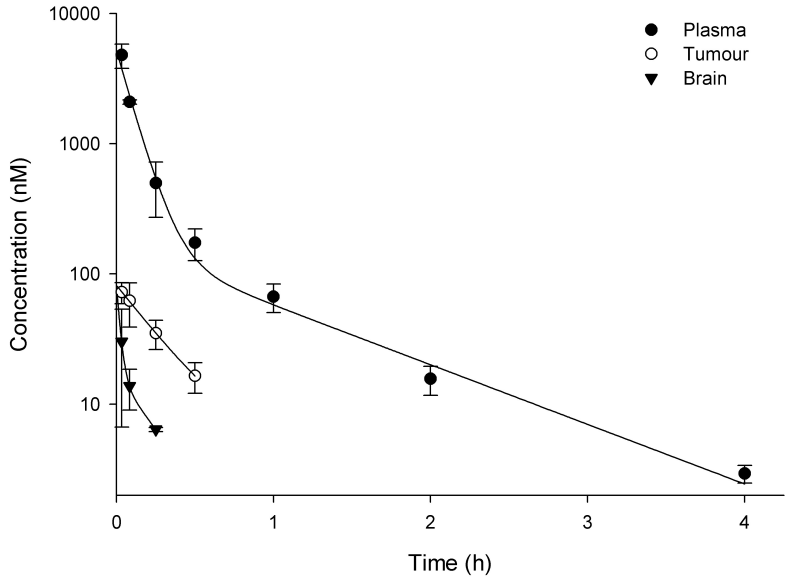

Figure 9.20 SJG-136 concentration versus time profile (mean ± SD; n = 3) in HL-60 tumour-bearing NCR-Nu mice, in plasma, tumour and brain following i.v. administration at the MTD (0.3 mg kg^{-1}).

LOQ for detection of SJG-136 in tumour was 20 nM, calculated from a 5 nM LOQ in spiked tumour homogenate, and corrected from the initial 4-fold dilution (w/v) of

tumour in buffer to calculate concentration in tissue. LOQ for detection of SJG-136 in brain was 8 nM, calculated from a 2 nM LOQ in spiked brain homogenate, and corrected from the initial 4-fold dilution (w/v) of brain in buffer to calculate concentration in tissue. This equates to an LOQ of 11.1 ng g^{-1} tumour tissue, and 2.8 ng g^{-1} in brain tissue. When considering the detection of SJG-136 in tumour or brain samples, it is important to be aware that it was not possible to remove blood that was perfused into the tissues after removal. Consequentially it is unknown whether there is enough blood within the tissue to result in the levels of drug detected, and thus detected compound may not accurately reflect the amount of agent within the tissue itself. In brain, it is suggested that there is 30 µl of blood per gram of tissue (Altman & Dittmer, 1971), as 200 µl of tissue homogenate was used for analysis (1:4 dilution w/v in PBS); this equates to 50 µg of brain per sample, a minute amount of tissue relative to the concentration detected. This indicates that it is unlikely that the concentration detected within the brain tissue is solely a result of blood present. It is difficult to estimate the volume of blood within the tumour, hence it cannot be assessed if the levels of SJG-136 detected can be accounted for by remaining blood.

9.5.4.2 Intravenous ⅓MTD pharmacokinetics

SJG-136 was also studied *in vivo* at ⅓MTD to determine linearity of the plasma pharmacokinetics at different dose levels (i.e. ⅓MTD should result in ⅓ of the AUC compared to the AUC for dosing at the MTD). Administration of SJG-136 via the i.v. route at ⅓MTD resulted in easily detectable levels of drug in plasma (Figure 9.21). The terminal elimination half-life of SJG-136 in plasma was calculated to be 1.44 h (calculated from an elimination rate constant of k_{el} = 0.48 h^{-1}; determined from a two-compartment model curve fit). A moderate plasma clearance of 12.88 ml min^{-1} kg^{-1}

(approximately 15% of murine hepatic blood flow) was calculated, and was observed to correlate closely to both the previous i.v. MTD study and the earlier i.p. MTD study. The AUC was calculated as 232.6 nM h (129.5 ng h ml^{-1}), approximately 31% of the i.v. MTD study, showing linearity of pharmacokinetics over a threefold concentration range with high linear correlation. C_{max} was observed at 2 min post dose as 1.6 μM (0.89 μg ml^{-1}). Volume of distribution was calculated as V_{ss} of 245 ml kg^{-1} or V_z of 368 ml kg^{-1}.

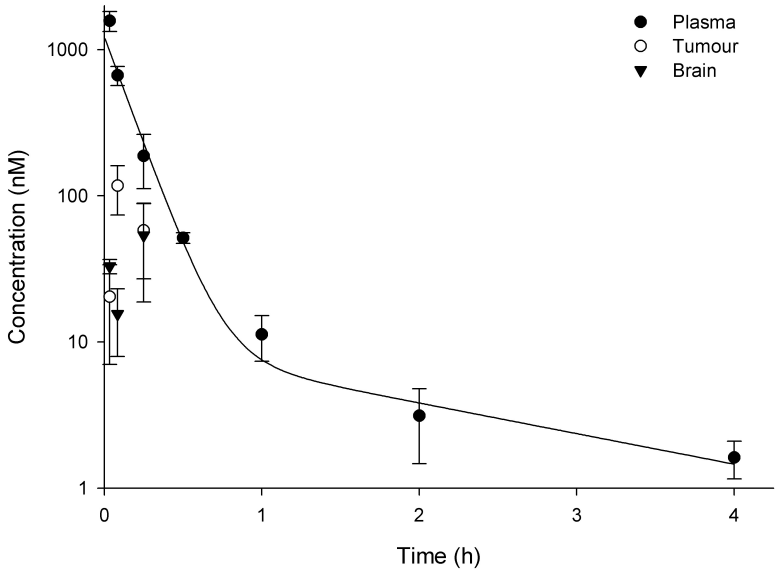

Figure 9.21 SJG-136 concentration versus time profile (mean ± SD) in HL-60 tumour bearing NCR-Nu mice, in plasma, tumour and brain following i.v. administration at ⅓MTD (0.1 mg kg^{-1}).

SJG-136 was detectable in both brain and tumour samples; however, detected levels were erratic and could not be fitted with a pharmacokinetically relevant curve fit. This produced difficulties in extrapolating back to the axis to predict $C(0)$ values and values for k_{el}. Consequentially tissue $t_{½}$ values could not be calculated and AUC values were

calculated as areas under detectable time points rather than by extrapolation to $t = 0$ and $t = \infty$. C_{max} was found to be 117.1 nM (65.1 ng ml^{-1}) at 5 min in the tumour, and 53.5 nM (29.8 ng ml^{-1}) at 15 min in the brain samples.

SJG-136 was below the limit of detection in plasma after 4 h or after 15 min in tumour and brain samples. The curve fit of the plasma time course showed good correlation ($r^2 > 0.9$).

9.6 Metabolic stability

The metabolic stability of SJG-136 was investigated using the analytical method developed for the pharmacokinetic studies (section 8.3). The aim of the metabolism study was to assess the stability of SJG-136 in liver-derived tissues and to identify the formation of any metabolites. *In vitro* models for murine metabolism were used in a predictive manner to identify potential *in vivo* metabolites.

9.6.1 Liver S9 fraction

The liver S9 subcellular fraction contains both microsomal and cytosolic enzymes and is capable of both phase I and phase II metabolism. While the S9 fraction is often considered a crude preparation for metabolism studies, the presence of both phases of metabolism suggested it was a good predictive *in vitro* model for hepatic metabolism of SJG-136 *in vivo*.

Experiments with the liver S9 fraction indicated rapid metabolism of SJG-136, resulting in a mean recovery of 9.9 ± 0.75% at time t = 0 h, with no significant metabolism after this point (Figure 9.22). SJG-136 was found to be stable in PBS and plasma over the time period investigated in this study. It was observed that the chromatographic profile of samples injected after extraction from S9 incubations showed remarkable similarity to other work investigating the reactivity of SJG-136 with GSH (section 12.3). Therefore it was possible the metabolism seen in the S9 fraction is skewed by reactivity of SJG-136 with GSH.

Preparation of the S9 fraction involves mechanical processing of liver tissue, and subsequent lysis of cells will therefore release the GSH contained therein, reported to be

(dependent on cell type) typically in the 5 – 20 mM range. Studies have shown that levels of GSH in murine liver homogenate are in the region of 5 mM (Kim *et al.*, 2003). Concentrations of GSH in this range were shown to drastically affect recovery of SJG-136, resulting in a poor recovery of drug (section 12.1). It was therefore concluded that results obtained from an S9 fraction may be an inaccurate reflection of metabolism of the drug as a result of this phenomenon.

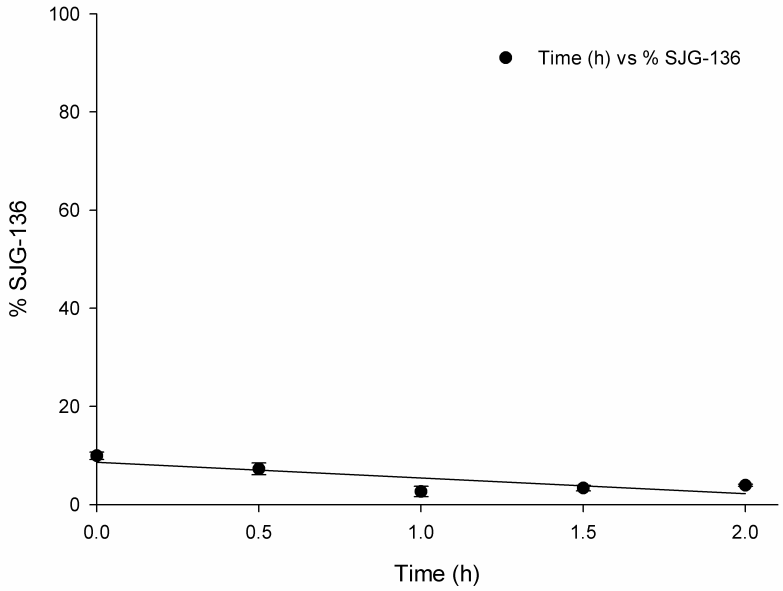

Figure 9.22 Percentage recovery of SJG-136 from liver S9 fraction relative to time after incubation at 37 °C (mean ± SD; n = 3).

9.6.2 Microsomal incubation

Hepatic microsomes are a subcellular fraction obtained from differential centrifugation of liver homogenate. Mainly consisting of membrane-bound endoplasmic reticulum fragments (vesicles), this preparation predominantly contains enzymatic capacity for phase I reactions due to a lack of the cofactors required for phase II conjugative reactions. A key factor in the use of hepatic microsomes for this study was the removal of GSH from the preparation via an ultracentrifugation step, in order to assess the

metabolic potential of SJG-136 without the effect of the non-enzyme-mediated reactivity of the compound with GSH.

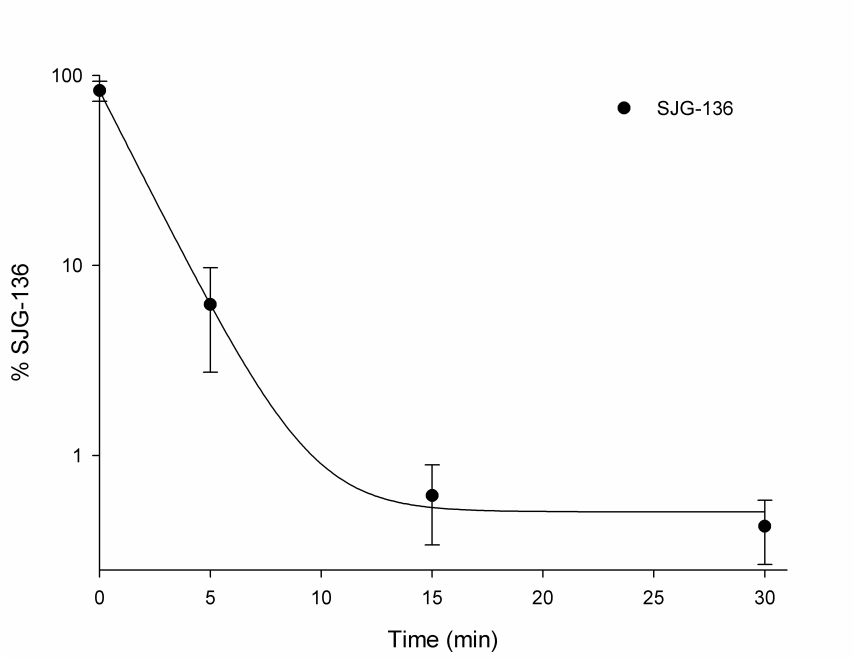

Figure 9.23 Metabolism of SJG-136 incubated with hepatic microsomes. Percentage recovery of SJG-136 from liver microsomal fraction relative to time after incubation at 37 °C (mean ± SD; n = 3). Line denotes a bi-exponential curve fit to illustrate biphasic nature of SJG-136 metabolism.

Incubation of SJG-136 with microsomes indicates a rapid metabolism of the compound over the first 15 min, with a half-life of SJG-136 in the microsomal incubation calculated from a biphasic curve fit equation as 0.96 min (Figure 9.23). Levels of SJG-136 in the microsomal incubation fell below the limit of detection after 30 min. There was no apparent metabolism / disappearance of SJG-136 in either heat inactivated microsomes or buffer (PBS) containing NADPH alone.

9.6.3 Metabolite identification

For metabolite identification studies, a high concentration of SJG-136 (50 μM) was incubated with hepatic microsomes, as a measure to produce high concentrations of metabolite. Metabolite identification was carried out by LC-MS analysis of the microsomal incubation of SJG-136, scanning from *m/z* 150 – 600, alongside fluorescence detection. It was necessary to use a high concentration of SJG-136 to compensate for the relatively insensitive (compared to fluorescence detection) scanning method of the mass spectrometer. After the HPLC run, these data were scrutinized for the presence of compound masses corresponding to potential SJG-136 metabolites, as defined from predictions of potential sites of metabolism based on compound structure.

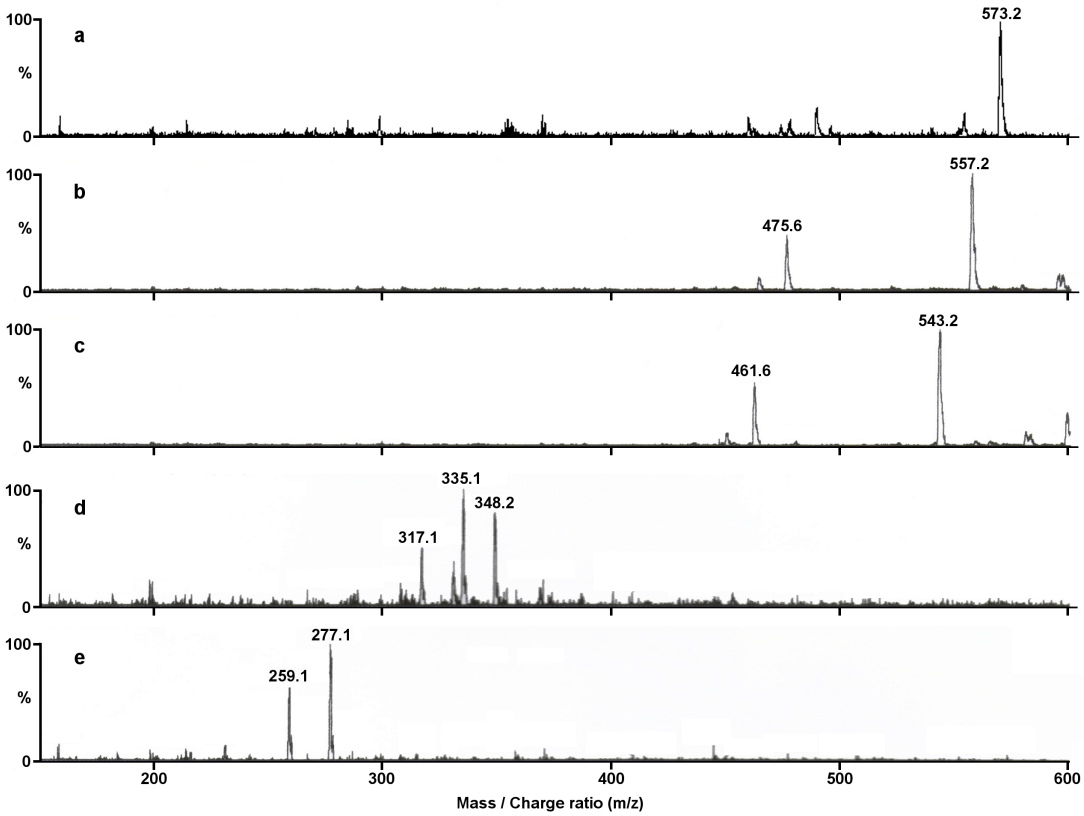

Figure 9.24 Mass spectra of SJG-136 and potential metabolites at a) 26.5 min, b) 25.3 min (SJG-136), c) 23.7 min, d) 18.1 min, and e) 15.5 min.

Several peaks at masses corresponding to potential metabolites were identified by examining the mass spectra extracted from scans performed during the sample run (Figure 9.24). The MW derived from the mass spectra were correlated to structures based on predictive metabolism from examination of the SJG-136 molecular structure (Table 9.6). These data were used to extract chromatograms of potential metabolites (see Figure 9.25).

Molecular weight (Exact MW)	Retention time (min)	Probable structure
572.61 (572.23)	26.5	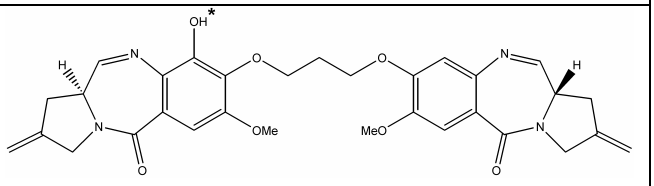
556.61 (556.23) SJG-136	25.3	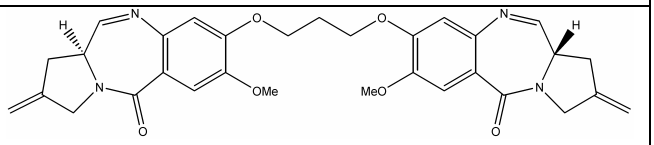
542.59 (542.22)	23.7	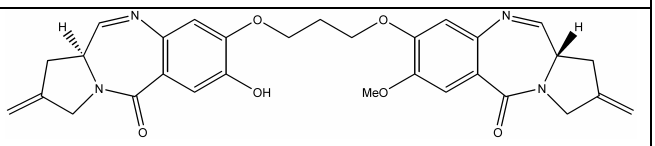
348.39 (348.17)	18.1	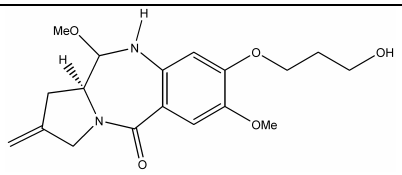
334.37 (334.15)	18.1	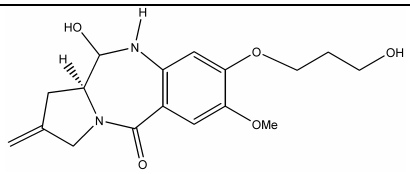
316.35 (316.14)	18.1	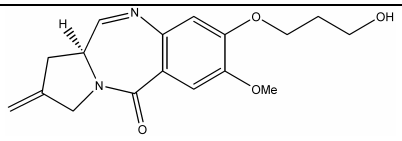
276.29 (276.11)	15.5	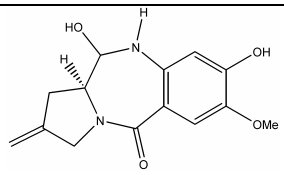
258.27 (258.10)	15.1	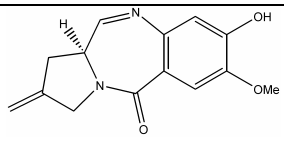

Table 9.6 Potential SJG-136 metabolites detected following incubation with hepatic microsomes, listed as MW with possible structures (* denotes hydroxyl group which may be attached to any similar ring position). Metabolites were detected using LC-MS (scan *m/z* 150 – 600).

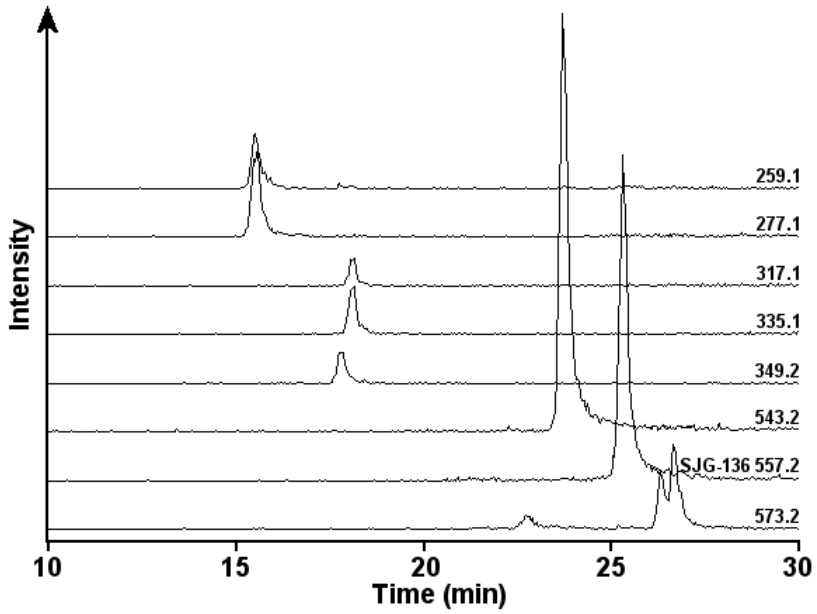

Figure 9.25 Chromatograms for SJG-136 and potential metabolites extracted from MS scan after incubation of SJG-136 with liver microsomes. Chromatograms are shown offset, and on the same scale to enable comparison of intensities for detected ions.

Of the several metabolites identified, the metabolite corresponding to *O*-dealkylation on one of either (but not both – interestingly this was not detected) benzene rings of SJG-136 produced the largest peak in the chromatogram. It is possible that metabolic dealkylation on one of the rings results in a 3-dimensional structural shift rendering the opposing group inaccessible to metabolic enzymes; further work with molecular modelling studies would be required to investigate this. Assuming equivalent response of the MS to this highly structurally similar metabolite compared to SJG-136 and other metabolites, this appears to be the major metabolite produced by microsomal metabolism. As expected due to the nature of the microsomal model, no phase II conjugative metabolic products were detected.

9.6.4 Metabolite detection *in vivo*

Following detection of a major metabolite at *m/z* 542.59, a highly sensitive LC-MS/MS method was developed to attempt to detect the metabolite in *in vivo* PK samples. A daughter ion for SJG-136 was identified at *m/z* 475.6 (seen in the mass spectra for SJG-136 after incubation with microsomes; Figure 9.24) and an apparent corresponding daughter ion is seen for the metabolite at *m/z* 461.6. These were used to tune the MS/MS to SJG-136, and to set up a multiple reaction monitoring (MRM) detection method. Due to lack of isolated metabolite, SJG-136 was used to tune the instrument for both compounds, therefore the method was optimised using SJG-136. To investigate the appearance of the metabolite *in vivo*, a 30 min PK sample (time point selected as maximum concentration of SJG-136 was detected at this time) from the i.p. pharmacokinetic study (section 9.5.3) was analysed using the optimised method for MS/MS detection of SJG-136 and metabolite.

The metabolite was detected *in vivo* (Figure 9.26). As metabolite was not available in an isolated form to produce calibration curves, for the sake of comparison of relative abundance of metabolite versus SJG-136 in the *in vivo* sample, it was assumed that the mass spectrometer gave an equivalent response per unit metabolite to SJG-136. This assumption is reasonable given the predicted high structural similarity of the compounds. Integration of the peaks gave peak areas for SJG-136 of 370555 versus a peak area in the sample of 4409 for the metabolite. This equates to approximately 1.2% of total detected SJG-136 converted to the metabolite at the 30 min time point *in vivo*. Comparison with the *in vitro* microsomal metabolism data (section 9.6.2), which indicate rapid metabolism of SJG-136, suggests a low metabolic potential for the SJG-136 dimer *in vivo*.

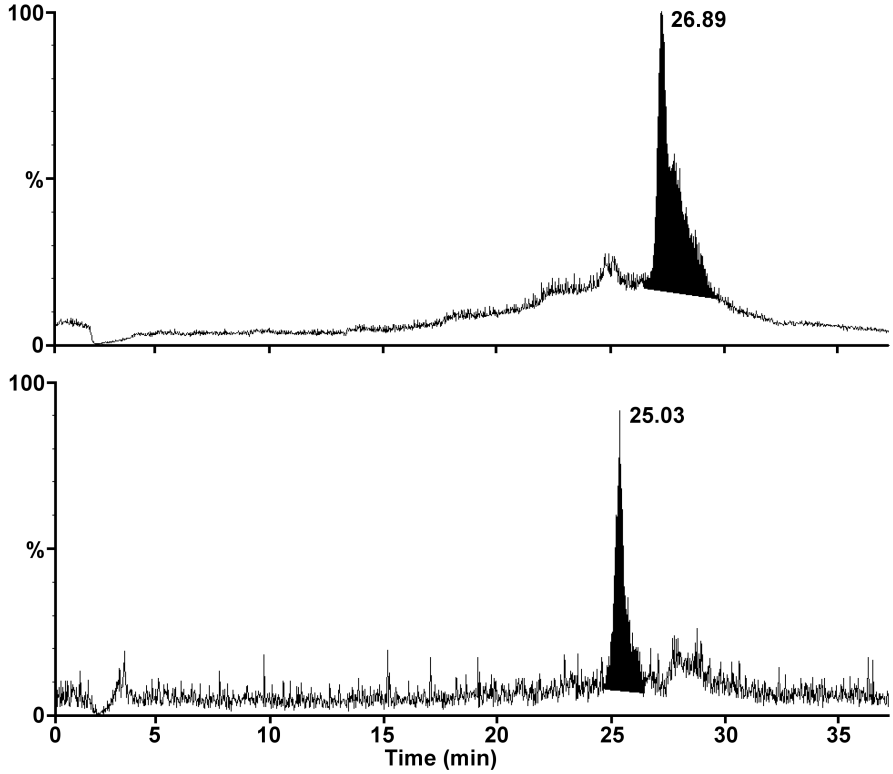

Figure 9.26 Detection of SJG-136 and major metabolite *in vivo* (30 min post-dose; i.p. dose @ 0.2 mg kg^{-1}) using LC-MS/MS. SJG-136 (a) was detected at 26.9 min, and metabolite (b) was detected at 25.0 min post injection.

Time constraints prevented a re-analysis of the full pharmacokinetic profiles (i.p. and both i.v. profiles) for characterisation of the total extent of metabolite production. It is entirely possible that further time points would show an increase detected metabolite as levels of SJG-136 decrease (possible conversion to metabolite). Furthermore, in an *in vivo* situation there is potential for further metabolism and formation of conjugates derived from phase II metabolic processes. However, this study demonstrates the usefulness of the *in vitro* microsomal model, as the predicted metabolite was detected.

9.7 Cellular effects of SJG-136

In order to better characterise the effects of SJG-136 at the cellular level, several models were used to assess toxicity, localisation and cell cycle effects of SJG-136. Cytotoxicity of the parent PBD dimer compound was assessed in selected cell lines to investigate reproducibility of previous data and to determine cell-type selective cytotoxicity.

The ability of SJG-136 to bind to chromosomal DNA was investigated to verify its DNA interactivity and to examine proposed sequence selectivity of the compound. In addition to this, as the pharmacodynamic endpoint of SJG-136 is interstrand DNA crosslinking *in vivo*, the level of crosslinking achieved in an *in vivo* murine system was assayed to assess pharmacodynamic efficacy of SJG-136 as a function of DNA crosslinking achieved.

The effect of SJG-136 on cell cycle was studied in an *in vitro* system to help elucidate the mechanism of action of this agent, and to correlate its behaviour with previous DNA interstrand crosslinking agents.

Five cell lines were chosen for study based on data from the NCI 60-cell line screen data for SJG-136. Cell lines were chosen from the "fingerprint" of data (Figure 9.27) based on relative sensitivity or resistance to SJG-136 in order to identify any cell-type selectivity of the compound. Chosen cell lines were: M14 (melanoma), SK-MEL-2 (melanoma), UACC-62 (melanoma), SK-OV-3 (ovarian) and DU-145 (prostate).

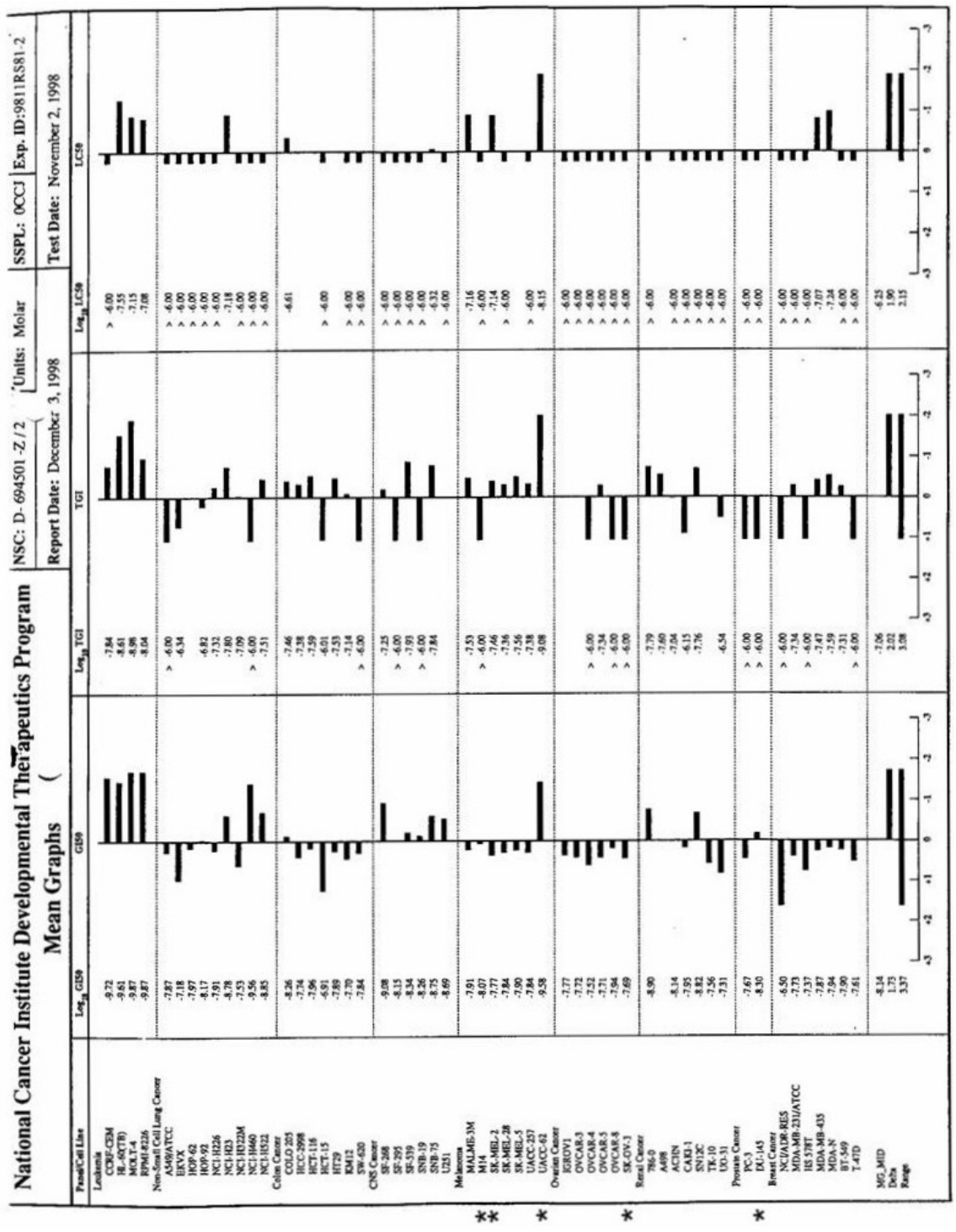

Figure 9.27 NCI 60-cell-line screen data for SJG-136. Data shows relative resistance or sensitivity of cell lines to SJG-136. * Denotes cell lines chosen for investigation in this study. From top to bottom, cell lines: M14, SK-MEL-2, UACC-62, SK-OV-3 and DU-145.

9.7.1 MTT cytotoxicity assay

The cytotoxicity of SJG-136 in the selected cell lines was assessed using the MTT assay method to determine the potential cell-type selectivity, and thus potential tumour selectivity of the compound. Growth curves were initially constructed to ensure that the seeding density of the cell lines allowed the cells to grow in the exponential growth phase for all five cell lines. It was found that at a seeding density of 2000 cells per well (i.e. 2000 cells per 200 µl; equivalent to 10000 cell per ml) for all cell lines showed exponential growth for each cell line studied over the eight day period (Figure 9.28).

Cytotoxicity of SJG-136 was investigated as either a continuous exposure of cells to the drug throughout the 96 h period of the experiment, or as a 1 h exposure to the drug after which drug was removed from culture medium; cells were washed and allowed to recover for the remaining 95 h of the experiment. The 1 h exposure allowed investigation of a more closely relevant *in vivo* exposure time of cells to SJG-136.

Exposure time (h)	IC50 value (nM) by cell line & cell type				
	DU-145 prostate	UACC-62 melanoma	SK-MEL-2 melanoma	SK-OV-3 ovarian	M14 melanoma
1	22.2 ± 2.6	16.6 ± 11	29.8 ± 5.5	18.38 ± 2.6	4.2 ± 0.7
96	0.5 ± 1.1	0.12 ± 0.33	1.3 ± 1.0	2.5 ± 1.4	0.4 ± 0.1

Table 9.7 IC_{50} values calculated for selected cell lines (mean ± SD; $n = 3$).

Cytotoxicity was assessed as IC_{50} (inhibitory concentration at which 50% growth reduction is observed versus untreated controls) values. IC_{50} values were calculated by plotting absorbance versus concentration of SJG-136 and the IC_{50} value was defined as the value at which 50% growth inhibition (defined as a 50% reduction in MTT absorbance) was seen (Figure 9.29, Figure 9.30). This was repeated in triplicate and

mean IC_{50} and standard deviation were calculated from these values. SJG-136 was observed to have a significant cytotoxic effect in each of the 5 cell lines studied, with both 96 h and 1 h exposure to the drug (Table 9.7). There is a range of cell sensitivities to SJG-136, up to 20-fold difference after 96 h exposure, and up to 7-fold difference after 1 h exposure. The IC_{50} values expressed for the SK-OV-3 cell line correlate closely with previously reported values of 9.1 nM for SJG-136 (Gregson *et al.*, 2001).

These data illustrate the potent cytotoxicity of SJG-136. Furthermore, the 1 h exposure data shown here indicates that a short exposure time of cells to SJG-136, as would be characteristic of an *in vivo* situation, can result in significant cytotoxic effect at low concentrations. Relating these data to the *in vivo* pharmacokinetic profiles of SJG-136 (section 9.5), it is shown that SJG-136 achieves concentrations well above the IC_{50} values in these cell lines, and maintains these levels for over the 1 h exposure used here, even when dosed at ⅓MTD.

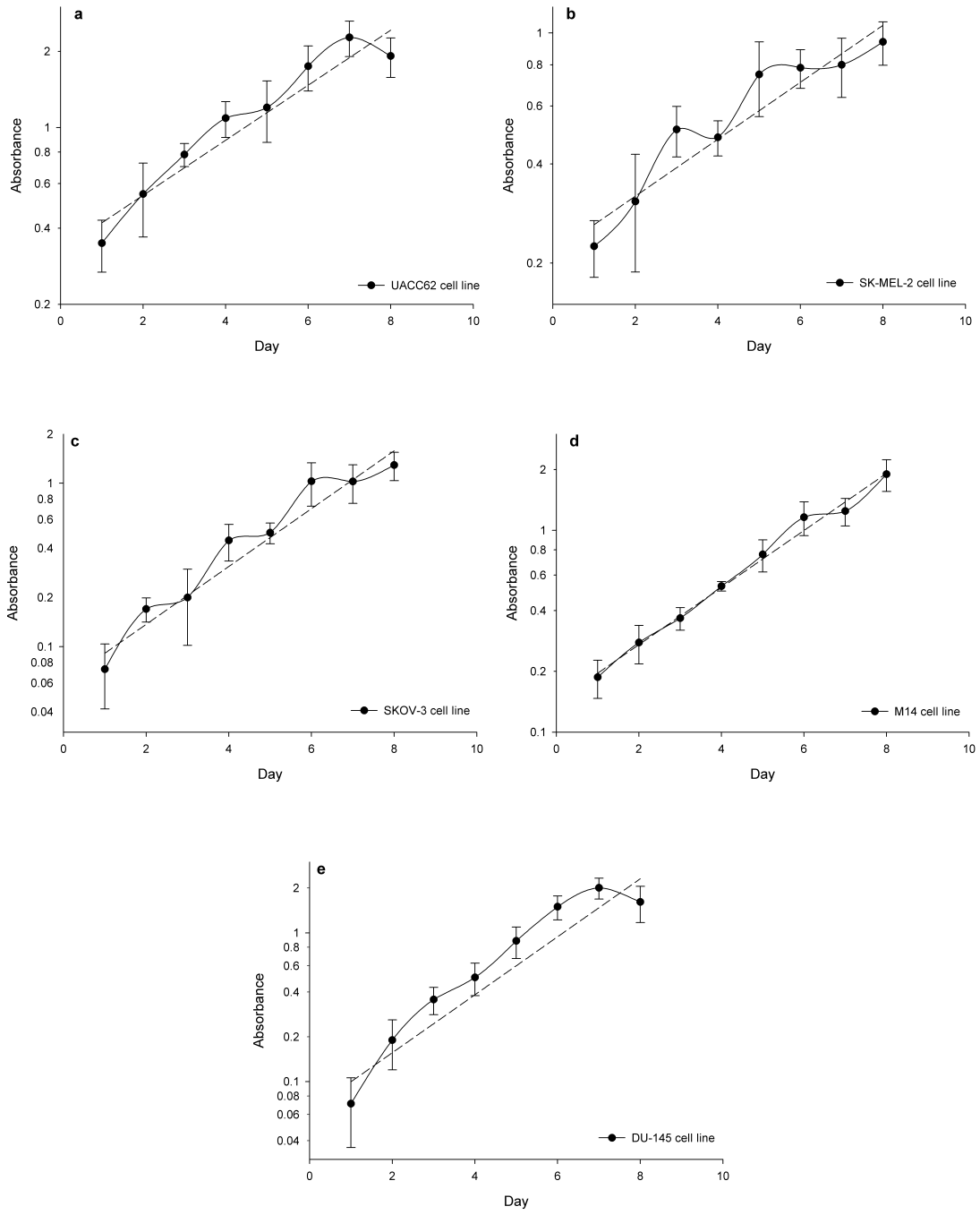

Figure 9.28 Growth curves for selected cell lines. Dashed line indicates exponential curve fit. Assayed as increase in absorbance using the MTT dye conversion assay over time (*y* axis plotted on log scale; mean ± SD). Cell lines (+ doubling times) a) UACC62 (2.8 days), b) SK-MEL-2 (3.2 days), c) SKOV-3 (1.7 days), d) M14 (2.1 days) and e) DU145 (1.5 days).

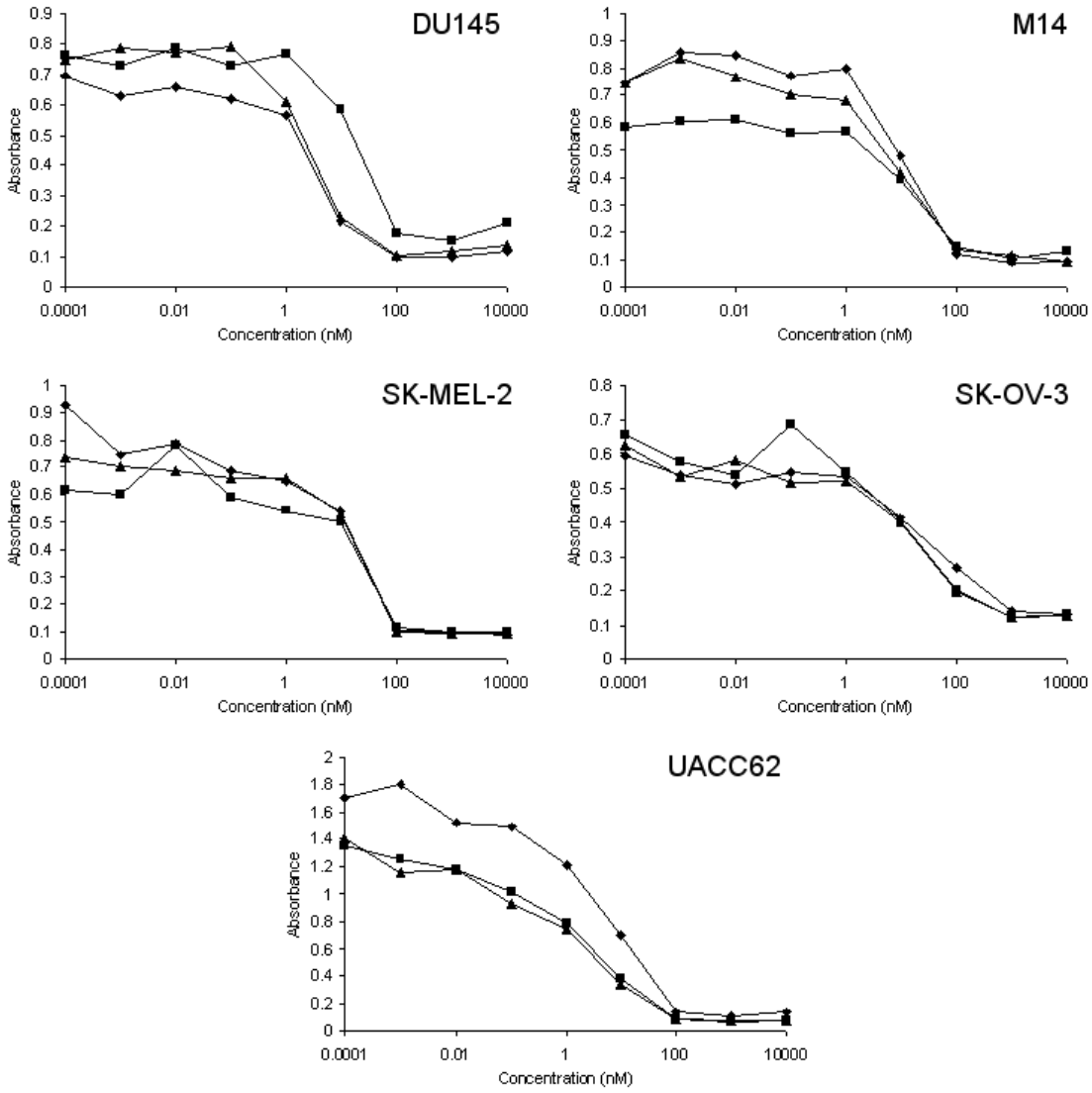

Figure 9.29 Dose response curves showing MTT absorbance (at 550 nm) versus concentration of SJG-136. Cells lines used noted on graph. Cells incubated with SJG-136 for 96 h continuously. 3 independent replicates.

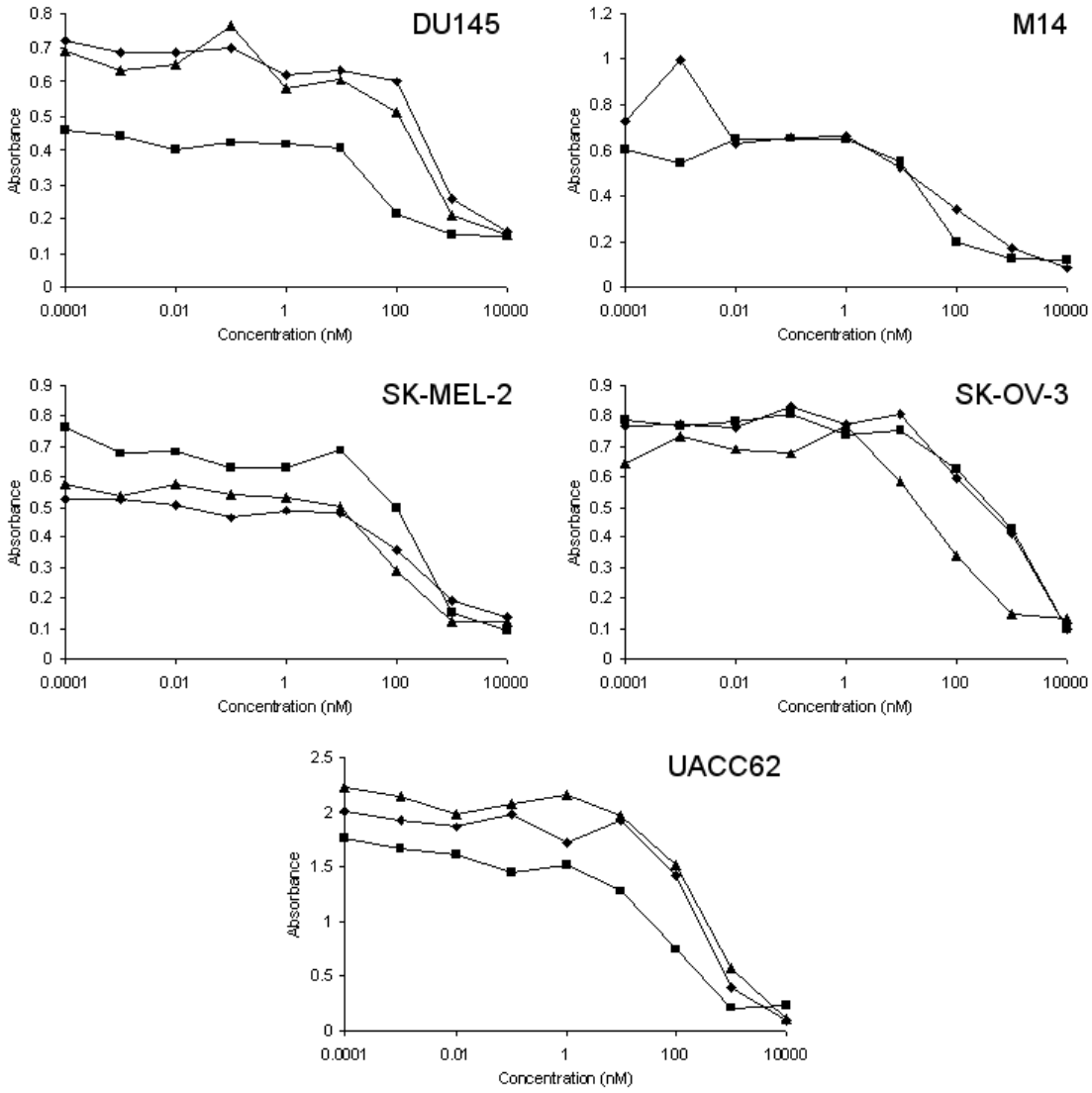

Figure 9.30 Dose response curves showing MTT absorbance (at 550 nm) versus concentration of SJG-136.Cell lines used noted on graph. Cells incubated with SJG-136 for 1 h, washed, and allowed to recover for remainder of 96 h period. 3 independent replicates.

9.7.2 Cellular localisation studies

SJG-136 is a fluorescent PBD dimer compound. In order to investigate the cellular distribution of the drug within cells, cells were treated with SJG-136 and viewed using UV fluorescence microscopy to determine the intracellular distribution of the agent.

Initial experiments examined cells at short time points of 1 h exposure to SJG-136, and concentrations of SJG-136 close to the IC_{50} values (as previously determined; Table 9.7). It was found that SJG-136 fluorescence was not sufficiently intense to be seen above background fluorescence level at these time points, presumably due to low concentrations of the agent. By increasing the concentration of SJG-136 to 1 mM, and incubating for 18 h, localisation of the drug became apparent. Intracellular SJG-136 could not be seen up to 8 h after incubation, and intermediate time points could not be investigated due to laboratory access restrictions. It was observed that SJG-136 localised within the nucleus of the cell in both the UACC62 (Figure 9.31) and DU145 (Figure 9.32) cell lines studied. Cells treated with SJG-136 at high concentration relative to the IC_{50} values appear distressed versus control cells; however, cell viability was tested using trypan blue exclusion and approximately 80% of cells were impermeable to trypan blue at the endpoint of the experiment.

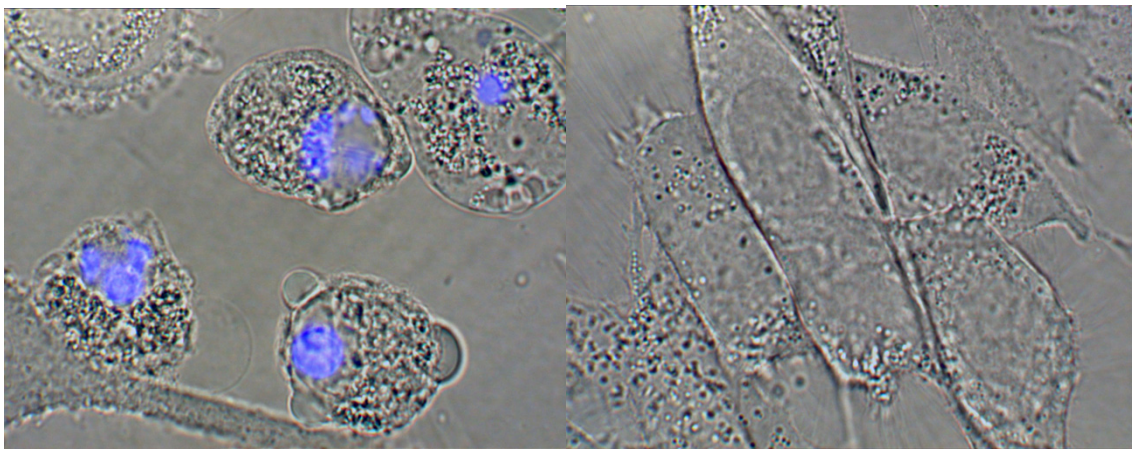

Figure 9.31 Localisation of SJG-136 within UACC62 cells after incubation with 1 mM SJG-136 for 18 h (left) versus control (right).

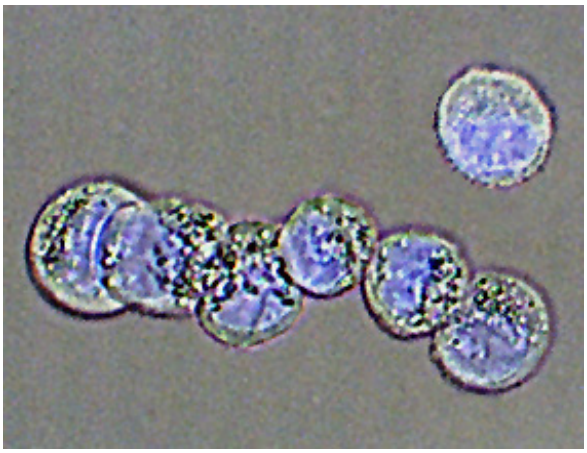

Figure 9.32 Localisation of SJG-136 within DU145 cells after incubation with 1 mM SJG-136 for 18h.

Cellular localisation of SJG-136 within the nucleus is especially relevant for SJG-136, as nuclear DNA is its proposed site of drug action. These data clearly show evidence of SJG-136 fixation within the cell nucleus. Further work planned, but unfortunately not completed, was to repeat these experiments with a counter-stain for elements known to be found exclusively within the nucleus. This would have enabled a less subjective assessment of localisation within the nucleus than observation of cellular morphology.

9.7.3 Chromosomal staining

SJG-136 is proposed to bind to cellular DNA in a sequence-selective manner. To investigate this visually chromosomal spreads were prepared from cultured cells and stained with SJG-136 at 100 μM overnight. Cells were then examined using confocal microscopy with a pseudo-UV laser (360 nm) to enhance sensitivity over UV microscopy and increase resolution. It was envisioned that sequence-selective binding may result in a "spotting" effect on chromosomal DNA.

SJG-136 was observed to stain chromosomal DNA (unstained chromosomal DNA showed no visible fluorescence), but no evidence of any spotting effect was seen (Figure 9.33). The concentration at which chromosomal DNA was treated with SJG-136 is much in excess of that used *in vivo*, hence it is possible that sequence-selective binding was masked as a result of increasingly unselective binding resulting from saturation of the DNA with SJG-136. Unfortunately, the sensitivity of this assay was such that binding of SJG-136 to DNA could not be detected at concentrations less than 100 μM with a 24 h incubation period. It is possible that assay sensitivity could be improved with use of UV laser confocal microscopy for further work.

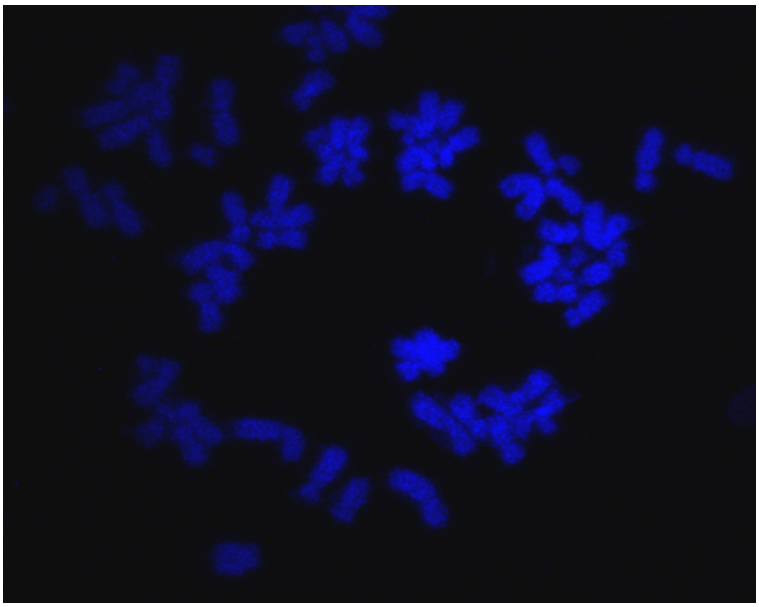

Figure 9.33 Staining of chromosomal DNA by SJG-136. Photograph shows chromosomal spread of cellular DNA after incubation with SJG-136 overnight. Image captured using confocal microscopy; fluorescence induced with 360 nm laser.

9.7.4 Cell cycle analysis

Flow cytometry was used to identify the effects of SJG-136 on cell cycle progression, and to establish how the effects of SJG-136 compare to that of other DNA interstrand crosslinking agents. Data from cytotoxicity assays (section 9.7.1) of SJG-136 was used to decide on concentration of exposure of cells to SJG-136. A drug concentration of 10 nM was selected, as this was close to the IC_{50} values for SJG-136 with all cell lines, thereby eliciting a substantial effect without 100% toxicity to all exposed cells.

Cells were treated with SJG-136 either chronically (continuous exposure for the course of the experiment) for up to 72 h, or to more accurately mimic an *in vivo* pattern of exposure cells, were exposed for 1 h after which drug was removed and cells were allowed to recover for up to 72 h. It was found that cells exposed to SJG-136

chronically for 24 h, exhibited a lower G1 peak area and increases in both S and G2 peak area along with a loss of histogram definition in all cell lines (Figure 9.34). At 48 h, loss of histogram definition was apparent in the treated cells; at 72 h histogram definition was completely lost in four of the five cell lines to the point of being un-analysable. All cell lines used grew adherent to tissue culture vessels under normal (untreated) conditions. Cells at 48 h and 72 h after initiation of exposure to SJG-136 were noted to be considerably less adherent than controls; a large proportion of cells were observed to be in suspension (however this was not quantifiable). This was indicative of levels of toxicity that would be predicted from earlier cytotoxicity studies (section 9.7.1) to produce maximal cell kill. This effect was noted in all cell lines. As a 10 nM concentration is in excess of the 96 h exposure IC_{50} values for all cell lines, it is inevitable that there will be a high degree of cytotoxicity.

Cells exposed to SJG-136 for 1 h with a wash step and recovery time showed a markedly different reaction to SJG-136. At 24 h post exposure, all cell lines showed a noticeable decrease in G1 peak area, with a similar S phase area and a clear increase in G2 peak area (Figure 9.35). This effect persisted to varying degrees in 3 of the 5 cell lines examined for 72 h, with the most apparent and enduring effects observed in the SK-MEL-2 cell line. After 72 h the DU-145 cell line appears to have recovered from the effects of SJG-136 exposure, showing a similar histogram to control cells. This is indicative of a cell cycle-blocking effect of SJG-136 during the G_2/M phase of the cell cycle.

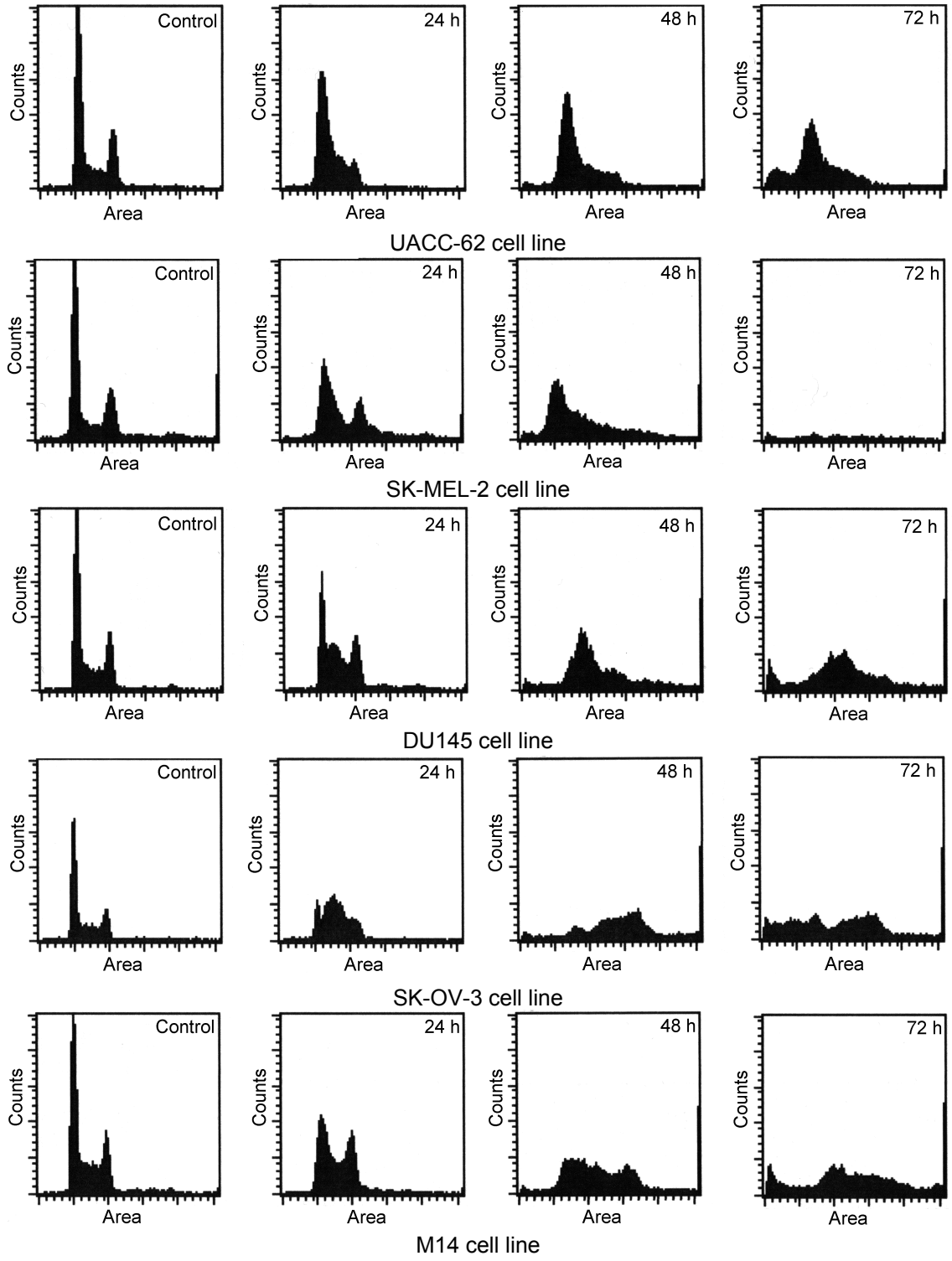

Figure 9.34 Disruption of the cell cycle by continuous exposure of cells to 10 nM SJG-136 after 24, 48 and 72 h versus control. Cells were harvested, fixed, and stained with propidium iodide. 10,000 stained cells were then subjected to FACScalibur analysis to determine distribution of cells throughout the cell cycle.

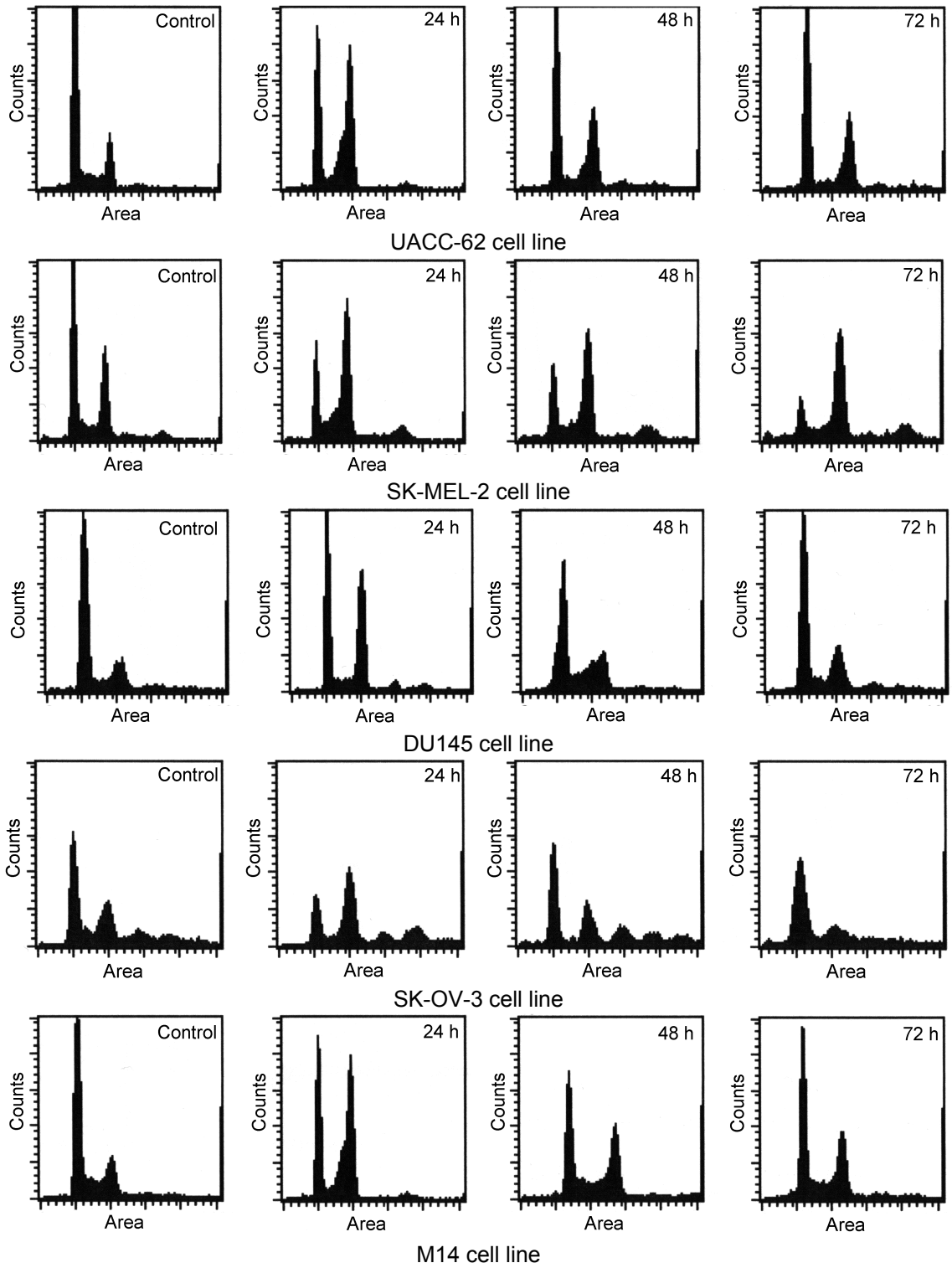

Figure 9.35 G_2/M phase arrest induced by exposure of cells to SJG-136 and subsequent recovery. Cells were exposed to SJG-136 at 10 nM for 1 h, washed, and allowed to recover for 24, 48 or 72 h. Cells were fixed and stained with propidium iodide and analysed using FACS. SJG-136 appeared to cause a G_2/M phase arrest in all cell lines, with cell populations recovering to differing degrees.

A block in G_2/M of the cell cycle is a common feature of DNA minor groove-binding agents (Erba *et al.*, 1995; Turner & Denny, 1996; Yamori *et al.*, 1999). These data indicate that chronic exposure of cells to SJG-136 at 10 nM (approximately an IC_{90} concentration for the cell lines studied with continuous exposure) results in rapid degradation of the cell cycle histogram (sub-24 h effects) such that it is not possible to identify the phase of the cell cycle in which SJG-136 is acting. Further studies investigating time points prior to 24 h may allow some elucidation.

Following 1 h exposure of cells to SJG-136 in an exposure pattern closer to that which may be expected to be seen *in vivo*, there is an obvious increase in the G_2/M peak indicating a block at this phase of the cell cycle. While earlier time-points need to be studied in order to establish how quickly following exposure this block will set in, these data indicate that the effects persist for at least 24 h following exposure, with obvious persistence of effects up to 72 h post-exposure in the UACC-62, SK-MEL-2 and M14 cell lines. Cycle perturbation was still apparent in both DU145 and SK-OV-3 up to 48 h post exposure. SJG-136 is proposed to evade DNA repair mechanisms by binding within the minor groove of DNA without causing distortion of the host double helix (Jenkins *et al.*, 1994; Gregson *et al.*, 2001), these data may be indicative of a reduced cellular repair capacity as a result of lack of lesion recognition due to minimal or no distortion (Sancar & Sancar, 1988). Distortion of DNA is believed to play a role in recognition of DNA damage and subsequent initiation of repair.

9.7.5 Comet assay for assessment of *in vivo* crosslinking

The Comet assay was used to detect and quantify the formation of DNA interstrand crosslinks (ICL) *in vivo* in murine lymphocytes extracted from blood samples at 1 h and

24 h after dosing via either the i.p. or i.v. route at the MTD and ⅓MTD. As the formation of DNA interstrand cross-links (ICL) is the proposed mechanism of toxicity of SJG-136, this was considered an appropriate pharmacodynamic endpoint for detection of SJG-136 activity *in vivo*. Experiments were also undertaken to attempt to identify the formation of ICL in tumour xenografts of the HL-60 cell line. However, it was found that untreated (control) cells prepared from this tumour showed DNA damage and strand breakage to the point where control cells were indistinguishable from irradiated cells. Hence, the presence of ICLs could not be quantified effectively. Project time constraints prevented further investigation into formation of ICLs within tumour tissues.

Typical examples of Comet images examined in this experiment are shown in Figure 9.36, taken from the i.v. studies. In control cells not irradiated or exposed to SJG-136, lymphocyte cells show no DNA damage (Figure 9.36a); characterised by the lack of a Comet tail due to unfragmented DNA and high-molecular-weight supercoiled DNA remaining intact. Following irradiation of untreated cells with 10 Gy to induce a fixed number of random DNA strand breaks, the shorted fragments of DNA can be observed to have migrated from the bulk of the DNA during electrophoresis giving the characteristic Comet tail (Figure 9.36b). SJG-136 was shown not to induce strand breaks in unirradiated, treated controls (Figure 9.36g). The extent of DNA damage was quantified by image analysis and defined as the percentage of DNA in the Comet tail combined with the distance between the means of the head and tail distributions as defined by Olive (Olive *et al.*, 1990).

It was found that SJG-136-induced ICLs could be easily detected in all samples, with detection of up to a 57% decrease in tail moment (Figure 9.37). There was no significant difference in formation of ICL between the i.p. and i.v. dosed routes. SJG-136 appeared to cause the formation of ICL in a non-dose-dependent manner, as there was no significant difference between levels of DNA crosslinking detected after dosing at the MTD or ⅓MTD (two-tailed, Students t-test; $p > 0.05$). This finding has significant implications, as it suggests that SJG-136 can be dosed at levels lower than the MTD without a significant decrease in the efficiency of DNA ICL formation.

It was observed anecdotally that extraction of lymphocytes from blood samples taken from mice dosed with SJG-136 yielded a drastically lower number of lymphocytes than from control mice in samples taken both 1 and 24 h post-dose. An average 20-fold decrease in lymphocytes extracted was observed. While the robustness of the extraction method was not extensively tested, the samples at 1 h were extracted alongside the control samples; this is indicative of drug induced lymphopenia rather than an extraction artefact. This apparent rapid elimination of lymphocytes indicates *in vivo* cytotoxicity of SJG-136, but is certainly in need of further study. Implications for lymphocyte cytotoxicity will be important in predicting overall toxicity of SJG-136; however, these will not be speculated on in the present work.

Repair of SJG-136 induced ICLs was studied at both doses via both routes 24 h after dosing. There was no evidence of repair of SJG-136 induced ICLs 24 h after dosing in any of the samples, suggesting a prolonged persistence of effect of SJG-136. These data corroborate suggestions from previous work performed with SJG-136 suggesting that the lack of distortion of DNA from the binding of SJG-136 may lead to impairment

of ICL detection and reduced DNA repair competency for SJG-136-mediated crosslinks.

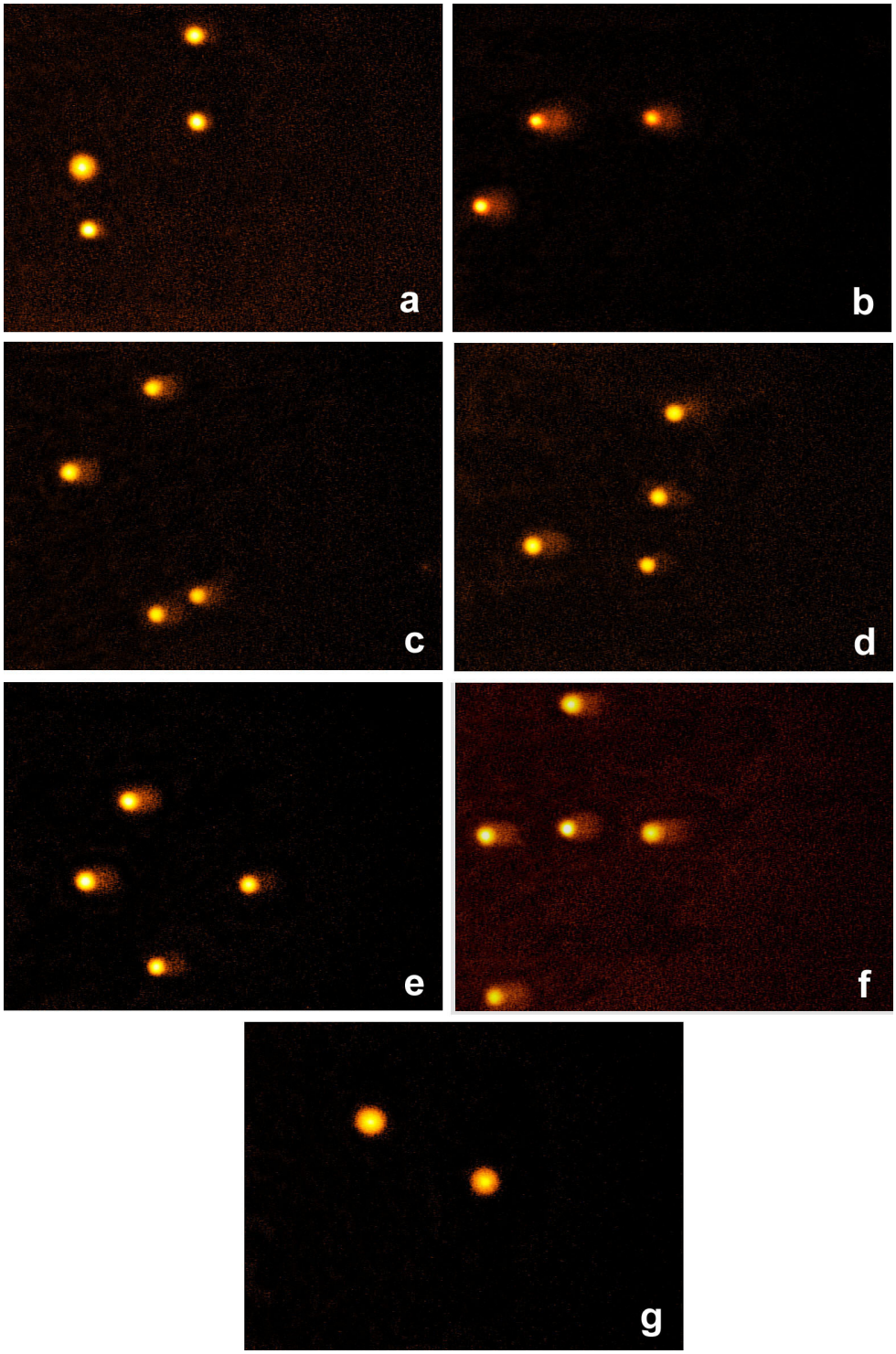

Figure 9.36 Comet images from i.v. *in vivo* lymphocyte study. Comparison of non-drug-treated unirradiated lymphocytes (a) with irradiated (10 Gy) non-drug-treated lymphocytes (b) showed distinct comets. After dosing at either the MTD (c & d) or ⅓MTD (e & f) *in vivo* and lymphocyte extraction, comet tails were visible but showed decreased tail length due to the presence of SJG-136 induce ICLs. There appeared to be no repair of DNA ICLs as comparison of 1 h (c & e; MTD and ⅓MTD respectively) with 24 h (d & f; MTD and ⅓MTD respectively) post-dose samples showed no significant difference in tail length. SJG-136 did not induce single strand breaks in treated unirradiated cells (g).

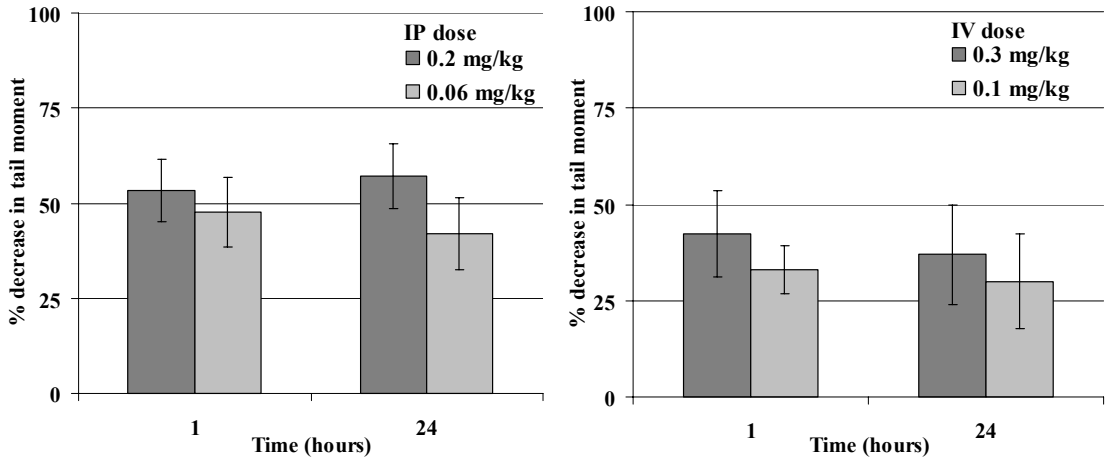

Figure 9.37 SJG-136 induced interstrand crosslinking. ICL formation, measured as percentage decrease in tail moment, showed no significant dose-dependent relationship between the MTD and ⅓MTD doses in i.v. or i.p. dosing *in vivo*. There was no significant indication of repair of ICLs 24 h after dosing at any dose level (mean ± SD; $n = 3$).

These data clearly demonstrate the efficacy of ICL formation by the PBD dimer SJG-136 *in vivo*. Furthermore, the apparent repair evasion of SJG-136-induced ICLs supports the proposed DNA repair evading binding mechanisms of SJG-136. SJG-136-induced ICLs in lymphocytes are formed at <1 h post-dose, and persist for >24 h post-dose with no significant repair of DNA ICLs. Additionally, there is no significant difference in the % decrease in tail moment induced by SJG-136 after treatment at the MTD versus ⅓MTD, after dosing via either the i.p. or i.v. route.

SJG-136 has been shown in this study to achieve its pharmacodynamic endpoint, formation of DNA crosslinks, *in vivo*. Activity of SJG-136 in lymphocytes does not, however, demonstrate the ultimate pharmacodynamic endpoint of formation of ICLs in tumour *in situ*. Experiments designed for this purpose did not work as planned, as tumour samples showed extensive DNA fragmentation that precluded the use of the

Comet assay for assessment of ICL formation. This may be a characteristic of the tumour type chosen (HL-60 tumour cell line), or may instead have been a result of the method used to prepare a single cell suspension for Comet analysis from the tumour. This would require further study to establish the cause.

9.8 Summary

This study has aimed to characterise SJG-136 pharmacokinetically and pharmacodynamically as fully as possible within the PhD research timeframe. The importance of this investigation has been further emphasised as SJG-136 is due to progress to clinical trials within the year. Consequentially, a better characterisation of the agent will allow more informed decisions to be made using data derived from man.

This investigation has provided the first example of characterisation of the analytical properties of SJG-136, identifying optimal detection parameters and using these to develop a sensitive and selective analytical method for the detection of SJG-136 in biological samples. This has included development of a robust extraction procedure for SJG-136 from pre-clinical murine samples, and initial method development for extraction from clinical samples. This work has formed the basis of other work which is currently ongoing to generate a validated analytical method for use in the phase I clinical trials.

For the first time, pharmacokinetic parameters have been defined for SJG-136 within this study. This has enabled the determination that SJG-136 shows linear pharmacokinetics over a 3-fold dose range (⅓MTD – MTD). Establishment of these parameters will allow scaling from murine pharmacokinetics in order to predict the

behaviour of SJG-136 in man. SJG-136 was detected in murine brain and tumour samples in these studies, indicating distribution of the SJG-136 agent across the blood/brain barrier and also into its target site. Levels of SJG-136 detected in brain samples exceed those that may be predicted from blood volume per weight tissue as cited in the literature (Kwon, 2001). Both factors are pharmacokinetically desirable characteristics for this agent. SJG-136 shows a moderate plasma clearance in the mouse of 11.8 and 12.8 ml min^{-1} kg^{-1} (MTD and ⅓MTD respectively) reproducible at two dose levels. Volume of distribution at steady state (V_{ss}) was shown to be low, and similar at both MTD (239 ml kg^{-1}) and ⅓MTD (245 ml kg^{-1}); typical total body water of a mouse is approximately 600 ml kg^{-1} (Davies & Morris, 1993), indicating poor distribution into tissues. V_z (volume of distribution of the terminal elimination phase) was slightly higher, at 849 ml kg^{-1} (MTD) and 488 mg kg^{-1} (⅓MTD).

The metabolism of SJG-136 *in vitro* has also been studied. The drug is shown to be metabolised rapidly in the liver microsomal model, with little or no metabolism in the liver S9 fraction model; behaviour derived from predicted glutathione reactivity of the compound (discussed in detail in section 12). Further work has characterised the metabolites of SJG-136, and predicted structures of these metabolites have been elucidated based on the molecular weight of detected metabolites and the probable metabolic processes for this compound. The major metabolite of SJG-136, a mono-demethylated form of the compound, was identified *in vivo*. Further studies are necessary to discover the extent of metabolite production *in vivo*, although these preliminary studies indicate that this *in vivo* metabolite does not contribute significantly to overall elimination of SJG-136.

The cytotoxicity of SJG-136 was investigated, based upon earlier data from the NCI, and IC_{50} values for chronic (96 h) and acute (1 h) exposure of cells to SJG-136 were defined. These results showed a similar level of cytotoxicity of the compound compared to previously reported data and NCI (unpublished) data. However, cell-specific cytotoxicity was apparent but less pronounced than previously described. Cell localisation studies indicated the localisation of SJG-136 within the cell nucleus, its proposed site of action, revealing cellular distribution desirable for a DNA-interactive agent. However, chromosomal staining studies did not indicate a determinable sequence-selective binding pattern of SJG-136.

Cell cycle effects were investigated using FACS analysis. This study demonstrated a G_2/M block of the cell cycle in all 5 cell lines investigated, persisting for up to 72 h post-exposure in acutely exposed cells. These data are consistent with the action of DNA minor groove-binding agents, indicating a similar mode of action of SJG-136 to this class of compound. Furthermore, this demonstrates a poor repair of SJG-136-induced cell cycle effects, likely a result of the formation of interstrand DNA crosslinks. This supports the proposed DNA-repair mechanism evading properties of SJG-136.

Comet analysis to determine the formation of SJG-136 induced ICLs *in vivo* clearly demonstrated the efficacy of ICL formation in lymphocytes, and thus the reaching of a pharmacodynamic endpoint of the compound. Further studies to identify the pharmacodynamic effects of SJG-136 *in vivo* in tumour models were unsuccessful due to problems with DNA strand breakage in control tumour-derived cells; this DNA damage is believed to be an inherent characteristic of the tumour. These data indicate rapid formation of DNA ICLs, and persistence of the formed crosslinks for up to 24 h.

This finding further supports the hypothesis that the minimal distortion of DNA structure by SJG-136 allows a degree of circumvention of DNA damage recognition and tracing repair mechanisms.

10 PBD monomer D709119

D709119 (Figure 10.1) is a PBD monomer compound selected for study based on indication of potent cytotoxicity and a novel mechanism of action, as defined by screening through the NCI 60-cell-line screen and COMPARE analysis. This compound is currently of interest and is being pursued here for further characterisation, although currently there has been no formal decision to move this compound toward the clinical trials stage. This study aims to characterise the preliminary pharmacokinetics of D709119 and to establish whether the compound exhibits favourable attributes; consequentially this will feed back and influence decisions on how investigation of D709119 proceeds.

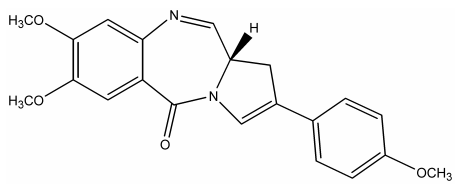

Figure 10.1 Structure of the PBD monomer, D709119.

This study is the first to develop an analytical detection method for D709119, and to characterise the pharmacokinetic properties of the compound.

10.1 Compound characterisation

In order to establish a reliable and optimal mode of analytical detection for the PBD monomer D709119, the compound was characterised using several methods. Each method will be described briefly, as follows. Fluorescence, UV absorbance and mass spectrometry typically facilitate sensitive and specific detection of compounds for

HPLC analysis. To determine optimal detection parameters, spectra for the compound were elucidated for each mode of detection.

10.1.1 Fluorescence characterisation

Scanning fluorescence detection was used to attempt to determine optimal excitation and emission wavelengths for D709119. Unfortunately, D709119 did not fluoresce sufficiently to be able to obtain fluorescence spectra for the compound.

10.1.2 UV absorbance spectra

UV absorbance spectra were obtained using a photodiode array detector (Figure 10.2). A simple MeCN/water HPLC method was developed and D709119 was injected onto the system. Spectral analysis of the eluted peak allowed determination of D709119 spectral properties.

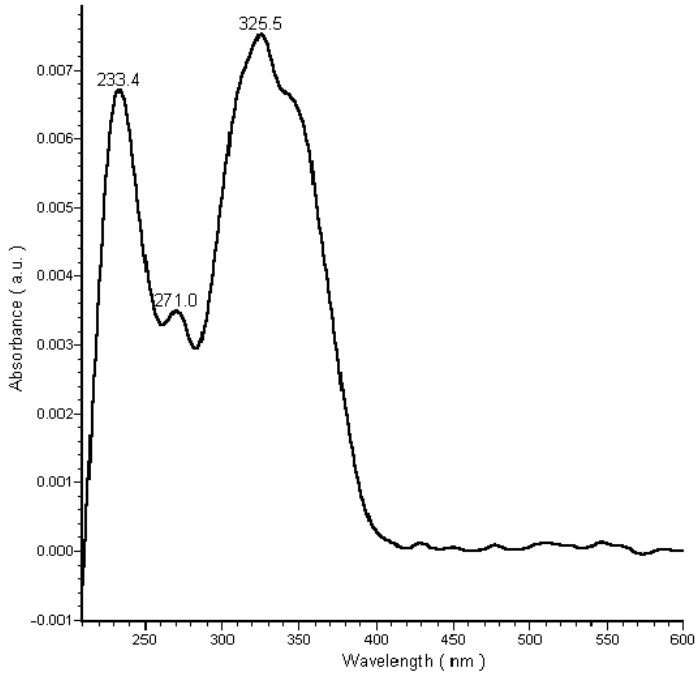

Figure 10.2 UV absorbance spectrum for D709119. Useful maxima for detection were observed at 233, 271 and 325 nm.

The UV absorbance spectrum for D709119 demonstrated useful wavelengths for detection at 233, 271 and 325 nm, however spectral peaks were broad.

10.1.3 Mass spectral characteristics

Mass spectral detection of D709119 was optimised by infusing a D709119 solution directly into the mass spectrometer without the use of a chromatographic component.

D709119 conditions were optimised using single quadrupole mass spectrometry. The exact monoisotopic molecular weight of D709119 was calculated as 364.1. D709119 was infused directly into the mass spectrometer in MeCN, and MS tune conditions were adjusted to give optimal detection of the parent ion at $[M + H]^{\bullet+}$; the compound was detected at an *m/z* of 365.2 (Figure 10.3a). The same phenomenon seen in Section 9.1.4 with SJG-136 was seen with D709119, in that the compound was observed to exist in both the imine (Figure 10.3a) and carbinolamine (Figure 10.3b) states dependent on the presence of water. The D709119 carbinolamine methyl ether form of the compound could not be detected in the presence of methanol.

The existence of alternate forms of D709119 dependent on the presence of water poses a similar potential difficulty to that discussed for the PBD dimer, SJG-136. Due to the presence of two forms of the compound during analysis, it is possible that method sensitivity may be affected. Optimisation of mass spectrometer tuning to D709119 in the presence of both water and MeCN resulted in the determination that the imine form of D709119 is the most intense ion when both solvents are present. However, the carbinolamine form could not be completely eliminated. Avoidance or elimination of

water from the HPLC method was considered impractical, due to the presence of water in the biological systems to be studied.

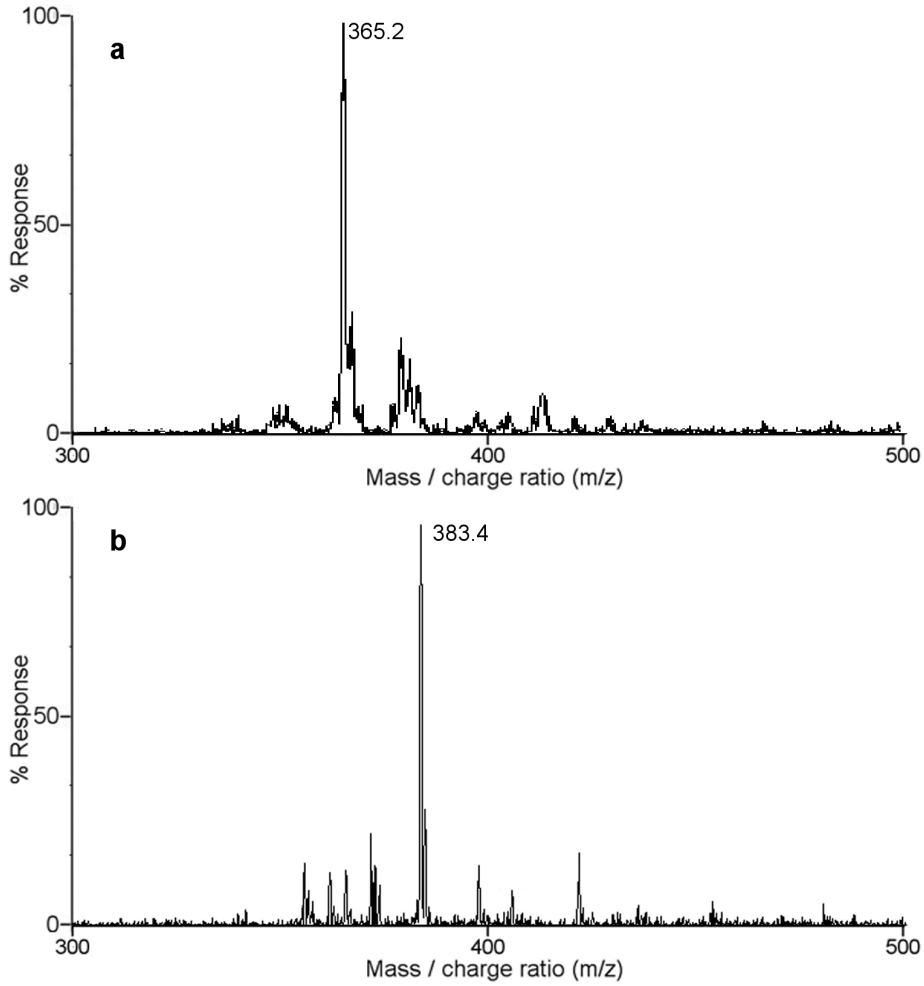

Figure 10.3 Mass spectra of D709119, showing the compound in: a) imine form ($[M + H]^{\bullet+}$), and b) carbinolamine form ($[M + H_2O + H]^{\bullet+}$).

These data suggest the presence of D709119 in both the imine and carbinolamine forms (Figure 10.4).

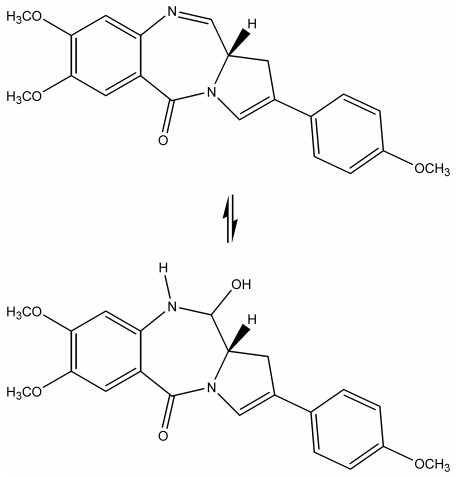

Figure 10.4 The imine (top) and carbinolamine (bottom) forms of D709119.

10.2 Analytical method development

Analysis of D709119 was performed using a MeCN-based HPLC method. Photodiode array or single quadrupole mass spectrometry was used for detection of the compound initially. However, although both modes of detection gave similar limits of detection, mass spectrometry was selected as this allowed selective detection of D709119 and prevented peak interference in samples extracted from biological matrices. Both isocratic and gradient HPLC methods were developed for D709119. However, due to the selectivity of mass spectrographic detection, the additional separation provided by the gradient method was not necessary.

10.2.1 Isocratic separation

Initial method development for D709119 analysis used an isocratic method (with photodiode array detection) to allow a short run-time for rapid sample throughput. However, it was observed that there was interference with plasma constituents in the chromatogram when this method was used following compound extraction from plasma. This led to a change of detection using mass spectrometry.

Injection of 70 µl of a 50 nM sample of D709119 using a mobile phase consisting of 25% MeCN: 75% 0.01 M ammonium formate (pH 4) gave a symmetrical peak with a reproducible retention time of 5.1 min (standard deviation of 0.06 min during a sample run; $n = 8$) (Figure 10.5).

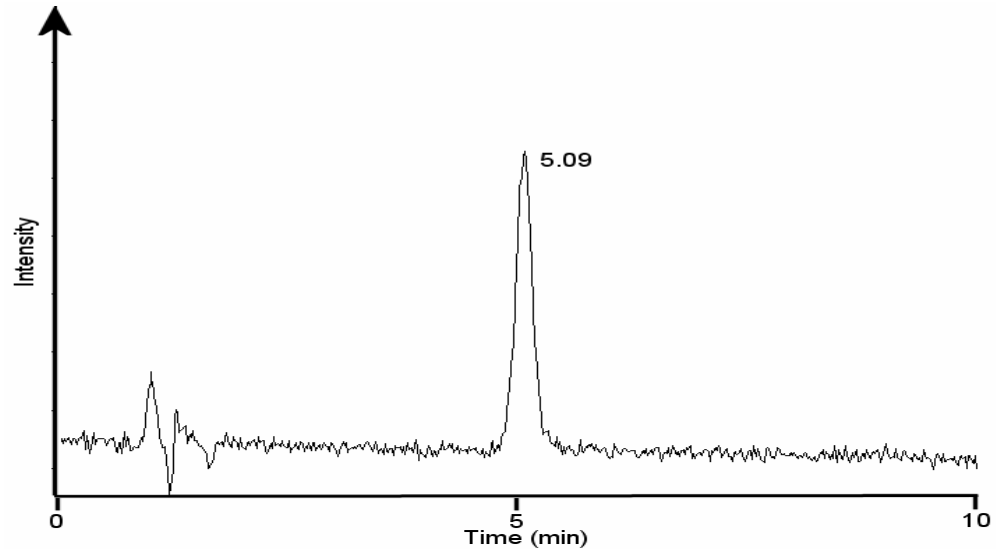

Figure 10.5 Example chromatographic trace showing D709119 eluted at 5 min using an isocratic HPLC method.

It was found that due to the ability of the mass spectrometer to select for specific analytes, it was unnecessary for complete separation from plasma constituents. This allowed the use of the isocratic method for analysis. In order to obtain maximal sensitivity for the compounds of interest, the MS protocol was set to use a "windowed" method so that during the sample run a single ion is monitored for a window of time during which the compound is eluted, as defined during HPLC method development. D709119 is eluted at ~5 min and its internal standard (SJG-303; see structure shown in Figure 11.1) was found to elute at ~3.2 min. Thus the MS instrument was set to monitor

only for SJG-303 from time 2.5 – 4.0 min, and for D709119 from time 4.0 – 6.0 min (Figure 10.6). This was found to give sensitive and selective detection of D709119; no interference from plasma components was detected using this method.

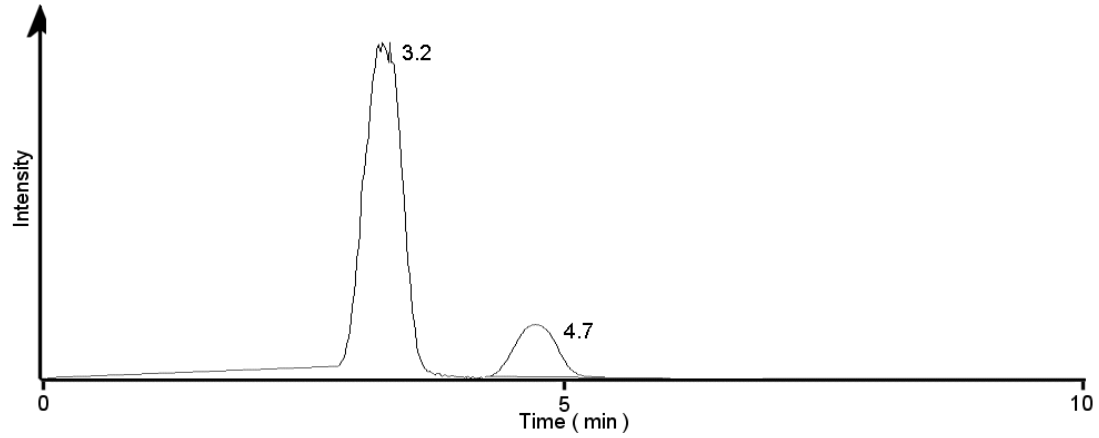

Figure 10.6 Example chromatogram showing D709119 (4.7 min) and internal standard (SJG-303; 3.2 min) detected using MS after extraction from 30 min (post-i.p. dosing) plasma PK sample.

10.2.2 Gradient separation

A gradient method was investigated to provide enhanced separation of D709119 from plasma constituents that were found to interfere with analysis of D709119 after extraction from plasma samples. This method was developed and found reliable, but was ultimately supplanted by the optimised isocratic method as the superior selectivity of mass spectral detection enabled detection of drug among potential interference components and a favourably shorter run-time.

10.3 Pre-clinical method development

10.3.1 Extraction from biological samples

Extraction efficiency of D709119 from murine plasma, tumour and brain tissues was performed using MeCN protein precipitation (Table 10.1). Preliminary studies using solid phase extraction indicated a much lower recovery from plasma and tissue (29% and 11%, respectively) than using MeCN protein precipitation; hence protein precipitation was selected as the optimal extraction method. Recovery of D709119 from tissue was appreciably lower than from plasma, but this was noted to be similar to that observed with SJG-136, and sufficient compound could be recovered to allow detection to approximately 50 nM in *in vivo* samples. Extraction efficiencies were calculated using a 100 nM final drug concentration in the biological sample, as this concentration was estimated to be pharmacokinetically achievable. Efficiency of extraction of D709119 from plasma should be considered alongside protein binding data for this agent (section 10.4.1), as protein binding studies indicate that approximately 80% of D709119 is protein-bound; thus there is only 20% unbound D709119 available in plasma. However, as approximately 80% of drug is recovered from plasma using the MeCN protein precipitation extraction procedure this indicates that the procedure acts to disrupt binding of the agent to plasma proteins.

Biological sample	**Extraction efficiency (% ± 1 SD)**
Plasma	79.2 ± 5.2
Brain	49.9 ± 6.5
Tumour	46.7 ± 4.3

Table 10.1 Plasma and tissue extraction efficiencies of D709119 using MeCN protein precipitation (n = 3; mean ± SD).

10.3.2 Calibration

10.3.2.1 Calibration curve

D709119 calibration curves were produced in murine plasma and found to be linear over the range 10 – 1000 nM (Figure 10.7). Intra-day variation was found to be low; the coefficient of variation was calculated as 6.5%. Limited calibration curves (points at 10, 100 and 1000 nM) were performed immediately before pharmacokinetic samples to (i) ensure accurate results, and (ii) to compensate for any inter-day variation.

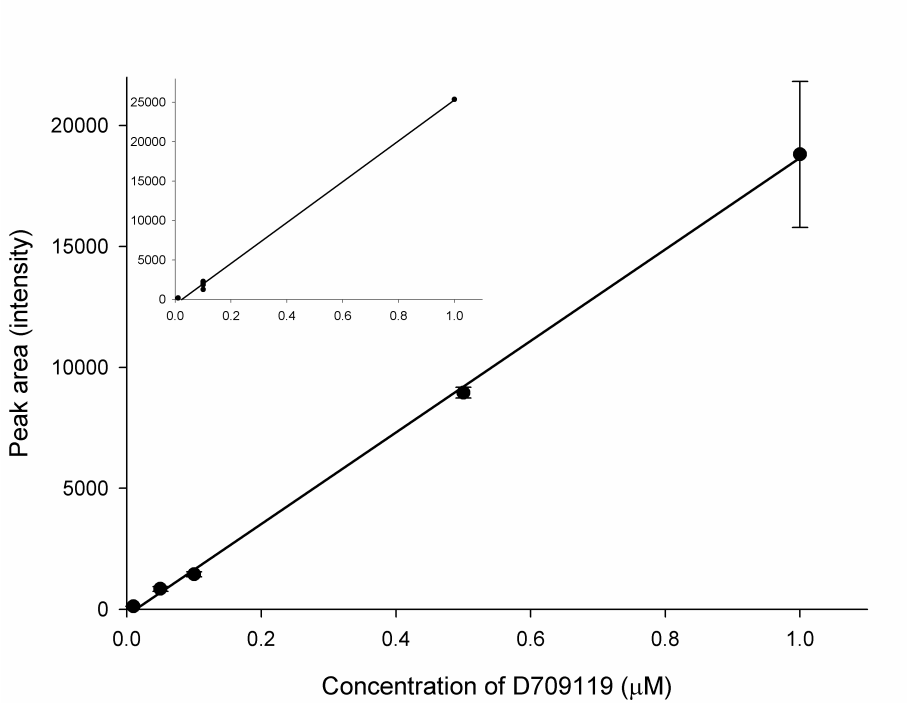

Figure 10.7 Calibration curve for D709119 in murine plasma (10 – 1000 nM; $n = 3$, mean ± SD); inset shows calibration curve over 10 – 1000 nM ($n = 6$ at 100 nM illustrating intra-day variability). ($r^2 = 0.99$; linear curve fit is defined as $y = 18909x - 246$).

Calibration of D709119 was observed to be linear over the range investigated with good correlation as assessed by the coefficient of determination (r^2, calculated by the method of least-squares regression).

10.3.2.2 Limit of detection

The limit of detection of D709119 in mouse plasma was found to be a 70 µl injection of extract from 10 nM of compound in mouse plasma, with a signal-to-noise ratio calculated as 12:1 (Figure 10.8). Figure 10.8 shows a 70 µl injection extracted from 100 µl of mouse plasma with D709119 spiked at 10 nM (extracted using protein precipitation).

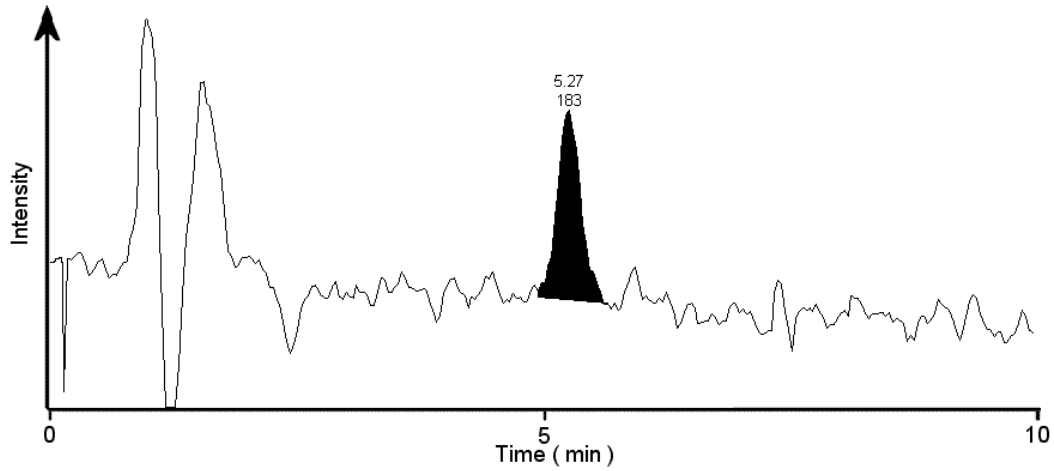

Figure 10.8 Chromatogram showing 10 nM D709119 extracted from mouse plasma. Signal-to-noise ratio calculated using MassLynx software as 12:1. D709119 eluted at 5.27 min. Evidence of baseline fluctuation as a result of injection artefact is seen at ~1 min post-injection.

10.3.3 Stability in blood and plasma

The stability of D709119 in murine plasma and blood was assessed at 37 °C over a 6 h period to assess potential degradation of D709119 *ex vivo* during sample handling.

D709119 was found to be stable in murine plasma and blood for up to 2 h (92 and 90% of T_0 sample recovered respectively), with a gradual decrease in recovery of drug at later time-points (Figure 10.9). The plasma and blood $t_{½}$ were calculated by extrapolation of a log-linear curve fit (mono-exponential decay) obtained from the time-points. Plasma $t_{½}$ was calculated as 6.5 h, blood $t_{½}$ was calculated as 10.3 h. The stability of the monitored compound indicates that rapid sample processing will be necessary to prevent degradation of D709119 in samples *ex vivo*.

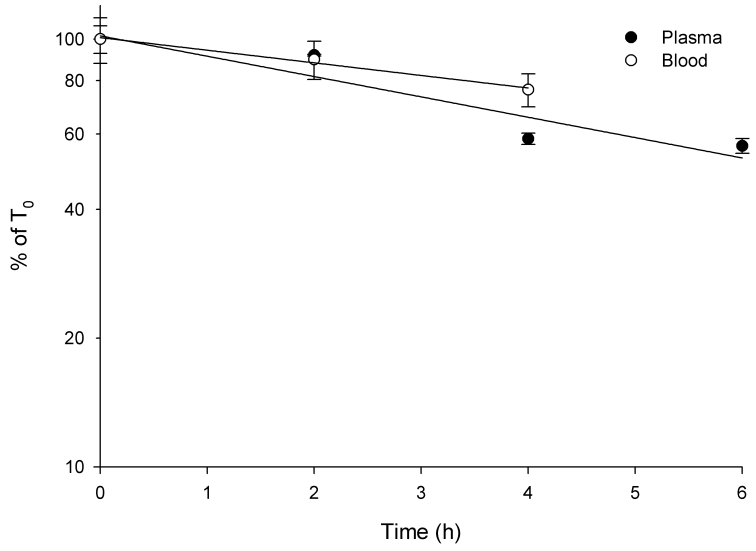

Figure 10.9 Stability of D709119 in murine blood and plasma relative to time at 37 °C. Values are expressed as a percentage of drug recovered at t = 0 h (mean ± SD; n = 3).

10.4 Pre-clinical pharmacokinetics

10.4.1 Protein binding

Ultracentrifugation was used to evaluate sera protein binding of D709119 as preliminary experiments with the PBD dimer SJG-136 indicated problems with binding to filter membranes for the structurally-similar PBD compound.

Ultracentrifugation was used to pellet out proteins in order to assess the proportion of unbound drug present in plasma water and thereby enable an estimation of the percentage of D709119 monomer bound to proteins. This was compared directly to ultracentrifuged standards (PBS containing D709119) in order to ensure recovery of drug after the procedure. Human serum was used for the study as it was not ethically justifiable to sacrifice the number of animals that would be required to obtain the volume of plasma necessary to perform this study using murine plasma.

D709119 concentration (nM) in human serum	% protein bound (mean ± SD)
1000	88.5 ± 4.1%
100	80.3 ± 10.5
10	n / d

Table 10.2 Assessment of % of D709119 bound to human sera protein using ultracentrifugation (n = 3).

Protein binding of D709119 was observed to be moderate, with 88% of drug bound at 1000 nM and 80% of drug bound at 100 nM (Table 10.2). D709119 could not be detected at 10 nM.

10.4.2 *In vivo* intra-peritoneal pharmacokinetics

Pharmacokinetic plasma time course of D709119 was investigated in the MAC15A tumour-bearing NMRI mouse following i.p. administration of the compound at the previously determined MTD of 0.5 mg kg^{-1} (Figure 10.10). At each time-point, tumour and brain tissue were also analysed to assess tumour and CNS penetration of the agent. A second study was performed in parallel administering D709119 at the MTD to MAC29 tumour-bearing NMRI mice, where plasma levels were not monitored but tumour and brain samples were again analysed for comparative penetration of drug in the different tumour types.

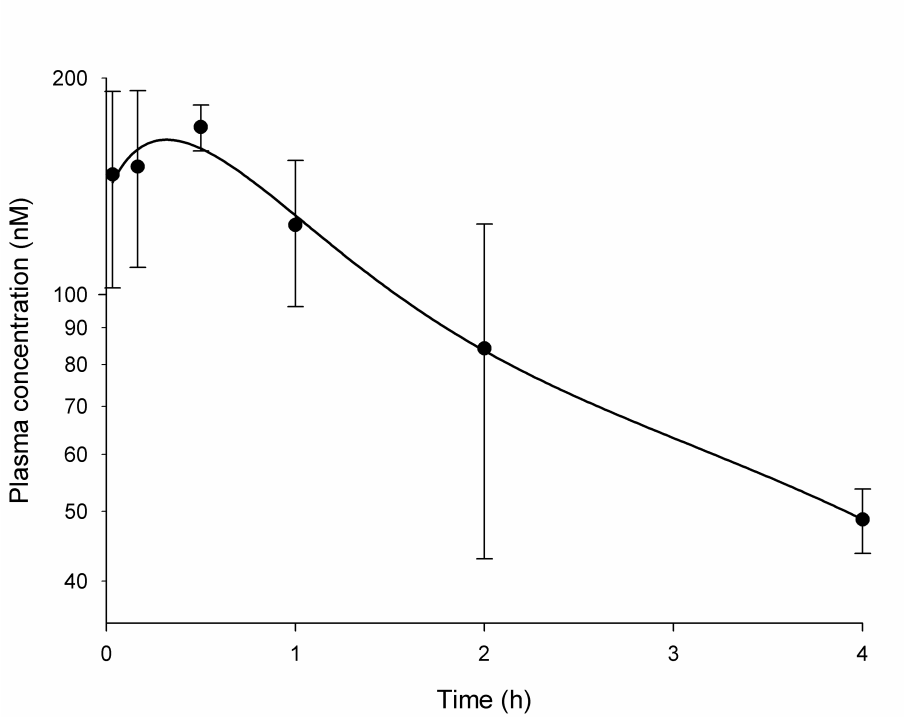

Figure 10.10 D709119 concentration (mean ± SD) versus time profile in MAC15A tumour-bearing NMRI mouse plasma following i.p. administration at 0.5 mg kg^{-1} (n = 3; LOQ 10 nM). Curve shows fit using 3 compartment model (Equation 4: C_1 = 165, C_2 = 120, k_a = 20, k_{el1} = 2.05, k_{el2} = 0.29).

The area under the concentration-time curve was calculated to be 540 nM h (197.1 ng h ml^{-1}). D709119 showed a terminal elimination half-life of 2.7 h (k_{el} calculated as 0.29 h^{-1} by curve fitting to the exponential decay portion of the plasma profile), although this data must be taken as tentative due to the high deviation seen at the 1 and 2 h time points. D709119 showed a moderate plasma clearance of 42.28 ml min^{-1} kg^{-1} (approximately half murine hepatic blood flow) estimated from the i.p. data. D709119 was detectable up to 4 h post-dose, but could not be detected after 4 h. The C_{max} detected for D709119 in this study was 171 nM (62.4 ng ml^{-1}), achieved at 30 min post-dose.

Volume of distribution of D709119 can be estimated as 3202 ml kg^{-1} (V_{ss}) or 742 ml kg^{-1} (V_z). Total body water of the mouse is estimated as 600 ml kg^{-1} (Davies & Morris, 1993). An volume of distribution greater than total body water but less than 5 l kg^{-1} is moderate. The larger volume of distribution of D709119 may account for the longer $t_{½}$ of this agent compared to that seen for SJG-136. While calculation of volume of distribution from i.p. data is not accurate compared to i.v. data, it is able to give an approximate value.

D709119 could not be detected at any time-points in tumour or brain tissue from either the MAC15A or MAC29 tumour-bearing mice.

10.5 Cellular effects of D709119

D709119 was assessed for cytotoxicity using the MTT cytotoxicity assay in cell lines selected based on data describing the agent obtained from the NCI 60-cell-line screen (Figure 10.11). Previous work by the NCI calculated a 96 h continuous exposure IC_{50}

for D709119 in SK-OV-3 cells at 9.8 nM (unpublished NCI data). The present work sought to confirm this and also to investigate the cytotoxicity of the compound for shorter exposure times.

10.5.1 MTT cytotoxicity assay

Cytotoxicity of D709119 was assessed over a range of concentrations in selected cell lines in order to investigate claims of cell-type selectivity of the compound. Exposure of cells to D709119 was either continuous for 96 h or as a short 1 h exposure to better reflect exposure of tumour cells to the agent in an *in vivo* situation. Growth curves for all cell lines were obtained as described previously (Section 9.7.1).

Exposure time (h)	IC_{50} value (nM) by cell line and cell type				
	DU-145 prostate	UACC-62 melanoma	SK-MEL-2 melanoma	SK-OV-3 ovarian	M14 melanoma
1	7.9 ± 0.8	41.0 ± 4.7	40.3 ± 3.1	47.9 ± 8.9	7.7 ± 2.1
96	0.14 ± 0.03	0.15 ± 0.01	0.7 ± 0.7	1.7 ± 0.2	0.02 ± 0.01

Table 10.3 IC_{50} values calculated for selected cell lines after either 96 h continuous or 1 h exposure to D709119 (mean ± SD; $n = 3$).

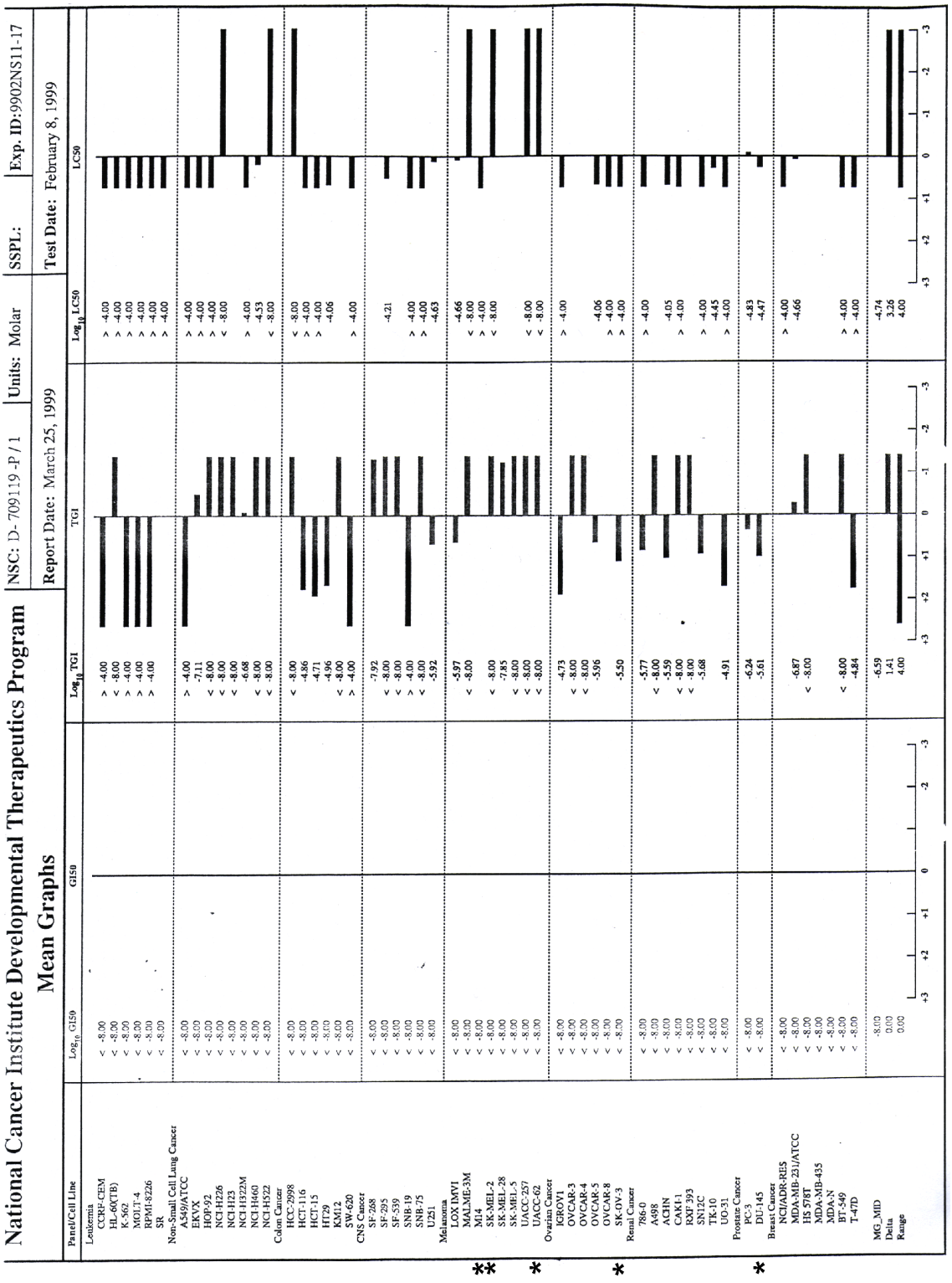

Figure 10.11 NCI 60-cell-line screen data for D709119. Data show relative resistance or sensitivity of cell lines to D709119. * Denotes cell lines chosen for investigation in this study. From top to bottom, cell lines: M14, SK-MEL-2, UACC-62, SK-OV-3 and DU-145.

These data support the NCI 60-cell-line screen data showing nM potency of D709119. Each cell line shows an approximate 100-fold increase in growth inhibition after 96 h exposure compared to the 1 h exposure (which would be expected with an approximate 100-fold longer exposure time), except for the SK-OV-3 cell line which appears less sensitive after prolonged exposure. This may be a result of compound degradation, metabolism or upregulation of drug resistance mechanisms (for example MRP1, P-gp) within the cell population. However, compound degradation is an unlikely cause as this effect would manifest across all cell lines studied. The UACC-62, SK-MEL-2 and SK-OV-3 cell lines appear approximately 4-fold less sensitive than the M14 and DU-145 cell lines after 1 h exposure, though this pattern is not reflected in the 96 h continuous exposure results. DU-145 and M14 remain the most sensitive cell lines to D709119 after either 96 h or 1 h exposure although there is a less marked difference in sensitivity compared to the other three cell lines after 96 h exposure. These data suggest a tumour cell-type selectivity for D709119, in this case as a more potent agent against the DU-145 (prostate-derived) and M14 (melanoma-derived) cell lines.

10.6 Summary

This study has aimed to characterise and develop a pre-clinical method, including extraction procedures, for analysis of D709119 in murine samples. This has included a preliminary pharmacokinetic study to establish basic pharmacokinetic parameters and to attempt to detect penetration of D709119 into the brain and tumour, two sites of specific interest with this compound. These studies are the first report for this compound (specifically on a C2-aryl-substituted PBD agent), and are intended to feed back to drug designer chemists in order to illustrate the pharmacokinetic properties of D709119 and relate the structural differences of this compound to its pharmacokinetics and cytotoxic

activity compared to other PBD agents. It is also intended that these data will provide a basis for decisions regarding further development of D709119.

This investigation is the first study to elucidate analytical properties for D709119, and to define optimal detection parameters for the compound. This has allowed the development of a sensitive and selective method for the detection of D709119 in biological fluids.

The pharmacokinetic profile of D709119 following i.p. dosing has demonstrated that D709119 is readily available in the systemic circulation, shows moderate clearance and plasma protein binding, and has a high initial volume of distribution (greater than total body water). It has also been established that D709119 is present *in vivo* in the systemic circulation at concentrations well in excess of those needed to achieve IC_{50} values *in vitro* for up to 4 h post-dose. This indicates potential for D709119 to be present in the body at efficacious concentrations. However, attempts to detect D709119 in murine tumour models or in the brain showed the levels of D709119 to be below the limit of detection. Further work needs to be performed to examine this finding, preferably in a human tumour xenograft model with optimisation of extraction procedures to enhance detection in tumour samples.

11 PBD monomer compounds

These agents were investigated in order to develop basic analytical methods to allow examination of levels of compounds in biological fluids. This was done with a view to providing a basis for future work allowing study of the pharmacokinetics of these compounds *in vivo*. DC-81 is a previously-studied compound that is the monomer unit of the first synthetic PBD dimer, DSB-120. The monomer also has proven activity as assessed by cytotoxicity and DNA binding studies (Bose *et al.*, 1992c; Puvvada *et al.*, 1993; 1997). DC-81 was included in these studies to (i) allow comparison with a previously characterised PBD, (ii) to broaden the limited available knowledge for PBD compounds, and (iii) allow further structure-activity relationships to be elucidated. There are currently no existing analytical methods available for the study of such compounds.

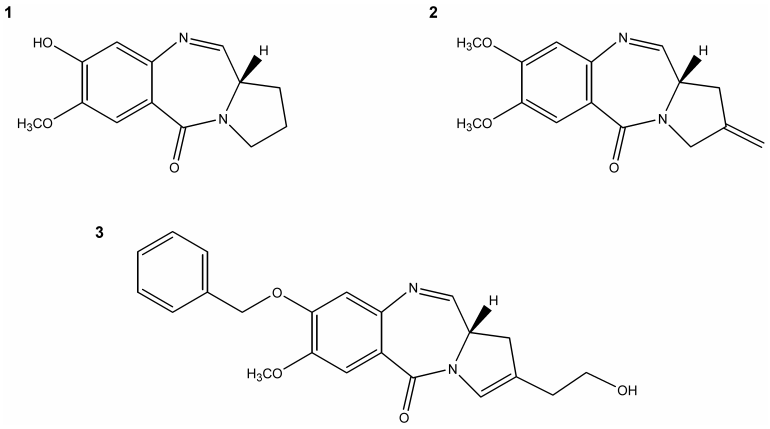

Figure 11.1 Structures of the PBD monomer compounds DC-81 (**1**), MMY-SJG (**2**), and SJG-303 (**3**).

11.1 Characterisation of compounds

The PBD monomers DC-81, MMY-SJG, and SJG-303 were characterised to allow determination of optimal parameters for their detection via fluorescence, UV absorption and mass spectrometry.

11.1.1 DC-81

The UV absorbance spectrum of DC-81 was determined using a photodiode array detector, and showed peaks for detection at 222, 233, 260 and 311 nm (Figure 11.2). Optimal wavelengths for detection using fluorescence were determined by scanning for excitation (Figure 11.3) and emission (Figure 11.4) peaks, and were found to peak at 230 and 400 nm, respectively, for excitation and emission.

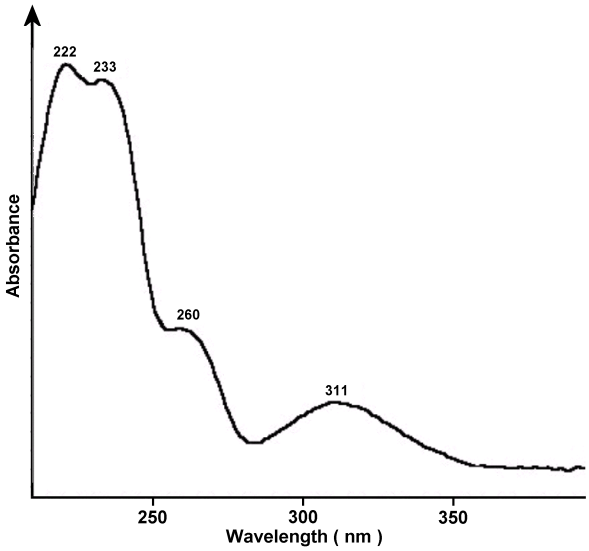

Figure 11.2 UV absorbance spectrum of DC-81. Useful maxima for optical detection seen at 222, 233, 260 and 311 nm.

Fluorescence detection was chosen over UV detection as it allowed a lower limit of detection for DC-81. However, the optimal excitation wavelength was found to be 260

nm as this reduced interference caused by biological materials (versus 230 nm) without any appreciable loss of sensitivity.

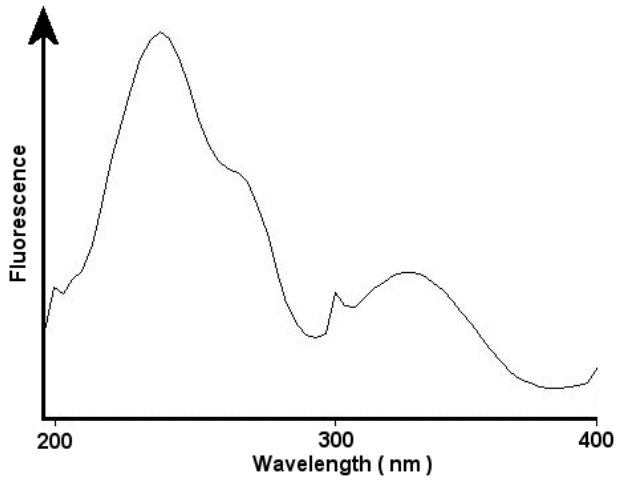

Figure 11.3 Fluorescent excitation spectral scan of DC-81 (emission wavelength 420 nm). Optimal sensitivity for excitation is seen at 230 nm.

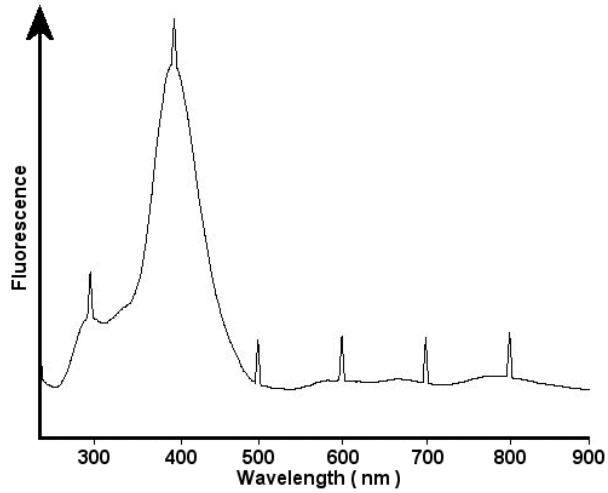

Figure 11.4 Fluorescent emission spectral scan of DC-81 (excitation wavelength 230 nm). Optimal sensitivity for emission is found at 400 nm.

11.1.2 MMY-SJG

The UV spectrum of MMY-SJG shows a similar pattern of absorbance to DC-81, with peaks at 223, 235, 262 and 324 nm (Figure 11.5). Fluorescence scans for emission and excitation of MMY-SJG indicated peak emission at 410 nm (Figure 11.6) and excitation

at 230 nm (Figure 11.7). As 260 nm was seen to give comparable intensity of signal, this was chosen for detection as it was less likely to be subject to interference from other materials at this higher wavelength. Fluorescence proved to be the most sensitive mode of detection for MMY-SJG as it allowed a lower limit of detection for the compound compared to UV absorbance detection.

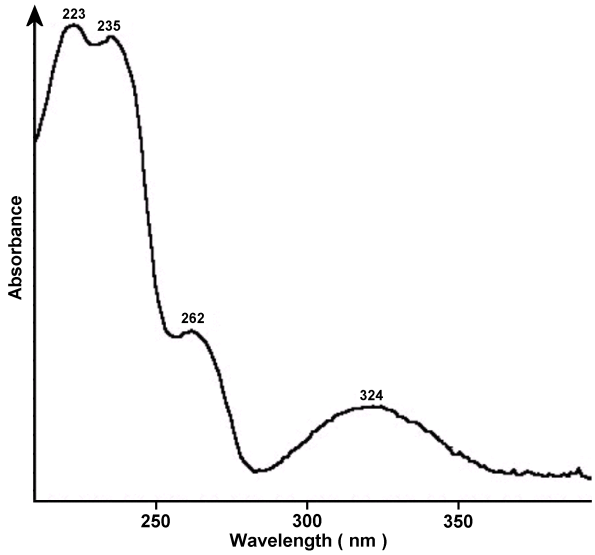

Figure 11.5 UV absorbance spectrum of MMY-SJG. Optimal peaks for detection seen at 223, 235, 262 and 324 nm.

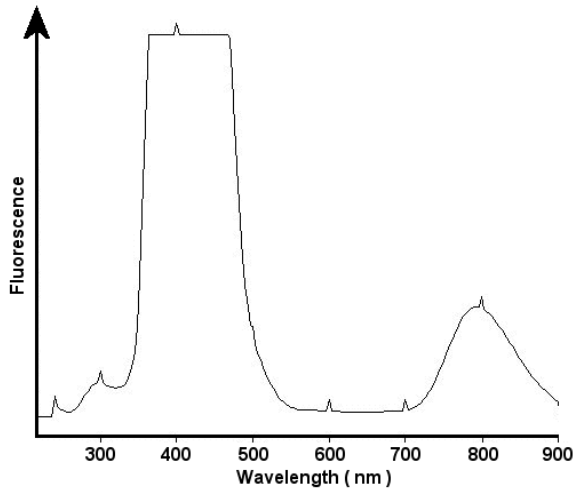

Figure 11.6 Fluorescent emission spectral scan of MMY-SJG (excitation wavelength 230 nm). Optimal sensitivity for emission is at 400 nm.

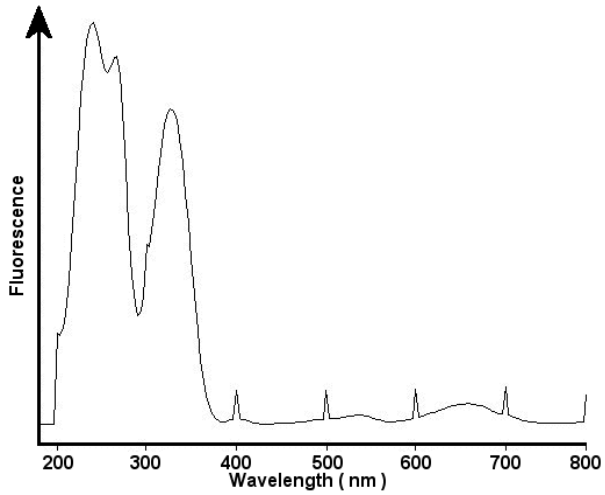

Figure 11.7 Fluorescent excitation spectral scan of MMY-SJG derived from an emission wavelength of 890 nm. Optimal sensitivity for excitation was 230 nm; selectivity is enhanced using 260 nm, with negligible loss of sensitivity.

11.1.3 SJG-303

The UV absorbance spectrum for SJG-303 showed peaks at 231, 261, 287 and 332 nm (Figure 11.8). Fluorescence spectra showed optimal emission and excitation wavelengths at 410 nm (Figure 11.9) and 260 nm (Figure 11.10), respectively. SJG-303 was less fluorescent than either DC-81 or MMY-SJG; it was found that UV absorbance

using a photodiode array detector offered the most sensitive mode of detection for this compound.

Intensity of fluorescence of SJG-303 was found to be relatively lower than for either DC-81 or MMY-SJG; consequentially a lower limit of detection was achieved using UV absorbance detection, which was selected as the mode of detection. Use of a photodiode array detector for SJG-303 detection allowed capture of wavelengths from 200 – 400 nm and selection of the most appropriate wavelength (260 nm) for data processing.

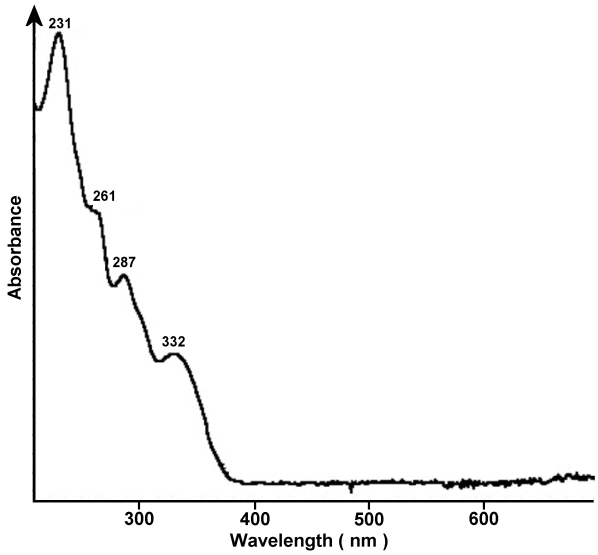

Figure 11.8 UV absorbance spectrum of SJG-303. Optimal peaks for detection appear at 231, 261, 287 and 332 nm.

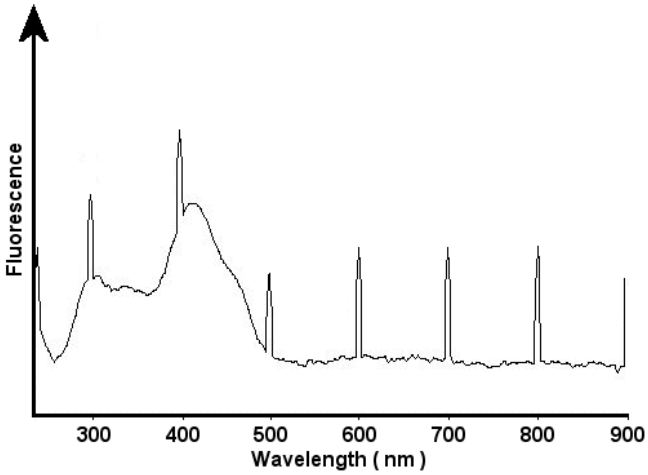

Figure 11.9 Fluorescent emission spectral scan of SJG-303 (excitation wavelength 230 nm). Optimal sensitivity for emission was 410 nm.

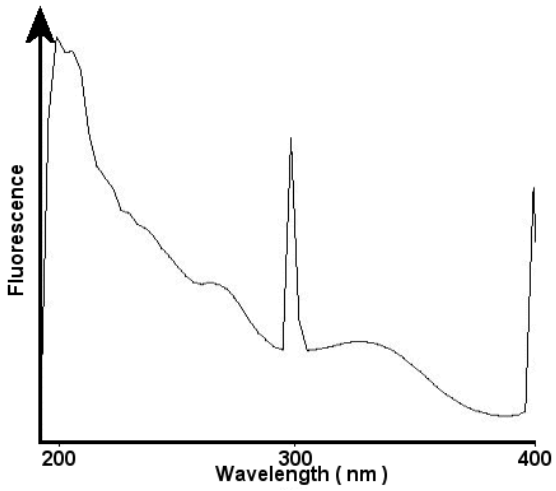

Figure 11.10 Fluorescent excitation spectral scan of SJG-303 (emission wavelength 410 nm). Optimal sensitivity for excitation was determined at 260 nm.

11.2 HPLC method development

11.2.1 Methanol-based method

The initial development of a methanol/water-based analytical method gave a satisfactory HPLC method for the initial purposes of this study. All three PBD

monomer compounds gave highly reproducible peak retention times with good symmetrical peak shape (Figure 11.11, Figure 11.12 and Figure 11.13 for DC-81, MMY-SJG and SJG-303, respectively).

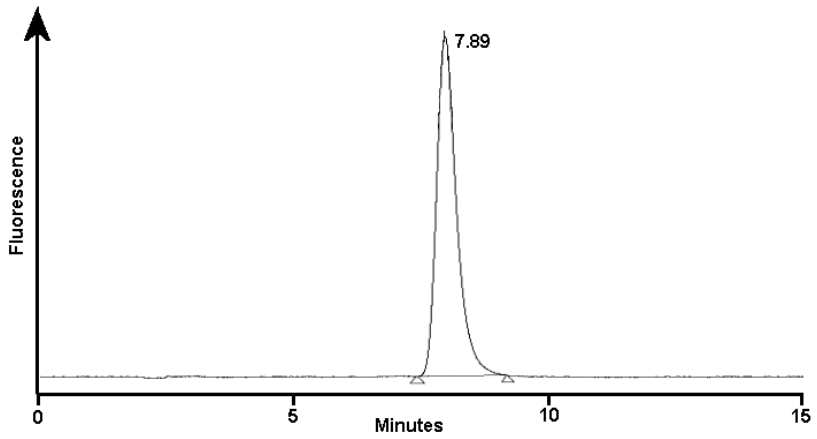

Figure 11.11 Example trace of DC-81 using a methanol/water-based HPLC method; peak retention time of 7.9 min.

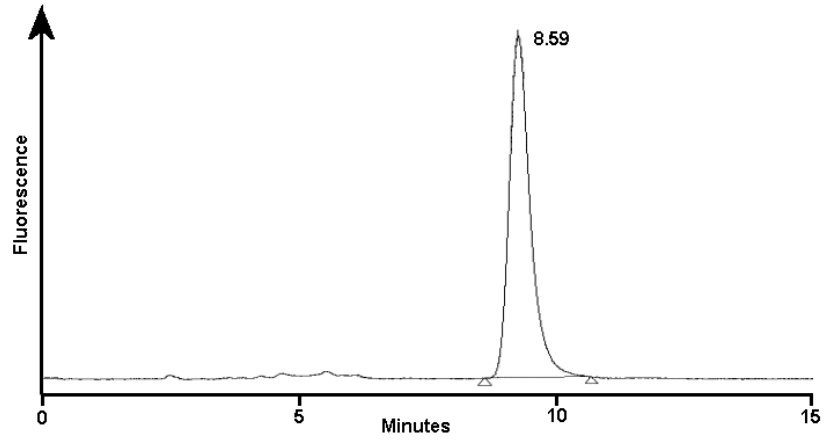

Figure 11.12 Example trace of MMY-SJG using a methanol/water-based HPLC method; peak retention time of 8.6 min.

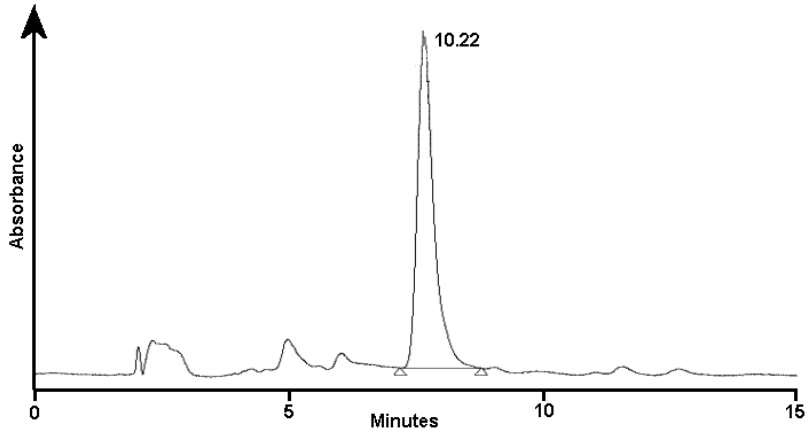

Figure 11.13 Example trace of SJG-303 using a methanol/water-based HPLC method; peak retention time of 10.2 min.

11.2.2 Acetonitrile-based method

In order to prevent formation of the carbinolamine methyl ether form of the PBD monomer compounds due to reaction with MeOH (see section 9.1.4.1), acetonitrile was substituted for MeOH. Optimisation of mobile phase conditions gave a robust method with reproducible retention times for each compound (Figure 11.14, Figure 11.15 and Figure 11.16, respectively).

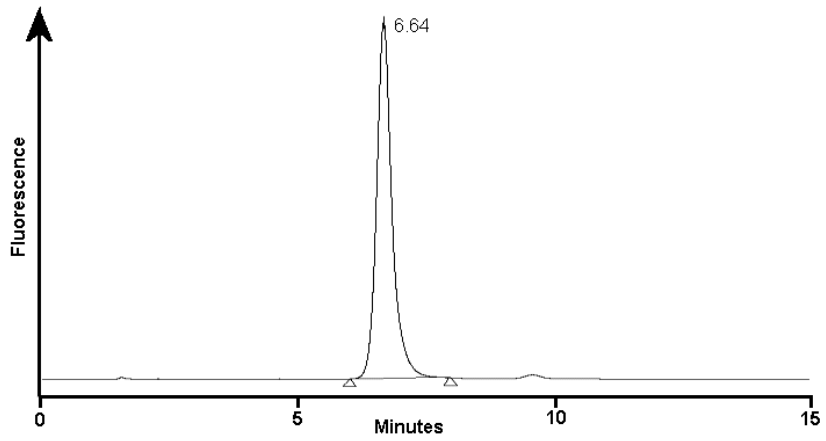

Figure 11.14 Example trace of DC-81 using an acetonitrile/water-based HPLC method, showing a peak at a retention time of 6.6 min.

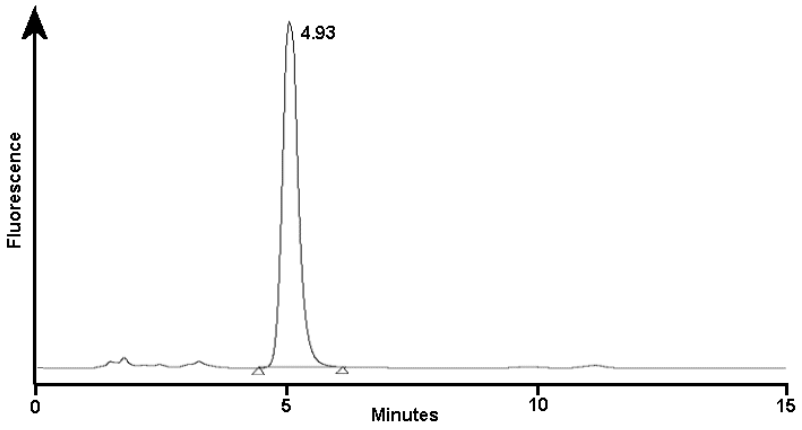

Figure 11.15 Example trace of MMY-SJG using an acetonitrile/water-based HPLC method, showing a peak at a retention time of 4.9 min.

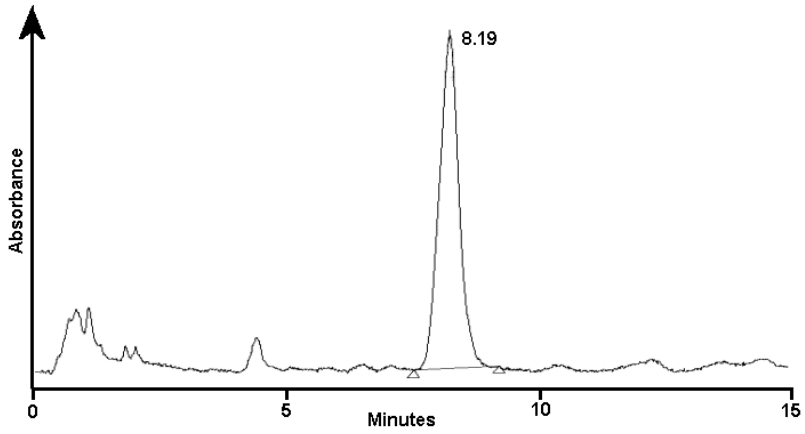

Figure 11.16 Example trace of SJG-303 using an acetonitrile/water-based HPLC method, showing a peak at a retention time of 8.2 min.

11.3 Mass spectrometry of compounds

Mass spectra for each of the three monomer compounds were obtained by direct infusion of compound into the mass spectrometer in order to (i) obtain optimal parameters for MS detection and (ii) identify the presence of alternate forms of the PBD monomer caused by the presence of water or methanol. It is possible for PBD compounds to exist in three forms due to reactions between the imine C11-N10 position of the PBD and water or MeOH. The forms present in solution will thus be the imine

(illustrated in Figure 11.17), the carbinolamine (hydrate) and the carbinolamine methyl ether (methanolate).

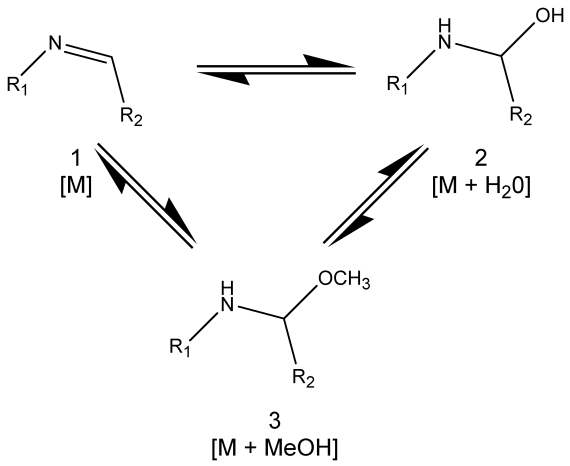

Figure 11.17 The three forms of a PBD compound present in solution. The imine (1) carbinolamine (2) and carbinolamine methyl ether (3) forms.

11.3.1 DC-81

DC-81 could be detected in both imine and carbinolamine methyl ether forms (Figure 11.18) as $[M + H]^{\bullet+}$ (imine) or $[M + MeOH + H]^{\bullet+}$ (carbinolamine methyl ether). However, DC-81 could not be detected in its carbinolamine form.

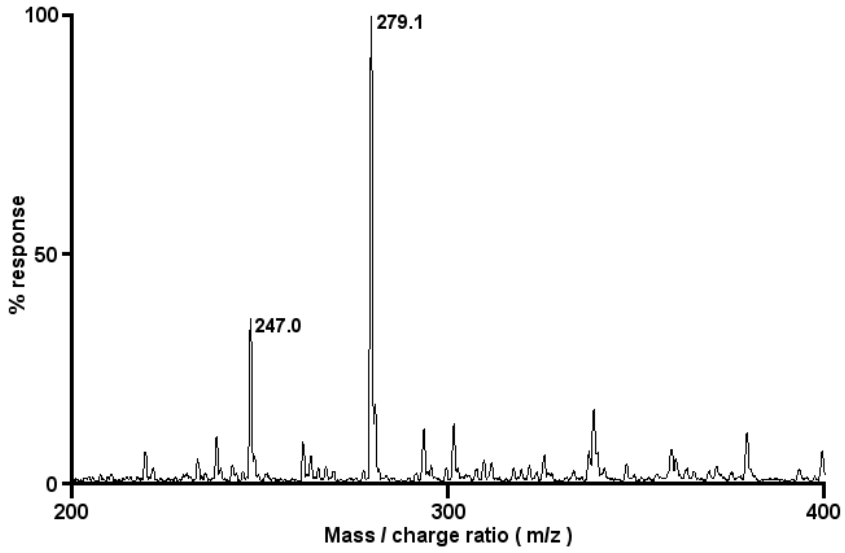

Figure 11.18 Mass spectrum of DC-81 showing the imine form (247.0; $[M + H]^{\bullet+}$) and carbinolamine methyl ether form (279.1; $[M + MeOH + H]^{\bullet+}$).

11.3.2 MMY-SJG

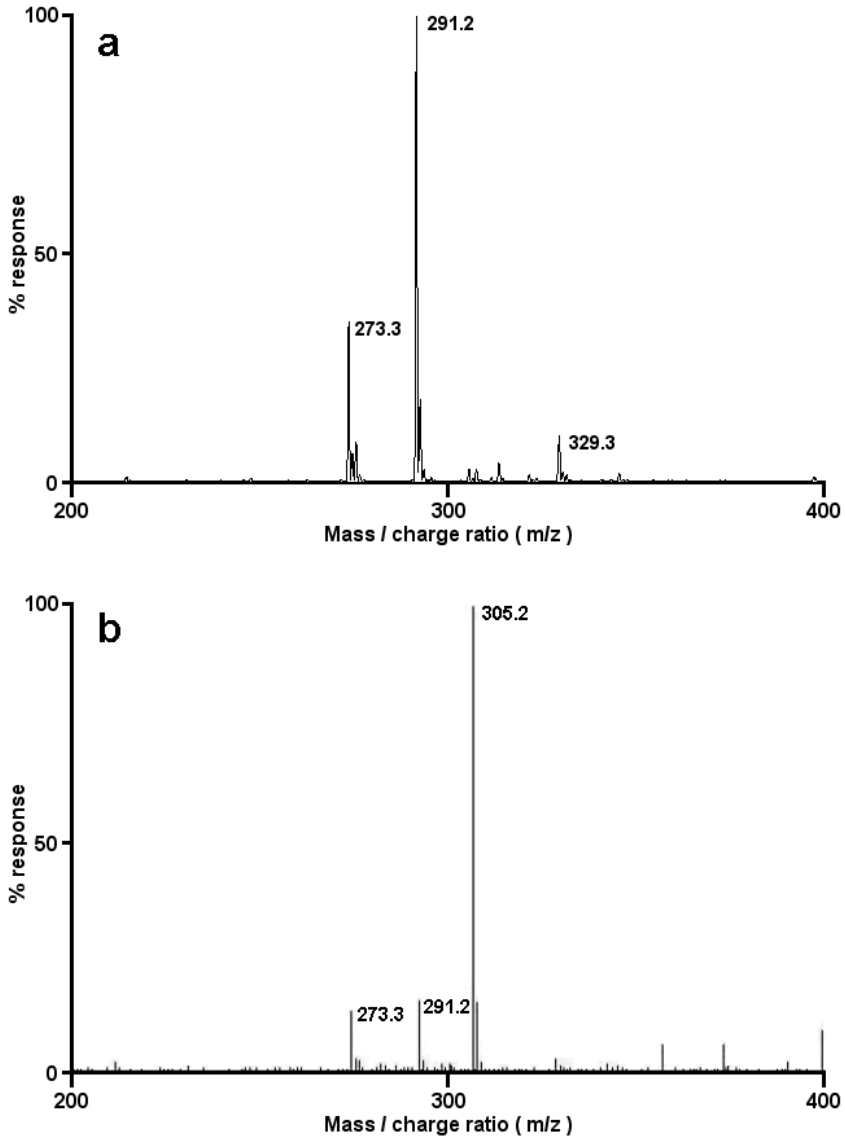

Figure 11.19 Mass spectra of MMY-SJG. a: Top trace; no methanol present, showing evidence of MMY-SJG in imine (273.3; $[M + H]^{\bullet+}$) and carbinolamine (291.2; $[M + H_2O + H]^{\bullet+}$) form. b: Bottom trace; methanol present, showing additional evidence of carbinolamine methyl ether (305.2; $[M + MeOH + H]^{\bullet+}$).

MMY-SJG could be detected in all three predicted forms. In the presence of aqueous solvent both the imine and carbinolamine could be detected (Figure 11.19a). In the presence of MeOH, the carbinolamine methyl ether could also be detected (Figure

11.19b). It is of note that, in the presence of MeOH, the carbinolamine methyl ether form of the compound becomes the most intense species detected. This has implications for mass spectral detection of the compounds, as the parent imine form is no longer the most intense ion, and therefore would not afford the most sensitive detection.

11.3.3 SJG-303

SJG-303 could be detected in all three forms. In the presence of water, the imine and more intense carbinolamine forms were detected (Figure 11.20, top trace). In the presence of methanol, the carbinolamine methyl ether could also be detected alongside the imine (Figure 11.20, bottom trace). Further, there was also evidence for the presence of carbinolamine and carbinolamine methyl ether plus sodium adducts (i.e. +23 for $[M + Na]^{\bullet+}$ instead of $[M + H]^{\bullet+}$) in both traces.

The formation of alternate forms of the monomer compounds was investigated as this influenced the choice of mobile phase for HPLC method development for this range of PBD compounds. The findings from this preliminary study resulted in changing from the initial MeOH based method to MeCN for all method development of PBD compounds. Ideally, working with one form of the compound is analytically favourable, but it was impractical to eliminate the aqueous element from the assay methods. Furthermore, there was no evidence during HPLC method development that the different forms of the PBD compounds could be separated chromatographically; therefore, it was unlikely to be of great import unless using mass spectrometry as the primary mode of detection.

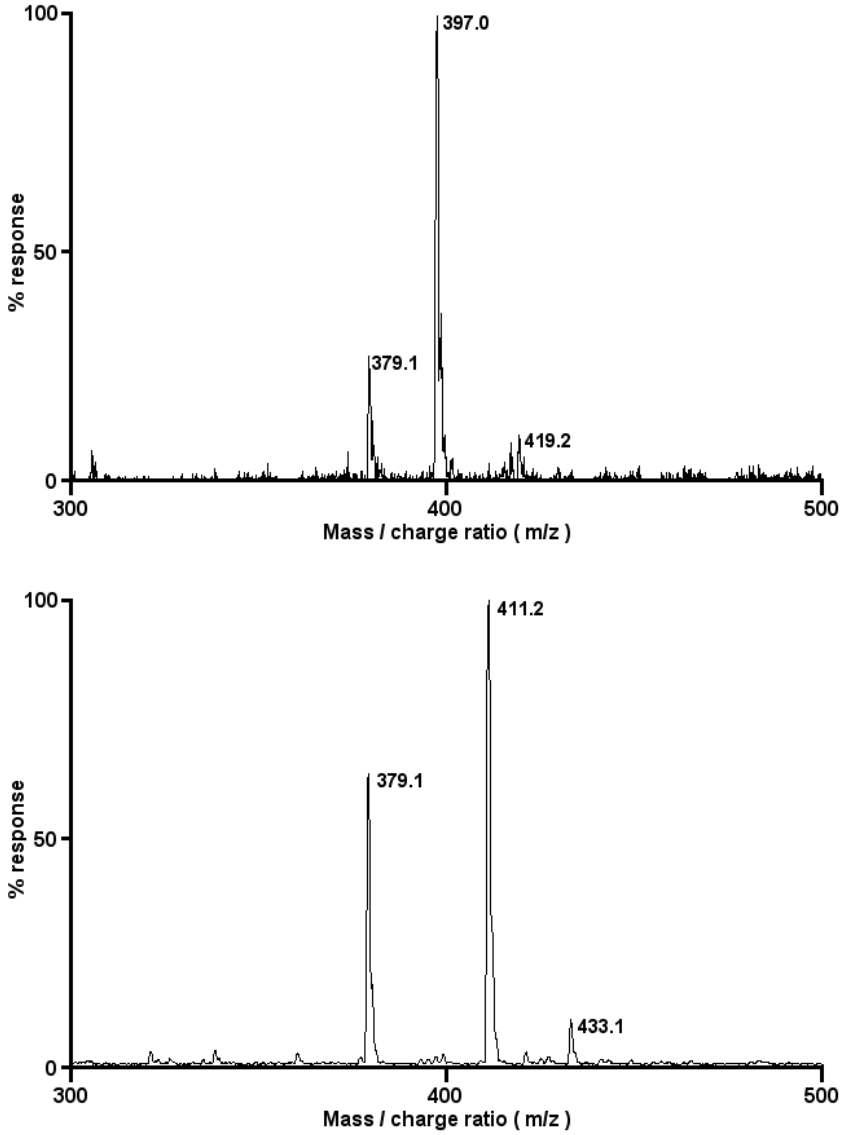

Figure 11.20 Mass spectra of SJG-303. Top trace; no methanol present, showing evidence of SJG-303 in imine (379.1; $[M + H]^{\bullet+}$) and carbinolamine (397.0; $[M + H_2O + H]^{\bullet+}$) form. Bottom trace; methanol present, showing additional evidence of carbinolamine methyl ether (411.2; $[M + MeOH + H]^{\bullet+}$).

11.4 Stability in blood and plasma

11.4.1 DC-81

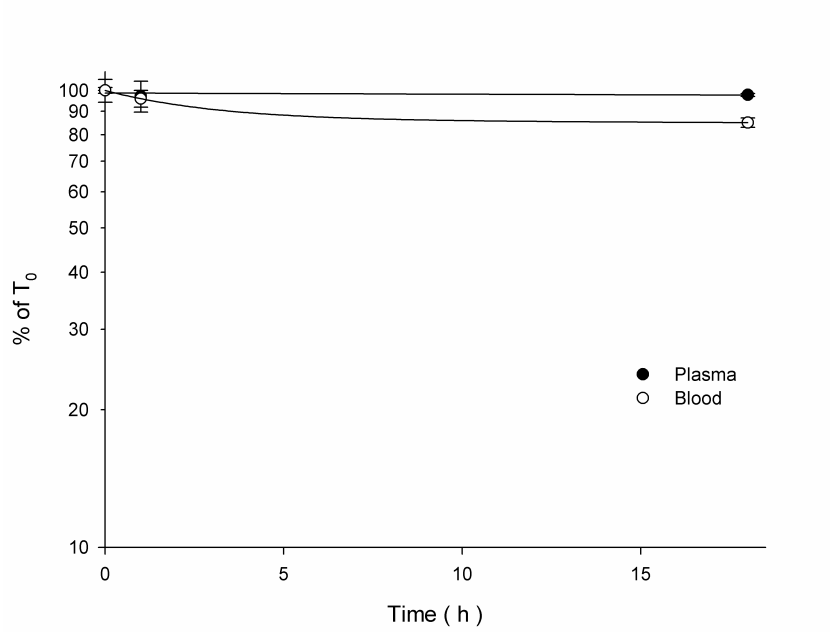

Figure 11.21 Stability of DC-81 in blood and plasma over 18 h. 50 µM compound incubated at 37°C (mean ± SD; *n* = 3).

The data in Figure 11.21 show the stability of DC-81 over an 18 h period when incubated with either mouse whole blood or plasma. DC-81 is relatively stable in plasma, with <5% loss of parent compound over 18 h. However, DC81 appears to be less stable in blood, with <5% loss of compound over the first hour, rising to a 15% loss over the 18 h period. These data indicate plasma and blood $t_{½}$ in excess of 18 h, and demonstrate DC-81 to be relatively stable. This indicates that it is unlikely that there will be extensive degradation of DC-81 in plasma or blood samples over this time period.

11.4.2 MMY-SJG

The data in Figure 11.22 show the stability of MMY-SJG in blood and plasma over an 18 h period. MMY-SJG is stable in plasma over 18 h, with <1% loss of parent compound over 18 h. However, MMY-SJG was less stable in blood showing a 21% loss of compound over the first hour, rising to 25% total loss of parent compound over 18 h.

These data indicate that MMY-SJG has a $t_{½}$ in blood and plasma greater than 18 h. However, it is apparent that there is loss of compound in blood samples over the initial 1 h period. To maximise recovery of MMY-SJG from samples this would suggest that rapid sample processing (centrifugation to separate plasma) once a blood sample is obtained may help to maximise recovery of compound.

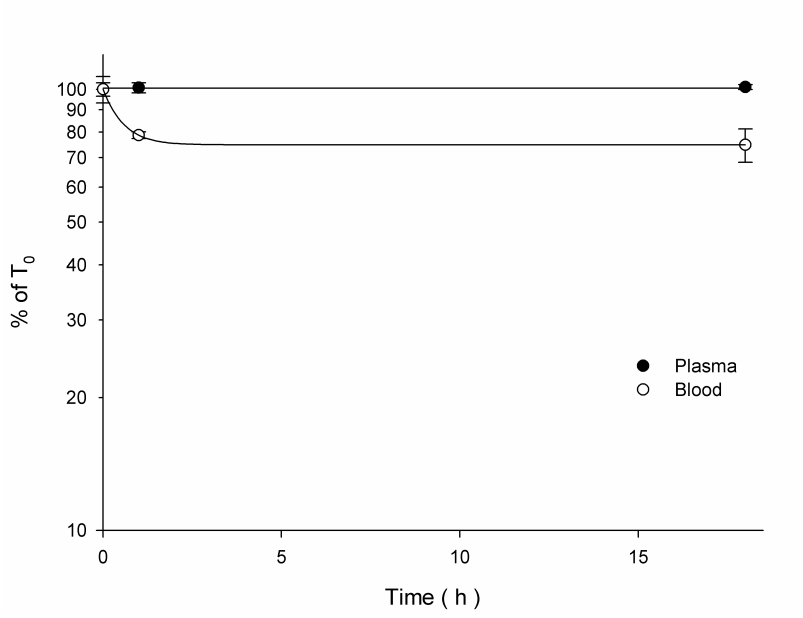

Figure 11.22 Blood and plasma stability of MMY-SJG over 18 h. 50 µM compound incubated at 37 ºC (mean ± SD; *n* = 3).

11.4.3 SJG-303

The PBD monomer SJG-303 was investigated in a similar fashion. SJG-303 is fairly stable in plasma, showing a 5% loss of parent compound over the 18 h period (Figure 11.23). The compound is less stable in blood, with a loss of 28% parent compound over the first hour, rising to 35% loss over 18 h.

As with both DC-81 and MMY-SJG, the SJG-303 compound shows plasma and blood $t_{½}$ of greater than 18 h. Similar to MMY-SJG though, there is appreciable loss of SJG-303 in blood over the first hour, indicating the need to separate plasma from blood rapidly to maximise recovery of compound from samples.

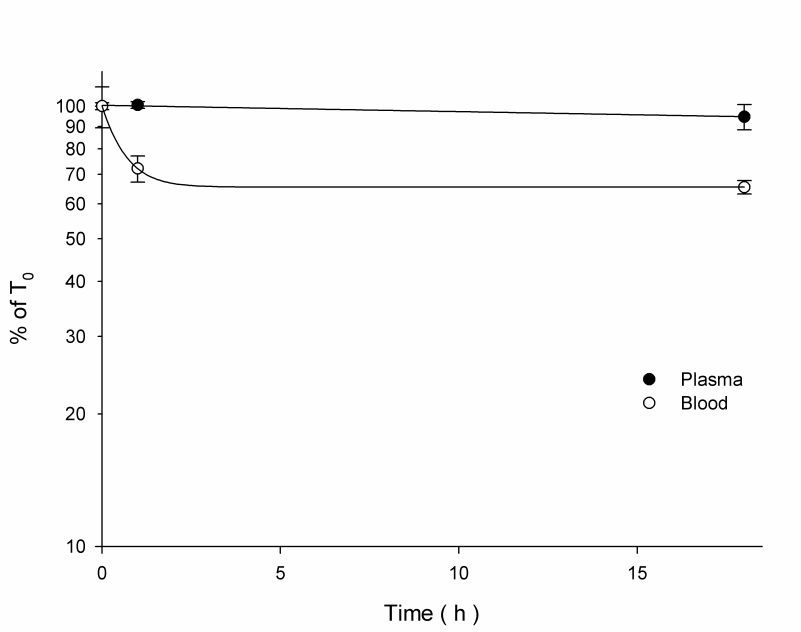

Figure 11.23 Blood and plasma stability of SJG-303 over 18 h. 50 µM compound incubated at 37 ºC (mean ± SD; *n* = 3).

11.5 Extraction efficiency

Efficiency of extraction of the PBD monomer compounds DC-81, MMY-SJG and SJG-303 from blood and plasma was investigated using a MeCN protein precipitation

method (Table 11.1). This method resulted in high levels of recovery for the PBD monomer compounds. On this basis, alternate methods of extraction were not investigated as this method proved to be both simple and effective.

High levels of extraction were seen from plasma samples for all compounds, and decreased levels of recovery were seen for extraction from blood. Analytically, extraction from plasma is more relevant as plasma samples are more commonly studied.

Compound	Extraction efficiency (%)	
	Plasma	Blood
DC-81	97.7 ± 13.9	46.8 ± 4.2
MMY-SJG	79.8 ± 3.1	64.1 ± 2.4
SJG-303	92.0 ± 7.3	70.0 ± 12.4

Table 11.1 Extraction efficiencies determined for PBD monomer compounds from murine blood and plasma using MeCN protein precipitation method (mean ± SD; $n = 6$).

11.6 Summary

The aim of this investigation was to develop analytical methods for the three PBD monomer compounds, DC-81, MMY-SJG and SJG-303 along with extraction methods to enable analysis of compound levels in biological fluids. DC-81 has been examined previously for cytotoxicity and DNA binding abilities (Bose *et al.*, 1992c; Puvvada *et al.*, 1993; 1997). Although of less interest as a potential clinical agent, DC-81 was included in this study to act as a point of reference for comparison with the novel PBD

monomers, MMY-SJG and SJG-303, along with further comparison to the PBD dimer SJG-136 in glutathione reactivity studies (Chapter 12).

This is the first study to demonstrate analytical methods and extraction procedures for DC-81, MMY-SJG and SJG-303. The compounds have been characterised to allow their optimal modes of detection to be selected. The relative stabilities of the PBD monomers in blood and plasma have also been investigated. Furthermore, the phenomenon observed with the other PBD compounds investigated, SJG-136 (chapter 9.1.4) and D709119 (chapter 10.1.3), showing reactivity of the compounds with water and methanol to produce carbinolamine and carbinolamine methyl ether derivatives of the compounds, was also seen with these monomer agents. This is an important issue to be considered for detection using mass spectrometry in future work.

12 Glutathione reactivity of PBDs

Studies have suggested a reactivity of GSH with PBD-based compounds (Morris, 1992; Smellie *et al.*, 1994; Zioga, 1999), both in cell-free and cell-based systems. A range of PBD compounds were investigated in order to better characterise the reactivity seen in the earlier studies. In order to put these data into a biologically relevant perspective, it is important to be aware that previously published work estimates the concentration of GSH in murine plasma to be in the range of 20-100 μM (Kim *et al.*, 2003). Intracellular concentrations of GSH are found to be approximately 1-20 mM, dependant on cell type (Liu & Hannun, 1997; Vahrmeijer *et al.*, 1999; Zhang, 2000; Hogg, 2002).

12.1 Reaction with GSH versus time

12.1.1 DC-81

Incubation of the PBD monomer DC-81 (50 μM in PBS) with 50 μM GSH over time showed an initial and immediate decrease in compound recovered, with little drop in recovery over the following 3 h. This experiment was conducted twice: once injecting the GSH reaction mixture directly onto the HPLC system, and secondly using a MeCN protein precipitation extraction procedure (Figure 12.1) to assess impact of extraction on the reaction. This study showed a lack of influence of time on the reaction of GSH with DC-81, indicating that the reaction occurs in t <5 min (estimated time required to handle and inject sample onto HPLC system), and the $t_{½}$ of DC-81 after this point is > 3h. Extrapolation of the curve fit estimates this at 7.6 h (for extracted samples) and 30.1 h (without extraction) relative to initial recovery from GSH. There is evidence of an effect of extraction on recovery of DC-81 as this increased drug recovered from approximately 60-80%, indicating possible disruption of binding of DC-81 to GSH by

MeCN. Calculation of a half-life for the PBD with GSH incubation is unlikely to be valid as the initial drop in compound levels occurs rapidly (t <5 min), and accounts for the largest decrease in compound recovery seen during the course of the experiment.

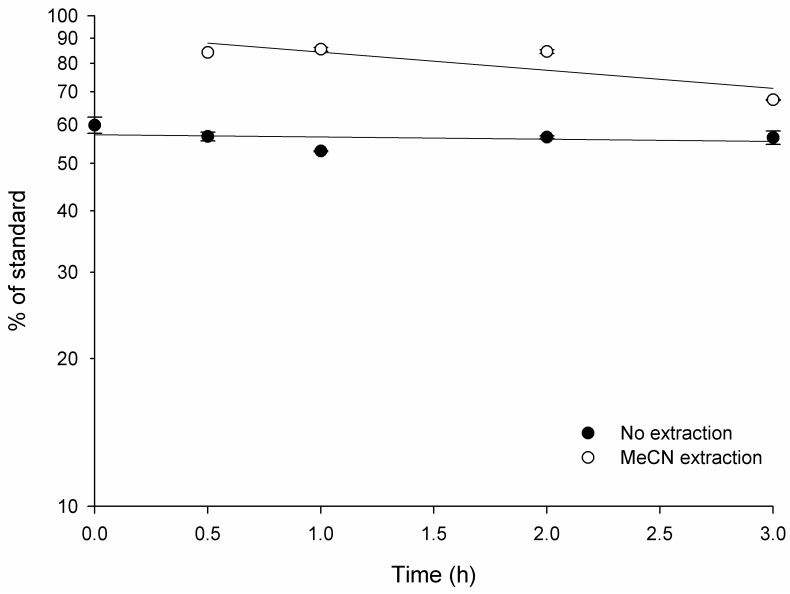

Figure 12.1 Reactivity of DC-81 (50 μM) over time with GSH (50 μM), relative to DC-81 control (0 μM GSH) (mean ± SD; n = 3). Open circles indicate MeCN extraction method used to recover DC-81, closed circles indicate no extraction used.

12.1.2 MMY-SJG

Similar to DC-81 (section 12.1.1), MMY-SJG shows an immediate and rapid drop in recovery of compound (t < 5 min). After the initial drop in compound level, there was only a small alteration in compound levels over the subsequent 3 h (Figure 12.2). The data indicated a $t_{½}$ > 3 h for both the extracted and non-extracted experiments (21.0 and 10.9 h, respectively, by extrapolation of curve fit; values relative to t_0 recovery of compound). The trend seen with DC-81 is repeated with MMY-SJG; extraction appears

to influence recovery of compound after incubation with GSH, but time does not seem to exert great influence on MMY-SJG levels relative to the initial drop in recovery.

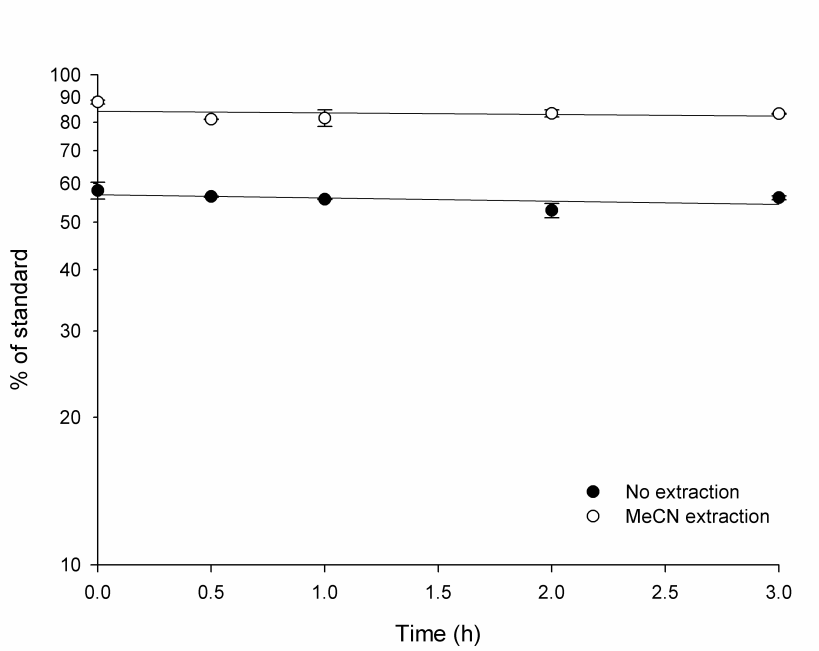

Figure 12.2 Reactivity of MMY-SJG (50 μM) over time with GSH (50 μM), relative to MMY-SJG control (0 μM GSH) (mean ± SD; n = 3). Open circle indicates MeCN extraction method used to recover DC-81, closed circle indicates no extraction used.

12.1.3 SJG-303

SJG-303 repeats the pattern of GSH reactivity seen with DC-81 and MMY-SJG, although it appears that time of incubation with GSH is more influential than with the other monomers, and almost 100% of SJG-303 could be recovered at the early time points (t = 0 and t = 0.5 h) compared to the other monomers when MeCN extraction is used (Figure 12.3). SJG-303 shows shorter $t_{½}$ (4.4 h in extracted samples, 6.1 h in non-extracted samples) than both DC-81 and MMY-SJG, although it maintains the initial rapid disappearance of parent compound when GSH is present.

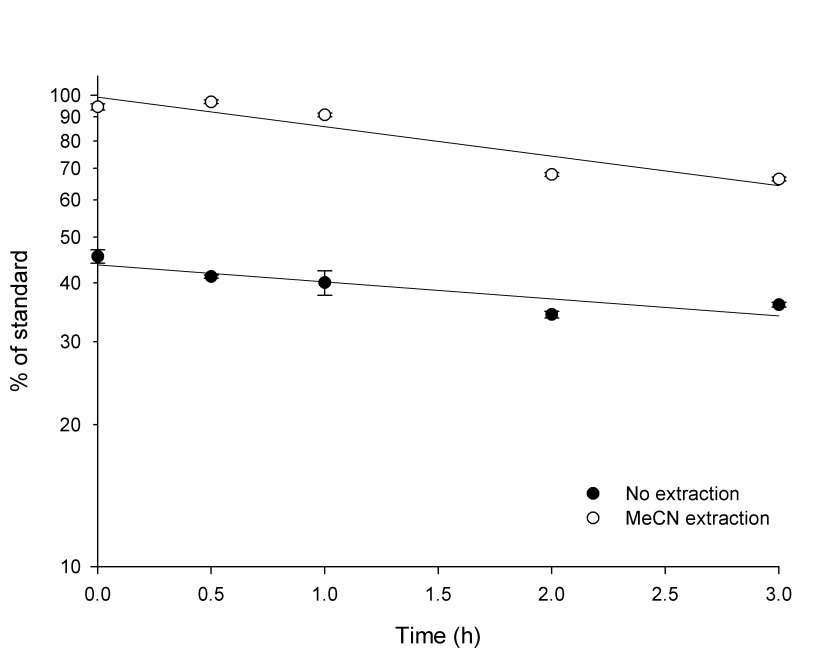

Figure 12.3 Reactivity of SJG-303 over time with GSH (50 μM), relative to SJG-303 control (0 μM GSH) (mean ± SD; n = 3). Open circle indicates MeCN extraction method used to recover DC-81, closed circle indicates no extraction used.

There is a clear trend across all three monomers investigated in this study. Disappearance of compound at t < 5 min (unfeasible to process and inject samples quicker than this onto the analytical system) is apparent in all three monomers (excepting SJG-303, where 100% recovery was achieved at early time-points with extraction). The MeCN extraction procedure has a noticeable effect, increasing the recovery of the monomers by approximately 20-40%; this is variable between compounds. All of the PBD monomers investigated had half-lives longer than the investigated period. The 3 h period reflects a reasonable estimate of the time of exposure likely to be seen *in vivo* based on previous pharmacokinetic studies performed with the PBD dimer DSB-120 (Walton *et al.*, 1996). These data indicate that GSH binding to the PBD compounds is likely to occur rapidly; the effect of a range of concentrations of GSH on compound recovery is investigated below to attempt to

ascertain how the range of GSH concentrations *in vivo* may influence PBD availability (section 12.2).

12.2 Concentration dependant reaction with GSH

The effect of a range of concentrations on PBD recovery was examined to assess the influence of GSH. The concentration range was selected to bracket physiologically relevant concentrations of GSH; plasma concentrations in the 20 – 100 μM range, and intracellular concentrations in the 1- 20 mM range. Extraction procedures were not used in order to minimise disturbance of drug-GSH reactivity.

12.2.1 DC-81

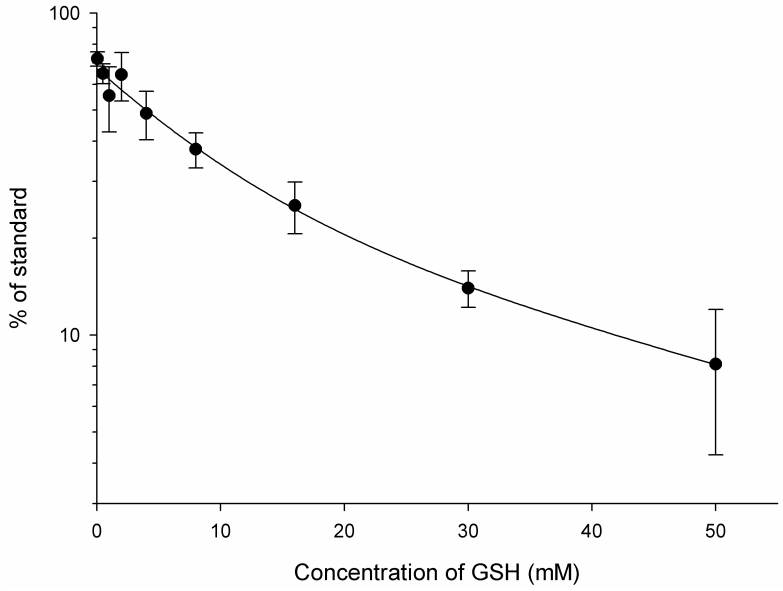

Figure 12.4 DC-81 recovery in the presence of increasing concentrations of GSH relative to standard (no GSH present). 50 μM DC-81 with GSH concentrations ranging from 0.05 – 50 mM (n = 3; mean ± SD).

As the concentration of GSH increased, it was observed that recovery of DC-81 decreased (Figure 12.4). Assuming plasma levels of GSH at approximately 100 μM, it can be estimated that 30% of DC-81 loss may be attributed to GSH binding. This decreased recovery increases as GSH levels approach intracellular concentrations (to approximately 80% DC-81 loss at 10 mM).

12.2.2 MMY-SJG

MMY-SJG recovery was observed to fall as levels of GSH were increased (Figure 12.5). At GSH levels approaching plasma concentrations, approximately >90% of compound was recovered. As concentrations of GSH approached intracellular levels this drops to approximately 30%.

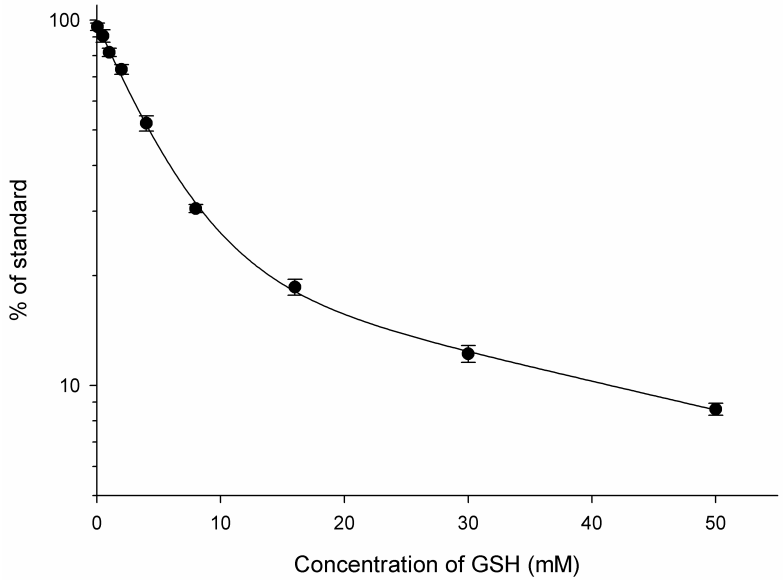

Figure 12.5 MMY-SJG recovery in the presence of increasing concentrations of GSH relative to standard (no GSH present). 50 μM MMY-SJG with GSH concentrations ranging from 0.05 – 50 mM (n = 3; mean ± SD).

12.2.3 SJG-303

Recovery of SJG-303 after incubation with GSH was >90% at plasma-relevant concentrations of GSH. Recovery of the compound decreased rapidly as concentrations of GSH were increased (Figure 12.6). Recovery of drug decreased to 40% at concentrations approximating intracellular levels.

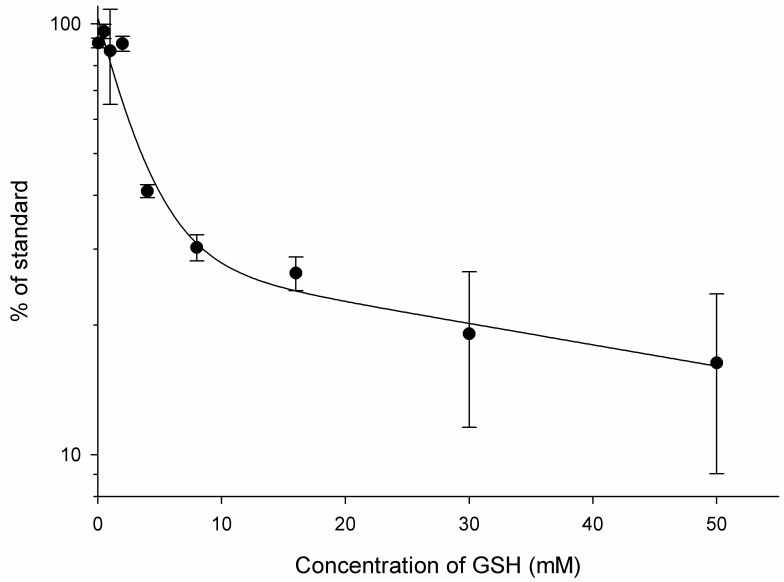

Figure 12.6 SJG-303 recovery in the presence of increasing concentrations of GSH relative to standard (no GSH present). 50 µM SJG-303 with GSH concentrations ranging from 0.05 – 50 mM (n = 3; mean ± SD).

12.2.4 SJG-136

Concentrations of SJG-136 were seen to decrease relative to increasing GSH concentration, as was found with the PBD monomer compounds. This was seen at the same molar concentration of SJG-136 as the monomer compounds (Figure 12.7) and at a lower concentration of SJG-136 (Figure 12.8).

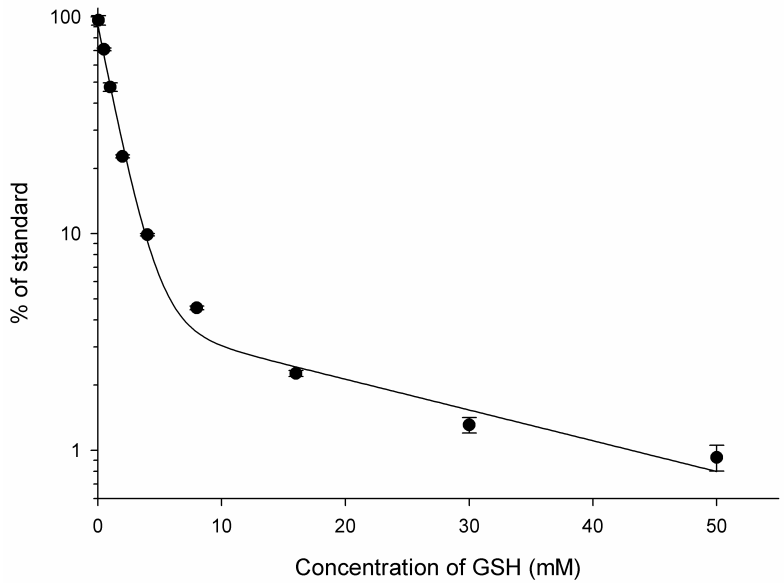

Figure 12.7 SJG-136 recovery in the presence of increasing concentrations of GSH relative to standard (no GSH present). 50 µM SJG-136 with GSH concentrations ranging from 0.05 – 50 mM (n = 3; mean ± SD).

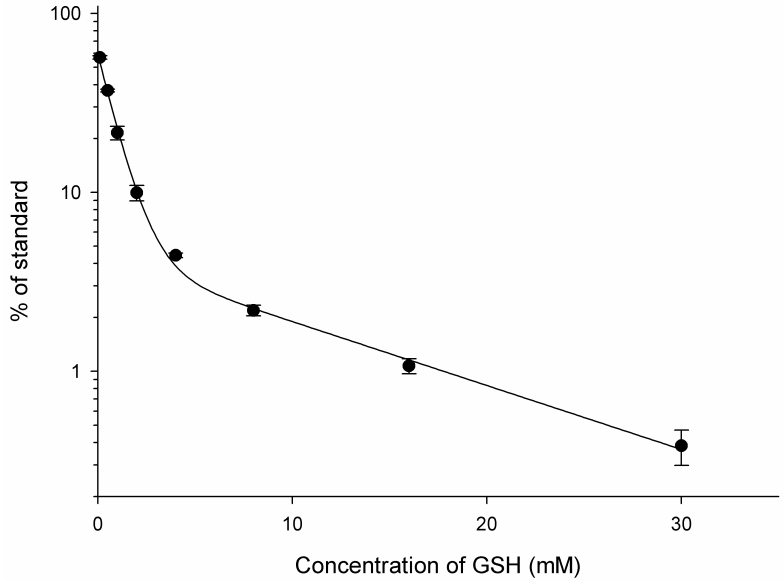

Figure 12.8 SJG-136 recovery in the presence of increasing concentrations of GSH relative to standard (no GSH present). 1 µM SJG-136 with GSH concentrations ranging from 0.1 – 30 mM (n = 3; mean ± SD).

12.3 GSH interference with metabolism

The metabolism of SJG-136 in liver S9 fraction was investigated in section 9.6.1. It was observed that the traces of SJG-136 (which appeared extensively and rapidly metabolised in S9 fraction; $t_{½} < 5$ min) after incubation with GSH appeared to closely correlate to those after incubation with murine liver S9 fraction. Further investigation showed that these traces matched (Figure 12.9). It is reported in the literature that typical intracellular concentrations of GSH are in the 1 - 20 mM range (Liu & Hannun, 1997; Vahrmeijer *et al.*, 1999; Zhang, 2000; Hogg, 2002). The tissue processing involved in S9 fraction preparation is likely to result in the lysis of cells and subsequent release of intracellular contents, including GSH. It is possible that this could increase the GSH content of the S9 fraction to the low mM range, although this has not been analytically confirmed. Therefore it can be concluded from these data that the incubation of SJG-136 with S9 fraction results in reaction of GSH with SJG-136. The appearance of metabolism in previous experiments is almost certainly due to reaction with glutathione. This is supported by data shown in section 12.2, indicating that a concentration of GSH in the low mM range will result in the loss of up to 90% of parent compound.

Attempts to identify a conjugate of SJG-136 and GSH were not successful, although the disappearance of the compound strongly suggests this is occurring. Furthermore, time constraints prevented the mass spectral characterisation of peaks b and c (Figure 12.9).

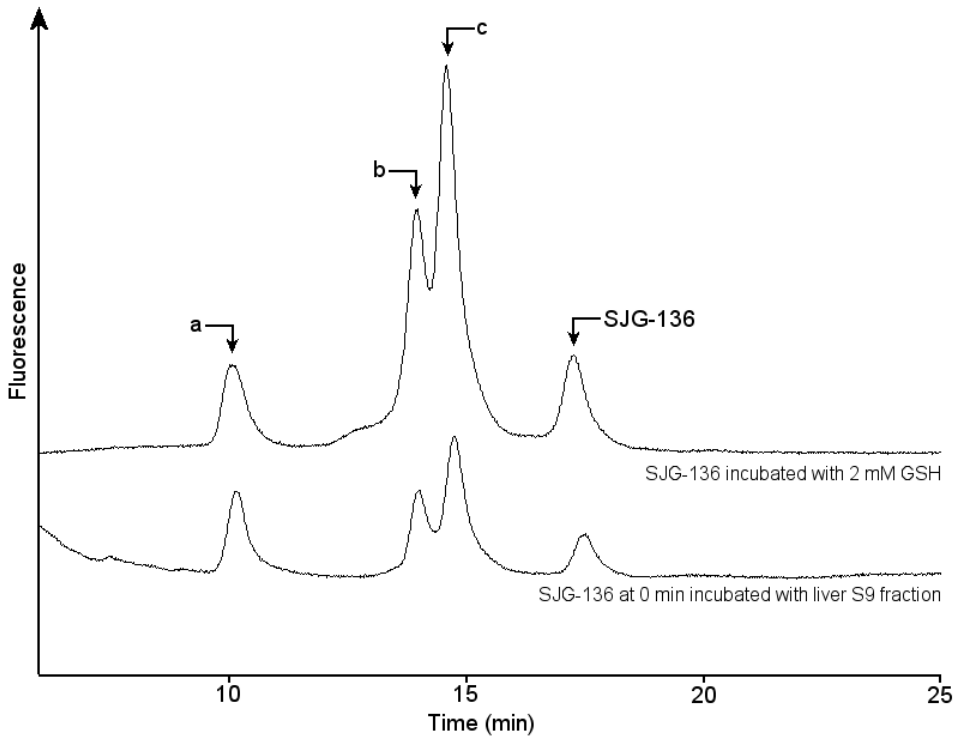

Figure 12.9 HPLC trace showing (top) SJG-136 at t_0 with 2 mM GSH and (bottom) SJG-136 incubated with S9 fraction (t_0). Traces show identical peak patterns despite no added GSH to S9 fraction experiment. Peak **a** (RT 10.2 min) present in SJG-136 standard also (possible impurity). Peaks **b** (RT 13.9 min) and **c** (RT 14.7 min) seen only when either GSH or S9 fraction present. SJG-136 seen at RT 17.5 min. RT = retention time.

12.4 Summary

With all PBD compounds investigated, it was observed that increasing concentrations of GSH resulted in lower recovery of PBD across a biologically relevant range of concentrations. These data have implications on the pharmacokinetics of PBD compounds within biological systems due to the high levels of GSH found *in vivo*. It has also been proposed that PBD compounds react readily with any thiol containing molecule (Morris *et al.*, 1990; Morris, 1992), further increasing the likelihood of reactivity of the compounds with endogenous molecules. The reactivity of the PBD compounds with GSH appears to be biphasic in all cases. It is possible that at higher

concentrations of GSH, the GSH molecules form dimers and thus the binding of GSH to itself acts as a competitive inhibitor of further reactions.

At concentrations of GSH found in the plasma there was observed to be a high recovery of PBD compounds (70 – 100%). Hence binding to GSH is not likely to influence plasma levels of PBD compounds, and therefore will not prevent distribution of the drug via the vasculature. However, due to the high levels of GSH found in the intracellular environment, the amount of free drug is likely to be significantly diminished. This effect was most marked with the clinical trial candidate molecule, SJG-136 (Figure 12.7), >90% recovery at plasma relevant concentrations and <10% recovery at intracellular relevant concentrations. Despite this drop in recovered drug at the higher concentrations of GSH, SJG-136 is still highly potent, and NCI human tumour xenograft data in the NCR-Nu mouse have indicated efficacy (personal communication, Prof. D. E. Thurston).

Relating specifically to SJG-136, it may be possible that, despite GSH binding, the inherent toxicity of the molecule is so potent that only a very small proportion of SJG-136 needs to be in an unbound state to elicit cytotoxic effects. It would be interesting to investigate this further in GSH-depleted cell lines, as one may expect increased toxicity of the compound with GSH-depleted cells if this suggestion is valid.

13 Discussion and conclusions

The pyrrolobenzodiazepine (PBD) class of compounds have been shown in several studies to have antitumour activity believed to result from cytotoxicity induced by interaction with cellular DNA. Although the use of DNA as an antitumour target has largely fallen out of favour over recent years, many of the most effective anti-cancer agents currently in use in the clinic are DNA-targeting drugs. This is due to the lack of specificity of current DNA-targeting agents and their associated toxicity. The PBD class of compound aims to improve specificity and reduce toxicity by a sequence-selective binding profile to cellular DNA (Puvvada *et al.*, 1997). Currently there are no PBD agents in the clinic, and agents that progressed to phase I trials were dropped due to high levels of toxicity (Fujita *et al.*, 1982). The main aim of this project was to characterise several PBD agents that have been flagged by the NCI 60-cell line screen as acting via a novel mechanism, and specifically to investigate the pharmacological actions of the PBD dimer SJG-136. This compound is of special interest due to its rapid progression to phase I clinical trials.

To enable accurate quantification of the PBD agents within the systems to be studied, sensitive and selective analytical methods were developed to enable extraction from the biological materials and HPLC analysis of the compounds. While mass spectroscopy was not considered an optimal mode of detection for all the compounds, it was important to ensure that a mass spectrometer-compatible HPLC method was developed in order to enable use of this mode of detection at later points of the study for purposes such as metabolite identification. As a consequence, mass spectrometer conditions for each compound were optimised. During this process it was discovered that all of the PBD agents are affected by an inherent reactivity with water and/or methanol that

causes the agents to interconvert between different forms (imine, carbinolamine, or carbinolamine methyl ether), depending on the presence of the aforementioned solvents. This became an issue as initial method development focused on a methanol/water-based separation, and interaction of the PBD agents with methanol caused the appearance of mass spectral peaks at *m/z* ratios corresponding to the discrete imine, carbinolamine, and carbinolamine methyl ether forms. While there was no evidence of chromatographic separation of these three forms, it posed a potential loss of sensitivity should single quadrupole mass spectral detection be used; the analytical sample of drug could potentially be split into three different masses each of lower intensity. This prompted the use of an acetonitrile-based method to prevent this issue. The carbinolamine (imine + water adduct) was still observed, but optimal tuning of the mass spectrometer enabled the imine form to be observed as the most intense ion, with elimination of the carbinolamine methyl ether (imine + methanol) form of the PBD compound. Furthermore, avoidance of water from the experimental protocol was deemed highly impractical for biological studies.

13.1 SJG-136

A sensitive and selective method for the analytical detection of SJG-136 was developed. Characterisation of the compound revealed fluorescence detection of SJG-136 to provide a comparable limit of detection to tandem quadrupole (MS/MS) detection, but with a higher degree of portability due to the expense and availability of MS/MS detectors. Consequentially, method development and analysis centred around HPLC separation and fluorescence detection, although MS and MS/MS detection methods were developed for further work. A simple and efficient method was developed for the extraction of SJG-136 from murine samples, allowing 98% recovery of compound from

plasma, and SJG-136 was found to be stable in plasma ($t_{½}$ > 12 h) *ex vivo*. The SJG-136 analytical method was calibrated and was found to be linear over the range 5 – 1000 nM, a range predicted to be appropriate for pre-clinical pharmacokinetic studies in view of the low MTD (0.2 mg kg^{-1} i.p., 0.3 mg kg^{-1} i.v.) for SJG-136 in the mouse.

The pre-clinical pharmacokinetic studies of SJG-136 revealed the agent to be easily detectable in the mouse at the MTD and ⅓MTD following i.v. administration, with peak plasma concentrations in the μM range; 4.8 and 1.6 μM C_{max} respectively, both at 2 min post-dose. Importantly, the observed C_{max} concentrations of SJG-136 demonstrate linear plasma pharmacokinetics for SJG-136 between the two doses, as the ⅓MTD C_{max} is 33% of the MTD, at 33% of the dose. Furthermore, using non-compartmental analysis (the linear trapezoidal method) to calculate the $AUC_{0-\infty}$ as a more accurate assessment of the linearity of the increase in detected SJG-136, the AUC of the ⅓MTD study showed as 31% of that of the value determined in the MTD study. As SJG-136 was dosed at the MTD, and linear pharmacokinetics were apparent over the 0.1 – 0.3 mg kg^{-1} range, it is likely that pharmacokinetics will be linear up to the murine MTD. However, study of SJG-136 pharmacokinetics at lower doses may be desirable to confirm linearity.

The low MTD determined for SJG-136 ensured that a highly sensitive analytical method could be developed, as it was expected that distribution of the agent within the mouse would result in low and difficult to detect plasma concentrations. Surprisingly, SJG-136 was present at high concentrations within murine plasma, and it was necessary to dilute plasma samples in order to bring the detected concentrations back within the range of the calibration curve. This arises from the low volume of distribution (V_{ss}) of

the compound, averaging at approximately 242 ml kg^{-1}, a volume lower than total body water (600 ml kg^{-1}) (Davies & Morris, 1993). The observed low volume of distribution indicates that the compound is not extensively distributed into tissues..

Parameter	SJG-136			DSB-120[a]
Structure	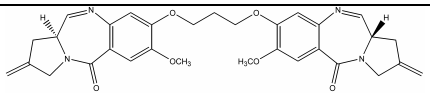			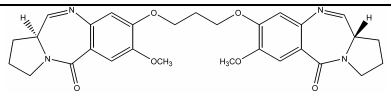
Dose (mg kg^{-1})	0.3 (MTD)	0.1 (⅓MTD)	0.2[b] (MTD)	5 (MTD)
V_{ss} (ml kg^{-1})	245	239		130
$t_{½}$ (h)	0.66	1.44	1.2	0.63
% protein bound		80.3		96.6
CL (ml min^{-1} kg^{-1})	11.8	12.9	17.7(12)	22
F (%)			67	n/a

Table 13.1 Comparison of SJG-136 (i.v. dose route) and DSB-120 (i.v dose route) pharmacokinetic properties. [a] Data taken from Walton *et al.* 1996. [b] SJG-136 i.p. data for comparison; value in brackets is corrected for incomplete absorption of SJG-136 via i.p. route.

A low volume of distribution may be the result of high plasma protein binding of SJG-136 reducing distribution of the agent outside of the bloodstream. However, protein binding studies show only a moderate level of protein binding of SJG-136. Protein binding levels of SJG-136 were established using human sera in these studies, due to the volume of biological fluid needed to perform the ultracentrifugation step. Consequentially, it would be useful to define the level of plasma protein binding in murine plasma to determine if there is a species difference between mouse and man, as a discrepancy between binding in man and mouse may lead to altered pharmacokinetics

when translating the data to man. More accurately, lower protein binding in man may result in a relatively higher proportion of free drug in plasma.

Interestingly, SJG-136 shows very similar pharmacokinetic properties to the earlier PBD dimer, DSB-120 (Table 13.1). Disappointingly, further development of DSB-120 was discontinued due to evidence of poor *in vivo* antitumour activity, despite demonstrable *in vitro* cytotoxicity (Walton *et al.*, 1996). However, SJG-136 has been shown to offer good *in vitro* antitumour activity across a wide range of human tumour xenografts *in vivo* (personal communication, D. Thurston). This is perhaps a result of the markedly increased cytotoxicity of SJG-136 compared to DSB-120; SJG-136 averages as approximately 1800-fold more cytotoxic than DSB-120 as assayed using the 96 h exposure MTT cytotoxicity assay (Gregson *et al.*, 2001). Consequentially, a much smaller concentration of SJG-136 would be required to elicit a cytotoxic effect; minimising the effect of the limited volume of distribution of SJG-136. It is apparent from these data that the small structural change from DSB-120 to SJG-136 has resulted in a significant increase in cytotoxicity of the compound without an appreciable effect on pharmacokinetics.

Plasma levels of SJG-136 were found to be well in excess of *in vitro* IC_{50} concentrations for 1 h exposure of tumour cell lines to SJG-136 for up to 2 h after dosing (section 9.5), indicating that SJG-136 is available in the systemic circulation at concentrations likely to be efficacious. SJG-136 was also detected in brain and tumour tissue at concentrations above the 1 h *in vitro* IC_{50} values; levels of SJG-136 were seen in brain samples at concentrations higher than would be expected to result solely from the

volume of blood/plasma present in the vasculature of the brain, blood volumes were not quantifiable in the tumour so this could not be estimated for tumour samples.

Intra-peritoneal pharmacokinetics of SJG-136 show a triphasic shape, indicating a rapid absorption phase, with subsequent distribution and elimination phases. Comparing the AUC of the MTD i.p. study with the i.v. study and correcting for dose indicates incomplete absorption of SJG-136 from the peritoneal cavity; approximately 68% absorbed. Values calculated for clearance and plasma half life were comparable to the i.v. dosed studies. Despite the incomplete absorption of SJG-136, back extrapolation of the distribution and elimination phases of the fitted curve to approximate an equivalent to the i.v. $C(0)$ results in the calculation of a V_i which is close to that calculated using i.v. data.

Metabolic stability of SJG-136 was studied initially using a murine liver S9 fraction preparation, however the glutathione reactivity of the compound limited the usefulness of this model (discussed below), and no discrete metabolites were identifiable. Incubation of SJG-136 with liver microsomes indicated a rapid breakdown of SJG-136 to several metabolites, with molecular weights identifiable using mass spectrometer analysis. The most abundant metabolite appeared to be a mono-demethylated form of SJG-136 (M = 542.6); the structure of this metabolite was determined by matching predictive metabolism to the detected mass spectral ion rather than via empirical determination, NMR studies on the metabolite would be required to confirm the structure. Other prospective metabolites were also detected that correspond to either ring hydroxylation of SJG-136 or breaking apart of the C8 linker into monomeric subunits.

To determine the relevance of the major metabolite determined *in vitro*, the 30 min plasma i.p. pharmacokinetic sample (corresponding to C_{max}) was reanalysed using LC-MS/MS. The metabolite was detectable *in vivo*, although assuming identical MS response to the metabolite and SJG-136, the metabolite represents only 1.2% of SJG-136 in plasma at this time point. Time constraints prevented reanalysis of further time points to establish a full pharmacokinetic profile of the metabolite and attempts to investigate potential formation of phase II metabolism derived metabolites.

Due to the fluorescence of SJG-136, it was possible to investigate cellular localisation of the agent. SJG-136 was observed to localise in the nucleus of the cells studied. However, the length of time and concentration at which cells were treated in order to detect intracellular SJG-136 resulted in obvious morphological changes to the cells arising from toxicity. While localisation in the nucleus is a desirable quality for SJG-136, as its mechanism of action is proposed to be via interaction with DNA, the concentrations of SJG-136 used (1 mM) were well in excess of the highest levels likely to actually be achieved *in vivo* (C_{max} *in vivo* from i.v. pharmacokinetic study = 4.8 μM). It is envisioned that further work using UV confocal microscopy may allow detection of SJG-136 and localisation at a more physiologically relevant concentration.

Cytotoxicity studies showed a degree of cell-type selective cytotoxicity. 96 h exposure of cells to SJG-136 indicated IC_{50} values ranging from 120 pM to 2.5 nM, dependent on cell type; a 20-fold difference between the sensitive UACC-62 melanoma cell line and the less-sensitive SK-OV-3 ovarian cell line. However, after 1 h exposure to SJG-136 there was a less pronounced difference in sensitivity to SJG-136, with only a 7-fold

difference between the sensitive M14 melanoma cell line and the less sensitive SK-MEL-2 cell line. These data are in line with previously published data indicating an IC_{50} value of 9.1 nM for 96 h exposure using the MTT assay with the SK-OV-3 cell line (found to be 2.5 nM in this study) (Gregson *et al.*, 2001), and data from the NCI 60-cell-line screen which found the GI_{50} of SJG-136 with SK-OV-3 to be 10 nM.

The effects of SJG-136 on the cell cycle were investigated to characterise the effects of the compound on cell growth and compare the actions of SJG-136 to other DNA interstrand crosslinking agents. The cells were treated at a concentration of SJG-136 achievable *in vivo* and midway between the 1 h and 96 h IC_{50} values. It was apparent that continuous exposure of cell lines to SJG-136 resulted in a decreased G_1 peak and increased S and G_2 peaks after 24 h exposure and loss of histogram definition after 48 h exposure with toxicity apparent due to the loss of adherence of the cell lines. Following 1 h exposure of the cells to SJG-136, a G_2/M block of the cell cycle was seen in all cell lines investigated after 24 h, apparent as an increase in G_2 peak area and a corresponding decrease in G_1 peak area. This effect persisted for up to 72 h post exposure in three of the five cell lines studied. This effect has been reported as a characteristic of DNA minor groove-binding agents (Erba *et al.*, 1995; Turner & Denny, 1996; Yamori *et al.*, 1999) and DNA crosslinking agents in general (Konopa, 1988). Furthermore, this study demonstrates a prolonged action of SJG-136 following a relatively short exposure of cells to SJG-136, perhaps indicative of evasion of DNA repair mechanisms by the agent arising from minimal distortion of the DNA double helix, previously proposed for the PBD dimer DSB-120 (Jenkins *et al.*, 1994) and for SJG-136 itself (Gregson *et al.*, 2001). In addition, these data are consistent with previously published data for the structurally similar but considerably less active

compound, DSB-120. Cell cycle analysis of DSB-120 revealed a dose-dependent block of the cell cycle in the G_2/M phase, with effects persisting for up to 96 h post-exposure following a 1 h exposure of cells to agent (Smellie *et al.*, 1994).

Assessment of the crosslinking effects of SJG-136 *in vivo* allowed a unique assessment of a pharmacodynamic endpoint for the agent, as DNA interstrand crosslinking of SJG-136 is the proposed mechanism by which SJG-136 elicits its cytotoxic effects. SJG-136 was shown to produce a high level of interstrand crosslinks in lymphocytes, as assessed using the Comet assay. Comparison of the crosslinking induced in lymphocytes after 1 h post dose to that present 24 h post dose revealed no significant decrease in the amount of crosslinking between the two time points; further evidence of a lack of cellular competency to repair SJG-136-induced lesions. Furthermore, there was no significant dose-dependent difference in the amount of crosslinking arising from dosing at the MTD versus ⅓MTD, although there was an observable (not-significant) decrease in crosslinking at ⅓MTD in both the i.p. and i.v. dosed studies. Detection of interstrand crosslinks within the HL-60 (acute myeloid leukaemia derived cell line) tumour was not possible, as there was a high level of DNA fragmentation observed in control tumour cells arising as a characteristic of the tumour therefore invalidating the assay for this tumour; time constraints prevented study of an alternate tumour type.

A point of note observed during the preparation of lymphocyte samples for Comet analysis is that there was appreciably less (approximately 20-fold) lymphocytes in samples from SJG-136 treated mice compared to control mice. While the investigation was not designed to investigate this and thus these data are not conclusive, it was

thought appropriate to mention this as it may provide an indication of potential toxicities of SJG-136 upon translation of the drug into man.

13.2 D709119

This study has produced a sensitive and selective LC-MS analytical method for the analysis of D709119 in biological fluids. D709119 was found to be relatively insensitive to detection via fluorescence or UV absorbance; consequentially, mass spectrometry was chosen as the mode of detection for use on the HPLC separation system. A simple and efficient acetonitrile-based protein precipitation method was developed for recovery of D709119 from murine plasma (79% extraction efficiency). The HPLC method was calibrated and D709119 was found to be linear over the 10 – 1000 nM range (10 nM limit of detection). The determined MTD for pharmacokinetic studies of D709119 was 0.5 mg kg^{-1} and it was estimated that this range would be appropriate for detection of D709119 *in vivo*.

Pre-clinical pharmacokinetic studies of D709119 at the MTD following i.p. dosing at the MTD (0.5 mg kg^{-1}) showed D709119 to be detectable well within the calibration limits of the HPLC assay. Peak plasma concentrations of D709119 were detected at 30 min post-dose as 171 nM (62.4 ng ml^{-1}). D709119 was detectable until 4 h post-dose, and non-compartmental analysis (using the linear trapezoidal method) showed the $AUC_{0-\infty}$ to be 540 nM h (197.1 ng h ml^{-1}). While it is not possible to accurately calculate the volume of distribution of D709119 from an i.p. dose due to the possibility of incomplete absorption of the compound via this route and the slow release of agent into the circulatory system, based on the rapid absorption seen in the pharmacokinetics profile $C(0)$ was estimated by back extrapolation of the distribution and elimination

portions of the fitted curve (fitted using a triphasic curve based on the two-compartment model; accounting for absorption, distribution and elimination phases) in order to allow an approximation of the initial volume of distribution for comparison to the PBD dimer compounds. The calculated V_{ss} of 3202 ml kg^{-1} tentatively indicates extensive distribution of the agent out of the central compartment, and is close to 8-fold higher that that seen for either DSB-120 (Walton *et al.*, 1996) or SJG-136 (reported in chapter 9). There is little reported data relating to the pharmacokinetic behaviour of PBD monomer agents. However, D709119 shows a much larger V_{ss} than neothramycin (3202 ml kg^{-1} versus 410 ml kg^{-1}), with a similar terminal $t_{½}$ (0.29 h versus 0.24 h) (Fujita *et al.*, 1982) (summarised in Table 13.2). These data are not strictly comparable due to the choice of differing dose routes (i.p. versus i.v.) and the disadvantages involved in predicting V_{ss} from non-i.v. data, so data should be treated with the appropriate caution. Furthermore, the plasma concentration versus time profile for D709119 showed several points with a high degree of standard deviation. Clearance of D709119 has likely been overestimated as calculation from i.p. data assumed complete absorption from the peritoneal cavity. Despite a larger volume of distribution, D709119 could not be detected in MAC29 tumour, MAC15A tumour or brain tissues in this study.

The structural differences between D709119 and neothramycin (Table 13.2) appear to have resulted in little difference in the $t_{½}$ between the compounds. The most apparent difference caused by the minor structural modifications between the two agents is the large increase in the V_{ss} of D709119 compared to neothramycin.

Parameter	D709119	neothramycin[a]
Structure	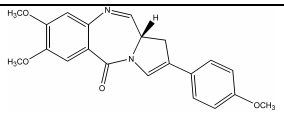	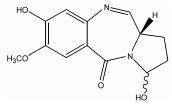
Dose (mg kg^{-1})	0.5	10
V_{ss} (ml kg^{-1})	3202	410
$t_{½}$ (h)	0.29	0.24
% protein bound	84.4	n / a
CL (ml min^{-1} kg^{-1})	42.3	20.2

Table 13.2 Comparison of D709119 (i.p. dose route) and neothramycin (i.v. dose route) pharmacokinetic properties. [a] Data taken from Fujita and co-workers (Fujita *et al.*, 1982).

The plasma time course of D709119 *in vivo* demonstrated that the agent is present in the mouse at concentrations well in excess of the 1 h IC_{50} values determined *in vitro* for up to 4 h post-dose. This indicates that D709119 is present in the circulatory system of the mouse at a concentration likely to produce a cytotoxic effect and for long enough to produce this effect. Unfortunately as levels of D709119 were not detected in the tumour it cannot be confirmed that the agent reaches the tumour at levels required to produce a cytotoxic effect.

13.3 PBD monomer compounds, MMY-SJG, SJG-303 and DC-81

Analytical methods were developed for detection of the PBD monomer compounds MMY-SJG, SJG-303 and DC-81. Characterisation of the compounds showed fluorescence detection to be the optimal mode of detection for MMY-SJG and DC-81, and UV absorbance detection using a photodiode array detector to be the optimal mode of detection for SJG-303. HPLC was used to provide chromatographic separation. An acetonitrile-based protein precipitation method was used to provide a straightforward

and efficient method for extraction of the agents from plasma and blood. Blood and plasma stability studies showed all three PBD monomer agents to be stable in murine plasma for up to 18 h, but less stable in blood.

Methods were developed for the analysis of these compounds to aid in future studies and to enable study of the glutathione reactivity of the PBD monomers. This investigation developed the first HPLC analytical method and extraction procedure for quantification of these compounds.

13.4 Reactivity of PBD compounds with glutathione

Glutathione (GSH) is a well documented agent involved in detoxification mechanisms for removal of xenobiotic compounds, including carcinogens and anticancer agents. This often involves glutathione S-transferases which act to catalyse the conjugation of GSH to a broad range of compounds. As a result of the major role of GSH in detoxification, its presence within biological systems is ubiquitous. Earlier work investigating the PBD compounds have shown an inherent, non-enzyme mediated, reactivity of this class of agents with thiol-containing molecules such as GSH (Morris *et al.*, 1990; Morris, 1992). The level of intracellular GSH has also been reported to influence cellular resistance to DSB-120; higher levels of GSH result in increased resistance (Smellie *et al.*, 1994). Consequentially the GSH reactivity of the PBD agents studied here was investigated to characterise this phenomenon and to predict the behaviour of these agents *in vivo*.

Study of the PBD monomer agents MMY-SJG, SJG-303 and DC-81 indicate that there is little influence of time on the reactivity of the compounds with GSH, as assessed by

recovery of the monomers after incubation with GSH. There appears to be an immediate (<5 min) reaction of the agents with GSH, resulting in rapid loss of detectable compound. Extraction using the acetonitrile precipitation method increased recovery of the compounds by 20-40%, indicating that this extraction procedure disrupts binding of the PBD monomers to GSH and that PBD-GSH binding is reversible. It is possible that GSH and the PBD monomers reach equilibrium rapidly, hence there is no further decrease in recovered agent after initial reaction. Further, acetonitrile may disturb binding sufficiently to increase recovery of agent by some small amount.

To investigate the effect of GSH concentration on recovery of PBD agents, the compounds were incubated with different concentrations of GSH in order to build a concentration versus percentage free PBD curve over a physiologically relevant range of concentrations. These data indicate that a higher concentration of GSH results in a lower recovery of PBD agent. To put these data in context, at concentrations of GSH found in plasma (20–100 μM), there is high recovery of PBD representative of a high amount of unbound compound, whereas at intracellular GSH concentrations (1 – 20 mM) there is a much lower recovery of PBD, representative of a lower amount of unbound compound.

Potential implications of this GSH reactivity were apparent when metabolism of SJG-136 was studied using the liver S9 fraction model. It became clear that the rapid disappearance of SJG-136 indicated in the study was attributable to the reactivity of the agent with GSH, as peaks seen in the HPLC trace after extraction from the liver S9 fraction matched exactly the peaks seen after incubation of SJG-136 with GSH alone.

GSH in the liver S9 fraction is likely to be in the mM range resulting from lysis of cells and subsequent release of intracellular GSH during preparation. Study of the metabolism of SJG-136 in the liver microsomal fraction did not show similarities to the S9 metabolism data or to the GSH studies; preparation of the liver microsomal fraction removes GSH, consequentially there is no evidence of the GSH-PBD conjugate in these data.

Thus, the innate reactivity of the PBD class of compounds is likely to affect unbound agent *in vivo* and therefore the distribution of the agents and free drug in tissue. Furthermore, this may have implications on the therapeutic usage of these compounds, as tumours expressing high levels of GSH may result in resistance.

13.5 Conclusions

The studies presented in this thesis have characterised several important factors for the progression of the PBD dimer SJG-136 into the clinic for use in man. A sensitive and selective HPLC analytical method has been developed for the analysis of pre-clinical samples, and early method development for an appropriate extraction procedure from human samples has been performed. Optimisation of the extraction procedure and full validation of the HPLC method should prove this method to be ideal for analysis of clinical samples.

The pharmacokinetics of SJG-136 in the mouse have been examined, and SJG-136 has been shown to be available *in vivo* at concentrations that produce cytotoxic effects *in vitro*. Furthermore, DNA crosslinking at these concentrations *in vivo* has been observed, demonstrating *in vivo* pharmacodynamic activity of SJG-136. Metabolism

studies of SJG-136 have identified the production of several metabolites *in vitro*, and the major metabolite is detected *in vivo*, although at low levels. Furthermore, SJG-136 has been shown to localise within the nucleus of the cell, and to cause a G_2/M block in the cell cycle, a feature characteristic of DNA-interactive agents.

A sensitive and selective HPLC based analytical method for the PBD monomer D709119 has been developed, with an accompanying extraction method for pre-clinical analysis of the agent *in vivo*. Pharmacokinetics of D709119 have shown the agent to be available following i.p. dosing at concentrations in excess of those required to elicit cytotoxic effects *in vitro*.

Glutathione reactivity towards the PBD monomers MMY-SJG, SJG-303 and MMY-SJG, and the dimer SJG-136 was investigated. The PBD agents studied all showed an inherent, non-enzyme-mediated reactivity with reduced glutathione. This is of particular interest as the agents showed highest levels of reactivity, as assessed by reduced recovery of compound, at concentrations of GSH in the intracellular range, and a markedly lower level of reactivity at levels of GSH found in plasma. This GSH reactivity suggests that activity of PBD agents may be affected by increased levels of GSH found in some tumours.

In summary, this study has shown that SJG-136 has favourable pharmacokinetics, with proven *in vivo* activity and is detectable in tumour tissue *in vivo*. D709119 possesses favourable pharmacokinetics similar to those of SJG-136, but with a larger apparent volume of distribution (further work using i.v. dosed studies needs to be done to confirm this), and may be of future interest if it shows to have anti-tumour activity. The

PBD compounds also have reactivity with GSH that may pose issues with tumours that over-express GSH.

14 Further work

The work carried out in the course of these investigations has gone some way further towards the characterisation of the compounds investigated, but has prompted the need for further investigation that time constraints have not allowed in the time-frame allocated.

Studies investigating the crosslinking of SJG-136 as assayed by Comet analysis *in vivo* in tumour were unsuccessful due to the characteristics of the tumour investigated. As a pharmacodynamic endpoint, proof of crosslinking of SJG-136 in tumour *in vivo* would be a desirable assessment of *in vivo* activity for the agent. Cell cycle analysis of the effects of SJG-136 showed a G_2/M block produced by the agent after 1 h exposure of cells to the compound 24 h post-exposure. Further characterisation of the rapidity of onset of the G_2/M block by study of cell-cycle effects at earlier time-points may prove useful. The identification of a major metabolite for SJG-136 *in vivo* is useful in predicting elimination of the compound from the body; however time did not allow a full pharmacokinetic profile to be generated for metabolite production from SJG-136 after dosing, or for the investigation of further metabolism of the metabolite. Consequentially it is not possible to estimate the AUC for the compound and therefore the proportion of SJG-136 converted to the metabolite. Synthesis of the metabolite and subsequent calibration and quantification along with full pharmacokinetic profiling would allow this to be assessed more accurately. Molecular modelling studies of the major metabolite of SJG-136 may allow elucidation of the effect of the possible dealkylation on the DNA-binding characteristics of the molecule. Combined with cytotoxicity studies, this would show the effect of the modification on the cytotoxic efficacy of the compound. However, NMR studies to confirm the predicted structure of

the metabolite would be necessary prior to further investigation. Additional sensitivity of detection provided by UV confocal microscopy may allow better visualisation of the subcellular localisation of SJG-136 at concentrations closer to those found *in vivo*. Furthermore, the use of cellular counter-stains to show the nucleus and/or other cellular organelles would allow a less subjective assessment of cellular localisation. UV confocal microscopy may also allow characterisation of selective binding of SJG-136 to DNA as assessed by the use of chromosomal spreads.

The pharmacokinetics of D709119 were investigated using an i.p. dosed *in vivo* model bearing murine tumours. Ideally to accurately predict pharmacokinetic parameters, i.v. dosing regimens such as those employed for SJG-136 should be used to eliminate the absorption phase seen with i.p. dosing as well as the possibility of incomplete absorption. Furthermore, additional studies of D709119 using two or more dose levels to establish whether or not the agent exhibits linear pharmacokinetics would be useful. Additional studies in i.v.-dosed mice bearing human tumour xenografts would allow a more accurate assessment of pharmacokinetic parameters and a closer approximation of tumour penetration to that which would be expected to be seen in man.

Of the monomer compounds studied, MMY-SJG is the monomer subunit of the dimer, SJG-136. It may be of interest to characterise this agent further to assess how the pharmacokinetics of the monomer vary compared to the dimer form.

The glutathione studies performed failed to conclusively identify the PBD-GSH adducts that were suspected to be formed and the cause of loss of recovery of the agents. Further investigations may be able to identify this adduct to confirm or disprove the

formation of this adduct using mass spectrometry and chromatography. If this adduct can be identified successfully, re-analysis of the SJG-136 pharmacokinetic samples would determine if this conjugate is seen *in vivo*. Study of the cytotoxicity of SJG-136 in GSH-depleted cell lines would also provide evidence to support GSH as a mechanism of cellular resistance to SJG-136 induced cytotoxicity.

15 References

Ackerknecht, E.H. (1953). *Rudolph Virchow: doctor, statesman, anthropologist*. University of Wisconsin Press: Madison,.

Altman, P.L. & Dittmer, D.S. (1971). *Respiration and circulation*. Biological handbooks. Federation of American Societies for Experimental Biology: Bethesda, Md.

Ames, B.N. (1983). Dietary carcinogens and anticarcinogens. Oxygen radicals and degenerative diseases. *Science*, **221,** 1256-64.

Aquilina, G., Ceccotti, S., Martinelli, S., Soddu, S., Crescenzi, M., Branch, P., Karran, P. & Bignami, M. (2000). Mismatch repair and p53 independently affect sensitivity to N-(2-chloroethyl)-N'-cyclohexyl-N-nitrosourea. *Clin Cancer Res*, **6,** 671-80.

Arima, K., Kosaka, M., Tamura, G., Imanaka, H. & Sakai, H. (1972). Studies on tomaymycin, a new antibiotic. I. Isolation and properties of tomaymycin. *J Antibiot (Tokyo)*, **25,** 437-44.

Baraldi, P.G., Cacciari, B., Guiotto, A., Romagnoli, R., Zaid, A.N. & Spalluto, G. (1999). DNA minor-groove binders: results and design of new antitumor agents. *Farmaco*, **54,** 15-25.

Barnes, D.E., Tomkinson, A.E., Lehmann, A.R., Webster, A.D. & Lindahl, T. (1992). Mutations in the DNA ligase I gene of an individual with immunodeficiencies and cellular hypersensitivity to DNA-damaging agents. *Cell*, **69,** 495-503.

Batty, D.P. & Wood, R.D. (2000). Damage recognition in nucleotide excision repair of DNA. *Gene*, **241,** 193-204.

Bazhanov, V.S. & Shepelevtseva, N.G. (1974). [Comparative study of the antitumor action and toxicity of the antibiotic sibiromycin and its sulfur derivative]. *Antibiotiki*, **19,** 714-7.

Bedford, P. & Fox, B.W. (1983). DNA-DNA interstrand crosslinking by dimethanesulphonic acid esters. Correlation with cytotoxicity and antitumour activity in the Yoshida lymphosarcoma model and relationship to chain length. *Biochem. Pharmacol.*, **32,** 2297.

Bell, W.R., Whang, J.J., Carbone, P.P., Brecher, G. & Block, J.B. (1966). Cytogenetic and morphologic abnormalities in human bone marrow cells during cytosine arabinoside therapy. *Blood*, **27,** 771-81.

Berdal, K.G., Johansen, R.F. & Seeberg, E. (1998). Release of normal bases from intact DNA by a native DNA repair enzyme. *Embo J*, **17,** 363-7.

Blackledge, G. & Averbuch, S. (2004). Gefitinib ('Iressa', ZD1839) and new epidermal growth factor receptor inhibitors. *Br J Cancer*, **90,** 566-72.

Bose, D.S., Thompson, A.S., Ching, J.S., Hartley, J.A., Berardini, M.D., Jenkins, T.C., Neidle, S., Hurley, L.H. & Thurston, D.E. (1992a). Rational Design of a Highly Efficient Irreversible DNA Interstrand Cross-Linking Agent Based on the Pyrrolobenzodiazepine Ring-System. *Journal of the American Chemical Society*, **114,** 4939-4941.

Bose, D.S., Thompson, A.S., Smellie, M., Berardini, M.D., Hartley, J.A., Jenkins, T.C., Neidle, S. & Thurston, D.E. (1992b). Effect of Linker Length on DNA-Binding Affinity, Cross-Linking Efficiency and Cytotoxicity of C8-Linked Pyrrolobenzodiazepine Dimers. *Journal of the Chemical Society-Chemical Communications***,** 1518-1520.

Bose, S.B., Jones, G.B. & Thurston, D.E. (1992c). New Approaches to Pyrrolo[2,1-c][1,4]benzodiazepines: synthesis, DNA-binding and cytotoxicity of DC-81. *Tetrahedron*, **48,** 751-758.

Boyd, M.R. (1997). The NCI *in vitro* anticancer drug discovery screen. In *Anticancer drug development guide.*, Teicher, B.A. (ed) pp. 23-42. Humana Press Inc.: New Jersey.

Braithwaite, E., Wu, X. & Wang, Z. (1999). Repair of DNA lesions: mechanisms and relative repair efficiencies. *Mutat Res*, **424,** 207-19.

Brazhnikova, M.G., Konstantinova, N.V. & Mesentsev, A.S. (1972). Sibiromycin: isolation and characterization. *J Antibiot (Tokyo)*, **25,** 668-73.

Bristow, R.G. & Hill, R.P. (1998). Molecular and Cellular Basis of Radiotherapy. In *The Basic Science of Oncology*, Tannock, I.F. & Hill, R.P. (eds) pp. 295-321. McGraw-Hill.

Brox, L.W., Gowans, B. & Belch, A. (1980). L-phenylalanine mustard (melphalan) uptake and cross-linking in the RPMI 6410 human lymphoblastoid cell line. *Cancer Res*, **40,** 1169-72.

Bulychev, N.V., Varaprasad, C.V., Dorman, G., Miller, J.H., Eisenberg, M., Grollman, A.P. & Johnson, F. (1996). Substrate specificity of Escherichia coli MutY protein. *Biochemistry*, **35,** 13147-56.

Buolamwini, J.K. (1999). Novel anticancer drug discovery. *Curr. Opin. Chem. Biol.*, **3,** 500-509.

Cancer Research UK. (2002). CancerStats Incidence - UK.

Cancer Research UK. (2003). CancerStats Mortality - UK.

Canman, C.E. & Kastan, M. (1995). Induction of apoptosis by tumour suppressor genes and oncogenes. *Cancer Biol.*, **6,** 17-25.

Chapman, J.D., Dugle, D.L., Reuvers, A.P., Meeker, B.E. & Borsa, J. (1974). Letter: Studies on the radiosensitizing effect of oxygen in Chinese hamster cells. *Int J Radiat Biol Relat Stud Phys Chem Med*, **26,** 383-9.

Chen, D.S., Herman, T. & Demple, B. (1991). Two distinct human DNA diesterases that hydrolyze 3'-blocking deoxyribose fragments from oxidized DNA. *Nucleic Acids Res*, **19,** 5907-14.

Chene, P. (2001). p53 as a drug target in cancer therapy. *Expert Opin. Ther. Patents*, **11,** 923-935.

Cheong, N., Wang, Y. & Iliakis, G. (1993). Radioresistance induced in rat embryo cells by transfection with the oncogenes H-ras plus v-myc is cell cycle dependent and maximal during S and G2. *Int J Radiat Biol*, **63,** 623-9.

Clayman, G.L., Frank, D.K., Bruso, P.A. & Goepfert, H. (1999). Adenovirus-mediated wild-type p53 gene transfer as a surgical adjuvant in advanced head and neck cancers. *Clin Cancer Res*, **5,** 1715-22.

Cole, R.S. (1973). Repair of DNA containing interstrand crosslinks in Escherichia coli: sequential excision and recombination. *Proc Natl Acad Sci U S A*, **70,** 1064-8.

Collins, J.M., Zaharko, D.S., Dedrick, R.L. & Chabner, B.A. (1986). Potential roles for preclinical pharmacology in phase I clinical trials. *Cancer Treat Rep*, **70,** 73-80.

Damia, G., Imperatori, L., Stefanini, M. & D'Incalci, M. (1996). Sensitivity of CHO mutant cell lines with specific defects in nucleotide excision repair to different anti-cancer agents. *Int J Cancer*, **66,** 779-83.

Davies, B. & Morris, T. (1993). Physiological parameters in laboratory animals and humans. *Pharm Res*, **10,** 1093-5.

De Silva, I.U., McHugh, P.J., Clingen, P.H. & Hartley, J.A. (2000). Defining the roles of nucleotide excision repair and recombination in the repair of DNA interstrand cross-links in mammalian cells. *Mol Cell Biol*, **20,** 7980-90.

Diamandopoulos, G.T. (1996). Cancer: an historical perspective. *Anticancer Res*, **16,** 1595-602.

Doetsch, P.W. & Cunningham, R.P. (1990). The enzymology of apurinic/apyrimidinic endonucleases. *Mutat Res*, **236,** 173-201.

Doll, R. & Peto, R. (1981). The causes of cancer: quantitative estimates of avoidable risks of cancer in the United States today. *J Natl Cancer Inst*, **66,** 1191-308.

Druker, B.J., Talpaz, M., Resta, D.J., Peng, B., Buchdunger, E., Ford, J.M., Lydon, N.B., Kantarjian, H., Capdeville, R., Ohno-Jones, S. & Sawyers, C.L. (2001). Efficacy and safety of a specific inhibitor of the BCR-ABL tyrosine kinase in chronic myeloid leukemia. *N Engl J Med*, **344,** 1031-7.

Dudnik, I.V., Karpov, V.L. & Netyksa, E.M. (1971). [Sulfur containing derivative of sibiromycin. Separation of sulfur during the interaction with DNA]. *Antibiotiki*, **16,** 6-8.

El-Hariry, I. & Pignatelli, M. (1997). Adhesion molecules: oppurtunities for modulation and a paradigm for novel therapeutic approaches in cancer. *Exp. Opin. Invest. Drugs*, **6,** 1465-1478.

Eliceiri, B.P. & Cheresh, D.A. (2001). Adhesion events in angiogenesis. *Curr. Opin. Cell Biol.*, **13,** 563-568.

e-Museum, N. (1926). The Nobel Prize in Physiology or Medicine 1926, Vol. 2004. Nobel e-Museum.

Erba, E., Mascellani, E., Pifferi, A. & D'Incalci, M. (1995). Comparison of cell-cycle phase perturbations induced by the DNA-minor-groove alkylator tallimustine and by melphalan in the SW626 cell line. *Int J Cancer*, **62,** 170-5.

Evans, E., Moggs, J.G., Hwang, J.R., Egly, J.M. & Wood, R.D. (1997). Mechanism of open complex and dual incision formation by human nucleotide excision repair factors. *Embo J*, **16,** 6559-73.

Farmer, P.B. (1987). Metabolism and reactions of alkylating agents. *Parmac. Ther.*, **35,** 301.

Feng, J., Funk, W.D., Wang, S.S., Weinrich, S.L., Avilion, A.A., Chiu, C.P., Adams, R.R., Chang, E., Allsopp, R.C., Yu, J. & et al. (1995). The RNA component of human telomerase. *Science*, **269,** 1236-41.

Ferber, D. (1999). Cancer research. A new way to combat therapy side effects. *Science*, **285,** 1651, 1653.

Fichtinger-Schepman, A.M., van Oosterom, A.T., Lohman, P.H. & Berends, F. (1987). cis-Diamminedichloroplatinum(II)-induced DNA adducts in peripheral leukocytes from seven cancer patients: quantitative immunochemical detection of the adduct induction and removal after a single dose of cis-diamminedichloroplatinum(II). *Cancer Res*, **47,** 3000-4.

Fojo, T. (2001). Cancer, DNA repair mechanisms, and resistance to chemotherapy. *J Natl Cancer Inst*, **93,** 1434-6.

Franks, L.M. & Teich, N.M. (1997). *Introduction to the cellular and molecular biology of cancer*. Oxford University Press: Oxford.

Frei, E. (1982). The national cancer chemotherapy program. *Science*, **217,** 600-606.

Friedberg, E.C., Walker, G.C. & Siede, W. (1995). *DNA repair and mutagenesis*. ASM Press: Washington.

Fujita, E., Mukasa, T., Tsukahara, T., Arahata, K., Omura, S. & Momoi, T. (1996). Enhancement of CPP32-like activity in the TNF-treated U937 cells by the proteasome inhibitors. *Biochem Biophys Res Commun*, **224,** 74-9.

Fujita, H., Ogawa, K., Okada, A., Kusama, T., Kajii, K., Suga, S. & Kimura, K. (1982). Pharmacokinetics of neothramycin in animals and man. *J Antibiot (Tokyo)*, **35,** 1093-100.

Garcia, S.T., McQuillan, A. & Panasci, I. (1988). Correlation between the cytotoxicity of melphalan and DNA crosslinks as detected by the ethidium bromide fluorescence assay. *Biochem Pharmacol*, **37**.

Gasco, M. & Crook, T. (2003). p53 family members and chemoresistance in cancer: what we know and what we need to know. *Drug Resist Updat*, **6,** 323-8.

Gauze, G.F., Preobrazhenskaia, T.P., Ivanitskaia, L.P. & Sveshnikova, M.A. (1969). [Production of the antibiotic sibiromycin by the Streptosporangium sibiricum sp. nov. culture]. *Antibiotiki*, **14,** 963-9.

Gauze, G.G., Dudnik Iu, V. & Dolgilevich, S.M. (1972). [Suppression of nucleic acid synthesis by atineoplastic antibiotic sibiromycin]. *Antibiotiki*, **17,** 413-9.

Gibaldi, M. (1984). *Biopharmaceutics and Clinical Pharmacokinetics*. Lea & Febiger.

Gilman, A. & Philips, F.S. (1946). The biological actions and therapeutic applications of β-chloroehtylamines and sulfides. *Science*, **103,** 409.

Glisson, B., Gupta, R., Hodges, P. & Ross, W. (1986). Cross-resistance to intercalating agents in an epipodophyllotoxin- resistant Chinese hamster ovary cell line: evidence for a common intracellular target. *Cancer Res*, **46,** 1939-42.

Gogos, A., Cillo, J., Clarke, N.D. & Lu, A.L. (1996). Specific recognition of A/G and A/7,8-dihydro-8-oxoguanine (8-oxoG) mismatches by Escherichia coli MutY: removal of the C-terminal domain preferentially affects A/8-oxoG recognition. *Biochemistry*, **35,** 16665-71.

Graves, D.E., Pattaroni, C., Krishnan, B.S., Ostrander, J.M., Hurley, L.H. & Krugh, T.R. (1984). The reaction of anthramycin with DNA. Proton and carbon nuclear magnetic resonance studies on the structure of the anthramycin-DNA adduct. *J Biol Chem*, **259,** 8202-9.

Gregson, S.J., Howard, P.W., Corcoran, K.E., Barcella, S., Yasin, M.M., Hurst, A.A., Jenkins, T.C., Kelland, L.R. & Thurston, D.E. (2000). Effect of C2-exo unsaturation on the cytotoxicity and DNA-binding reactivity of pyrrolo[2,1-c][1,4]benzodiazepines. *Bioorg Med Chem Lett*, **10,** 1845-7.

Gregson, S.J., Howard, P.W., Hartley, J.A., Brooks, N.A., Adams, L.J., Jenkins, T.C., Kelland, L.R. & Thurston, D.E. (2001). Design, synthesis, and evaluation of a novel pyrrolobenzodiazepine DNA- interactive agent with highly efficient cross-linking ability and potent cytotoxicity. *J Med Chem*, **44,** 737-48.

Gregson, S.J., Howard, P.W., Jenkins, T.C., Kelland, L.R. & Thurston, D.E. (1999). Synthesis of a novel C2/C2'-exo unsaturated pyrrolobenzodiazepine cross-linking agent with remarkable DNA binding affinity and cytotoxicity. *Chem Commun***,** 797-798.

Harker, W.G., Slade, D.L., Dalton, W.S., Meltzer, P.S. & Trent, J.M. (1989). Multidrug resistance in mitoxantrone-selected HL-60 leukemia cells in the absence of P-glycoprotein overexpression. *Cancer Res*, **49,** 4542-9.

Harris, C.C. (1996). Structure and function of the p53 tumour suppressor gene: clues for rational cancer chemotherapeutic strategies. *J. Natl. Cancer Inst.*, **88,** 1442-1455.

Harris, M. (2004). Monoclonal antibodies as therapeutic agents for cancer. *Lancet Oncol*, **5,** 292-302.

Heise, C., Sampson-Johannes, A., Williams, A., McCormick, F., Von Hoff, D.D. & Kirn, D.H. (1997). ONYX-015, an E1B gene-attenuated adenovirus, causes

tumour-specific cytolysis and antutumoural afficacy that can be augmented by standard chemotherapeutic agents. *Nat. Med.*, **3,** 639-645.

Hertzberg, R.P., Hecht, S.M., Reynolds, V.L., Molineux, I.J. & Hurley, L.H. (1986). DNA sequence specificity of the pyrrolo[1,4]benzodiazepine antitumor antibiotics. Methidiumpropyl-EDTA-iron(II) footprinting analysis of DNA binding sites for anthramycin and related drugs. *Biochemistry*, **25,** 1249-58.

Hisamatsu, T., Uchida, S., Takeuchi, T., Ishizuka, M. & Umezawa, H. (1980). Antitumor effect of a new antibiotic, neothramycin. *Gann*, **71,** 308-12.

Hodgson, S.V. & Maher, E.R. (1999). *A practical guide to human cancer genetics*. Cambridge University Press: Cambridge.

Hogg, N. (2002). The biochemistry and physiology of S-nitrosothiols. *Annu Rev Pharmacol Toxicol*, **42,** 585-600.

Hollingshead, M.G., Alley, M.C., Camalier, R.F., Abbott, B.J., Mayo, J.G., Malspeis, L. & Grever, M.R. (1995). In vivo cultivation of tumor cells in hollow fibers. *Life Sciences*, **57,** 131-141.

Hollstein, M., Hergenhahn, M., Yang, Q., Bartsch, H., Wang, Z.Q. & Hainaut, P. (1999). New approaches to understanding p53 gene tumour mutation spectra. *Mutat Res*, **431,** 199-209.

Horwitz, S.B. (1975). In *Antineoplastic and Immunosuppresive Agents*, Sartorelli, A.C. & Johns, D.G. (eds) pp. 642-648. Springer-Verlag: New York.

Huang, J.C., Svoboda, D.L., Reardon, J.T. & Sancar, A. (1992). Human nucleotide excision nuclease removes thymine dimers from DNA by incising the 22nd phosphodiester bond 5' and the 6th phosphodiester bond 3' to the photodimer. *Proc Natl Acad Sci U S A*, **89,** 3664-8.

Hurley, L.H. (1977). Pyrrolo(1,4)benzodiazepine antitumor antibiotics. Comparative aspects of anthramycin, tomaymycin and sibiromycin. *J Antibiot (Tokyo)*, **30,** 349-70.

Hurley, L.H. & Petrusek, R. (1979). Proposed structure of the anthramycin-DNA adduct. *Nature*, **282,** 529-31.

Hurley, L.H., Reck, T., Thurston, D.E., Langley, D.R., Holden, K.G., Hertzberg, R.P., Hoover, J.R., Gallagher, G., Jr., Faucette, L.F., Mong, S.M. & Johnson, P.K. (1988). Pyrrolo[1,4]benzodiazepine antitumor antibiotics: relationship of DNA alkylation and sequence specificity to the biological activity of natural and synthetic compounds. *Chem Res Toxicol*, **1,** 258-68.

Ivanetich, K.M. & Santi, D.V. (1988). Thymidylate synthase and fluorouracil. *Adv. Exp. Med. Biol.*, **244,** 113.

Jenkins, T.C., Hurley, L.H., Neidle, S. & Thurston, D.E. (1994). Structure of a covalent DNA minor groove adduct with a pyrrolobenzodiazepine dimer: evidence for sequence-specific interstrand cross-linking. *J Med Chem*, **37,** 4529-37.

Jones, G.B., Davey, C.L., Jenkins, T.C., Kamal, A., Kneale, G.G., Neidle, S., Webster, G.D. & Thurston, D.E. (1990). The non-covalent interaction of pyrrolo[2, 1-c] [1, 4]benzodiazepine-5, 11-diones with DNA. *Anticancer Drug Des*, **5,** 249-64.

Kanaar, R., Hoeijmakers, J.H. & van Gent, D.C. (1998). Molecular mechanisms of DNA double strand break repair. *Trends Cell Biol*, **8,** 483-9.

Kaplan, D.J. (1982). Variation in the inhibition of restriction enzyme cleavage of lambda phage DNA produced by two covalent binding antitumor agents: anthramycin and mitomycin C. *Biochem Biophys Res Commun*, **109,** 639-48.

Katcher, H.L. & Wallace, S.S. (1983). Characterization of the Escherichia coli X-ray endonuclease, endonuclease III. *Biochemistry*, **22,** 4071-81.

Kim, K.J., Li, B., Winer, J., Armanini, M., Gillett, N., Phillips, H.S. & Ferrara, N. (1993). Inhibition of vascular endothelial growth factor-induced angiogenesis suppresses tumour growth in vivo. *Nature*, **362,** 841-4.

Kim, N.W., Piatyszek, M.A., Prowse, K.R., Harley, C.B., West, M.D., Ho, P.L., Coviello, G.M., Wright, W.E., Weinrich, S.L. & Shay, J.W. (1994). Specific association of human telomerase activity with immortal cells and cancer [see comments]. *Science*, **266,** 2011-5.

Kim, S.K., Choi, K.H. & Kim, Y.C. (2003). Effect of acute betaine administration on hepatic metabolism of S-amino acids in rats and mice. *Biochem Pharmacol*, **65,** 1565-74.

Kohn, K.W. (1975). Anthramycin. In *Antibiotics III. Mechanism of Action of Antimicrobial and Antitumour Agents*, Gottleib, D., Shaw, P.D., Corcoran, J.W. & Hahn, F.E. (eds) pp. 3-11. Springer-Verlag: New York.

Kohn, K.W. (1979). DNA as a target in cancer chemotherapy:Measurement of macromolecular DNA damage produced in mammalian cells by anticancer agents and carcinogens. *Methods Cancer Res*, **16,** 291-345.

Kohn, K.W., Glaubiger, D. & Spears, C.L. (1974). The reaction of anthramycin with DNA. II. Studies of kinetics and mechanism. *Biochim Biophys Acta*, **361,** 288-302.

Kohn, K.W. & Spears, C.L. (1970). Reaction of anthramycin with deoxyribonucleic acid. *J Mol Biol*, **51,** 551-72.

Konishi, M., Ohkuma, H., Naruse, N. & Kawaguchi, H. (1984). Chicamycin, a new antitumor antibiotic. II. Structure determination of chicamycins A and B. *J Antibiot (Tokyo)*, **37,** 200-6.

Konopa, J. (1988). G2 block induced by DNA crosslinking agents and its possible consequences. *Biochem Pharmacol*, **37,** 2303-9.

Kopka, M.L., Goodsell, D.S., Baikalov, I., Grzeskowiak, K., Cascio, D. & Dickerson, R.E. (1994). Crystal structure of a covalent DNA-drug adduct: anthramycin bound to C- C-A-A-C-G-T-T-G-G and a molecular explanation of specificity. *Biochemistry*, **33,** 13593-610.

Korman, S. & Tendler, M.D. (1965). Clinical investigation of cancer chemotherapeutic agents for neoplastic disease. *J New Drugs*, **5,** 275-85.

Krokan, H.E., Standal, R. & Slupphaug, G. (1997). DNA glycosylases in the base excision repair of DNA. *Biochem J*, **325 (Pt 1),** 1-16.

Kwon, Y. (2001). *Handbook of Essential Pharmacokinetics, Pharmacodynamics, and Drug Metabolism for Industrial Scientists*. Kluwer Academic: New York.

Lewis, N.L. & Weiner, L.M. (2002). Translational Research (Overview of Phase I, II, and III Clinical Trials). In *The Cancer Handbook*, Vol. 102. Macmillan.

Li, Q., Gardner, K., Zhang, L., Tsang, B., Bostick-Bruton, F. & Reed, E. (1998). Cisplatin induction of ERCC-1 mRNA expression in A2780/CP70 human ovarian cancer cells. *J Biol Chem*, **273,** 23419-25.

Lissauer. (1865). II. Zwei Faille von Leucaemie. *Berl. Klin. Wochenschr.*, **40,** 403.

Liu, B. & Hannun, Y.A. (1997). Inhibition of the Neutral Magnesium-dependent Sphingomyelinase by Glutathione. *J. Biol. Chem.*, **272,** 16281-16287.

Lobell, R.B. & Kohl, N.E. (1998). Pre-clinical development of farnesyltransferase inhibitors. *Cancer Metastasis Rev.*, **17,** 203-210.

Loo, T.W. & Clarke, D.M. (1999). The human multidrug resistance P-glycoprotein is inactive when its maturation is inhibited: potential for a role in cancer chemotherapy. *Faseb J*, **13,** 1724-32.

Lum, G. & Gambino, S.R. (1974). A comparison of serum versus heparinized plasma for routine chemistry tests. *Am J Clin Pathol*, **61,** 108-13.

Manuel, R.C., Czerwinski, E.W. & Lloyd, R.S. (1996). Identification of the structural and functional domains of MutY, an Escherichia coli DNA mismatch repair enzyme. *J Biol Chem*, **271,** 16218-26.

Martin, N.M. (2001). DNA repair inhibition and cancer therapy. *J Photochem Photobiol B*, **63,** 162-70.

Massey, A., Offman, J., Macpherson, P. & Karran, P. (2003). DNA mismatch repair and acquired cisplatin resistance in E. coli and human ovarian carcinoma cells. *DNA Repair (Amst)*, **2,** 73-89.

Masuda, H., Ozols, R.F., Lai, G.M., Fojo, A., Rothenberg, M. & Hamilton, T.C. (1988). Increased DNA repair as a mechanism of acquired resistance to cis-diamminedichloroplatinum (II) in human ovarian cancer cell lines. *Cancer Res*, **48,** 5713-6.

Matsumoto, Y. & Kim, K. (1995). Excision of deoxyribose phosphate residues by DNA polymerase beta during DNA repair. *Science*, **269,** 699-702.

Matter, A. (2001). Tumour angiogenesis as a therapeutic target. *DDT*, **6,** 1005-1024.

McHugh, P.J., Sones, W.R. & Hartley, J.A. (2000). Repair of intermediate structures produced at DNA interstrand cross-links in Saccharomyces cerevisiae. *Mol Cell Biol*, **20,** 3425-33.

McHugh, P.J., Spanswick, V.J. & Hartley, J.A. (2001). Repair of DNA interstrand crosslinks: molecular mechanisms and clinical relevance. *Lancet Oncol*, **2,** 483-90.

McVie, J.G. (1999). Cancer treatment: the last 25 years. *Cancer Treat Rev*, **25,** 323-331.

Middleton, M.R. & Margison, G.P. (2003). Improvement of chemotherapy efficacy by inactivation of a DNA-repair pathway. *Lancet Oncol*, **4,** 37-44.

Mistry, P., Kelland, L.R. & Harrap, K.R. (1991). The relationships between glutathione, glutathione-S-transferase and cytotoxicity of platinum drugs and melphalan in eight human ovarian carcinoma cell lines. *Br. J. Cancer.*, **64,** 215-220.

Mitsiades, N., Mitsiades, C.S., Richardson, P.G., Poulaki, V., Tai, Y.T., Chauhan, D., Fanourakis, G., Gu, X., Bailey, C., Joseph, M., Libermann, T.A., Schlossman, R., Munshi, N.C., Hideshima, T. & Anderson, K.C. (2003). The proteasome inhibitor PS-341 potentiates sensitivity of multiple myeloma cells to conventional chemotherapeutic agents: therapeutic applications. *Blood*, **101,** 2377-80.

Moertel, C.G., Lefkopoulo, M., Lipsitz, S., Hahn, R.G. & Klaassen, D. (1992). Streptozocin-doxorubicin, streptozocin-fluorouracil or chlorozotocin in the treatment of advanced islet-cell carcinoma. *N Engl J Med*, **326,** 519-23.

Mol, C.D., Parikh, S.S., Putnam, C.D., Lo, T.P. & Tainer, J.A. (1999). DNA repair mechanisms for the recognition and removal of damaged DNA bases. *Annu Rev Biophys Biomol Struct*, **28,** 101-28.

Moore, M.J. & Erlichman, C. (1998). Pharmacology of Anticancer Drugs. In *The Basic Science of Oncology*, Tannock, I.F. & Hill, R.P. (eds) pp. 370-391. McGraw-Hill.

Morris, S.J. (1992). Design, synthesis and evaluation of a sequence-selective DNA-cleaving agent based on the pyrrolobenzodiazepine ring system. In *Division of Medicinal Chemistry and Pharmacognosy.* pp. 196. University of Portsmouth: Portsmouth.

Morris, S.J., Thurston, D.E. & Nevell, T.G. (1990). Evaluation of the electrophilicity of DNA-binding pyrrolo[2,1-c][1,4]benzodiazepines by HPLC. *J Antibiot (Tokyo)*, **43,** 1286-92.

Mosmann, T. (1983). Rapid colorimetric assay for cellular growth and survival: application to proliferation and cytotoxicity assays. *J Immunol Methods*, **65,** 55-63.

Mountzouris, J.A., Wang, J.J., Thurston, D. & Hurley, L.H. (1994). Comparison of a DSB-120 DNA interstrand cross-linked adduct with the corresponding bis-tomaymycin adduct: an example of a successful template-directed approach to drug design based upon the monoalkylating compound tomaymycin. *J Med Chem*, **37,** 3132-40.

Myers, C.E., Mimnaugh, E.G., Yeh, G.C. & Sinha, B.K. (1988). Biochemical mechanisms of tumour cell kill by the anthracyclines. In *Anthracycline and Anthracenedione-based anticancer agents*, Lown, J.W. (ed) pp. 527-569. Elsevier: Amsterdam.

NCI. (2001). Development therapeutics program NCI/NIH.

Neddermann, P. & Jiricny, J. (1993). The purification of a mismatch-specific thymine-DNA glycosylase from HeLa cells. *J Biol Chem*, **268,** 21218-24.

Newell, D.R., Burtles, S.S., Fox, B.W., Jodrell, D.I. & Connors, T.A. (1999). Evaluation of rodent-only toxicology for early clinical trials with novel cancer therapeutics. *Br J Cancer*, **81,** 760-8.

Olive, P.L., Banath, J.P. & Durand, R.E. (1990). Heterogeneity in radiation-induced DNA damage and repair in tumor and normal cells measured using the "comet" assay. *Radiat Res*, **122,** 86-94.

Orlowski, R.Z. & Baldwin, A.S., Jr. (2002). NF-kappaB as a therapeutic target in cancer. *Trends Mol Med*, **8,** 385-9.

Orlowski, R.Z., Eswara, J.R., Lafond-Walker, A., Grever, M.R., Orlowski, M. & Dang, C.V. (1998). Tumor growth inhibition induced in a murine model of human Burkitt's lymphoma by a proteasome inhibitor. *Cancer Res*, **58,** 4342-8.

Ormerod, M.G. (2000). *Flow cytometry : a practical approach*. Practical approach series ; 229. Oxford University Press: Oxford.

Ostrander, J.M., Hurley, L.H., Balakrishnan, M.S. & Krugh, T. (1981). Determination of the structure of the anthramycin-DNA adduct by ^{1}H and ^{13}C-NMR spectroscopy. *J. Supramol. Struct. Cell. Biochem.*, **Suppl. 5,** 168.

Parikh, S.S., Mol, C.D. & Tainer, J.A. (1997). Base excision repair enzyme family portrait: integrating the structure and chemistry of an entire DNA repair pathway. *Structure*, **5,** 1543-50.

Peapack, N.J. (2004). Pharmacia Corporation's (PHA) Cancer Drug SU5416 (Semaxanib) Not Effective; Ends Phase III, Vol. 2004. CCIS Biospace.

Petrusek, R.L., Anderson, G.L., Garner, T.F., Fannin, Q.L., Kaplan, D.J., Zimmer, S.G. & Hurley, L.H. (1981). Pyrrol[1,4]benzodiazepine antibiotics. Proposed structures and characteristics of the in vitro deoxyribonucleic acid adducts of anthramycin, tomaymycin, sibiromycin, and neothramycins A and B. *Biochemistry*, **20,** 1111-9.

Pierce, A.J., Stark, J.M., Araujo, F.D., Moynahan, M.E., Berwick, M. & Jasin, M. (2001). Double-strand breaks and tumorigenesis. *Trends Cell Biol*, **11,** S52-9.

Plowman, J., Dykes, D.J., Hollingshead, M., Simpson-Herren, L. & Alley, M.C. (1997). Human tumor xenograft models in NCI drug development. In *Anticancer drug development guide.*, Teicher, B.A. (ed). Humana Press Inc.: New Jersey.

Pratt, W.B., Ruddon, R.W., Ensminger, W.D. & Maybaum, J. (1994). Antimetabolites. In *The Anticancer Drugs* pp. 69-107. Oxford University Press.

Puvvada, M.S., Forrow, S.A., Hartley, J.A., Stephenson, P., Gibson, I., Jenkins, T.C. & Thurston, D.E. (1997). Inhibition of bacteriophage T7 RNA polymerase in vitro transcription by DNA-binding pyrrolo[2,1-c][1,4]benzodiazepines. *Biochemistry*, **36,** 2478-84.

Puvvada, M.S., Hartley, J.A., Jenkins, T.C. & Thurston, D.E. (1993). A quantitative assay to measure the relative DNA-binding affinity of pyrrolo[2,1-c] [1,4]benzodiazepine (PBD) antitumour antibiotics based on the inhibition of restriction endonuclease BamHI. *Nucleic Acids Res*, **21,** 3671-5.

Remers, W.A. (1988). Pyrrolo(1,4)benzodiazepines. In *The Chemistry of Antitumour Antibiotics*, Vol. 2. pp. 28-92. Wiley: New York.

Roberts, J.J., Know, R.J. & Rera, M.F. (1988). The role of platinum-DNA interactions in the cellular toxicity and the anti-tumour effect of platinum coordinated compounds. *Dev. Oncol.*, **54,** 16-31.

Roth, J.A., Nguyen, D., Lawrence, D.D., Kemp, B.L., Carrasco, C.H., Ferson, D.Z., Hong, W.K., Komaki, R., Lee, J.J., Nesbitt, J.C., Pisters, K.M., Putnam, J.B., Schea, R., Shin, D.M., Walsh, G.L., Dolormente, M.M., Han, C.I., Martin, F.D., Yen, N., Xu, K., Stephens, L.C., McDonnell, T.J., Mukhopadhyay, T. & Cai, D. (1996). Retrovirus-mediated wild-type p53 gene transfer to tumors of patients with lung cancer. *Nat Med*, **2,** 985-91.

Rowland, M. & Tozer, T.N. (1989). *Clinical Pharmacokinetics : Concepts and Applications*. Lea & Febiger: Philadelphia.

Ruddon, R.W. (1995). *Cancer biology*. Oxford University Press: Oxford.

Rusch, V., Klimstra, D., Venkatraman, E., Oliver, J., Martini, N., Gralla, R., Kris, M. & Dmitrovsky, E. (1995). Aberrant p53 expression predicts clinical resistance to cisplatin-based chemotherapy in locally advanced non-small cell lung cancer. *Cancer Res*, **55,** 5038-42.

Sadee, W., Beelen, G.C.M. & Lin, E.T. (1980). *Drug level monitoring*. Wiley: New York ; Chichester.

Sancar, A. & Sancar, G.B. (1988). DNA repair enzymes. *Annu Rev Biochem*, **57,** 29-67.

Shah, V.P., Midha, K.K., Dighe, S., McGilveray, I.J., Skelly, J.P., Yacobi, A., Layloff, T., Viswanathan, C.T., Cook, C.E., McDowall, R.D., Pittman, K.A. & Spector, S. (1992). Analytical methods validation: bioavailability, bioequivalence and pharmacokinetic studies. *Pharm Res*, **9,** 588-592.

Shimizu, K., Kawamoto, I., Tomita, F., Morimoto, M. & Fujimoto, K. (1982). Prothracarcin, a novel antitumor antibiotic. *J Antibiot (Tokyo)*, **35,** 972-8.

Shindell, S. & Goldberg, H.M. (1981). Surveillance systems: what to include and why. *Occup Health Saf*, **50,** 34-5, 38-9, 56.

Simon, R., Freidlin, B., Rubinstein, L., Arbuck, S.G., Collins, J. & Christian, M.C. (1997). Accelerated titration designs for phase I clinical trials in oncology. *J Natl Cancer Inst*, **89,** 1138-47.

Skehan, P., Storeng, R., Scudiero, D., Monks, A., McMahon, J., Vistica, D., Warren, J.T., Bokesch, H., Kenney, S. & Boyd, M.R. (1990). New colorimetric cytotoxicity assay for anticancer-drug screening. *J Natl Cancer Inst*, **82,** 1107-12.

Slupphaug, G., Eftedal, I., Kavli, B., Bharati, S., Helle, N.M., Haug, T., Levine, D.W. & Krokan, H.E. (1995). Properties of a recombinant human uracil-DNA glycosylase from the UNG gene and evidence that UNG encodes the major uracil-DNA glycosylase. *Biochemistry*, **34,** 128-38.

Smellie, M., Kelland, L.R., Thurston, D.E., Souhami, R.L. & Hartley, J.A. (1994). Cellular pharmacology of novel C8-linked anthramycin-based sequence-selective DNA minor groove cross-linking agents. *Br J Cancer*, **70,** 48-53.

Sorenson, C.M. & Eastman, A. (1988). Mechanism of cis-diamminedichloroplatinum(II)-induced cytotoxicity: role of G2 arrest and DNA double-strand breaks. *Cancer Res*, **48,** 4484-8.

Soussi, T. (2003). p53 mutations and resistance to chemotherapy: A stab in the back for p73. *Cancer Cell*, **3,** 303-5.

Soussi, T., Dehouche, K. & Beroud, C. (2000). p53 website and analysis of p53 gene mutations in human cancer: forging a link between epidemiology and carcinogenesis. *Hum. Mutat.*, **15,** 105-213.

Spanswick, V.J., Hartley, J.M., Ward, T.H. & Hartley, J.A. (1999). Measurement of drug-induced DNA interstrand crosslinking using the single cell gel electrophoresis (Comet) assay. In *Methods in Molecular Medicine: Cytotoxic Drug Resistance Mechanisms*, Brown, R. & Boger-Brown, U. (eds), Vol. 28. pp. 143-154. Humana Press: Totowa, NJ.

Sumner, W., 2nd & Bennett, G.N. (1981). Anthramycin inhibition of restriction endonuclease cleavage and its use as a reversible blocking agent in DNA constructions. *Nucleic Acids Res*, **9,** 2105-19.

Swenson, D.H., Li, L.H., Hurley, L.H., Rokem, J.S., Petzold, G.L., Dayton, B.D., Wallace, T.L., Lin, A.H. & Krueger, W.C. (1982). Mechanism of interaction of CC-1065 (NSC 298223) with DNA. *Cancer Res*, **42,** 2821-8.

Takeuchi, T., Miyamoto, T., Ishizuka, M., Naganawa, H. & Kondo, S. (1976). Neothramycins A and B, new antitumor antibiotics. *J Antibiot (Tokyo)*, **29,** 93-6.

Teicher, B.A. (1997). *Anticancer drug development guide : preclinical screening, clinical trials, and approval*. Cancer drug discovery and development. Humana Press: Totowa.

Thurston, D.E. (1993). Advances in the Study of Pyrrolo[2,1-*c*][1,4]benzodiazepine (PBD) Antitumour Antibiotics. In *Molecular Aspects of Anticancer Drug-DNA Interactions*, Neidle, S. & Waring, M.J. (eds), Vol. 1. pp. 54-88. Macmillan Press U.K.

Thurston, D.E. (1999). Nucleic acid targeting: therapeutic strategies for the 21st century. *Br J Cancer*, **80 Suppl 1,** 65-85.

Thurston, D.E., Bose, D.S., Howard, P.W., Jenkins, T.C., Leoni, A., Baraldi, P.G., Guiotto, A., Cacciari, B., Kelland, L.R., Foloppe, M.P. & Rault, S. (1999). Effect of A-ring modifications on the DNA-binding behavior and cytotoxicity of pyrrolo[2,1-c][1,4]benzodiazepines. *J Med Chem*, **42,** 1951-64.

Tong, W.P. & Ludlum, D.B. (1980). Crosslinking of DNA by busulfan formation diguanyl derivatives. *Biochim. Biophys. Acta.*, **608,** 174.

Toppmeyer, D.L. (1997). Phase I trial design and methodology. In *Anticancer drug development guide.*, Teicher, B.A. (ed). Humana Press Inc.: New Jersey.

Tozuka, Z., Takasugi, H. & Takaya, T. (1983). Studies on tomaymycin. II. Total syntheses of the antitumor antibiotics, E-and Z-tomaymycins. *J Antibiot (Tokyo)*, **36,** 276-82.

Tsugaya, M., Washida, H., Hirao, N., Hachisuka, Y., Sakagami, H. & Iwase, Y. (1986). The treatment of bladder cancer by neothramycin. *Hinyokika Kiyo*, **32,** 1443-8.

Turner, P.R. & Denny, W.A. (1996). The mutagenic properties of DNA minor-groove binding ligands. *Mutat Res*, **355,** 141-69.

UKCCCR. (1997). *Guidelines for the Welfare of Animals in Experimental Neoplasia.* UKCCCR, 20 Park Crescent London, WIN 4AL, UK.

Vahrmeijer, A.L., van Dierendonck, J.H., Schutrups, J., van de Velde, C.J. & Mulder, G.J. (1999). Effect of glutathione depletion on inhibition of cell cycle progression and induction of apoptosis by melphalan (L-phenylalanine mustard) in human colorectal cancer cells. *Biochem Pharmacol*, **58,** 655-64.

Verweij, J. & de Jonge, M.J.A. (2000). Achievements and future of chemotherapy. *Eur J Canc*, **36,** 1479-1487.

Voorhees, P.M., Dees, E.C., O'Neil, B. & Orlowski, R.Z. (2003). The proteasome as a target for cancer therapy. *Clin Cancer Res*, **9,** 6316-25.

Walton, M.I., Goddard, P., Kelland, L.R., Thurston, D.E. & Harrap, K.R. (1996). Preclinical pharmacology and antitumour activity of the novel sequence-selective DNA minor-groove cross-linking agent DSB-120. *Cancer Chemother Pharmacol*, **38,** 431-8.

Wang, Z.M., Chen, Z.P., Xu, Z.Y., Christodoulopoulos, G., Bello, V., Mohr, G., Aloyz, R. & Panasci, L.C. (2001). In vitro evidence for homologous recombinational repair in resistance to melphalan. *J Natl Cancer Inst*, **93,** 1473-8.

Wattel, E., Preudhomme, C., Hecquet, B., Vanrumbeke, M., Quesnel, B., Dervite, I., Morel, P. & Fenaux, P. (1994). p53 mutations are associated with resistance to chemotherapy and short survival in hematologic malignancies. *Blood*, **84,** 3148-57.

Whang-Peng, J., Leventhal, B.G., Adamson, J.W. & Perry, S. (1969). The effect of daunomycin on human cells in vivo and in vitro. *Cancer*, **23,** 113-21.

White, L.K., Wright, W.E. & Shay, J.W. (2001). Telomerase inhibitors. *Trends in Biotechnology*, **19,** 114-120.

Wilkinson, G.P. (2000). Development of a High Throughput assay for the assessment of drug interaction with P-glycoprotein. Kings College London: London.

Wils, P., Phung-Ba, V., Warnery, A., Lechardeur, D., Raeissi, S., Hidalgo, I.J. & Scherman, D. (1994). Polarised transport of docetaxel and vinblastine medited by P-glycoprotein in human intestinal epithelial cell monolayers. *Biochem Pharmacol*, **48,** 1528-30.

Wilson, D.M., 3rd & Barsky, D. (2001). The major human abasic endonuclease: formation, consequences and repair of abasic lesions in DNA. *Mutat Res*, **485,** 283-307.

Wood, R.D. (1997). Nucleotide excision repair in mammalian cells. *J Biol Chem*, **272,** 23465-8.

Woodburn, J.R. (1999). The epidermal growth factor receptor and its inhibition in cancer therapy. *Pharmacol Ther*, **82,** 241-50.

Wright, W.E. & Shay, W.E. (1992). The two-stage mechanism controlling cellular senescence and immortalization. *Exp. Gerontol.*, **27**.

Yamori, T., Matsunaga, A., Sato, S., Yamazaki, K., Komi, A., Ishizu, K., Mita, I., Edatsugi, H., Matsuba, Y., Takezawa, K., Nakanishi, O., Kohno, H., Nakajima,

Y., Komatsu, H., Andoh, T. & Tsuruo, T. (1999). Potent antitumor activity of MS-247, a novel DNA minor groove binder, evaluated by an in vitro and in vivo human cancer cell line panel. *Cancer Res*, **59,** 4042-9.

Zhang, Y. (2000). Role of glutathione in the accumulation of anticarcinogenic isothiocyanates and their glutathione conjugates by murine hepatoma cells. *Carcinogenesis*, **21,** 1175-82.

Zioga, G. (1999). Studies on the reaction of pyrrolobenzodiazepines with nucleophiles. In *Division of Medicinal Chemistry and Organic Chemistry.* pp. 185. University of Portsmouth: Portsmouth.

Zubrod, C.G. (1979). Historic milestones in curative chemotherapy. *Semin. Oncol.*, **6,** 490-505.

16 Publications

Accepted for publication in *Investigational New Drugs* December 2003.

Preliminary Pharmacokinetic and Bioanalytical Studies of SJG-136 (NSC 694501), A Sequence-Selective Pyrrolobenzodiazepine Dimer DNA-Cross-Linking Agent

Gary P. Wilkinson BSc MSc[1], James P. Taylor BSc, Steve Shnyder PhD[1], Patricia Cooper BSc[1], Phil W. Howard PhD[3], David E. Thurston PhD[3], Terry C. Jenkins PhD[2], Paul M. Loadman PhD[1]

[1] *Cancer Research UK Cancer Research Unit, Tom Connors Cancer Research Centre, University of Bradford, All Saints Road, Bradford, West Yorkshire, BD7 3AY, UK*
[2] *Yorkshire Cancer Research Laboratory of Drug Design, Tom Connors Cancer Research Centre, University of Bradford, All Saints Road, Bradford, West Yorkshire, BD7 3AY, UK*
[3] *Cancer Research UK Gene Targeted Drug Design Research Group, The School of Pharmacy, University of London, 29/39 Brunswick Square, London, WC1N 1AX, UK*

Address for offprints: Dr Paul Loadman
Cancer Research UK Cancer Research Unit,
Tom Connors Cancer Research Centre,
University of Bradford,
All Saints Road,
Bradford, West Yorkshire, BD7 3AY, UK
Tel [044] (0)1274 233228
Fax [044] (0)1274 233234
E-mail P.M.Loadman@bradford.ac.uk

Summary
SJG-136 is a synthetic pyrrolobenzodiazepine (PBD) dimer in which two DNA-alkylating subunits are linked through an inert propanedioxy tether. Biophysical and biochemical studies of SJG-136 have shown a remarkable affinity for DNA and potent cytotoxicity *in vitro*. On this basis, together with its unique sequence selectivity and interstrand DNA cross-linking activity, SJG-136 has been selected for clinical trials. This study examines the pharmacological characteristics of SJG-136 and provides the first report of pharmacokinetic properties for this agent. A sensitive, selective and reproducible reversed-phase gradient LC/MS assay has been developed for detection and analysis, where a molecular ion (*m/z* 557.2) is detectable for the SJG-136 parent imine. Fluorescence detection (260 nm excitation, 420 nm emission) gives a limit of sensitivity of 5 nM (2.5 ng ml^{-1}) for analysis of SJG-136 in mouse plasma. Extraction efficiencies from plasma were >65% across a range of concentrations (5–1000 nM). Following administration to mice at the MTD (i.p., 0.2 mg kg^{-1}), high peak plasma concentrations of SJG-136 were seen (C_{max} = 336 nM) at 30 min after dosing. A calculated terminal $t_{1/2}$ of 0.98 h and AUC of 0.34 μM·h resulted in a clearance rate of 17.7 ml min^{-1} kg^{-1}. The PBD dimer binds only moderately to proteins (65–75%), and *in vitro* cytotoxicity studies confirmed IC_{50} values of 4–30 nM with a panel of human cell lines. This finding demonstrates that plasma concentrations achieved in the mouse are substantially higher than those required to elicit an anti tumour response *in vitro*. This report forms an important phase in the pre-clinical characterization of the compound.

Keywords: plasma, protein binding, DNA cross-linking, mass spectrometry, HPLC, PBD.

Introduction

Many clinically useful anti-cancer agents produce their anti-tumour effects by targeting DNA (*1*). Thus, for example, classical intercalating agents such as the anthracyclines (e.g., mitoxantrone or daunomycin/doxorubicin) form "cleavable complexes" involving DNA topoisomerase II, whereas covalent modifiers such as cisplatin induce cross-links in double-stranded DNA. These mechanisms are intimately linked to their cytotoxic and biological potency. However, few drugs in current clinical use show sequence recognition for DNA tracts greater than 2–3 base pairs (bp) in length (*2*), and hence do not target defined gene sequences. Strategies for selective targeting of tumours with DNA-interactive agents generally exploit their rapid cell cycling rather than the targeting of any cellular flaw at a genomic level. Compounds should ideally be able to selectively recognise and inhibit stretches of DNA to prevent the transcription and subsequent translation of oncogenic DNA, and thereby inhibit tumour progression. However, for this level of selectivity to be feasible such agents must recognise individual sequences of duplex DNA to achieve inhibition at the gene level (*2*).

The pyrrolo[2,1-*c*][1,4]benzodiazepines (PBDs) are antitumour antibiotics where a large number of natural (e.g., anthramycin) and synthetic derivatives are known (*2–4*). PBD compounds form covalent adducts by alkylation at the exocyclic 2-NH_2 positions of guanines via the minor groove of double-stranded DNA, and have been shown to span a 3-bp region of duplex DNA in a sequence-selective manner, with preferential binding to guanines flanked by purine bases, i.e. 5'-Pu-**G**-Pu (*4–6*).

While PBDs behave as monofunctional DNA alkylating agents, a dramatic increase in cytotoxicity and sequence selectivity can be achieved by linking two PBD units to form a PBD dimer that can cross-link appropriately separated guanines on opposite DNA strands (e.g., interstrand cross-links) (*7–11*). The first synthetic PBD dimer DSB-120 offered selectivity toward embedded 5'-GATC target DNA sites that are 6–7 bp in length (*9*,*11*), although it is accepted that recognition of ~15 bp will be required for DNA sequences within the human genome (*12)*. Molecular tailoring of PBD monomers and judicious linkage to form dimeric compounds has culminated in improved anti-cancer efficacy and has recently enabled recognition of longer DNA sequences (e.g., 5'-Pu-GATC-Pu in the case of SJG-136) [*13*].

SJG-136 (Figure 1) is a synthetic PBD dimer that comprises two C2-*exo*-methylene-substituted DC-81 subunits linked via their C8 positions through an inert $–O(CH_2)_3O–$ diether bridge (*13*,*14*). DC-81 (for ring numbering and nomenclature, see Figure 1) is a simple, synthetic PBD monomer "building block" that has been used extensively to probe DNA-binding events for this unique class of agent. Biophysical and biochemical assay methods have shown that SJG-136 has remarkable affinity for DNA and acts as a highly efficient interstrand DNA cross-linking agent. Further, the dimer is a potent cytotoxic agent *in vitro*, with an IC_{50} of ~25 pM in sensitive cell lines (*13*,*14*). On the basis of this activity, SJG-136 has been selected for clinical trials. It is therefore essential to have an understanding of the pharmacokinetic (PK) and pharmacological characteristics of SJG-136 at likely therapeutic doses to enable prediction of PK parameters in man. This study examines the pharmacological characteristics of SJG-136 and provides the first report of pharmacokinetic properties for this novel agent in mice. This forms an important phase in the pre-clinical characterisation of the compound. *In vitro* cytotoxicity has also been assessed in a panel of cells selected from data produced by the NCI 60-cell-line screen (*15*,*16*) in order to further investigate tumour selectivity and to confirm the likely exposure parameters required to produce an in vivo antitumour

response. The cytotoxicity data obtained can also be used to assess the significance of plasma concentrations achieved *in vivo*.

Materials and Methods

Chemicals and reagents

SJG-136 was synthesised as described previously (*13*,*14*) and supplied by the National Cancer Institute (Bethesda, Batch No Z/5) . The PBD dimer was supplied as an almost colourless powder. Stock solutions were shown to be stable when dissolved in dimethyl sulfoxide (DMSO) at 1.0 mg ml^{-1} and stored in polypropylene tubes at –80 °C. High-purity HPLC-grade solvents (Fisher Scientific, Loughborough, UK), analytical-grade chemicals (Sigma-Aldrich Ltd, Poole, UK) and triple-distilled water were used throughout. Heparinised polypropylene tubes were used for collection of blood samples. Polypropylene microcentrifuge tubes (Sigma-Aldrich Ltd, Poole, UK) were used throughout for sample handling and storage, and polypropylene autosampler vials (Sigma-Aldrich Ltd, Poole, UK) were used to load samples for HPLC analysis. Following approval from the Local Ethical Review Committee human plasma was kindly donated by The National Blood Service, Leeds, UK.

Animals

Female NCR nude mice (NCR/nu) aged 6–8 weeks were obtained from the National Cancer Institute (NCI Bethesda, MD, USA) and were fed a CRM pellet diet (CRM, Special Diets Service, Witham, Essex, UK) and water *ad libitum*. Mice were kept in cages in an air-conditioned room with regular alternating cycles of light and darkness. All animal procedures were carried out under a project licence issued by the UK Home Office, and UKCCCR guidelines (*17*) were followed rigorously.

Instrumentation

The HPLC chromatographic system used consisted of a Waters Alliance 2690 separations module (Waters, Manchester, UK), fitted with a Waters 996 photodiode array detector for absorbance monitoring and a Merck-Hitachi 4780 fluorescence detector. Data were collected and chromatograms processed using MassLynx 3.4 software (Micromass, Manchester, UK). Fluorescence spectra for SJG-136 were obtained using a Varian-Cary Eclipse fluorimeter (Varian, Warrington, UK).

Chromatography conditions

The chromatographic separation of SJG-136 was performed using a binary gradient on a reversed-phase Hypersil phenyl column (150 mm × 4.6 mm i.d.; Sigma-Aldrich Ltd, Poole UK). A 0.5-μm pre-column filter was used to protect the column from any residual particulate matter. Mobile phase A consisted of 5% acetonitrile (MeCN) and 95% aqueous 0.01 M ammonium formate buffer (HCO_2NH_4, pH 5.0); mobile phase B consisted of 50% MeCN and 50% 0.01 M HCO_2NH_4 buffer (pH 5.0). Gradient conditions (flow rate 1.8 ml min^{-1}) were used with linear gradient changes between intervals: 0–5 min, 80→70% A; 5–26 min, 70→53% A; 26–30 min, 53→5% A; 30→45 min, 5% A. The column was equilibrated with 80% A for 15 min before re-injection. The use of MeCN as eluting solvent was preferred to methanol to avoid MeOH-adduct formation with SJG-136 (see below).

Mass spectrometry

LC/MS analysis was carried out using a ZMD quadrupole mass spectrometer (Micromass, Manchester, UK) linked in series to the Waters Alliance 2690

chromatography system. The mass spectrometer was operated in positive-ion electrospray mode with an ionising voltage of +3.00 kV applied to the capillary. A solvent flow rate of 1.8 ml min^{-1} (1:10 volume split), a N_2 gas flow of 400 l h^{-1} and a source temperature of 125 °C were employed to produce stable spray conditions. A cone voltage of 35 V resulted in clear mass spectra for the PBD dimer compound. Mass spectra were continuously scanned in the *m*/*z* 250–700 range at 3.5 s intervals throughout the HPLC separation. MassLynx 3.4 software (Micromass, Manchester, UK) was used to process the mass spectral data and to produce total ion chromatograms (TICs) for the separations. A single-ion recording (SIR) channel was established at *m*/*z* 557.1 to monitor the $[M + H]^+$ molecular ion for the parent bis-imine form of SJG-136. All HPLC conditions, column, solvents and flow rates were as described earlier.

Sample preparation and drug extraction
Plasma was prepared immediately by centrifugation of a mouse blood sample at 5000 *g* for 3 min and removal of the plasma to a fresh tube. Plasma was stored at –80 °C prior to analysis. Drug was extracted from plasma (100 µl) by addition of MeCN (200 µl) at 4 °C. Samples were briefly vortex-mixed, then centrifuged at 20,000 *g* for 20 min at room temperature. The supernatant was removed to a fresh microcentrifuge tube and transferred to a Jouan RC 10.10 centrifugal evaporator (Jouan Ltd, Ilkeston, UK), where the sample was evaporated to dryness under vacuum at room temperature. The dried sample was reconstituted in 100 µl of mobile phase, vortex-mixed briefly and centrifuged at 20,000 *g* for 10 min to remove any residual particulate matter; a 70 µl aliquot was used for HPLC analysis. Extraction efficiencies were calculated by comparing samples extracted from plasma (n = 6) to standards prepared in the same mobile phase.

Calibration
Calibration curves were generated by spiking drug-free mouse plasma (90 µl) with SJG-136 (10 µl), diluted from stock in PBS to give final concentrations in plasma in the 0–1000 nM range, and a final concentration of DMSO of <0.2%. Samples were then extracted as described. Calibration curves were determined by linear regression analysis of a plot of the peak areas obtained for the analyte versus concentration. Replicate samples (n = 6) at a midpoint of the calibration curve were examined to ensure reproducibility.

In vivo pharmacokinetic studies
For *in vivo* studies, SJG-136 was dissolved in DMSO and then diluted in physiological saline to give a final solution containing <1% v/v DMSO. The drug was administered via the intraperitoneal (ip) route at the maximum tolerated dose (MTD) of 0.2 mg kg^{-1} . Blood samples from three mice at each time point (5, 15, 30, 60, 120, 240 and 360 min) were taken by cardiac puncture under terminal anaesthesia using heparinised syringes, and placed into heparinised tubes on ice. Plasma was prepared immediately by centrifugation of a mouse blood sample at 5000 *g* for 3 min and removal of the plasma to a fresh tube. Plasma samples were stored at –80 °C prior to analysis.

16.1.1.1.1 Pharmacokinetic analysis
Pharmacokinetic parameters were calculated using the trapezoidal rule for area under the plasma concentration–time curve (AUC) to the final time point, and the remaining area to ∞ was calculated from C_t/k_{el} (where C_t is the final time point at which

concentration can be determined, and k_{el} is the elimination rate constant). Other parameters were calculated using standard techniques, as described previously (*18*).

16.1.1.1.2 Stability in plasma and blood

Stability of SJG-136 in plasma and blood was assessed at concentrations and times likely to be pharmacokinetically relevant. SJG-136 was spiked into pooled *NCR/nu* mouse blood or plasma to give a final concentration of 100 nM. The plasma or blood samples were incubated at 37 °C for up to 6 h, with aliquots removed at 2 h intervals for HPLC analysis. Drug was extracted from each sample as described previously.

16.1.1.1.3 Plasma protein binding studies

Initial plasma protein binding studies were performed using ultrafiltration; however, this method was discontinued as SJG-136 shows a high affinity for usual filter membranes. Subsequent plasma protein binding studies were carried out using ultracentrifugation and human plasma as multiple large volumes (>500 µl) were required. Pooled human plasma (990 µl) was spiked with SJG-136 (10 µl diluted from stock in PBS) to give final concentrations of 1 µM, 100 nM and 10 nM (n = 4) in plasma. Identical volumes of phosphate-buffered saline (PBS) in ultracentrifuge tubes were spiked with SJG-136 to give the same final concentrations of SJG-136 to provide controls. Samples were then centrifuged at 20 °C for 18 h at 150,000 *g* (Beckman Optima TL ultracentrifuge) to pellet the plasma proteins. Supernatant was removed from the plasma or PBS samples and analysed using the HPLC method described. The percentage of SJG-136 bound to plasma proteins was calculated from the difference in drug levels present in plasma water and the PBS control.

16.1.1.1.4 *In vitro* cytotoxicity studies

All cell lines were grown under similar conditions to those used by the National Cancer Institute (NCI): RPMI 1640 medium containing 10% fetal calf serum supplemented with 2 mM L-glutamine, maintained at 37 °C with 5%:95% CO_2/air and no added antibiotics. Drug-induced cytotoxicity was determined using a 96 h growth inhibition by the MTT dye conversion assay. Five cell lines were selected based on data from the NCI 60-cell-line screen for relative sensitivity or resistance to SJG-136. The selected cell lines used were UACC-62 (melanoma), M-14 (melanoma), DU-145 (prostate), SK-OV-3 (ovarian) and SK-MEL-2 (melanoma), and were obtained from NCI. Growth curves were generated for each cell line using the MTT dye conversion assay to establish exponential growth phase. Cells were seeded at 10^4 cells ml^{-1} into cell culture-treated 96-well plates, and allowed to attach overnight. For *in vitro* studies, SJG-136 stock solution in DMSO was diluted to the required concentrations in cell culture growth medium immediately before use. SJG-136 solution was added to cells in medium, to give ≤0.1% v/v DMSO working concentrations. IC_{50} values were determined for SJG-136 after 1 h and 96 h continuous exposure.

Results

Chromatographic analysis

Initial chromatographic separation was attempted using a reversed-phase C18 column (HiChrom RPB) with a MeOH / 0.01 M HCO_2NH_4-based mobile phase. The organic solvent in the mobile phase was ultimately replaced with MeCN due to reactivity of the SJG-136 dimer with MeOH (Figure 2A), and analytical difficulties that arise from possible mixtures containing the parent bis-imine and possible dihydrate or bis-carbinolamine methyl ether forms (Figure 2A). Peak shape was found to be optimal

using these mobile phase conditions in conjunction with a reversed-phase Hypersil phenyl column. Isocratic conditions were used in preliminary studies; however, optimal separation and peak shape were subsequently achieved using gradient elution. Gradient conditions were refined to include a strong organic phase at the end of the gradient as this significantly improves peak reproducibility by preventing accumulation of adsorbent particles on the column and ensures prompt elution of any potential late-eluting peaks. The limit of detection on the column was found to be 39 pg of SJG-136 (i.e., 70 µl injection of a 1 nM standard solution); the limit of quantitation for drug in plasma was found to be 5 nM. The PBD dimer compound was eluted after 17.8 min (Figure 3). Optimal conditions for fluorescence detection of SJG-136 were determined as 260 nm (excitation) and 420nm (emission), respectively, as shown by the excitation and emission spectra (Figure 4).

Mass spectrometry

PBD monomer compounds are reactive towards nucleophilic species due to the N10–C11 imine moieties, and this reactivity is responsible for their biological efficacy. Dissolution of a PBD in water results in an equilibrium mixture (*4*) containing the imine and both *R*/*S*-carbinolamine (or hydrate) enantiomeric forms of the compound (Figure 2B). Analogous reversible reaction with an anhydrous alcohol results in a mixture that contains the *R*/*S*-carbinolamine alkyl ether (or alcoholate) adduct forms (Figure 2B). The situation is more complex for alcohol solvents containing water (or mixed alcohol/water solutions), where the imine, hydrate and alcoholate can co-exist; the equilibrium composition for the PBD solute will be governed by the level of water present, the relative stabilisation afforded by the organic solvent, and (chiefly) the inherent reactivity of the PBD compound. However, this factor is unimportant for biological efficacy as interconversion to the DNA-reactive PBD imine (or protonated iminium) species is facile and not rate-limiting at low drug concentrations. Nevertheless, these solvent-mediated equilibria will have implications for the reliable detection and monitoring of PBD drug levels in analytical samples.

SJG-136 is supplied as a bis-imine (Figure 1), but the compound will react with the water present in most solvents to generate the bis-carbinolamine or dihydrate form (Figure 2A). Equivalent dual adduct formation in the presence of MeOH leads to the bis-carbinolamine methyl ether or dimethanolate form of the drug (Figure 2B). This was demonstrated by mass spectrometry to identify the signatures for the parent bis-imine at *m*/*z* 557.1 ($[M + H]^{\cdot +}$ in Figure 5.1), the dihydrate at *m*/*z* 615.1 ($[M + 2H_2O + Na]^{\cdot +}$ in Figure 5.2) and the dimethanolate adduct at *m*/*z* 643.4 ($[M + 2MeOH + Na]^{\cdot +}$ in Figure 5.3).

Avoidance of drug or sample contact with MeOH solvent at all stages prevents formation of the dimethanolate adduct of SJG-136 and hence possible complications for HPLC analysis. There was no apparent chromatographic separation of the possible discrete forms of the drug under the HPLC protocol used, presumably as a result of rapid equilibrium interconversion during elution. Use of a chiral column may enable separation of the *R*/*S*-enantiomeric species but was not investigated in this study. Switch of solvent from MeOH to acetonitrile (MeCN) resulted in a marked improvement in detection sensitivity. In MeCN solution, the majority of SJG-136 was detected as the imine form appearing at *m*/*z* 557.1 (i.e., $[M + H]^{\cdot +}$), and this molecular ion was chosen for detection using single-ion recording in our mass spectrometric assays. No mass spectral peaks of interest were seen outside the *m*/*z* 540–680 range. While appearance of the dihydrate species in mass spectra of samples is unavoidable due to water traces this has no significant effect upon the overall analysis. Use of MeCN serves to maximise

detection of SJG-136 as the parent bis-imine, presumably as equilibrium formation and/or stabilisation of the dihydrate is disfavoured compared to the more polar alcohol solvents.

Aqueous solutions of SJG-136 will contain both the bis-imine and the mono-/di-hydrate (i.e., mono- and di-carbinolamine) species formed by reaction with water, although most drug is detected by MS in the unreacted parent form. Dimer reaction appears to favour equilibrium formation of the dihydrate rather than intermediate monohydrate, presumably due to the overwhelming concentration of water reactant (~55 M) in the solution. The dihydrate species can be detected by NMR analysis, albeit at higher concentration (unpublished data). Interconversion between the hydrate forms of SJG-136 and the biologically relevant bis-imine form is judged to be facile from kinetic studies of equilibrium processes for monomeric PBD compounds. The imine/hydrate balance in aqueous solution is governed by stereoelectronic factors involving the structural complexion of the 5-membered C-ring in the PBD. It is noteworthy that the C2-*exo*-methylene substitution in SJG-136 (Figure 1) appears to displace the equilibrium in favour of the imine species.

Extraction from biological matrices and calibration

Efficiency of recovery of SJG-136 from spiked plasma was reliably found to be 67.8 ± 8.8%, 84.5 ± 2.1%, 115.1 ± 0.6% for 10, 100 and 1000nM respectively (n = 6, mean ± SEM). Calibration curves for SJG-136 in plasma were linear in the 0.01–1 μM range, where this spans the drug levels examined in the present study. Intra-day variation of extraction of SJG-136 from plasma was low, with a co-efficient of variation of 6.0% at 100 nM.

Plasma pharmacokinetics

The plasma time-course of SJG-136 in NCR/Nu mice is shown in Figure 6. The pharmacokinetics show a tri-exponential behaviour, illustrating absorption, distribution and elimination phases following ip dosing. SJG-136 was detectable in mouse plasma up to 4 h after administration. C_{max} was observed at 30 min after dosing, with a peak plasma concentration of 336 nM. The $t_{1/2}$ of the elimination phase for SJG-136 was determined as 0.98 h, with a total clearance of 17.72 ml min^{-1} kg^{-1}. The $AUC_{0-\infty}$ value was calculated as 0.34 μM h.

Stability in plasma and blood

The stability of SJG-136 was investigated in whole blood and plasma over a 6-h period at 37 °C (Figure 7). There was no significant loss of SJG-136 in plasma over this time. However, there was a progressive but slow loss of SJG-136 in blood during 6 h, resulting in a 31% loss of parent drug over this period. The $t_{1/2}$ was >6 h for both whole blood and plasma. These data indicate that blood samples should be processed promptly in order to minimise degradative loss of SJG-136 *ex vivo*. To this end, all blood PK samples were immediately placed on ice and processed within 15 min of sample collection.

Plasma protein binding

Binding of SJG-136 to plasma proteins was examined by incubation of fresh human plasma with 10, 100 and 1000 nM drug for 10 min, followed by ultracentrifugation as described. Binding of drug to plasma proteins was found to be moderate at 65 ± 11% and 76 ± 5% for initial 100 and 1000 nM concentrations of SJG-136, respectively (mean ± SEM, n = 4 at each concentration). SJG-136 was not detectable in the 10 nM samples.

In vitro *cytotoxicity*
Cytotoxicity data obtained for SJG-136 against the selected panel of cell lines are collected in Table 1. SJG-136 shows high *in vitro* potency, with IC_{50} values in the 4–30 nM range. These values are still 100-fold higher than previously reported for the very sensitive A2780 cell line (*13*). However, IC_{50} values reported here for the SK-OV-3 ovarian cell line are comparable to earlier reported data (*13*). There is evidence of cell type selectivity for the five cell lines examined, with 20-fold differences for the 96 h drug exposures.

Discussion
SJG-136 is a DNA-targeting cross-linking agent and the NCI 60-cell-line screen and COMPARE analysis have indicated a pattern of *in vitro* cell line sensitivity that differs markedly from that of established clinical agents (15,16). Reported work has shown SJG-136 to be an exceptionally cytotoxic compound achieving sub-nanomolar IC_{50} values in four different cell lines (13,14). There is considerable interest in the compound due to its progress into phase I clinical trials in the UK during 2004; the compound is also under consideration for US trials with the NCI. We describe here a sensitive and selective analytical method to enable the study of SJG-136 in the murine *in vivo* model prior to clinical trial. SJG-136 represents a logical progression in the development of potent sequence-selective interstrand DNA cross-linking agents.

This is the first report of the mass spectral analysis of SJG-136 in aqueous, MeCN or MeOH solution and illustrates the predicted reactivity of the two imine groups present in this PBD dimer. The bis-imine form of SJG-136 can be detected when the compound is analysed in MeCN, with a predominant mass peak at *m*/*z* 557.1 ($[M + H]^{\cdot +}$) (Figure 5.1). Additional peaks can be seen at *m*/*z* 615.1 and 631.1 when water is introduced that correspond to the hydrate or carbinolamine form of the drug on each PBD unit of the dimer (i.e., $[M + 2H_2O]^{\cdot +}$), where the adduct further combines with either a sodium or potassium in the detected ion species. In this case, the $[M + H]^{\cdot +}$ ion for the agent is no longer seen (Figure 5.2). Further, the addition of MeOH results in the formation of mono- and di-methanolate forms of the drug, as evident from peaks at *m*/*z* 589.4 ($[M$+H+MeOH$]^{\cdot +}$), 611.1 ($[M$+Na+MeOH$]^{\cdot +}$), 643.4 ($[M$+Na+2MeOH$]^{\cdot +}$) and 659.1 ($[M$+K+2MeOH$]^{\cdot +}$[Figure 5.3]). As it proved possible to avoid use of MeOH in the HPLC method, this strategy was adopted to prevent loss of sensitivity due to untoward methanolate formation. No apparent chromatographic separation could be achieved for the three different forms of SJG-136 in solution (i.e., imine, hydrate or methanolate forms; see Figure 2B). Mass spectrometry (MS) was also investigated as an alternate means of HPLC detection, but was found to be less sensitive than fluorescence monitoring.

The plasma time course of SJG-136 in the NCR-Nu mouse indicates the concentration of SJG-136 that can be achieved *in vivo*. It is notable that the peak plasma concentrations reached (C_{max} = 336 nM) are over 10-fold higher than the IC_{50} values necessary for anti tumour activity *in vitro* suggesting likely efficacy *in vivo*. Furthermore, no metabolites of the compound were detected in this study indicating a low metabolic potential of the compound and consequentially less chance of complications that may arise from metabolite production.

SJG-136 was surprisingly stable in plasma over 6 h at 37 °C, with <10% loss. However, it was less stable in blood during the same period. Comparison of the blood stability data for SJG-136 and the structurally similar PBD dimer DSB-120 (*7*) reveals a

marked difference in stability. Earlier reports showed an 80% loss of DSB-120 within 10 min (*19*), whereas SJG-136 shows a loss of only ~30% over 6 h (Figure 6). SJG-136 showed a $t_{1/2}$ of > 6 h in both blood and plasma. This difference may reflect a lower level of plasma protein binding evident for SJG-136 compared to DSB-120 (i.e., ~70% and 97% bound, respectively).

Based on the NCI data a panel of 5 cell lines were selected for relative sensitivity or resistance to SJG-136 and were assayed for *in vitro* IC_{50} values. This study also suggests a degree of selectivity of SJG-136 according to cell type, as there was a 20-fold difference in sensitivity between the five cell lines examined. The 1 h exposure regimen was chosen alongside the often studied 96 h exposure in an attempt to more accurately reflect the time of exposure likely to be seen in an *in vivo* environment following iv or ip bolus administration. It is of note that the IC_{50} value of 2.5 nM obtained for 96 h exposure of SJG-136 to the SKOV-3 cell line correlates closely to that previously reported for this cell line (9.1 nM, [13]).

In summary, these preliminary studies are the first report of plasma concentrations achievable in animal models. Peak plasma concentrations are high, suggesting that a therapeutic index is achievable as plasma drug concentrations are over 10-fold greater than that needed for cytotoxicity *in vitro*. SJG-136 also shows potent *in vitro* cytotoxicity with evidence of cell-type selectivity. The pharmacokinetic parameters described will inform the forthcoming clinical trial. Further more detailed pharmacological studies are currently underway.

16.1.1.1.4.1 Acknowledgements

This work was supported by Cancer Research UK programme grant C459/A2579 (JPT, SS, PC, PML); C180/A1060, SP1938/0402, SP1938/0201 and SP1938/0301 to DET and TCJ] and Yorkshire Cancer Research (to TCJ). The authors would also like to thank Dr Rosendo Obach (Ipsen Pharma S.A.) for his helpful comments.

References

1. Hurley, LH: DNA and associated targets for drug design. J Med Chem 32: 2027–33, 1989.
2. Thurston, DE: Nucleic acid targeting: therapeutic strategies for the 21st century. Br J Cancer 80 Suppl 1: 65–85, 1999.
3. Remers, WA: The Chemistry of Antitumour Antibiotics, Vol. 2. Wiley, New York, 1988, pp 28–92.
4. Thurston, DE: Advances in the Study of Pyrrolo[2,1-*c*][1,4]benzodiazepine (PBD) Antitumour Antibiotics. In: Neidle, S, Waring, MJ (eds) Molecular Aspects of Anticancer Drug-DNA Interactions, Vol. 1. Macmillan Press UK, 1993, pp 54–88.
5. Hurley, LH, Reck, T, Thurston, DE, Langley, DR, Holden, KG, Hertzberg, RP, Hoover, JR, Gallagher, G, Faucette, LF, Mong, SM, Johnson, PK: Pyrrolo[1,4]benzodiazepine antitumor antibiotics: relationship of DNA alkylation and sequence specificity to the biological activity of natural and synthetic compounds. Chem Res Toxicol 1: 258–2**, 1988.
6. Puvvada, MS, Forrow, SA, Hartley, JA, Stephenson, P, Gibson, I, Jenkins, TC, Thurston, DE: Inhibition of bacteriophage T7 RNA polymerase in vitro transcription by DNA-binding pyrrolo[2,1-*c*][1,4]benzodiazepines. Biochemistry 36: 2478–2484, 1997.
7. Bose, DS, Thompson, AS, Ching, JS, Hartley, JA, Berardini, MD, Jenkins, TC, Neidle, S, Hurley, LH, Thurston, DE: Rational design of a highly efficient irreversible DNA interstrand cross-linking agent based on the pyrrolobenzodiazepine ring system. J Amer Chem Soc 114: 4939–4941, 1992.
8. Bose, DS, Thompson, AS, Smellie, M, Berardini, MD, Hartley, JA, Jenkins, TC, Neidle, S, Thurston, DE: Effect of linker length on DNA-binding affinity, cross-linking efficiency and cytotoxicity of C8-linked pyrrolobenzodiazepine dimers. Chem Commun: 1518–1520, 1992.
9. Jenkins, TC, Hurley, LH, Neidle, S, Thurston, DE: Structure of a covalent DNA minor groove adduct with a pyrrolobenzodiazepine dimer: evidence for sequence-specific interstrand cross-linking. J Med Chem 37: 4529–4537, 1994.
10. Thurston, DE, Bose, DS, Thompson, AS, Howard, PW, Leoni, A, Croker, SJ, Jenkins, TC, Needle, SS, Hartley, JA, Hurley, LH: Synthesis of sequence-selective C8-linked pyrrolo[2,1-*c*][1,4]benzodiazepine DNA interstrand cross-linking agents. J Org Chem 61: 8141–8147, 1996.
11. Smellie, M, Bose, DS, Thompson, AS, Jenkins, TC, Hartley, JA, Thurston, DE: Sequence-selective recognition of duplex DNA through covalent interstrand cross-linking with pyrrolobenzodiazepine (PBD) dimers: kinetic and molecular modelling studies. Biochemistry 42: 8232–8239, 2003
12. Neidle, S, Puvvada, MS, Thurston, DE: The relevance of drug DNA sequence specificity to anti-tumour activity. Eur J Cancer 30A: 567–568, 1994.
13. Gregson, SJ, Howard, PW, Hartley, JA, Brooks, NA, Adams, LJ, Jenkins, TC, Kelland, LR, Thurston, DE: Design, synthesis, and evaluation of a novel pyrrolobenzodiazepine DNA-interactive agent with highly efficient cross-linking ability and potent cytotoxicity. J Med Chem 44: 737–748, 2001.
14. Gregson, SJ, Howard, PW, Jenkins, TC, Kelland, LR, Thurston, DE: Synthesis of a novel C2/C2'-*exo* unsaturated pyrrolobenzodiazepine cross-linking agent with remarkable DNA binding affinity and cytotoxicity. J Chem Soc Chem Commun: 797–798, 1999.
15. Hartley, JA, Spanswick, VJ, Brooks, N, Clingen, PH, McHugh, PJ, Hochhauser, D, Pedley, B, Kelland, LR, Guichard, S, Jodrell, DI, Alley, MC, Schultz, R,

Hollingshead, MG, Sausville, EA, Gregson, SJ, Howard, PW, Thurston, DE: SJG-136 (NSC 694501) A novel rationally designed DNA minor groove interstrand cross-linking agent with potent and broad spectrum antitumour activity. Part 1: Cellular pharmacology, *in vitro* and initial *in vivo* antitumor activity. Cancer Res 2003 (in press).

16. Alley, MC, Hollingshead, MG, Pacula-Cox, CM, Waud, WR, Hartley, JA, Howard, PW, Gregson, SJ, Thurston, DE, Sausville, EA: SJG-136 (NSC 694501) A novel rationally designed DNA minor groove interstrand cross-linking agent with potent and broad spectrum antitumour activity. Part 2: Efficacy evaluations. Cancer Res 2003 (in press).
17. Workman, P, Twentyman, P, Balkwill, F, Balmain, A, Chaplin, D, Double, JA, Embleton, J, Newell, D, Raymond, R, Stables, J, Stephens, T, Wallace, J: United Kingdom Co-Ordinating Committee on Cancer Research (UKCCCR) Guidelines for the Welfare of Animals in Experimental Neoplasia (Second Edition). Brit J Cancer, **77:** 1–10, 1998.
18. Rowland, M, Tozer, TN: Clinical Pharmacokinetics - Concepts and Applications. Lea & Febiger, Philadelphia, 1989.
19. Walton, MI, Goddard, P, Kelland, LR, Thurston, DE, Harrap, KR: Preclinical pharmacology and antitumour activity of the novel sequence-selective DNA minor-groove cross-linking agent DSB-120. Cancer Chemother Pharmacol 38: 431–438, 1996.

Table 1. *In vitro* cytotoxicity of SJG-136 toward selected cell lines

Exposure time (h)	IC_{50} (nM)[a] by cell line and cell type				
	DU-145 prostate	UACC-62 melanoma	SK-MEL-2 melanoma	SK-OV-3 ovarian	M14 melanoma
1	22 ± 3	17 ± 1	30 ± 6	18 ± 3	4 ± 0.7
96	0.6 ± 1.1	0.12 ± 0.33	1.3 ± 1.0	2.5 ± 1.4	0.4 ± 0.1

[a] Determined using the MTT dye conversion assay after exposure of cells to the PBD dimer for either 1 h or 96 h.

Figure Legends

Figure 1. Structure of the PBD monomer DC-81 (left) and the synthetic dimer SJG-136 (right) selected for anti-cancer clinical trials. The PBD ring numbering scheme used is indicated for DC-81.

Figure 2. A: Illustration showing the reversible covalent reactions of a PBD imine with either water or an alcohol to form carbinolamine (hydrate) and carbinolamine alkyl ether (alkanolate) forms that can be detected in solutions. The equilibrium composition is influenced by the choice of solvent. R^1 and R^2 denote the PBD ring attachments, and ROH the reactive nucleophile species. B: The ions detected for each form of PBD dimer SJG detected by MS in solution are indicated (see text).

Figure 3. Example HPLC trace showing detection of SJG-136 (peak at 17.8 min) after extraction from mouse plasma following ip dose at the MTD (0.2 mg kg^{-1}), time-point shown is 30 min post-dose

Figure 4. Fluorescence spectra of SJG-136. Excitation spectrum (left) with emission at λ 400 nm, showing peaks at 235, 260 and 313 nm. Emission spectrum (right) with excitation at 235 nm, showing an emission peak at 420 nm.

Figure 5. Mass spectra for SJG-136: (1) parent imine form [*m*/*z* of 557.1]; (2) in aqueous solution as the bis-imine [*m*/*z* 557.1], dihydrate+Na adduct [*m*/*z* 615.1], and dihydrate+K adduct [*m*/*z* 631.1] forms, and (3) in MeOH solution as the imine [*m*/*z* 557.1], monomethanolate [*m*/*z* 589.1] and its Na adduct [*m*/*z* 611.1], and dimethanolate+Na adduct [*m*/*z* 643.4] or +K adduct [*m*/*z* 659.1]. No spectral peaks of interest were seen outside the *m*/*z* 540–680 range.

Figure 6. Pharmacokinetic profile of SJG-136 in plasma in the NCR/Nu mouse after dosing at the MTD (0.2 mg kg^{-1}) via the intraperitoneal (ip) route. C_{max} = 336 nM and the calculated terminal $t_{1/2}$ = 0.84 h.

Figure 7. Stability of SJG-136 in mouse plasma (open circles) and whole blood (closed circles) at 37 °C.

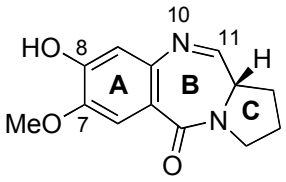

DC-81

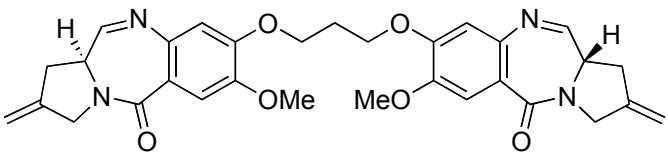

SJG-136
(NSC 694501)

Figure 1

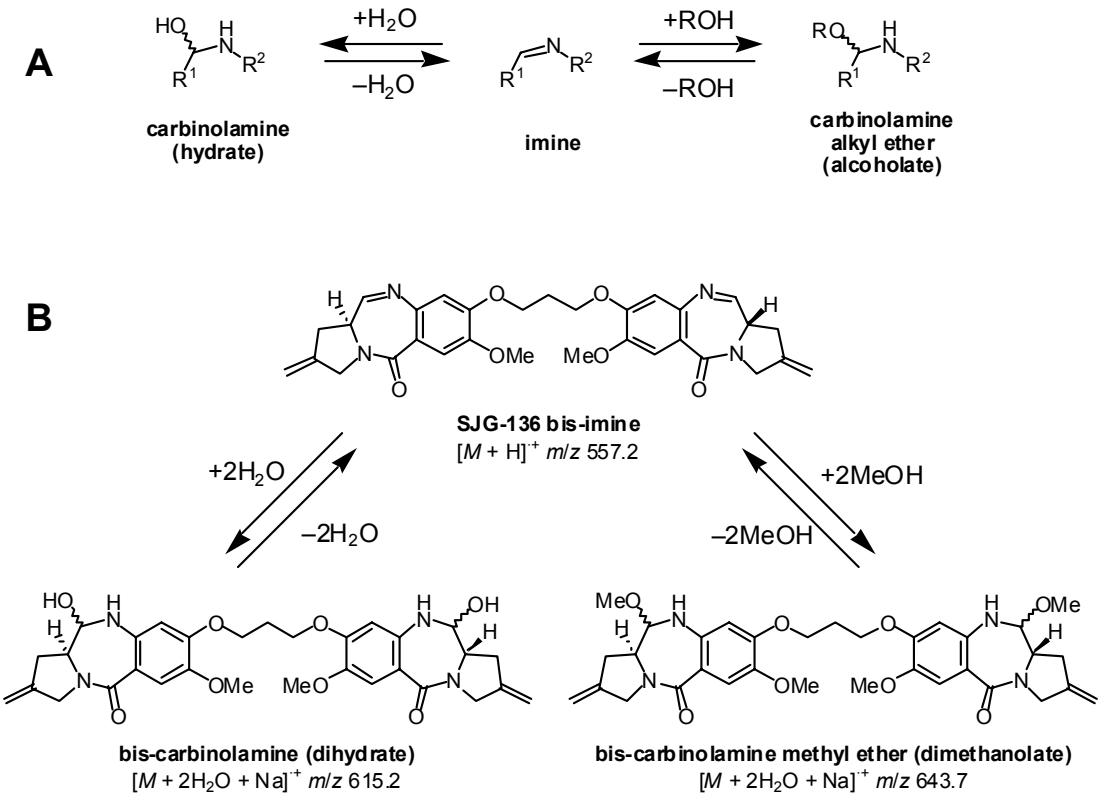
A
+H2O
–H2O
+ROH
–ROH
carbinolamine (hydrate)
imine
carbinolamine alkyl ether (alcoholate)
B
SJG-136 bis-imine
[M + H]+ m/z 557.2
+2H2O
–2H2O
+2MeOH
–2MeOH
bis-carbinolamine (dihydrate)
[M + 2H2O + Na]+ m/z 615.2
bis-carbinolamine methyl ether (dimethanolate)
[M + 2H2O + Na]+ m/z 643.7

Figure 2

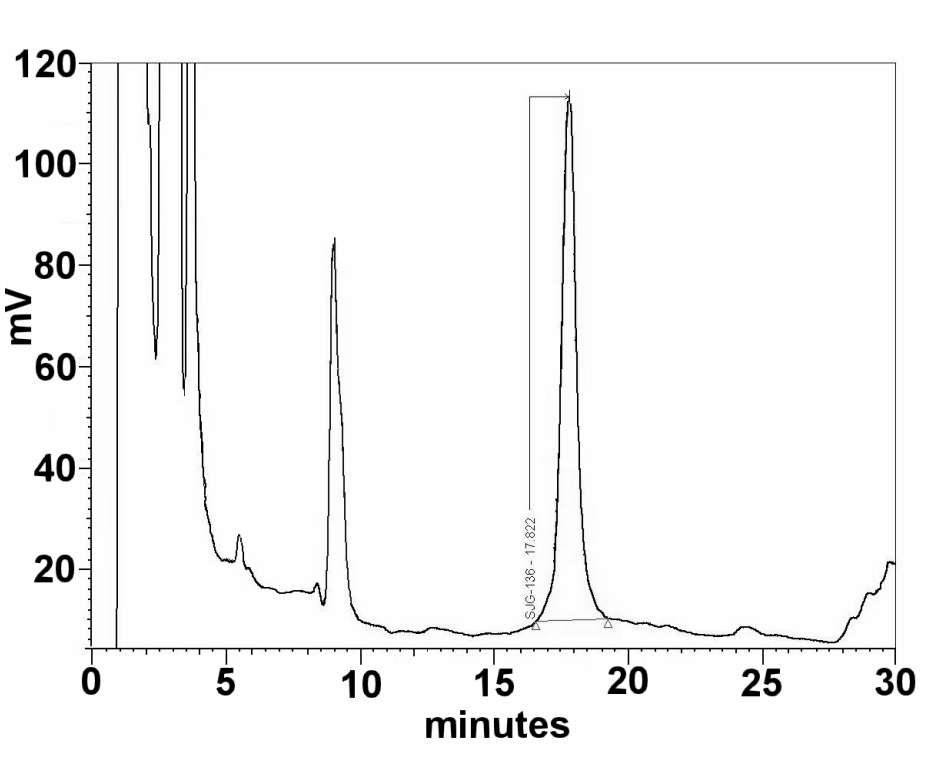

Figure 3

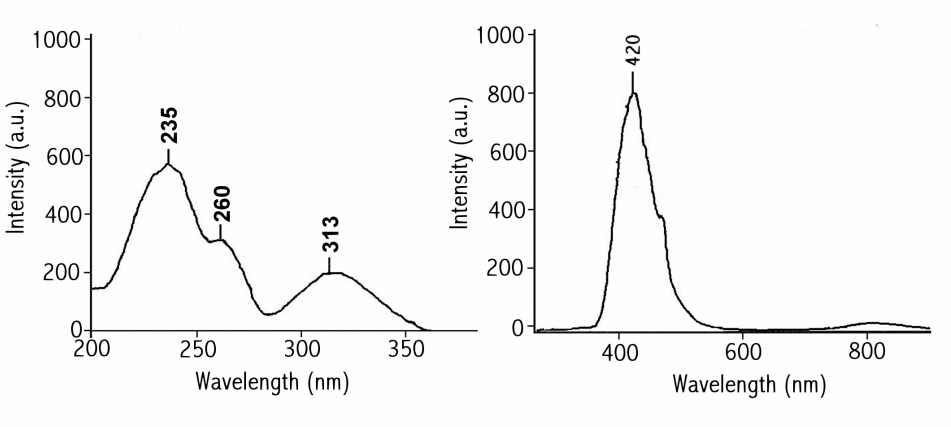
1000
800
600
400
200
0
Intensity (a.u.)
235
260
313
200
250
300
350
Wavelength (nm)
1000
800
600
400
200
0
Intensity (a.u.)
420
400
600
800
Wavelength (nm)

Figure 4

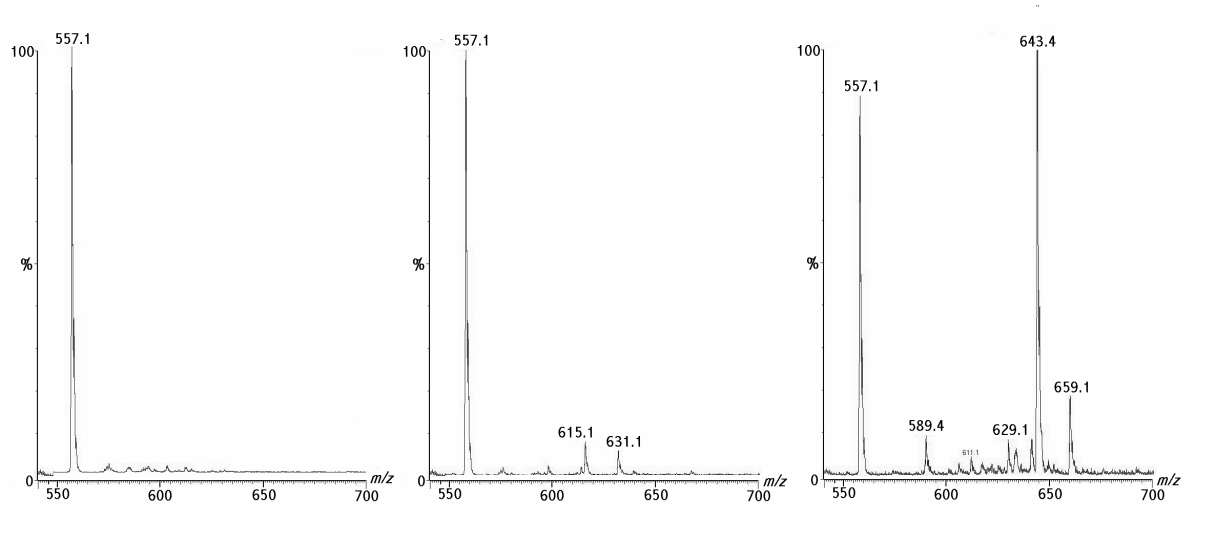
100
%
0
557.1
550
600
650
700
m/z
100
%
0
557.1
615.1
631.1
550
600
650
700
m/z
100
%
0
557.1
643.4
659.1
589.4
629.1
550
600
650
700
m/z

Figure 5

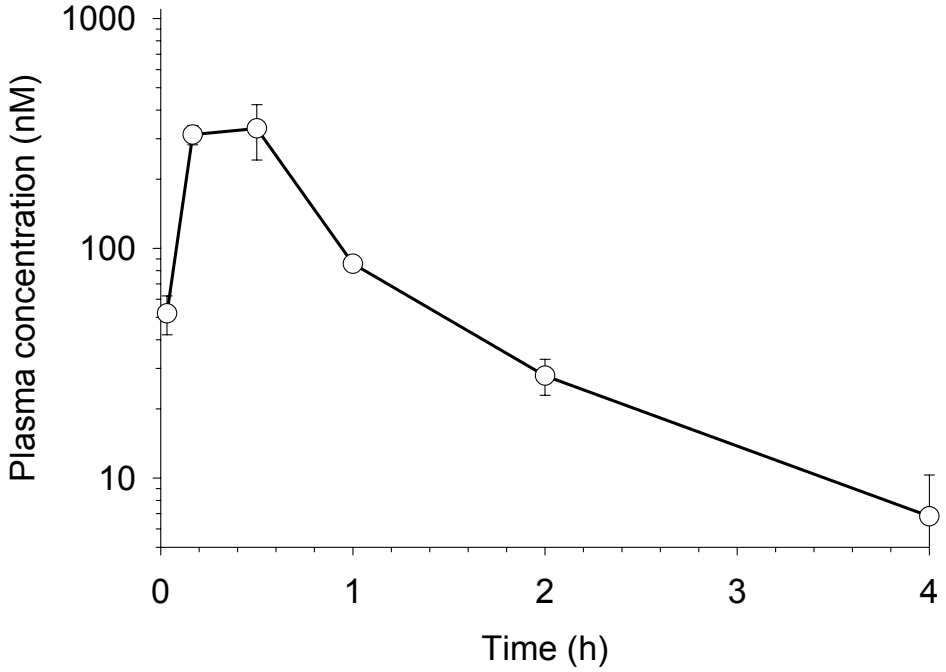

Figure 6

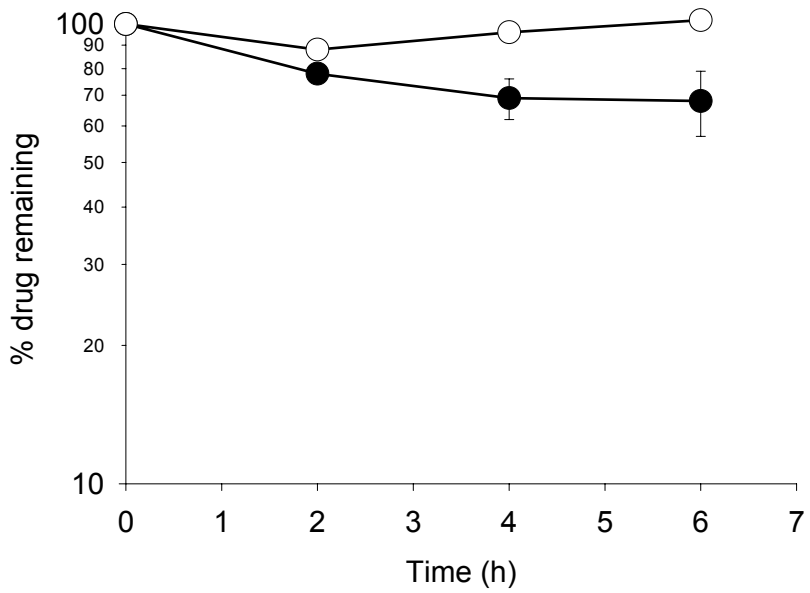

Figure 7

Published Abstract

Pharmacokinetics of D709119 (DRH-417), a DNA minor groove-binding pyrrolobenzodiazepine monomer with a novel mechanism of action

G.P. Wilkinson [1] , T.C. Jenkins [2], D.E. Thurston [3] , P.W. Howard [3] , J.A. Double [1] , M.C. Bibby [1] , P.M. Loadman [1].
[1]University of Bradford, Cancer Research UK Cancer Research Unit, Bradford, United Kingdom; [2] University of Bradford, Yorkshire Cancer Research Laboratory of Drug Design, Bradford, United Kingdom; [3] University of London, Cancer Research UK Gene Targeted Drug Design Group, London, United Kingdom

D709119 is a DNA minor groove-binding pyrrolobenzodiazepine derivative that shows significant *in vitro* cytotoxicity towards a select number of cell lines in the 60-cell line NCI screen. This activity translates into human tumour xenograft models where *in vivo* antitumour activity has been demonstrated for a number of models including melanoma, renal and ovarian. On the basis of this *in vivo* activity, together with the novel mechanism of action of D709119 as suggested by findings from an NCI COMPARE analysis, the compound is now in pre-clinical development with the EORTC. The aim of this study was to develop a highly selective LC/MS analytical method in order to investigate the pre-clinical pharmacokinetics of D709119 in mice. A further goal was to measure tumour concentrations of the drug, and also brain concentrations in order to assess the degree of CNS penetration. An LC/MS-based method has been developed using an acetonitrile/ammonium formate mobile phase with a Hypersil phenyl reversed-phase HPLC column. Selective detection is achieved using electrospray MS analysis with a SIR of m/z 368.4 to detect the parent ion, the limit of detection is 50 nM. All *in vivo* studies have been approved by the UK Home Office. Pharmacokinetic studies have been carried out in NMRI mice bearing either MAC29 or MAC15A murine colon tumours. Although an extraction efficiency of ~50 % was achieved from plasma and brain homogenates, only ~15 % extraction was achieved from spiked tumour homogenate suggesting extensive binding to tumour proteins. After i.p. administration at the MTD of 0.5 mg/kg, D709119 was easily detectible in mouse plasma up to 4 h post-dose, with peak concentrations of 171 nM after 30 min and a tl/2 of 2.3 h. The AUC was calculated to be 0.54 uM h. D709119 levels were below the limit of detection in both brain and tumour homogenates. An IC50 value for D709119 was determined experimentally in the human ovarian adenocarcinoma cell line SK-OV-3 to be 2.75 nM. These studies suggest that D709119 is bioavailable following i.p. injection at plasma concentrations well in excess of those necessary to achieve *in vitro* cytotoxicity. Further studies are now underway to probe the extensive binding of D709119 in tumour tissue.

Presented at the 14th EORTC/NCI/AACR Symposium on Molecular Targets and Cancer Therapeutics held in Frankfurt, November 2002.
Published in *European Journal Of Cancer* 38: 77 Suppl. 7 (2002).

Published Abstract

Intracellular and *in vivo* distribution of the pyrrolobenzodiazepine dimer SJG-136, a novel sequence-selective DNA minor groove cross-linking agent

G.P. Wilkinson 1 , P.M. Loadman 1 , J.P. Taylor 1 , T.C. Jenkins 2, J.A. Double 1 , S.J. Gregson 3 , P.W. Howard 3 , D.E. Thurston 3.
1University of Bradford, Cancer Research UK Cancer Research Unit, Bradford, United Kingdom; 2 University of Bradford, Yorkshire Cancer Research Laboratory of Drug Design, Bradford, United Kingdom; 3 University of London, Cancer Research UK Gene Targeted Drug Design Resear, London, United Kingdom

The pyrrolobenzodiazepine dimer SJG-136 is a novel sequence-selective DNA minor groove cross-linking agent with potent DNA stabilising activity and remarkable *in vitro* cytotoxicity (e.g. IC50 value of 23 pM in A2780 cells). The aim of this study was to characterise the *in vitro* cellular distribution of the agent and to establish its *in vivo* preclinical pharmacokinetic properties. SJG-136 is highly fluorescent and this enables its *in vitro* visualisation. Cell lines selected from the NCI's 60-cell line panel were treated with SJG-136 and fluorescence microscopy was used to monitor cellular uptake. It was demonstrated to produce a high level of nuclear-specific staining in HCT-116, UACC62, SK-MEL-2, SK-OV-3 and M14 cell lines, indicating both cellular penetration of the drug and Iocalisation by covalent fixation within the nucleus, the proposed site of drug action. A sensitive and reproducible HPLC-based analytical method has been developed for SJG-136 that will be used to obtain pharmacokinetic data in forthcoming clinical trials. Using an acetonitrile/ammonium formate gradient with a reversed-phase phenyl column and fluorescence detection, a limit of detection for SJG-136 of 1 nM in serum has been achieved. Extraction efficiencies from serum were >60% across a range of concentrations (1-100 nM). All *in vivostudies* have been approved by the UK Home Office. In pilot pharmacokinetic studies where SJG-136 was administered i.p. to NMRI mice at the MTD of 0.2 mg/kg, the drug could be observed at detectible levels with a Cmax of 336 nM after 30 min in mouse plasma. A calculated terminal tl/2 of 0.98 h and an AUC of 0.34 uM h resulted in a clearance of 17.72 ml / min kg. Preliminary plasma protein-binding studies demonstrate that the agent is poorly bound to proteins (<20 %), suggesting that SJG-136 is readily bioavailable in the blood with peak plasma concentrations substantially higher than those needed for *in vitro* cytotoxicity. Studies are currently in progress to establish the levels of SJG-136 that can be achieved in tumours.

Presented at the 14th EORTC/NCI/AACR Symposium on Molecular Targets and Cancer Therapeutics held in Frankfurt, November 2002.
Published in *European Journal Of Cancer* 38: 78 Suppl. 7 (2002).

Published Abstract

Pharmacokinetics, Metabolism & Glutathione Reactivity Of SJG-136

Gary P. Wilkinson*, Paul M. Loadman, Terence C. Jenkins, James Taylor, Steve D. Shnyder, Patricia A. Cooper & David E. Thurston
Tom Connors Cancer Research Centre, University of Bradford, All Saints Road, Bradford, West Yorkshire, BD7 3AY

SJG-136 is a novel DNA-crosslinking agent with sequence selective properties. The PBD dimer shows potent in vitro cytotoxicity and DNA-stabilising activity, and has been selected for clinical development on the basis of impressive preclinical activity.

The aim of this study was to investigate the in vitro & in vivo pharmacological characteristics of SJG-136 and to identify any potential metabolites. The proposed reactivity of PBDs with thiol containing macromolecules (e.g. GSH) was also investigated due to the potential influence of this on the pharmacology of SJG-136.

An HPLC method was developed using fluorescence and MS/MS detection. Intraperitoneal administration of SJG-136 to NMRI mice at the MTD (0.2 mg/kg) gave peak plasma concentrations of 336 nM after 30 min and an AUC of 0.34 uM. In vitro metabolism studies of SJG-136 in the mouse liver S9 fraction showed rapid drug depletion (< 10% at t0) likely to be due to GSH conjugation. SJG-136 is freely metabolised to a demethylated form in mouse liver microsomes & this metabolite was detected in in vivo samples at low concentrations. This metabolite is not detectible in the S9 fraction suggesting that GSH reactivity inhibits metabolic degradation of the drug. SJG-136 reacts with GSH in a concentration-dependant manner, suggesting increased adduct formation at higher GSH levels. Analytically, these adducts appear to be identical to those found in the S9 fraction.

Such low metabolic potential in vivo simplifies the pharmacology of the compound and enhances its therapeutic potential.

All in vivo studies complied with UK home office regulations.

Presented at the BACR British Cancer Research Meeting held in Bournemouth, July 2003.
Published in *British Journal Of Cancer* 88: S29 Suppl. 1 (2003).

Published Abstract

Pharmacokinetics and intracellular pharmacological characteristics of the novel pyrrolobenzodiazepine (PBD) dimer SJG-136.

Wilkinson G. P.[1] , Loadman P. M.[1] , Taylor J.[1], Swaine D.[1], Jenkins T. C.[2] , Double J. A.[1] , Spanswick V. J.[3], Hartley J. A.[3], Gregson S. J.[4] , Howard P. W.[4] , Thurston D. E.[4]

[1] Cancer Research UK Cancer Research Unit, University of Bradford, All Saints Road, Bradford, West Yorkshire, BD7 3AY, UK; [2] Yorkshire Cancer Research Laboratory of Drug Design, University of Bradford, All Saints Road, Bradford, West Yorkshire, BD7 3AY, UK; [3] Cancer Research UK Drug-DNA Interactions Group, Dept of Oncology, UCL, London, W1W 7BS, UK; [4] Cancer Research UK Gene Targeted Drug Design Research Group, School of Pharmacy, University of London, 29/39 Brunswick Square, London, WC1N 1AX, UK

SJG-136 is a novel sequence-selective DNA minor-groove binding pyrrolobenzodiazepine (PBD) dimer that spans six DNA base pairs forming interstrand cross-links at Pu-GATC-Py sites. It is remarkably cytotoxic *in vitro* and has significant antitumour activity with a clear therapeutic index in a large number of human tumour xenograft models. As a result of these pre-clinical data, SJG-136 has been selected for Phase I clinical trials in the UK (Cancer Research UK) and the USA (NCI). The aim of this study was to characterise the pre-clinical pharmacokinetics and cellular pharmacological properties of SJG-136.

A gradient reversed-phase HPLC method using ES^+-mass spectrometry and fluorescence detection has been developed to enable the analysis of SJG-136 in biological samples. The assay has limits of detection of 10 nM and 0.5 nM for mouse and human plasma, respectively. Following ip administration to NMRI mice at the MTD of 0.2 mg/kg, SJG-136 was easily detectable with a C_{max} of 336 nM after 30 min. A calculated terminal $t_{½}$ of 0.98 h and an AUC of 0.34 μM h resulted in a clearance of 17.72 ml/min/kg. During these pharmacokinetic studies, DNA interstrand crosslinks were measured in mouse lymphocytes using a modification of the Comet assay. Crosslinks could be detected at 1 h following ip drug administration and remained at the same level for 18 h.

The fluorescence of SJG-136 enabled studies of its intracellular distribution in living cells using fluorescence microscopy. Cell lines (UACC-62, DU-145, SK-MEL-2, SK-OV-3 and M14) showing a range of sensitivities to SJG-136 were selected from the NCI's 60-cell line panel and exposed to SJG-136 at concentrations close to peak plasma concentrations in the mouse. Nuclear-specific staining was observed in all cell lines demonstrating cellular penetration and localisation within the nucleus, the proposed site of drug action. IC_{50} concentrations for selected cell lines were determined using the MTT dye conversion assay. These ranged from 4.2 - 29.8 nM for a 1 h drug exposure. FACS studies indicated that at these concentrations, SJG-136 caused a G_2/M block in the cell cycle for all selected cell lines.

Further pharmacokinetic and pharmacodynamic studies are in progress to monitor drug concentrations and DNA crosslinking in solid tumours in *in vivo* models using therapeutic concentrations. These data will help in the clinical development of SJG-136.

Presented at the AACR 94th Annual Meeting held in Washington D.C., July 2003. Published in Proceedings of the American Association of Cancer Research 44;1634 (2003).

Published Abstract

Pyrrolobenzodiazepine-polyamide libraries: synthesis and DNA binding selectivity

G. Wells*, T. Gale*†, A. Hardy*†, A. Hamaguchi†, J. A. Hartley†‡, **G. P. Wilkinson**§, P. M. Loadman§, T. Jenkins§, P. W. Howard*† and D. E. Thurston*†
*CRUK Gene Targeted Drug Design Research Group, The School of Pharmacy, 29–39 Brunswick Square, London, WC1N 1AX; †Spirogen Ltd, 29–39 Brunswick Square, London, WC1N 1AX; ‡CRUK Drug-DNA Interactions Research Group, Department of Oncology, University College London, London, W1W 7BS and §CRUK Cancer Research Unit & Yorkshire Cancer Research Laboratory of Drug Design, University of Bradford, All Saints Road, Bradford, UK

The ability to modify gene transcription by inhibiting the activity of specific transcription factors or blocking transcription in the coding region of a gene has potential applications in the treatment of cancer. A sufficient number of base pairs must be recognised in order to obtain a specific effect. At the molecular level the minor-groove binding pyrrolobenzodiazepine (PBDs) recognise and covalently bind to Pu-G-Pu sequences (Thurston 1993; Hardy *et al* 2003), whereas heterocyclic polyamide (HPAs) interact reversibly with a variety of sequences depending on the nature of the heterocycle and the binding stoichiometry. The aim of this work is to synthesise hybrid molecules that combine the recognition characteristics of both molecules. Solution phase peptide coupling methods have been used to synthesise a series of PBD-HPA hybrids with polyamide components (N-methylpyrroles) of varying length with a long-term view of studying the effect of polyamide length on DNA binding-site size and selectivity, binding affinity, cellular penetration and in-vitro cytotoxicity. GW6 consists of a PBD attached to three N-methylpyrrole heterocycles. Footprinting studies have shown that the molecule binds to a GATAATC sequence suggesting that it possesses DNA-recognition properties characteristic of both the PBD and HPA portions of the molecule. Using fluorescence microscopy we have shown that, unlike Dervan hairpin polyamides (Belitsky *et al* 2002) that bind to a similar number of base pairs, GW6 penetrates the nucleus of cultured MCF-7 cells. It also has in-vitro cytotoxic properties with a mean GI50 of 5 10 n M in the NCI's 60 cell line screen. Synthesis of the PBD-HPA conjugates has been successfully transferred to solid phase methodology using a variety of heterocyclic building blocks, and has been extended to the preparation of PBD-heterocycle combinatorial libraries. These libraries have been synthesised in conjunction with a peptide coding strand to enable identification of an individual DNA-binding molecule. A 100 000 member library has been screened against a number of rhodamine labelled gene fragments including one taken form *bcr-abl* and a number of hits have been obtained. Edman degradation of the tag sequences has revealed the structures of 10 lead molecules which are currently being resynthesized for further biological evaluation.

Published in Proceedings of the American Association of Cancer Research 44;452 (2003).